Generic Analysis Methods
for
Gas Turbine Engine Performance

The development of

the gas turbine simulation program GSP

Wilfried Visser

Generic Analysis Methods
for
Gas Turbine Engine Performance

The development of

the gas turbine simulation program GSP

PROEFSCHRIFT

ter verkrijging van de graad van doctor
aan de Technische Universiteit Delft,
op gezag van de Rector Magnificus Prof. Ir. K.Ch.A.M. Luyben,
voorzitter van het College voor Promoties,
in het openbaar te verdedigen op
dinsdag 6 januari 2015 om 12:30 uur

door

Wilhelmus Petrus Jozef VISSER
Werktuigkundig ingenieur
geboren te Bovenkarspel

Dit proefschrift is goedgekeurd door de promotor:

Prof. Ir. J.P. van Buijtenen

Samenstelling promotiecommissie:

Rector Magnificus	Voorzitter
Prof. Ir. J.P. van Buijtenen,	Technische Universiteit Delft, promotor
Prof. Dr. Ir. Piero Colonna,	Technische Universiteit Delft
Prof. Dr. Ir. Tiedo Tinga,	Universiteit Twente
Prof. Dr. Ir. D.M.J. Smeulders,	Technische Universiteit Eindhoven
Prof. Dr. Tomas Grönstedt	Chalmers University of Technology
Dr. Arvind Gangoli Rao	Technische Universiteit Delft
Dr. Joachim Kurzke	GasTurb GmbH
Prof. Dr. Ir. Leo Veldhuis	Technische Universiteit Delft, reservelid

Keywords: gas turbine, simulation, performance modelling, object orientation

This thesis is dedicated to my brother Robert

"Scientists discover the world that exists;
engineers create the world that never was."

Theodore von Karman

Summary

Numerical modelling and simulation have played a critical role in the research and development towards today's powerful and efficient gas turbine engines for both aviation and power generation. The simultaneous progress in modelling methods, numerical methods, software development tools and methods, and computer platform technology has provided the gas turbine community with ever more accurate design, performance prediction and analysis tools. An important element is the development towards *generic* tools, in order to avoid duplication of model elements for different engine types. This thesis focuses on the development of generic gas turbine system performance simulation methods. This includes the research required to find the optimal mathematical representation of the aero-thermodynamic processes in the gas turbine components in terms of fidelity, accuracy and computing power limitations. The results have been applied in the development of the Gas turbine Simulation Program GSP.

GSP is a modelling tool for simulation and analysis of gas turbine system performance. This involves 0-D (i.e. zero-dimensional or parametric) component sub-models that calculate averaged values for parameters such as pressures and temperatures at the gas path stations between the components. The component sub-models are configured ('stacked') corresponding to the gas turbine configuration. Component performance is determined by both aero-thermodynamic equations and user specified characteristics, such as turbomachinery performance maps. If higher fidelity is required at a specific location in the system model, 1-D component models can be added to predict the change in gas state or other parameters as a function of a spatial (usually in the direction of a streamline) parameter. Non-linear differential equations (NDEs) are used to represent the conservation laws and other relations among the components. The sets of NDEs are automatically configured depending on the specific gas turbine configuration and type of simulation. Simulation types include design point (DP), steady-state off-design (OD) and transient simulations.

The research and development challenge lies in the development of generic, accurate and user friendly system modelling methods with sufficient flexibility to represent any type of gas turbine configuration. The accuracy and fidelity is enhanced by the development of modelling methods capturing secondary effects on component and system performance in 0-D or 1-D sub-models. Object oriented software design methods have been used to accomplish the flexibility objectives, also resulting in a high degree of code maintainability. This allows easy adaptation and extension of functionalities to meet new requirements that are emerging since

the start of the development of GSP in its current form (1997). The object oriented architecture and how it relates to the system and component modelling and the ensuing solving of the NDEs, is described in the thesis.

An important element has been the development of the gas model with chemical equilibrium and gas composition calculations throughout the cycle. Fuel composition can be specified in detail for accurate prediction of effects of alternative fuels and also detailed emission prediction methods are added. The gas model uses a unique and efficient method to iterate towards chemical equilibrium.

The object oriented architecture enabled the embedding of a generic *adaptive modelling* (AM) functionality in the GSP numerical process and NDEs, providing best AM calculation speed and stability. With AM, model characteristics are adapted for matching specified (often measured) output parameter values for engine test analysis, diagnostics and condition monitoring purposes. The AM functionality can be directly applied to any GSP engine model.

The recent trend towards the development of micro turbines (with very high surface-to-volume ratios in the gas path) requires accurate representation of thermal (heat transfer) effects on performance. For this purpose, GSP has been extended with an object oriented thermal network modelling capability. Also, a 1-D thermal model for representing the significant heat soakage effects on micro turbine recuperator transient performance has been developed.

For *real-time* transient simulation, the Turbine Engine Real-Time Simulator (TERTS) modelling tool has been derived from GSP. In TERTS, the methods from GSP are used with fidelity reduced to some extent in order to meet the real-time execution requirements.

GSP has been applied to a wide variety of gas turbine performance analysis problems. The adaptive modelling (AM) based gas path analysis functionality has been applied in several gas turbine maintenance environments. Isolation of deteriorated and faulty turbofan engine components was successfully demonstrated using both test rig data and on-wing data measured on-line during flight.

For a conceptual design of a 3kW recuperated micro turbine for CHP applications, design point cycle parameters were optimized based on careful component efficiency and loss estimates. Worst and best case scenarios were analysed with GSP determining sensitivity to deviations from the estimates. The predictions have proven very accurate after a test program showing 12% (electric power) efficiency on the first prototype. For increasing the efficiency towards 20%, GSP was used to predict the impact of several design improvements on system efficiency.

GSP was used to study the effects on performance and losses of scaling micro turbines in the range of 3 to 36 kW. At small scales, turbomachinery losses become relatively large due to the smaller Reynolds number (larger viscous losses) and

other effects. The scale effects have been analysed and modelled for the turbine and compressor and GSP has been used to predict the effects on system efficiency.

Other applications include prediction of cumulative exhaust gas emissions of the different phases of commercial aircraft flights, simulation of thermal load profiles for hot section lifing studies, alternative fuel effect studies, performance prediction of vertical take-off propulsion systems and reverse engineering studies.

The object oriented design of GSP has proven its value and has provided the building blocks for an ever increasing number of component models, adaptations and extensions. The flexibility of GSP is demonstrated with the modelling of novel cycles, including a parallel twin spool micro turbine with a single shared combustor, a rotating combustor micro turbine concept, a modern heavy duty gas turbine with a second (reheat) combustor and a multi-fuel hybrid turbofan engine, also with a reheat combustor. Several new capabilities have been developed following new requirements from the user community, using the original object oriented framework and component model classes.

In the future, new technologies may replace today's simulation tools. Maybe even the concept of modelling and simulation as we know it today will entirely change. However, as long as gas turbines and related systems will be developed and operated, there will be a need to understand their behaviour. The fundamental physics behind this will not change nor will the equations describing the processes. In that sense, GSP can be seen as a phase in the development of gas turbine modelling and simulation technology. An interesting question would be, how long will GSP remain before it is left behind for new ways. A lot will depend on the ability of GSP and its developers to adapt to future needs and also future opportunities emerging from new modelling, simulation, and computer and software technologies. So far however, GSP has proven a remarkable track record and will be around for quite a while, serving many scientists and engineers interested in gas turbine system performance analysis and simulation.

Samenvatting

Numerieke simulatiemethoden hebben een essentiële rol gespeeld bij de ontwikkeling van moderne gasturbinemotoren voor zowel vliegtuigvoortstuwing als energieopwekking. Door de gelijktijdige ontwikkeling van numeriek methoden, moderne methoden voor software ontwikkeling en de ontwikkeling van computer technologie, kan de gasturbinewereld beschikken over steeds nauwkeuriger middelen voor analyse en voorspelling van gasturbineprestaties. Een belangrijk element is de ontwikkeling van *generieke* methoden waarmee 'dubbel werk' kan worden voorkomen bij het opstellen van steeds dezelfde soort modelelementen voor verschillende gasturbine types. Dit proefschrift focust op de ontwikkeling van generieke methoden voor het modelleren van gasturbineprestaties en -gedrag. Dit omvat onderzoek naar de optimale mathematische beschrijvingen van de aerodynamische en thermodynamische processen in de gasturbinecomponenten. Hierbij gaat het om de optimale combinatie van detail en nauwkeurigheid bij de gegeven beperkingen in computerrekenkracht. De resultaten zijn toegepast bij de ontwikkeling van het Gasturbine Simulatie Programma GSP.

GSP is een computerprogramma voor simulatie van het gedrag van gasturbines als systeem. In 0-D (nuldimensionale of 'parametrische') submodellen van de componenten worden gemiddelde waarden van parameters zoals drukken en temperaturen berekend op de gaspad locaties tussen de componenten. De submodellen worden gerangschikt overeenkomstig de gasturbineconfiguratie. De prestaties van de componenten worden bepaald door aero-thermodynamische vergelijkingen en door de gebruiker te specificeren prestatiekarakteristieken van de componenten, zoals de 'maps' van compressoren en turbines. Voor een meer gedetailleerde beschrijving van de processen op een specifieke locatie in de gasturbine kunnen 1-D (eendimensionale) component modellen worden toegevoegd. Dan worden gastoestands- of andere parameters functies van een ruimtelijke parameter (meestal in de richting van de gasstroming). Met niet-lineaire differentiaalvergelijkingen (NDEs) worden de behoudswetten en andere relaties tussen componenten beschreven. De sets van NDEs worden automatisch opgesteld afhankelijk van de specifieke configuratie van de gasturbine en het type simulatie: ontwerppunt (design point DP), off-design (OD) stationaire, of dynamische simulatie.

De uitdaging voor het onderzoek is het ontwikkelen van generieke, nauwkeurige en ook gebruikersvriendelijke methoden met voldoende flexibiliteit voor het modelleren van alle mogelijke soorten gasturbines. De nauwkeurigheid en de mate

van detail kan door de gebruiker worden verhoogd door de ontwikkeling van 0-D of 1-D submodellen voor tweede orde effecten op component- en systeemprestaties. Object-georiënteerde software-ontwikkelmethoden zijn gebruikt om de doelen ten aanzien van flexibiliteit te realiseren. Dit verbetert ook in sterke mate de onderhoudbaarheid van de software code. Aanpassingen en uitbreidingen van de functionaliteit, nodig voor steeds weer nieuw eisen aan GSP, kunnen hierdoor efficiënt geïmplementeerd worden. De object-georiënteerde softwarearchitectuur en haar relatie met het modelleren van het gasturbinesysteem en de componenten, en vervolgens de oplossing van de NDEs, is beschreven in deze thesis.

Een belangrijk element is de ontwikkeling van het gasmodel met chemisch evenwicht en de berekeningen van de gassamenstelling op de verschillende locaties in de gasturbine. Brandstofsamenstelling kan in detail gespecificeerd worden en nauwkeurige voorspelling van effecten van alternatieve brandstoffen op prestaties en op uitlaatgasemissies is hierdoor mogelijk. Het gasmodel gebruikt een unieke methode voor iteratie naar chemisch evenwicht.

De object georiënteerde architectuur maakte de integratie van een generieke *adaptive modelling* (AM) functionaliteit mogelijk in het numerieke proces en in de NDEs voor optimale AM rekensnelheid en numerieke stabiliteit. Met AM worden modeleigenschappen aangepast met het doel specifieke uitvoerparameters met (vaak gemeten) waarden overeen te laten komen. De toepassingen hiervan zijn onder meer analyse van testresultaten, diagnostiek en conditiebewaking. De AM functionaliteit kan direct worden toegepast op elk GSP gasturbinemodel.

De recente trend richting de ontwikkeling van microturbines (met zeer hoge oppervlakte-inhoud verhoudingen in het gaspad) vereist nauwkeurige modellering van thermische effecten op de prestaties. Hiervoor is GSP uitgebreid met een object georiënteerd 'thermal network' model. Ook is een 1-D thermisch model ontwikkeld voor de effecten van 'heat soakage' in de recuperator op het dynamische gedrag van microturbines.

Voor *real-time* dynamische simulatie is het Turbine Engine Real-Time Simulator (TERTS) simulatie programma ontwikkeld. In TERTS worden de methoden van GSP gebruikt met een gereduceerde mate van detail, en dus minder benodigde rekenkracht, om zo aan de real-time snelheidseis te kunnen voldoen.

GSP is toegepast op een breed scala van gasturbineprestatieanalyse-problemen. De 'adaptive modelling' (AM) functionaliteit is toegepast in verschillende gasturbine-onderhoudsbedrijven. De identificatie van turbofan motorcomponenten met afwijkende conditie of storingen is met succes gedemonstreerd met zowel meetgegevens van de motorproefbank als on-line tijdens de vlucht gemeten gegevens.

Voor een conceptueel ontwerp van een 3kW gerecupereerde microturbine voor warmte-kracht koppeling, zijn de kringproces-ontwerpparameters geoptimaliseerd

na nauwkeurige schattingen van componentrendementen en thermodynamische verliezen. 'Worst / best case' scenario's zijn geanalyseerd op basis van met GSP berekende effecten van afwijkingen van de schattingen. De voorspellingen bleken zeer nauwkeurig na voltooiing van een testprogramma waarbij 12% rendement (op basis van elektrisch uitgangsvermogen) gemeten werd op een eerste prototype. Voor verhoging van het rendement richting de 20% is GSP vervolgens gebruikt bij het voorspellen van the effecten van verschillende ontwerpverbeteringen.

GSP is verder gebruikt bij een studie naar de effecten op prestaties en verliezen van het schalen van micro turbines met vermogens tussen 3 en 36 kW. Verliezen in stromingsmachines nemen toe bij kleiner wordende afmetingen door o.a. het kleiner wordende Reynolds getal (en dus grotere viskeuze verliezen). De schaaleffecten zijn geanalyseerd en gemodelleerd voor turbines en compressoren en GSP is gebruikt voor het voorspellen van deze effecten op gasturbine-systeemniveau.

Andere toepassingen zijn: de voorspelling van uitlaatgasemissies tijdens de verschillende fasen de vlucht met civiele vliegtuigen; simulatie van thermische belastingsprofielen voor gasturbine 'hot section' levensduuranalyses; studies naar effecten van alternatieve brandstoffen; voorspelling van prestaties van vliegtuigmotoren voor verticaal opstijgen en voor 'reverse engineering' studies.

De object oriëntatie in GSP heeft haar nut bewezen en de bouwstenen geleverd voor de verdere ontwikkeling van meer componentmodellen, aanpassingen en uitbreidingen. De flexibiliteit van GSP is gedemonstreerd met het modelleren van nieuwe soorten gasturbine-kringprocessen zoals een microturbine met 2 parallelle assen en een enkele gedeelde verbrandingskamer, een concept met een roterende verbrandingskamer, een moderne 'heavy duty' gasturbine met een tweede verbrandingskamer voor herverhitting en een 'multi-fuel hybrid turbofan engine met herverhitting. Verschillende nieuwe functionaliteiten zijn ontwikkeld naar aanleiding van nieuwe eisen afkomstig van de GSP gebruikers. Hierbij is steeds weer het originele object georiënteerde raamwerk gebruikt.

In de toekomst zullen nieuwe technologieën wellicht de huidige simulatie methoden en middelen vervangen. Misschien dat het gehele concept van modelleren en simulatie zoals we dat nu kennen ooit geheel gaat veranderen. Echter, zolang gasturbines en aanverwante systemen ontwikkeld en gebruikt worden zal de behoefte blijven bestaan hun gedrag te analyseren. De fundamentele fysica hierachter zal niet veranderen en ook niet de vergelijkingen die de processen beschrijven. In die zin kan GSP gezien worden als een fase in de ontwikkeling van gasturbine-simulatietechnologie. Een interessante vraag is hoe lang het zal duren voordat GSP wordt vervangen door nieuwe methoden en middelen. Veel zal afhangen van de mate waarin GSP en haar ontwikkelaars zich kunnen aanpassen aan toekomstige behoeften en ook nieuwe kansen afkomstig van nieuwe simulatie-, computer- en softwaretechnologie. Tot dusver heeft GSP echter bewezen dat het

nog jaren voor de boeg heeft als een waardevol stuk gereedschap voor veel onderzoekers en ingenieurs met interesse in simulatie en analyse van gasturbineprestaties.

Contents

CONTENTS 19

CONTENTS   21

(289 pages total)

PART I

INTRODUCTION

Chapter 1   Background

1.1   History

It has been more than 60 years since the gas turbine was developed and successfully applied. The initial applications included both aircraft propulsion and land-based power generation. The greatest impact of the gas turbine engine has been on aviation with the development of the jet engine. Aircraft gas turbines were developed by the former piston aero engine manufacturers, while steam turbine manufacturers started developing gas turbines for land based applications. Later, aircraft gas turbine derived engines were used for industrial use as well.

From the very start, modelling the processes inside the gas turbine has been critical for successful development towards a working concept [1, 2]. Models were required to predict performance of the Joule-Brayton cycle that takes place in the gas turbine, to predict performance of the components and to predict structural and thermal loads. Obviously, the first models consisted of only manual cycle and component performance and structural stress calculations. These models had limited potential and consequently in those early days a lot of experimental work was needed for development of optimized gas turbine designs. At the same time, the rapidly growing scientific gas turbine community was working hard to minimize this trial-and-error approach, developing new modelling techniques and, after the introduction of computers, exploiting the utmost from available computer power.

1.2   Modern simulation tools for engine development

The last few decades have provided gas turbine engineers with increasingly powerful modelling tools for engine design disciplines such as aero-thermodynamics, structural and thermal analysis, controls, lifing and cost analysis. Today, these include detailed engine system performance models, multi-dimensional computational fluid dynamics (CFD) for component performance analysis and finite element method (FEM) models to analyse structural stress. The resulting improvements in performance prediction accuracy have reduced the need for test facilities. While testing still remains a major element in engine development programs, for *test analysis* performance models play a critical role using 'analysis by synthesis' methodology.

Recent developments are focused on integral simulations in different disciplines for 'multi- disciplinary optimization' (MDO) in new engine designs [3-7]. An important element in this is the 'zooming' concept where engine system models are coupled on-line with detailed models simulating local phenomena in a limited section in the engine with higher fidelity and accuracy.

1.3   Models in the operational and maintenance environment

More recently, engine models are entering the operational and maintenance environment in the form of diagnostic tools: either off-line with engine testing or during operation embedded in condition monitoring and/or control systems. Advanced *adaptive* control system concepts exist [8] where control laws may be adapted depending on on-line model based assessment of engine condition.

1.4   Computer platforms and software implementation

The more comprehensive models for gas turbine research and development (R&D) generally involve solving multiple differential equations. For multi-dimensional models the number of equations can become very large. Computers are required to solve the equations using numerical methods such as Newton-Raphson based or other solvers. An essential element in gas turbine simulation therefore is the computer implementation.
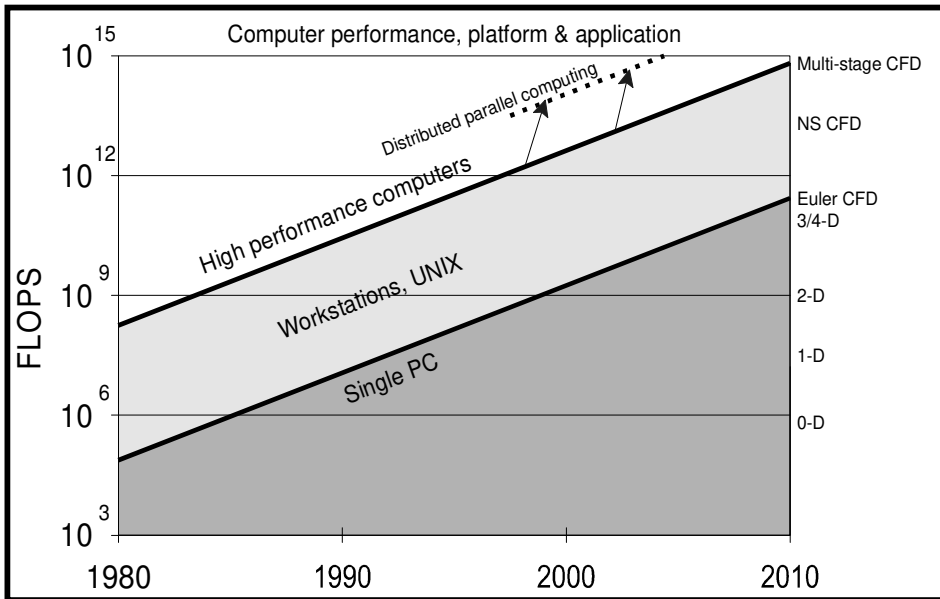
Figure 1.1 Trends in performance simulation computing power (from [9])

Today, computing power is extremely cheap compared to several decades ago. CFD simulations already run on single personal computers (PCs) and when clustering PCs computing power can be increased to perform simulations that earlier could only be done on very expensive dedicated super computers. Figure 1.1 shows performance simulation computing power trends determined around 2001 by [9]. As a consequence, computer power has ceased to be the bottleneck for all but

the high-fidelity CFD gas turbine simulations. For all types of simulations, implementation effort, user interface including visualization and code maintenance have become critical for successful and efficient use of the models.

For high fidelity CFD simulations a bottleneck remains in the available computer power and memory, especially when combustion is included or the time domain is added as an extra dimension for dynamic simulations. Simultaneous simulation at high spatial resolution and high time domain resolution for instance remains limited as indicated by Figure 1.2. As a consequence, trade-offs are required with respect to spatial and temporal resolution, number of dimensions and the scope of the model.
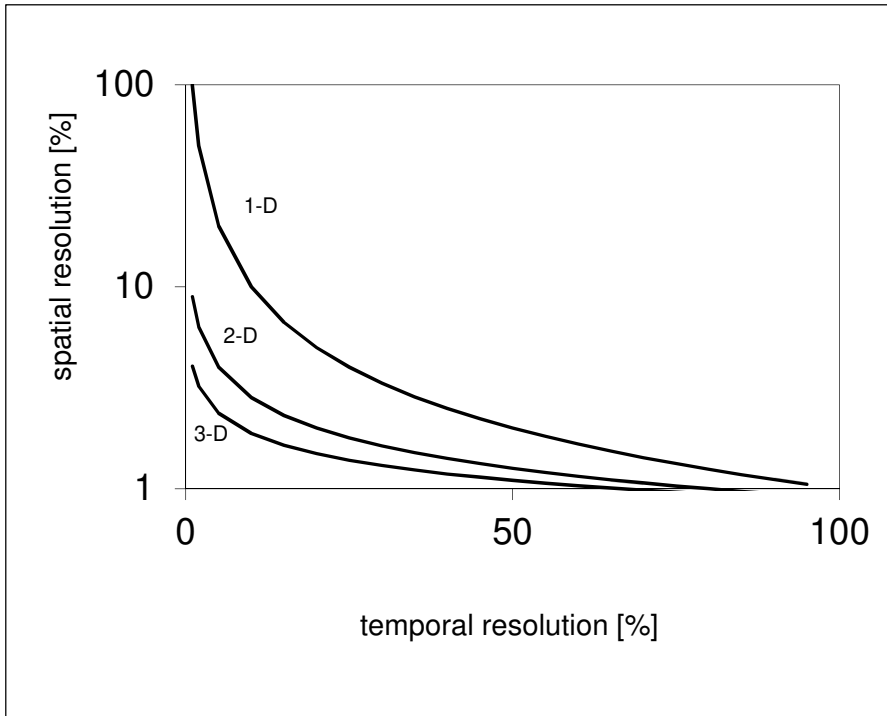
Figure 1.2 Spatial vs. temporal resolution for a given computing power (from [9])

1.5   Legacy codes versus new modelling tools

A challenge remains to implement the models on the computing platform in a cost effective manner. Excellent software development tools exist to develop models and generic modelling environments for today's relatively low-cost computers. However, such projects still involve significant investments compared to the cost of using existing models. Since the 1970s, a huge legacy of gas turbine model codes has been accumulated and a substantial part of it is still in use.

Especially the lower fidelity models still function quite well and, until using them becomes impossible due to phasing-out of the old platforms, maintaining them instead of developing new models may seem the most cost effective way.

1.6   Configuration and case management

Management of gas turbine model configurations and simulation cases and related data requires specific attention, especially when large numbers of different model versions are involved. Also when the number of people involved with using or developing a model increases, configuration management becomes increasingly important. Often special tasks need to be defined in order to maintain integrity of the model configurations. These tasks may be performed either inside modern modelling environment or using special software tools.

1.7   Generic modelling environments

The legacy codes, developed in times where today's development and application life cycle management (ALM, [10]) tools were not yet available, present significant maintenance problems. Often, code documentation is limited and without the employees that once developed the codes, adaptation or upgrading is difficult.

As a result, since the 1990s projects have started to develop generic gas turbine simulation tools and standards using modern software development methodology [11, 12]. With these, models for new studies and engines could be developed and maintained more efficiently and old codes replaced.

This thesis describes the development of the Gas turbine Simulation Program GSP which represents a generic gas turbine system performance simulation environment. The development of GSP started in 1996 and still continues today.

Chapter 2   Gas turbine performance simulation

2.1   Application areas

Gas turbine performance models have traditionally been developed by engine manufacturers (OEMs) and related institutes. Today, models are used for a wide variety of tasks throughout the engine life cycle (see Figure 2.1). From conceptual design to performance monitoring, engine performance is simulated in some form. In Figure 2.1 the cycle restarts using operational experience for design of derivative engines, showing the value of performance monitoring simulation models.
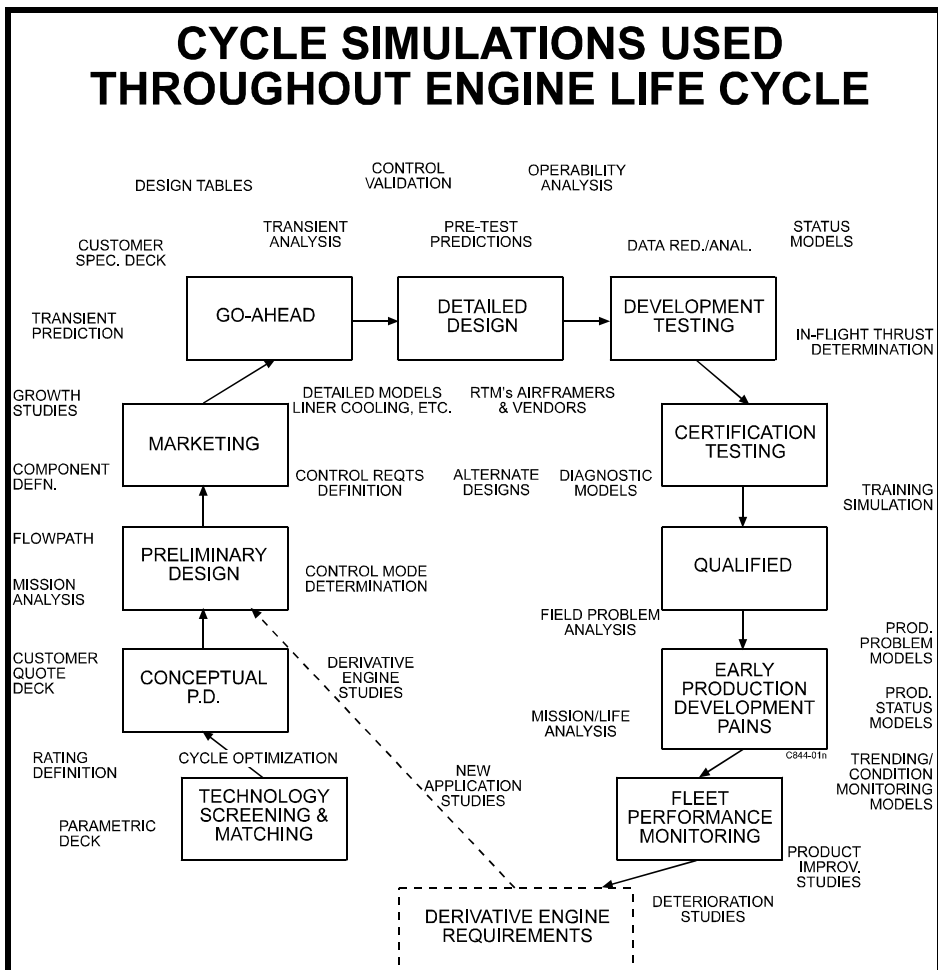
Figure 2.1 Engine simulations throughout the engine life cycle (from [9])

Naturally, for a particular engine design, the models will evolve from early stage conceptual design studies, where the cycle design parameters are varied and optimized, towards models that accurately represent specific performance aspects of the eventual engine design. For the different model types, different platforms and tools will be used that ideally are integrated in a single framework in order to minimize data entry and/or copy work.

In addition, modelling tools have been developed outside the engine OEM environment for applications other than pure engine development. These applications include performance prediction in aircraft design studies, flight simulation, power generation studies, operating condition effect analysis, deterioration effects, emission prediction etc. Arguments to develop these models were often the usually very limited availability of engine performance data and models ('engine decks') from the OEM.

2.2   Model creators and users

Figure 2.2 shows the relationship between the users and creators of aero-engine models at various levels, from the generally highly detailed models in the research environment to the lower detail engine performance decks used by system integrators, such as aircraft designers and industrial power plant integrators.
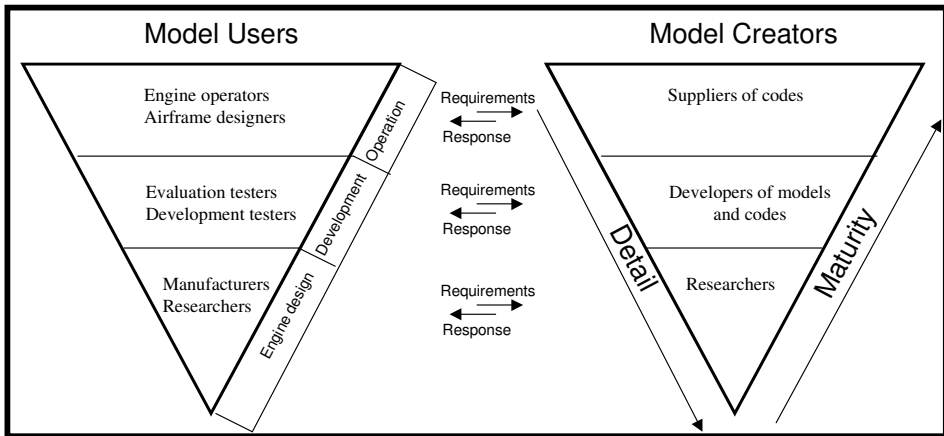
Figure 2.2 Model users and creators (from [9])

The figure also indicates that today, gas turbine modelling is often done by specialized developers based on requirements coming from the users. An overview of aero-engine gas turbine simulation applications is given in [9, 13].

Today's OEM engine modelling environments are often based on a legacy of tools and software codes, resulting in series of engine specific models. This means development of models for new engines requires significant efforts including

significant coding work. From the nineties onwards, the OEMs have started to develop generic tools that enable rapid set-up of new models including MDO (Multi-Disciplinary Optimization) capabilities [3-7]. Meanwhile, outside the OEM community user friendly modelling tools are required with high degrees of flexibility to model different engine types using limited engine performance data. With the range of applications gradually expanding outside the engine design area these 'non-OEM' models are of increasing importance and are covering an increasing number of applications shown in Figure 2.1. Applications include failure analysis, performance prediction, gas path analysis, diagnostics, emission prediction and life cycle management studies. Several OEMS seek collaboration with the 'non-OEM' model makers and other OEMS to combine efforts in developing powerful generic modelling tools for many different applications [14, 15].

2.3   Performance simulation scope

Cycle performance models represent performance of the whole gas turbine engine. These usually simulate the processes in the engine with limited fidelity. 0-D (i.e. zero-dimensional or parametric) models calculate averaged values for pressures and temperatures at the gas path stations between the components. More advanced cycle models may also include 1-D and/or mean-line models to predict the change in gas state parameters as a function of a spatial parameter (often in the direction of a streamline).

Higher fidelity multi-dimensional models usually are representing phenomena in a limited area within the engine. Examples are compressor or turbine stage CFD models or complete component models that are capable of predicting component maps. The interaction between the detailed phenomena and the whole engine performance can be simulated by combining 0-D and multi-dimensional models. One approach is to run the multi-dimensional model as a component of the whole engine model. This approach, also referred to as 'zooming', requires transformations between multi-dimensional model boundary conditions and 0-D averaged gas and flow conditions at some *station* in the cycle [15, 16].

Another extension of modelling scope is applied with multi-disciplinary modelling where the relations between properties of different disciplines such as aero-thermodynamics, structural stress analysis, life and cost analysis are defined in order to obtain optimized engine or component designs using multi-disciplinary optimization (MDO) methods [15, 17].

This thesis will be primarily focused on *cycle* (or '*system'* or *'whole engine'*) *performance modelling and simulation.*

2.4   Joule-Brayton cycle

A gas turbine converts thermal power into mechanical power using the Joule-Brayton thermodynamic cycle shown by the h-s diagram and process scheme in Figure 2.3. The nature of this cycle and how it is realized in hardware by a particular configuration of gas turbine engine components largely determines the engine performance modelling approach.
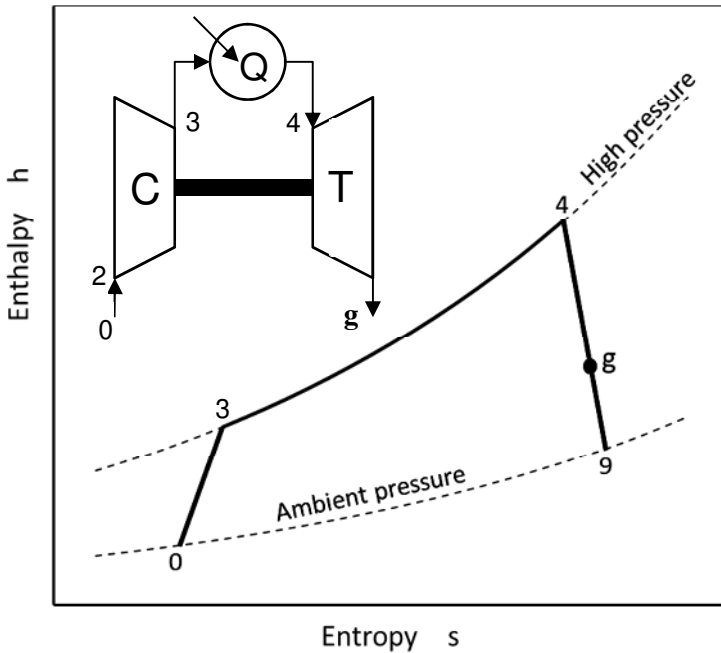
Figure 2.3 Simple Joule-Brayton cycle process scheme and h-s diagram

In Figure 2.3, station numbers 2, 3, 4, 9 and g represent the transition points of the inlet (0-2), compression (2-3), heat addition with heat flux Q (3-4) and expansion (4-9) phases of the Joule-Brayton cycle. The power generated by expansion in the turbine T from 4 to g is required to drive the compressor C. Station 'g' indicates the end point of the gas generator process. Gas turbines normally have a *gas generator* that converts the thermal power added to the cycle into 'gas power'. Gas power here is defined as the maximum mechanical power that can be obtained from expanding the hot pressurized gas exiting the gas generator at station g. This maximum is equal to the kinetic power that would be obtained after isentropic expansion of the gas at station g.

The expansion power from g to 9 can be used to generate a jet by expansion in a nozzle for aircraft propulsion, or to generate mechanical shaft power to drive a generator for example. In the latter case the expansion from g to 9 may take place in additional turbine stages.

Either an open or closed cycle may be used. With an open 'air-breathing' cycle, the heat Q can be added by internal combustion of fuel.

2.5   Gas turbine engine configurations

2.5.1   Simple configurations

In this thesis, the scope is limited to open cycle gas turbines with internal combustion. Then the gas generator consists of a compressor (C), combustor or burner (b) and turbine (T) as shown in Figure 2.4 (with station numbers corresponding to Figure 2.3). Figure 2.4a represents a turbojet engine with a diffuser shaped inlet (0-2) and an exhaust nozzle (5-8) to generate a propelling jet. Figure 2.4b shows a simple turboshaft engine with a bell mouth inlet. Depending on the application, the exhaust (5-9) in Figure 2.4b may include a diffuser to maximize expansion in the turbine.
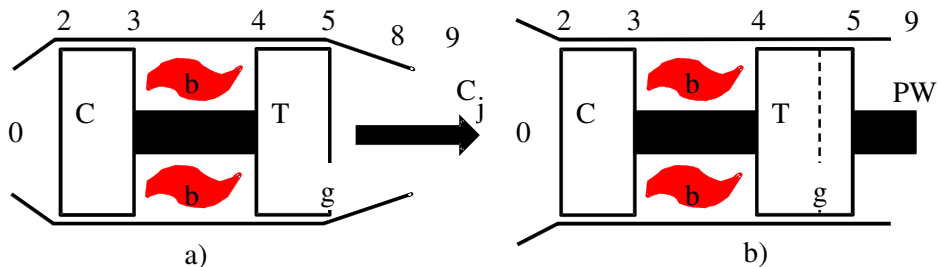
Figure 2.4 Simple turbojet (a) and turboshaft (b) configurations

The configurations in Figure 2.4 only represent simple gas turbine engine configurations. Depending on the application, many variations exist in configurations with multiple shafts, compressors, turbines, diffusers, combustors, afterburners/reheat combustors, recuperators and intercoolers.

If component design performance parameters such as inlet mass flow, pressure ratios and fuel flow are given, cycle design performance can be calculated, as will be explained in section 2.6.4. As the end of the thermodynamic process is different for the turbojet and turboshaft configurations, also the cycle calculations are different for these configurations.

2.5.2   Aircraft propulsion

For large commercial aircraft propulsion, turbofan engines are used. These configurations have multiple shafts, compressors and mixers or separate hot and

cold exhaust nozzles. Smaller aircraft often use turboprop gas turbine engines which usually comprise of a gas generator and a free power turbine. The turboprop provides both shaft power to the propeller and some (minor portion of) thrust with the exhaust nozzle jet. Finally, helicopters, except for the very small ones, use turboshaft engines which also have a gas generator and free power turbine but usually no exhaust nozzle thrust.

2.5.3   Power generation

For large scale power generation, the configuration shown in Figure 2.4b is often used, often in combined cycle configuration where the exhaust heat is used to power a Rankine (steam) cycle for example. Advanced configurations exist with multiple combustors to maximize performance and efficiency. For smaller scale power generation often 'aero derivative' turboshaft designs are used, derived from turbofan aero engines.

2.5.4   Implications to models

The h-s diagrams for these engine cycles often have additional compression, combustion, expansion and other elements. Naturally, the complexity of performance models strongly depends on the complexity of the engine configuration. In addition, the gas turbine configuration usually determines the types of boundary conditions for the simulation. With a jet engine model for example, a steady-state operating point can be calculated for a given fuel flow or turbine entry temperature. Then thrust, rotor speeds and other parameter values are calculated as simulation output, since these are determined by the thermodynamic equilibrium of the stabilized engine operating point. For a turboshaft engine however, often the output shaft speed is specified as a constant and then shaft output torque and power can be calculated for a given fuel flow.

It is often practical to specify a power output parameter as simulation input instead and calculate fuel flow required. Power output can be specified as shaft power for a turboshaft or turboprop model for example. For a turbofan engine model, thrust or fan rotor speed or some other parameter representing power setting can be specified as simulation input.

Considering the model boundary conditions (i.e. the simulation input and output parameters) is important in view of their impact on the equations that must be solved during the simulations and the meaning of the simulation results.

2.6   Modelling the gas turbine cycle

2.6.1   The gas turbine cycle versus reciprocating engine cycles

In the gas turbine engine's Joule-Brayton cycle, combustion takes place at constant pressure, and compression, combustion and expansion are continuous processes. This is the primary difference with reciprocating engine cycles in piston

engines, such as Diesel and Otto cycles. Note that these are all open cycles taking place in 'air breathing engines' as opposed to closed cycle engines such as externally fired closed cycle gas turbines, Rankine cycle engines (such as steam turbines) and Stirling engines. Closed cycle gas turbine engines are outside the scope of this thesis.

In *reciprocating* engines, compression, combustion and expansion take place intermittently on separate charges of air or gas that are repeatedly supplied to the engine by 'scavenging'. Primary parts of the process are described in prescribed volumes with valves that are opened and closed during specific phases of the cycle. Combustion or heat addition does not take place at constant pressure but (ideally) at constant volume instead. Simulation of steady-state operation (constant power and rpm) of a reciprocating engine cycle requires modelling the dynamics of the scavenging, heat release and piston movement effects. Since the compression, combustion/heat release and expansion processes are separated in time they can be simulated sequentially. Only if the exhaust gas condition somehow affects the inlet air conditions (pressure and temperature), for example via a turbocharger, an outside iteration would be required to determine the operating point. Naturally, this simulation can be easily extended to a quasi-steady-state transient simulation where engine torque is translated into engine acceleration in the form of a small stepwise increase of engine speed.

2.6.2   Gas turbine cycle dynamics

Contrary to reciprocating engines, the gas turbine cycle (for a steady-state operating point) can be modelled as a full steady-state process. Unsteady effects in turbomachinery and combustion can be ignored since these do not have specific effects on performance parameters that usually are of primary interest with an engine system simulation. However, with the continuous flow through the subsequent engine components without separation in time of compression, combustion and expansion phases such as with reciprocation engines, these processes directly affect each other. Pressure effects propagate with the speed of sound downstream the engine gas path, and also upstream unless the flow chokes at some point. Temperature effects propagate along with the gas flow, often with velocities in the order of Mach 0.5. While engine rotor speed dynamics as determined by rotor inertia or control system dynamics have time constants in the order of 1 second, propagation of gas state changes happens within fractions of a second and can usually be considered instant and not affecting system performance. A slight change in compressor pressure ratio will immediately affect turbine performance for example, which in turn will affect the compressor operating point through the shaft connection. A change in fuel flow will increase turbine inlet temperature, and therefore density which in turn will require a higher compressor pressure ratio to maintain the flow rate. Changes in operating conditions such as inlet conditions and fuel flow will cause the engine to 'find' a new 'equilibrium'

steady-state operating point. A free running gas generator with no shaft connection to the outside will accelerate or decelerate to a new steady-state rotor speed and consequently new internal pressure levels.

2.6.3   Differential equations

As a result, a gas turbine engine system performance model must be able to determine these equilibrium operating points. Equilibrium states of systems can be represented by solutions of sets of differential equations describing the relations among the system state variables. Gas turbine engine system performance characteristics depend on the characteristics of the individual components. A gas turbine system model therefore must include appropriate representations of component performance characteristics. It further must represent the relations among the components in a set of differential equations. These include the equations for conservation of mass, energy and momentum and the specific component characteristics (relations among parameters such as flow rate, rotor speed and power, pressure and temperature change etc.). The solution of the set of equations is a number of parameter values uniquely defining the engine operating point (all other parameters depend on these). This way, the model represents the overall engine system performance as a function of operating conditions such as inlet pressure and -temperature and fuel flow.

2.6.4   Design point calculations

Prior to simulating performance of a particular engine, the engine design has to be determined in terms of component configuration, design parameters and component characteristics. These may either come from engine specifications (an existing engine design) or from a cycle design exercise (a 'paper engine'). In general, a design point (DP) simulation must be performed calculating the design point operating point parameters from a set of given DP operating conditions and cycle design parameters such as mass flows, pressure ratios and turbine entry temperatures for example. The DP calculation result determines the particular engine design and size and represents the *cycle reference point CRP* for subsequent off-design (OD) operating point calculations[1].

The DP calculation may be merely a straight forward calculation from inlet to exhaust without iteration if all primary cycle parameters are given. A good example is the DP calculation for a single spool turbojet with given inlet conditions and mass

---

[1] Note that a model DP is not necessarily the same as a design point in an engine development project where often multiple design points are defined with specific performance requirements. For a turbofan engine for example design points may be defined for take-off, end-of-climb and cruise. The single DP (i.e. CRP) for a cycle model may be any of these or even a separate one if desired. Usually though, the model DP corresponds to a high power operating point such as take-off power at ISA conditions for a turbofan engine.

flow, cycle pressure ratio, fuel flow and component efficiencies and losses (see example in section 11.4, Figure 11.3). Often iterations are involved if specific relations are required between cycle parameters such as air flow rate and pressure ratio and/or power output. Typically, during series of DP calculations with cycle parameters varying over specific ranges ('parameter sweeps'), the engine size is adapting to the cycle parameter variations. For example, turbine nozzle through-flow area will have to adapt to variations in volume flow that result from the variations in cycle parameters if mass flow is to be kept constant. Often, the objective of DP iterations is optimization of particular performance parameters such as specific fuel consumption, thrust or power.

2.6.5 Off-design calculations

An off-design (OD) calculation involves iteration towards an operating point of a fixed given engine design. The result is a set of cycle parameters satisfying all conservation equations for operating conditions (see section 5.5) deviating from the DP operating conditions. The engine design usually has been determined by an initial DP calculation. Due to the iterations, the OD calculations normally involve much more numerical processing time than the DP ones.

For *steady-state* OD point simulations, all time derivatives and time dependent terms in the equations are inactive and equal to zero.

Transient operation analysis requires a more complex form of OD simulation. By adding time derivatives to the shaft power conservation equations and specifying rotor inertia, the major transient effects on system performance can be captured accurately using a quasi-steady-state approach with steady-state component characteristics. This is a valid method since the gas dynamics effects are orders of magnitude higher in frequency bandwidth and therefore usually do not significantly affect system performance. In some cases, effects of heat transfer and mass- and energy content dynamics in the volumes become significant and then must be added to the model.

2.7   Relation to other process simulation tools

The above described methodology is specific to gas turbine and similar system simulations where both design point and off-design performance prediction is required. System models are composed of sub-models representing gas path components in which a specific compressible medium flows continuously between one or more inlets and outlets.

This is different from typical process flow sheet simulation tools (e.g. AspenONE [18], Cycle Tempo [19]) that usually cover larger systems often including gas turbine models as sub-elements, usually with limited or no off-design or transient simulation capability. A common example is a combined cycle system in which a steam cycle is used to convert gas turbine exhaust heat to additional

mechanical power. The steam cycle simulation involves processes with both compressible (steam) and incompressible media (water). The gas turbine sub-model inside the flow sheet model often requires only limited fidelity in view of the overall system model requirements.

Dedicated higher fidelity gas turbine simulation models can be coupled to flow sheet programs using modern interface technology, providing the flow sheet model with accurate gas turbine design, OD or even transient performance data repeatedly upon request. For steady state system performance analysis, a simpler approach may be used in the form of look-up tables pre-calculated by the gas turbine model. These would typically represent performance parameters as function of operating condition parameters such as ambient or inlet conditions, fuel flow, fuel properties and power setting.

Chapter 3   Research and development scope

3.1   Gas turbine performance modelling challenges

The development and efficient operation of improved and more environmentally friendly engines and engine systems require more and more sophisticated modelling and simulation tools. Efficient and accurate gas turbine engine performance prediction and analysis have proven to be essential for further improvements relative to today's state of the art. The 'law of diminishing returns' means the performance improvement potential left in today's engine designs is often in detailed design adaptations whose effects can only be efficiently analysed using accurate models. Examples are detailed cycle models used to optimize system performance by analysing effects of small component design changes, and CFD simulations generating 3-D optimized turbomachinery blade geometries (curved in all directions). Consequently, for system performance simulation there is a challenge in improving the following aspects:

3.1.1   Physical modelling

The methodology of 0-D modelling of the basic thermodynamic processes in gas turbines is well known. [9, 13]. In 0-D models, the averaging of gas properties at flow cross sections in the gas path implies limitations in terms of model fidelity. However, for accurate simulations, many small and secondary effects must be captured, requiring specific extensions, sometimes in the form of 1-D or even multi-dimensional sub-models. Moreover, analysis of detailed phenomena and particular effects requires new innovative modelling elements embedded in the system model. An important example is adaptive modelling in order to establish relations between performance and engine component condition.

3.1.2   Numerical methods

The numerical methods to model *whole engine* 0-D gas turbine DP and OD operation can be implemented in code for a particular engine fairly straightforward. However the very non-linear nature of gas turbine performance characteristics requires specific attention to the numerical methods to mitigate the consequent numerical instabilities. An important factor here originates from the component maps (especially of compressors), that often show very non-linear behaviour. Sometimes the maps have limited accuracy or even discontinuities severely hindering numerical iteration stability and convergence.

3.1.3   Generic components

Instead of repeatedly implementing models in computer code for every new engine it is more efficient to invest in generic methods to speed up the modelling and simulation work that will have to be done many times for different engines and applications. Advanced software engineering technologies are required to work towards a fully generic and flexible gas turbine modelling environment.

3.1.4   User interface

The user interface is an essential element for the effectiveness and efficiency of the performance analysis work. This means the user must have the best overview possible of his model configuration, data and also simulation results. He must be able to produce advanced graphical presentations of the results that clearly show relations among parameters. In addition, error reporting and debugging options must be added to provide clues why simulations get stuck, errors occur or other unexpected results emerge. With a poor or limited interface, the user becomes prone to hidden errors compromising results and may well miss valuable analysis results and insights.

In larger engine research and development organizations, many different models are used and many types of simulations run. In order to maintain an overview of the rapidly accumulating model and result data, model configuration- and case management functionality becomes important, enabling the user to rapidly get back to existing model configurations and simulation cases.

3.1.5   External interfaces

There is an increasing need to couple gas turbine models with other models in order to simulate performance of larger systems. Examples are combined cycle installations or aircraft models including detailed engine performance sub-models. Also, models from different disciplines can be coupled to represent interaction between engine performance and other aspects such as structural loads or noise aspects for example. This is usually done for multi-disciplinary optimization purposes. Also, high fidelity multi-dimensional CFD models can be coupled to a gas turbine system simulation in order to predict interaction between detailed aerodynamics in some location (e.g. a compressor stage) and system performance.

As a consequence, efficient external interfaces are required including data export and import options (for example performance deck tables), local interfaces transforming 0-D averaged gas properties to profiles for multi-dimensional CFD models and interfaces to structural load (FEM) models. In addition, Application Programming Interfaces (API's) may be required to control gas turbine model simulations with another simulation tools. An example would be Matlab® running an aircraft model that obtains propulsion system performance data from a separate engine model via API calls.

3.2   Objectives

Already during the 1980s, at both Delft University of Technology (DUT) and Dutch National Aerospace Laboratory NLR a need for accurate cycle performance simulation of a variety of gas turbine engines emerged. Aircraft engine performance analysis using tests became expensive and was limited by OEM restrictions on adding instrumentation. Flexible generic tools for gas turbine system simulation were not available. DYNGEN [20] was available but very instable and limited in terms of engine configuration flexibility. This prompted the start of collaborative efforts by NLR and DUT to develop generic tools suitable to simulate performance of different types of gas turbine engines. Over the years and with the increasing user community many new requirements emerged related to applications such as adaptive modelling for diagnostics and test analysis, real-time simulation and industrial gas turbine simulation applications. Complex cycles including recuperated and intercooled cycles, engines with complex multiple shaft arrangements, various gas turbine sub-systems and loads such as propellers also had to be covered (also for these, there were no generic simulation tools). Most recent requirements include configuration and case management functions and detailed modelling of micro-turbine specific aspects.

The main objective of the research and development work described in this thesis is to meet these requirements and to develop a gas turbine system simulation environment that

1. enables accurate modelling of the physical processes that determine gas turbine system performance characteristics,

2. represents the thermo- and aerodynamic processes in the components using 0-D or 1-D sub-models with sufficient fidelity to predict their effects on system performance,

3. includes consistent representation of the energy and mechanical power transformations among components,

4. enables accurate prediction of effects of design parameter- and operating condition variations on steady state and transient performance,

5. employs the optimal mathematical representation of the aero-thermodynamic processes in the gas turbine components in terms of fidelity, accuracy and computing power limitations,

6. employs mathematical models that can be implemented in a modern programming language.

Additional requirements must be met to assure sufficient usability, software maintainability and extendibility over a long period. These include

7. a user-friendly user interface,

8. flexibility to model any gas turbine configuration using a user configurable component stacking concept,

9. flexibility to easily extend the functionality to improve fidelity, new applications and effects and to couple the models with other modelling environments,

10. a configuration and case management functionality to efficiently manage model- and simulation result data.

Chapter 4   Outline of this thesis

This thesis describes a synthesis of the gas turbine system performance modelling and simulation work focused on the objectives described in Chapter 3. This includes the research required to find the optimal mathematical representation of the aero-thermodynamic processes in the gas turbine components in terms of fidelity, accuracy and computing power limitations.

The work has been performed at DUT and NLR during the period from 1996 to 2014 where GSP has evolved from a FORTRAN based derivative of the NASA public DYNGEN code [20] to today's GSP version 11 for the Microsoft Windows[®] platform. As such, the thesis may serve as baseline for further modelling development work inside or outside GSP and also as a guide to using GSP for new performance analysis problems. The work described in the thesis is divided in three major parts:

PART I   INTRODUCTION

The material already discussed in this part, including historical background, an overview of gas turbine performance simulation methods and applications, research and development scope and objectives.

PART II   MODEL DEVELOPMENT

In PART II the model development work and results are described. Several chapters are based on publications. Most publication content however is distributed over multiple chapters with some irrelevant parts omitted.

Chapter 5 gives an introduction with an overview of modelling methods for whole engine system steady-state and transient simulation and a global description of the GSP gas turbine modelling methodology

In Chapter 6 GSP's object oriented design architecture providing the flexibility, code maintainability and extendibility is described.

In Chapter 7 the gas model is described including the chemical equilibrium and gas composition calculations for prediction of emissions and fuel type effects.

Chapter 8 describes the scheduler and limiter numerical model elements for controlling simulation boundary conditions.

Chapter 9 describes the modelling of thermal effects.

The GSP object oriented graphical user interface is described in Chapter 10. Different model configurations run cases can be stored in a GSP project and inheritance is used to rapidly derive adapted model configurations and run cases.

Chapter 11 describes the internal processes in a GSP simulation session, including the subsequent steps from model creation to running the simulation itself.

A description of the numerical initialisation setting up the NDEs and of the Newton-Raphson iteration itself is given using the example of a simple turbojet model. This chapter is valuable for the more advanced users and also developers of GSP who need to understand the numeric internals.

Chapter 12 describes the generic Adaptive Modelling (AM) capability added to GSP for gas path analysis diagnostics and test analysis applications.

In Chapter 13 the TERTS real-time transient simulation tool is described, derived from GSP and implemented in Matlab®.

Finally, an outlook into the future of GSP development is given in Chapter 14.

PART III APPLICATIONS

In PART III a number of applications are described, demonstrating GSP's capabilities and also showing best practices for users. Most chapters are based on publications.

Chapter 15 provides an introduction and overview of application areas.

Chapter 16 gives a number of application examples developed for demonstration purposes only. The *lift fan driven by a turbofan* example is quite complex due to the addition of a special custom component representing a clutch. Simulations of engine transient response to lift fan clutch engagement and disengagement are demonstrated.

Chapter 17 describes the application of the AM (adaptive modelling) capability for gas path analysis, engine diagnostics and condition monitoring.

Chapter 18 describes the use of GSP for development of a 3kW recuperated micro turbine for CHP applications, including conceptual design, performance improvement and loss effect analysis and analysis of scale effects.

Chapter 19 briefly describes a number of GSP applications focused on novel cycles, including a parallel twin spool micro turbine with a single shared combustor, a rotating combustor micro turbine concept, a modern heavy duty gas turbine with a second reheat combustor and a multi-fuel hybrid turbofan engine, also with a second reheat combustor.

Chapter 20 lists a number of other applications and references to publications. These application areas include exhaust emission prediction, alternative fuels, lifing, in-flight gas path analysis and reverse engineering of component map data.

Important to note is that much of the model development work described in PART II has been performed following new requirements that emerged from performance analysis problems and challenges in the application cases described in PART III.

An epilogue is added with concluding remarks, an overview of the development of GSP seen from the developer's perspective and an outlook into the future.

PART II

MODEL DEVELOPMENT

Chapter 5   Gas turbine performance models

5.1   Model types

There are several types of gas turbine performance simulation models, ranging from simple manual cycle calculation procedures to high-fidelity 3-D CFD models. As already described in section 2.3, simpler models usually represent engine performance using a parametric (0-D) model in which only averaged gas states are defined at 'stations' in a thermodynamic cycle or process. These gas states are related by equations (or algorithms in case of a computer model). A 0-D simulation of a pure steady-state operating point or process allows for the assumption that all time derivatives are equal to zero. Adding time as a factor for a transient simulation usually adds significant complexity to the model, especially if also high fidelity is required such as in unsteady CFD simulations for example. Other model types are real-time models. These are used for (flight) simulators, hardware-in-the loop simulations and similar applications. Depending on the application, model fidelity can be traded for costs and execution speed, such as in training simulators for example which do not have an R&D purpose and therefore usually no interest in internal details of the gas turbine cycle process.

Multi-dimensional CFD models usually limit themselves to only a specific part of the engine or engine components in the gas path. Objectives often are to analyse local effects such as rotor-stator interactions that affect average component performance, results of which can be represented in a 0-D system model (by component maps) to predict effects on system performance. Limiting detailed CFD simulation to local areas saves time (setting up CFD models) and computing power as explained in section 1.4. Also, computation power requirements for simulating the whole engine in high fidelity 3-D cannot be met by today's computers [9].

Advanced simulation tools employ various forms of the 'zooming' concept (see section 2.3) where local CFD models run simultaneously with system models, communicating boundary condition changes over special interfaces [3, 16].

5.2   Whole-engine system models

The models that represent whole-engine (or 'engine system') performance usually are 0-D *component stacking models*. These models represent the gas turbine engine by component models 'stacked' in a particular arrangement corresponding to the engine configuration. The component models represent gas path components such as inlets, compressors, fans, turbines, ducts and exhaust nozzles that pass air or gas to one another through their gas path connections. See Figure 5.1 for an example of a simple GSP turbojet component model configuration.
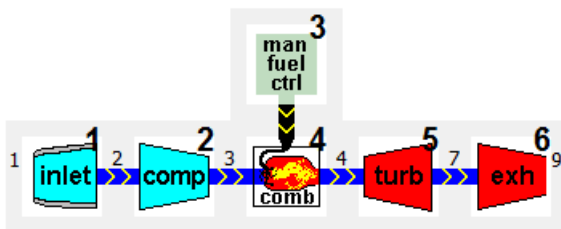
Figure 5.1 GSP turbojet model configuration

In this section, the general approach followed in GSP is described which can be considered fairly common for all component stacking models. An excellent overview of gas turbine system performance methods and the generally accepted numerical methodology is given in [9, 13].

5.3   Engine system performance representation

As with a real gas turbine, for a given operating condition (inlet conditions and fuel flow rate for example) the engine system model must 'stabilize' at a steady-state equilibrium operating point. For this steady-state point, a number of equations can be derived that must be satisfied in order for the operating point to be valid. The operating point can be represented by a set of *independent* performance parameters that are the unknown variables in the equations to be solved. The equations are based on the conservation equations for mass, energy and momentum along the gas path and include algorithms that look up values from compressor characteristics, such as compressor maps for example. Component characteristics potentially introduce strong non-linearity and in some cases discontinuity, especially in cases where the maps are inaccurate or obtained from poor or incomplete measurements.

Note that for a design point (DP) simulation, the calculation may be straight forward in simple cases, not requiring iteration (see section 2.6.4).

The number of *independent* variables is limited to the minimum set of parameters that uniquely defines the engine operating point. From these parameters all other cycle parameters can be calculated using the specific thermodynamic relations; these are the *dependent* parameters. Interesting to note is that with generic simulation tools that are not specifically developed for gas turbine engines such as PROOSIS [14], the specific relations among gas turbine cycle parameters are not explicitly used. Then the model state is often represented by an unnecessarily high number of parameters with many dependent on others through known relations. A generic simulation tool is not 'aware' it is simulating a gas turbine and consequently has to solve for a large amount of unknowns and equations (up to even a 100 where a dedicated tool such as GSP would need less than 10 for the same fidelity). This is consuming a lot of extra processing time. In addition, the solver will have to cope with an ill conditioned system of non-independent variables.

5.4   Engine system operating point

Component operating point parameters such as rotor speed and pressure ratio (for a compressor for example) depend on the engine system operating point. For off-design (OD) simulations, these usually are the unknowns, or 'state parameters' in a system of non-linear differential equations (NDEs). For DP simulations the number of NDEs usually is small or even 0 (see section 2.6.4). Depending on the type, each component model depends on a number of these state parameters. As a result, for the whole-engine system model, a set of state parameters distinctively defines the engine operating point. The equilibrium of an OD steady-state operating point then is represented by a vector of n state variable values S that is the solution of a set of n NDEs. The state variables thus are the unknowns in a set of NDEs that are composed of thermodynamic conservation laws and component performance characteristics.

Apart from the engine component characteristics, the engine operating point is depending on the operating conditions (see section 5.5).

5.5   Operating conditions

For a given engine, the operating point depends on the operating conditions. Consequently, the engine operating conditions represent the boundary conditions to be specified as simulation input to the model. Varying the operating conditions (away from the design point operating conditions) implies off-design simulation (see section 2.6.5). The following categories can be defined:

5.5.1   Power setting

The power setting is usually determined by the operator to obtain a required or desired level of power of some form depending on the application. This may be power in the form of shaft power or torque, jet engine thrust or pneumatic power if compressed air is produced. The parameter directly affecting power of the gas turbine usually is fuel flow and this also is the simplest way to specify power in a gas turbine model. In practice however, power setting is usually specified in different terms, such as:

- Turbine inlet temperature (TIT) often used to specify a maximum power condition as determined by the hot part temperature limitation.
- Turbine exit temperature or Exhaust gas temperature (EGT), used when simulating cases including control system effects. Because usually TIT cannot be measured easily due the very high temperatures, EGT is measured instead by the control system to indicate hot section temperature level (and indirectly TIT). With multi-spool engines EGT usually is measured at the exit of the gas generator or high pressure (i.e. the first) turbine or turbine stages.

- Rotor speed. This usually implies the inclusion of control schedules in the model. For a turbofan aero-engine fan rotor speed N1 is often used as primary power setting indicator in the cockpit.
- Engine pressure ratio (EPR), a typical jet engine power setting indicator similar to rotor speed N1, used in aircraft operation. EPR is generally defined as gas generator exit or exhaust pressure divided by inlet pressure.
- Shaft power or torque output, specified in cases where a turboshaft engine operating point simulation is required depending on the load. Examples are large heavy duty or helicopter gas turbines with operating points at given torque levels and rotor speeds.
- Thrust, specified in cases where a jet engine operating point simulation is required depending on required thrust. Examples include large turbofan operating points at specific thrust levels and flight conditions.

Using the above mentioned power setting parameters instead of fuel flow usually implies the addition of an equation in the model to find the unknown fuel flow that corresponds to the specified power setting value (see section 5.5.5).

5.5.2 Ambient and engine inlet and exhaust conditions

Gas turbine inlet and exhaust conditions usually depend on ambient conditions. These strongly affect engine performance, especially with aero-engine applications where static and stagnation pressures and temperatures in flight and at altitude may deviate substantially from sea level static conditions. When ambient or flight conditions are given, pressure loss models may need to be added to determine the conditions at the inlet of the first compressor ('station 2'). Alternatively, the losses can be ignored and station 2 conditions directly specified. The exhaust condition can either be the ambient static pressure or a specific engine 'back-pressure'.

In addition to pressure and temperature, inlet flow medium (or air) properties or composition may be specified. An example is the specification of the liquid water fraction in the inlet air to analyse the effect of water injection.

5.5.3 Installation effects

Installation effects may be specified in many forms. Usually they represent some extra loss associated to a particular application or installation. Examples are inlet or exhaust system pressure losses, power off-takes and compressor bleed flows.

5.5.4 Engine condition

In this thesis, engine *condition* (or 'health') is also considered an operating condition. However, other than the external boundary conditions mentioned above, it is not a real model boundary condition. Instead it directly affects the engine performance characteristics. Since it is considered an *off-design condition* similar to the other operating conditions, for practical reasons engine condition is treated as an operating condition here also.

5.5.5   Equations and operating conditions

The operating conditions used to specify the boundary conditions for the simulation may affect the set of model equations. This especially applies to power setting. For example, fuel flow can simply be an input for explicit calculation of the combustion process without having to add equations. Turbine exit temperature as the input however makes the combustor operating point relations implicit since fuel flow cannot directly be calculated from it if an enthalpy based gas model is used (with varying c_p, see section 7.2). An extra equation has to be solved satisfying conservation of energy in a relation between fuel flow and combustor exit temperature (or turbine inlet temperature TIT). In this case, since both parameters are calculated during the combustion process simulation, a local iteration procedure may be used inside the combustor model. When HP turbine rotor inlet temperature (RIT) is specified instead of TIT (and 1st stage guide vane cooling is applied), the problem moves outside the combustor and the approach described below is required with an extra equation on the system level.

If power output is specified as operating condition input, the implicit nature of the problem comes to the system level. For a given fuel flow, a cycle calculation can produce power output as a result and the reverse is not directly possible. In this case, an equation has to be added to the set of system equations (NDE's) described in section 5.9. Alternatively, a separate iteration loop outside the model may be used, but this usually is less efficient and prone to instability due to ignoring the non-linear relations with the model. The extra unknown added to the system then usually is the fuel flow. After convergence of the extended set of NDE's the fuel flow corresponding to the specified power output is found.

Many other operating conditions in terms of simulation output are used both for DP and OD simulation depending of the objectives of the analysis, including mass flows, rotor speeds, pressure ratios and, pressures and temperatures at specific engine stations.

In GSP, specification of operating conditions requiring extra equations usually means the model user has to add one of the scheduling and equation components described in section 8.2.

5.6   Conservation laws

In GSP, the following relations are used for the conservation laws:

The conservation of mass for flow through a component:

$$\frac{dM_v}{dt} = W_{in} - W_{out} \tag{5.1}$$

The relations between density, temperature, pressure, mass and component internal volume:

$$M_v = \rho . V_{comp} \tag{5.2}$$

$$\frac{dM_v}{dt} = \left(\frac{1}{RT} . \frac{dp}{dt} - \frac{p}{RT^2} . \frac{dT}{dt} \right) . V_{comp} \tag{5.3}$$

Assuming the adiabatic isentropic compression relation between dp and dT, equation (5.3) can be worked into:

$$\frac{dM_v}{dt} = \frac{V_{comp}}{\gamma RT} . \frac{dp}{dt} \tag{5.4}$$

The conservation of energy for a component:

$$\frac{dM_v}{dt} . u + M_v . \frac{du}{dt} - Q = w_{in} . h_{in} - w_{out} . h_{out} + PW_{abs} \tag{5.5}$$

Q and PW_{abs} are the heat and power absorbed by the component. Note that in a 0-D model such as GSP, for most components, equation (5.5) can only be evaluated by dividing the process in steps. Turbomachinery power for example is calculated using isentropic or polytropic efficiency from a performance map, assuming an adiabatic process without volume effects (i.e. changing mass and energy in the internal volume). This means the terms on the left in equation (5.5) are first assumed 0. Then after calculation of PW_{abs}, they are calculated for entry, exit or averaged conditions and used to correct power (as described in section 9.4.5) and component exit conditions (using equation (5.4)).

The conservation of energy for a drive shaft:

$$I . \frac{d\omega}{dt} . \omega = PW_{abs} + PW_{del} \tag{5.6}$$

The conservation of momentum for joining flows (in a mixer for example) or calculating propulsive thrust:

$$\sum (w_{in} . c_{in} + A_{in} . p_{s\,in}) + F_x = w_{out} . c_{out} + A_{out} . p_{s\,out} \tag{5.7}$$

The relations for conservation of energy for a heat transfer between the gas (g) and a heat sink (hs) element in the heat transfer and thermal network component models (see section 9.4):

$$Q_{hs} = U.A.(T_{hs} - T_g)$$
(5.8)

$$M_{hs}.c_{p_{hs}}.\frac{dT_{hs}}{dt} = \Sigma Q_{hs}$$
(5.9)

The time derivatives only are non-zero for transient simulation. As a result, the equations are reduced to fewer terms for a steady-state simulation.

5.7   Component performance models

In the component models, for given state parameter values, exit flow and gas conditions are calculated as a function of inlet conditions and sometimes other parameters such as rotor speed, heat release, bleed flows, heat transfer effects etc. The models may use both thermodynamic equations and/or empirical relations. The compressor component for example calculates exit conditions as a function of inlet conditions and compressor operating point, obtaining compressor efficiency and pressure ratio from empirical component performance *characteristics*.

5.8   Component performance characteristics

Component performance characteristics are relations among two or more component performance parameters. These relations can be defined by analytical or semi-empirical equations or experimentally determined with component tests, and presented in graphical form such as the compressor *map* in Figure 5.2.

Usually one or two properties are required to determine the state of an engine component. The turbo machinery components (e.g. compressors, turbines) have the most complex characteristics. The map in Figure 5.2 shows the relation between the 4 compressor characteristic parameters W_c, PR, N_c and η_{is}. Any two out the first 3 parameters W_c, PR, N_c determine the compressor operating point.

Dimensional analysis of turbomachinery as described in [21] and [22] shows that turbomachinery performance is described by 6 dimensionless groups. One of the groups is the ratio of specific heats γ which only significantly affects characteristics in case of large variations of gas properties. As this is not the case with open cycle gas turbines, this group is omitted, leaving five properties to define component performance:

Corrected mass flow

$$W_c = \frac{W\sqrt{\theta}}{\delta} \cdot \frac{\sqrt{\frac{R}{\gamma}}}{\sqrt{\frac{R_{std}}{\gamma_{std}}}}$$

Corrected rotor speed

$$N_c = \frac{N}{\sqrt{\theta} \cdot \sqrt{\frac{\gamma R}{\gamma_{std} R_{std}}}}$$

Pressure ratio

$$PR = \frac{p_{t_{in}}}{p_{t_{out}}}$$

Component isentropic or polytropic efficiency

$$\eta$$

Reynolds number

$$Re_D = \frac{\rho c D}{\mu}$$

with $\quad \theta = \frac{T_{t_{in}}}{T_{std}}$ and $\quad \delta = \frac{P_{t_{in}}}{P_{std}}$.

N_c and W_c are derived from true dimensionless parameters (with dimensional parameters such as diameters left out) and are proportional to blade tip Mach number and axial inlet flow Mach number respectively. With the accounting for variations of R and γ, real gas effects are included providing accurate *Mach similitude* for corrected mass flow and rotor speed. As such, rotor speed N and mass flow W are *corrected* to standard conditions T_{std} and p_{std} using the correction factors θ and δ, and standard gas properties R_{std} and γ_{std}. As a result, N_c and W_c represent the performance parameter relations independent of inlet conditions.

Often real gas effects on corrected mass flow and rotor speed are ignored and then the first two equations reduce to

Corrected mass flow

$$W_c = \frac{W\sqrt{\theta}}{\delta}$$

Corrected rotor speed

$$N_c = \frac{N}{\sqrt{\theta}}$$

In GSP, real gas effects for corrected mass flow and rotor speeds in maps are optional.

The Reynolds number *Re* makes the fifth property determining the effects of viscosity on the turbomachinery operating point. It is often omitted since it only has a relatively small effect on component performance [21]. This is due to the relatively high value of *Re* where its effects on friction become very small. Sometimes, for example at high altitude operation of aero engines were *Re* is much lower than at design conditions, the *Re* deviation is used in simple empirical correction relations for efficiency and corrected mass flow.
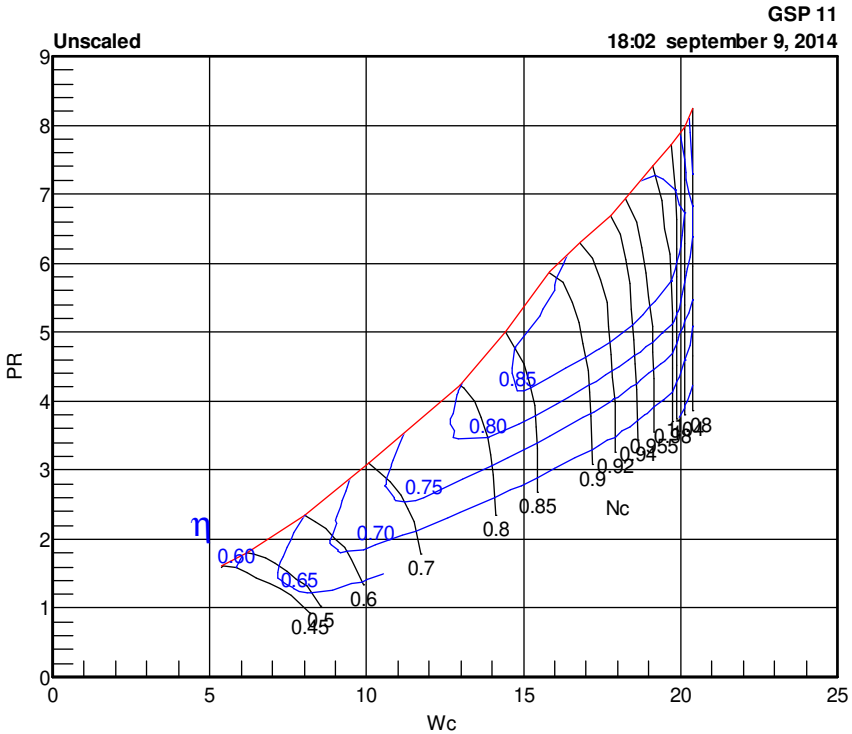
Figure 5.2 Example of a compressor map

In computer models, component characteristics usually are represented by multi-dimensional lookup tables. The component operating point is determined by one or more input parameters that are used for interpolation in the table to obtain the output parameters. In a compressor map table for example, N_c and W_c can be used to lookup *PR* and *η*. Sometimes additional 'helper' input parameters are used to avoid cases where parameters become insensitive to changes of others (causing system simulation iteration problems) such as the extra 'Beta' polar coordinate used in the MTU map format [23]. Components other than turbomachinery usually have simpler relations, such as

- a duct or inlet with a pressure loss – corrected mass flow relation lookup table for example. The operating point then can be defined by the corrected mass flow,
- a heat exchanger or recuperator with effectiveness – heat capacity rates ($W.C_p$) relations,
- a heat sink, with an empirical temperature - heat transfer relation,
- engine specific control system relations.

Often, component characteristics are used in OD simulations only. In that case, the initial DP simulation then scales the map to the DP, saving the scaling factors for subsequent OD simulations. In case a map is used for a DP simulation, often DP iterations (i.e. equations and corresponding unknowns) must be added to satisfy the conservation equations.

5.9   System performance differential equations

For a numerical solution of the set of differential equations representing the engine model, error variables are introduced. For each equation, an error variable represents the deviation from the solution and therefore the deviation from the physical relation among component states.

The choice of error variables is closely related to the choice of state variables. The desired relation between state variables and error variables is, that each error variable is sensitive to at least one state variable. A set of state variables $\bar{S}$ has to be found yielding the value 0 for the error variable e in each equation, or in vector notation:

$$\bar{E}(\bar{S}) = \bar{0} \tag{5.10}$$

The error variables (in vector $\bar{E}$) are a function of the state variables (in vector $\bar{S}$). In GSP, normalized states and errors are used, i.e. they are divided by their corresponding reference (often design point) values.

5.9.1   Solution method

The solution procedure is based on the multi-variable Newton-Raphson numerical method. Linearization of equation (5.10) in a small region around the state $\bar{S}$ yields the set of first order equations:

$$\delta\bar{E} = J.\delta\bar{S} \quad or \quad \Delta\bar{E} = J.\Delta\bar{S} \tag{5.11}$$

A set of partial derivatives of the error variables to the state variables is now determined

$$J_{i,j} = \frac{\Delta e_i}{\Delta s_j} \quad (i,j = 1 \dots n) \tag{5.12}$$

where i is the index for the error variable E and j is the index for the state $\bar{S}$. J is the *Jacobian matrix* determined by calculating $(n+1)$ times through the gas turbine model from front to rear: once with $\bar{S}$, and n times (for each element of $\bar{S}$) with a

small perturbation Δs_j of element j of $\bar{S}$, in order to determine the sensitivities $\Delta e_{1..n}$ to the change of s_j and thereby all elements $\Delta e_i / \Delta s_j$ in J.

By multiplying the left and right hand side of equation (5.11) by J^{-1}, we obtain

$$\Delta \bar{S} = J^{-1}.\Delta \bar{E} \qquad\qquad (5.13)$$

Equation (5.13) indicates how much $\bar{S}$ has to change to reduce $\bar{E}$ in a linearized area. We can now iterate towards $\bar{S}$ where $\bar{E} = 0$ by subtracting $\Delta \bar{S}$ and recalculating J^{-1} in small steps using

$$\bar{S}_{i+1} = \bar{S}_i - f.J_i^{-1} .\bar{E}_\iota \qquad\qquad i = 1, 2 ... \qquad (5.14)$$

f is a combined automatic and user controlled factor limiting the magnitude of correction steps thereby improving stability and rate of convergence. The initial $\bar{S}$ can be represented by the design operating point at the beginning of a simulation session (all elements of $\bar{S}$ equal to 1) or by the previously determined off-design operating point. The iteration continues while decreasing $\bar{S}$ until the absolute value of each element of $\bar{E}$ is smaller than a user-defined inaccuracy. To reduce calculation time, the Jacobian matrix J^{-1} is not re-calculated for every new $\bar{S}$ per step i. Instead, the same J^{-1} is used repeatedly until convergence does not meet a certain requirement anymore and then re-calculated. The convergence requirement may expressed by the sum-square of the $\bar{E}$ elements for example.

In addition, Broyden's Method [24] may be used to 'update' (instead of re-calculate) the Jacobian matrix J based on the previous iteration step to save calculation time. Broyden's method was particularly useful when computer power was still relatively low, saving time to re-calculate J^{-1}. While still an option in GSP, it is today rarely used due to the increased risk of iteration instability.

The GSP solver also contains algorithms protecting against instability and options to reduce f if oscillation or singularity of $\bar{S}$ is detected. Step size is varied automatically to jump over local extremes in $\bar{E}(\bar{S})$, to avoid the iteration from getting stuck. Oscillation is a problem preventing convergence near the solution that often occurs due to strong non-linearities in the model NDEs or 'unsmooth' maps. Both oscillation on a single state variable (a single state variable oscillating and causing errors to remain beyond the tolerance margin) and multiple state variables (e.g. two state variables intermittently jumping up and down) can be detected and automatically compensated by reducing f. f and other iteration control parameters can be manually adjusted to optimize iteration speed or prevent singularity of J in case the equation set is ill conditioned.

5.9.2   Steady-state simulation

For steady state simulation, the time derivatives in the conservation equations are all assumed zero and solving the set of equations directly provides the state vector representing a steady-state operating point. It is possible that there is no solution, which normally means the steady-state operating point cannot exist. This happens for example if one tries to simulate a sub-idle steady-state operating point of a gas turbine: in reality the engine would not be able to sustain rotor speed, decelerate and finally stop.

5.9.3   Transient simulation

For transient simulation the time derivatives in the conservation equations are integrated with the modified Euler method:

$$x_{i+1} = x_i + \Delta t. (f_e. x_i' + (1 - f_e). x_{i+1}') \tag{5.15}$$

with f_e as the Euler equation factor. For $f_e = 1$ the normal (explicit) Euler form is obtained. With $f_e < 1$, the stability and accuracy improve compared to the normal Euler method. In GSP, $f_e = 0$.

Due to the implicit nature of equation (5.15) with $f_e = 0$, x must be solved iteratively. Since the dynamic equation terms (the time derivatives in the conservation equations) are embedded in the conservation equations, equation (5.15) is solved implicitly with the Newton-Raphson method solving the error equations for every time step. Apart from the time derivatives in the conservation equations, there are transient effects on component performance not captured by the steady-state performance characteristics. This is why this type of simulation is usually referred to as 'quasi-steady state' simulation. Quasi-steady state models however still have the potential to very accurately simulate engine system simulation (i.e. within error margin of typically 1%).

5.10   The Gas turbine Simulation Program GSP

The main focus of this thesis is on the development of the Gas turbine Simulation Program GSP whole engine system modelling environment. In the next sub-sections a brief overview is given of the history of this development until today.

5.10.1 Early FORTRAN GSP versions

Model development work initially involved the early work developing GSP as it was still in FORTRAN code. Around 1986 GSP was derived from the public NASA DYNGEN code [20] by W. Bouwmans, who added significant improvements to the code structure and user interface for running on a main frame environment with command line user interface. He also added some new modelling functionality.

From there on it was further developed and used at NLR where stability and usability was enhanced. Already with the FORTRAN based GSP versions prior to version 7, elements of *object orientation* (see section 6.4) had been applied that facilitated enhanced code maintenance and user friendliness. A sort of 'manual object orientation' was applied using indexed arrays of procedures representing different gas turbine components and their data blocks. This way, the user could compose an arrangement of model components representing a particular gas turbine.

This was already a great improvement over the common practice (seen well into the 1990s) of implementing specific gas turbine performance characteristics directly in the code, thereby requiring a recompilation for almost every change in engine characteristics. The latter practice has led to a large legacy of gas turbine model codes that later become almost unmanageable. As a result, the generic nature of the FORTRAN based GSP had already some advanced capabilities.

In [25] an overview is given of gas turbine simulation tools and methods used at NLR including FORTRAN based GSP.

5.10.2 Modern software implementation

With the introduction of 32 bit operating systems on PC's (Windows 95) around 1995, advanced software development tools (Borland Delphi [26]) became available. These were offering optimal software flexibility and maintainability, minimizing the problems such as experienced with the old legacy codes described in section 1.5 and above. Consequently, GSP 7 was developed for the Windows platform and modularity was maximized using object orientation. Also, a separate gas model was developed that can relatively easily be adapted. A similar approach was followed with TERTS (described in Chapter 13) for real-time engine modelling for applications such as research flight-simulators.

The GSP software design methodology is described in [12] and Chapter 6.

5.10.3 GSP 7

For GSP 7, a completely new architecture including a graphical user interface concept was designed using Delphi's Object Pascal language. The FORTRAN code of the component models was translated and embedded in the new framework. Code maintainability, user interface, speed, execution costs (no tariffed mainframe) was radically enhanced. Key in this development was the application of object orientation to the GSP architecture providing ultimate flexibility for further model enhancements and extensions.

GSP 7 for Windows was the first practical object oriented gas turbine simulation tool in 1996 and became the example for several others such as [14]. From version 7 onwards, many improvements and extensions were developed (described in the following chapters) with the help of an increasing number of engineers, researchers and students. GSP became internationally recognized and now has many users.

In this thesis, the modelling methodology is described with a focus on the elements that are unique or otherwise merit attention. For general gas turbine system methodology, references are given to public literature such as [9, 13, 21].

5.10.4 GSP today

To date, significant contributions have been made to developing generic modelling methodologies with the Gas turbine Simulation Program GSP [12, 25, 27]. The objectives defined above have been successfully pursued and the major elements and results of the research and development work done at both DUT and NLR are described in this thesis.

The latest version is GSP 11 which is available from www.gspteam.com both as a free non-commercial version with limited capabilities and a full version for registered users. A user manual [28] and a technical manual [29] provide the primary information required by most users. In addition to the standard version, custom component model libraries are offered and developed with modelling methods and elements specific to customers' needs.

GSP's flexibility has proven valuable to many applications, examples of which are described in Part III of this thesis.

5.10.5 Model development publications

The next chapters are mostly derived from publications. The GSP modelling environment is described from different perspectives including aero-thermodynamic modelling methods, gas thermodynamic properties model, software architecture, model extensions to facilitate test analysis (adaptive modelling) and more. The publications are particularly focused on innovative elements in gas turbine modelling methodology.

Chapter 13 addresses the 'TERTS' real-time gas turbine engine simulation environment. TERTS has been developed using elements of GSP that were adapted in order to meet the real-time calculation speed requirements. GSP models were used to validate TERTS real-time simulation results.

Chapter 6   GSP, a generic object-oriented gas turbine simulation environment[2]

6.1   Introduction

The 'Gas turbine Simulation Program' (GSP) is a component based performance modelling environment for gas turbine engines. Both steady-state and transient simulation of any gas turbine configuration can be performed by establishing a specific arrangement of engine component models in a model window as displayed in Figure 6.1. Typical applications include design optimization studies and off-design performance simulation for analysis of effects of varying operating conditions including deterioration and effects of control system characteristics.
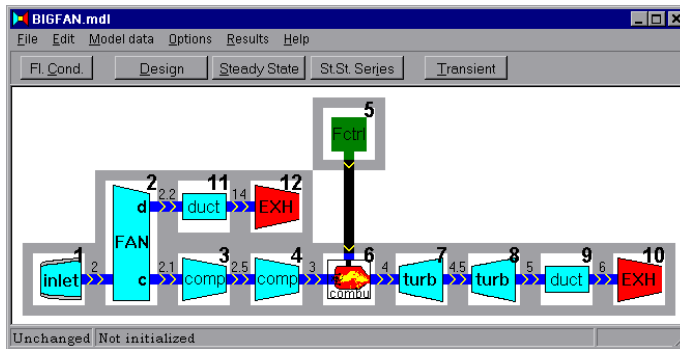
Figure 6.1 GSP model window with simple turbofan model

GSP has been developed at National Aerospace Laboratory NLR, Amsterdam.in a collaborative effort with Delft University of Technology. Since NLR is presented with a wide variety of gas turbine performance problems, simulation tools with a high degree of flexibility are required [30]. In order to minimize model development and software maintenance costs, *generic* gas turbine system simulation tools are required for new modelling tasks. Thus, GSP was developed to allow rapid adaptation to various problems rather than being dedicated to a specific task. MS-Windows® was selected as platform in view of the rapid increase in cheap available computer power, combined with the wide scale use of this operating system. GSP is implemented in the Embarcadero Delphi® object-oriented

---

[2] This chapter is based on: [12]   W. P. J. Visser and M. J. Broomhead, "GSP A generic object-oriented gas turbine simulation environment", ASME 2000-GT-0002, presented at the ASME TURBO EXPO, Munich, Germany, 2000.

development environment [26], offering excellent means to maintain and extend the program.

GSP has a user-friendly graphical *drag-and-drop interface* (see Chapter 10) with on-line help allowing quick implementation of new engine models and rapid analysis of a wide variety of problems. During continuous development, GSP has been extended and improved with new features including a chemical gas model and several advanced 0-D and 1-D component models described in the following chapters.

6.2   Overview

GSP calculates gas turbine performance, relative to a reference operating point, usually the design point. Apart from design point analysis, GSP is particularly suitable for off-design analysis. Off-design steady-state and transient performance is calculated using the customary numerical methods of defining engine system states and solving the equations for the conservation of mass, energy and momentum, see section 5.5.

An *information analysis* exercise [31] indicated that, for meeting the requirements defined in [30], a GSP gas turbine model must consist of a user-specified arrangement of components in a model window (see Figure 6.1) corresponding to the particular gas turbine configuration. A single model window must provide access to all features necessary for the engine system simulation. Component icons, drag-and-dropped and positioned on a special panel, must be able to represent any sub-system model (thereby providing GSP's flexibility). Each component model requires user specification of data such as design point data values and component maps using its own specific interface.

6.3   Architecture

GSP's power in terms of flexibility and user-friendly interface is owed to its object-oriented architecture, designed with primarily these two qualities in mind. The flexibility is to a large extent reflected in the component modelling approach. The GSP component class hierarchy is given in Figure 6.2. With efficient ways to develop or adapt component models, simulations of new gas turbine configurations with different degrees of detail and fidelity can easily be realized. More details on the architecture are given in [31].

For this approach, a generic solver was developed that is able to automatically solve and integrate the equations for any gas turbine configuration. The solver is implemented in the *engine system model* (Figure 6.3) and calculates steady-state or transient operating points for any valid configuration of components. The system model also includes code for simulating items and processes in the gas turbine which are not related to single components such as the ambient/flight conditions,

shafts transmitting torque or power between components, secondary air flows such as cooling flows or compressor bleeds and transfer functions which simulate the behaviour of sensors, control system functions etc.

6.4   Object orientation

The engine system model solver must be able to handle a set of *abstract components*, each with an undefined number of states. Different components will have different methods to add states and equations to the modelling system, depending on their specific characteristics.

Object-orientation offers an excellent mechanism for this problem. Many publications on object-oriented software design (such as [32]) show the three basic principles of object-orientation: *encapsulation*, *inheritance* and *polymorphism*. These principles offer significant potential to efficient gas turbine simulation software development.

Encapsulation enhances code maintainability and readability by concentrating all data declarations and procedures related to a particular *object class* (such as the compressor component model class in GSP) in a single code unit. *Classes* are 'types' of objects. Implementation details (i.e. code not relevant to the scope outside the object) are 'hidden', enhancing the overview over the different functional levels in the code. For example, it enables developers to change the implementation of a gas turbine component model with minimal impact on the system model. It also provides means to strictly control access to the internal component data from outside (i.e. by the system model), thereby preventing unintended data operations and leaving only relevant control methods visible to the programmer.

Inheritance is used to concentrate code common to multiple component types in *abstract* component *classes*, preventing code duplication and enhancing code maintainability. For example, the abstract 'Turbomachinery component class' in Figure 6.2 represents an *abstract* ancestor incorporating all functionality common to compressors, fans and turbines. These classes inherit this functionality from their ancestor turbomachinery component class. Thorough a-priori analysis of the modelling elements is essential for a well-designed and efficient inheritance structure.

Polymorphism is the ability of parameters to represent objects of different classes and is extensively applied in GSP. For example, the system model code has an *abstract* (*polymorph*) identifier able to represent any component in the model. During simulation, the abstract identifier is able to access the data and run the simulation procedures of the specific component class. This way, the component objects in a system model are *virtualized*.

Figure 6.2   Component inheritance architecture

6.5   Virtualisation

The GSP flexibility and user friendliness is established using 3 essential polymorphism elements in the architecture:

1. Virtual component performance simulation methods
2. Virtual component interaction with system model equations
3. Virtualized linking and interacting with adjacent or connected components

6.5.1   Virtual component performance simulation methods

Virtualization of component performance simulation procedures (*methods*) is essential for flexibility. This applies to any modelling environment for simulating systems of heterogeneous components. As described in section 6.4, the system model controls a collection of *abstract* components.

Abstract components may represent different *classes* that, once *instantiated*[3] during program execution and simulation (after loading the model from the project file) define the actual component state and behaviour, both in terms of simulation performance, user interface and other procedures.

Consequently, all component procedures used by the system (e.g. the simulation code) have been made *abstract* or *virtual* which means that they are 'known' in the abstract components but not implemented. Before instantiation, the *abstract* components only know the *class* they will have to represent. After instantiation the *abstract* or *virtual* methods will refer to the actual component class dependent code. *Abstract methods* have no implementation at all inside the owning class. *Virtual methods* are similar, but may have already some functionality implemented that applies to all inheriting classes. The abstract and virtual methods are *overridden* by the corresponding methods in the component specific classes that are to be instantiated.

6.5.2   Virtual component interaction with system model equations

The different components have different relations to the system states and equations. Some components will need states to define the operating point (e.g. a mass flow state); others need to provide information for an equation (e.g. shaft power for a power balance equation) and yet others may need both. Similar to virtual performance simulation methods described above, also abstract or virtual methods have been developed for controlling the component's relations with the system model states and equations. The abstract components in the system have abstract methods for this task. In the inherited specific component classes, states and errors are controlled in *overridden* code implementations.

6.5.3   Virtualized linking and interacting with connected components

The components are arranged by the user corresponding to a gas turbine system configuration using a drag-and-drop interface. Gas path components have gas path inlet and exit 'ports' to connect to other gas path components. This way a component can discharge its exit flow into the next component's inlet. Other connections need to be made with internal shaft and secondary airflow components. Control components have their own connectors to the control ports of components

---

[3] Instantiation is the creation of an *instance* of a particular object class, including the allocation of computer memory and initialization of parameters; for example, the creation of a compressor object that is ready to run in a simulation.

requiring control inputs. Al these relations must be established automatically during arranging of the components and assigning connections to shaft and secondary air flow numbers. If not, the GSP graphical user interface would appear useless and the user friendliness benefits lost. For all this to work consistently for all components, these processes must be virtualized using abstract methods in the abstract component classes.

6.6   Designing the component model class inheritance tree

It is up to the software architect to decide on how to build up the inheritance tree for optimal code maintainability and reusability and avoiding code duplication. Thorough information analysis is required, classifying different sets of component model data and calculation routines and algorithms for corresponding *classes* in an optimally consistent inheritance tree. Although changes can be made in the inheritance tree at a later stage, this is undesirable in view of breaking the backward compatibility of improved GSP versions with older model files. However, there is no single best solution here and different choices may be made. For example, the *Map component* class in Figure 6.2 is the ancestor of most gas path component model classes, except Nozzles and Mixers. This is because Nozzles and Mixers component models do not require lookup maps in GSP's current version. However, if maps would be used for these components also in a future version, all gas path components would become child classes of the *Map component* class. In that case however, this class would become obsolete since there is no added value in having parent classes with only single childs (and no saving on code duplication). Then all map functionality could be moved to it's parent (*Gas Path Component class*) and the *Map component* class removed. Also Fans are now childs of compressors and afterburners of combustors and this surely has benefits, but there are also arguments to make them siblings instead. When moving particular classes in the inheritance tree, or moving data or modeling code among classes, the associated user specified model data will be lost when opening old model projects. Although GSP's backward compatibility always enables opening of older project files, due to its generic XML model data storage capability, some data will have to be re-entered by the user.

6.7   Gas turbine model structure

A GSP model can be decomposed into model (data) elements and model procedures as depicted in Figure 6.3. The model elements include a series of component model *objects* configured in a particular arrangement corresponding to the gas turbine engine system to be simulated. The component model objects are *instantiated* model component *classes* (see section 6.5.1). The object's data

structure and behaviour is defined by the code declarations and implementation in the particular class.
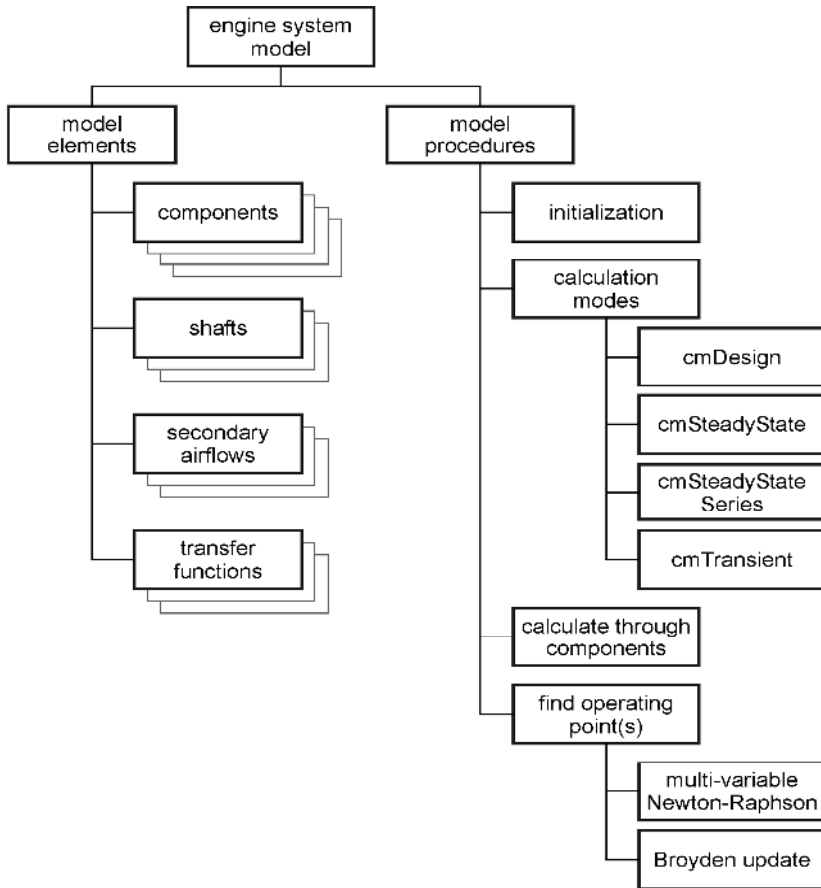
Figure 6.3   Engine system model architecture

Besides component models, also classes exist for shafts, secondary airflows and transfer functions (mostly to represent sensor dynamics) that are automatically instantiated into objects in a model depending on the user defined engine configuration component model elements.

The model procedures control the manipulation and simulation of the particular arrangement of component model objects and other model elements. This includes reading and writing model data to and from hard disk memory, initializing the model, providing a user interface for model editing (specifying component arrangement and editing component model data), selecting simulation mode and numerical iteration control options, and controlling simulation execution.

6.8   Component models

GSP component models are kept in component libraries. To the user, these are windows with component icons that can be copied onto the model panel using the drag-and-drop interface.

For many simulations the *GSP standard component libraries* are sufficient, which include gas path components such as an inlet, compressor, turbine etc. and several controls ranging from 'manual' controls, allowing the user to directly specify fuel flow or nozzle area, to components with PID (Proportional Integral Differential) control logic and customary fuel flow/burner pressure maximum acceleration and deceleration schedules. A number of primary standard components are shown in Figure 6.2. For all standard components, refer to [28].

In Chapter 8 a number of special components for scheduling parameter inputs, adding equations to the models for establishing user defined relations among specific parameters or parameter limits.

All standard gas path component models are 0-dimensional (processes inside components are not described along a spatial parameter). There are a number of special component models derived (inherited) from the standard ones with 1-D properties: The GSP 1-D multi-reactor combustor model includes the calculation of semi 1-dimensional combustion kinetics and requires detailed geometrical combustor data, see [33] and Chapter 7. In section 9.6 a 1-D model for recuperator thermal effects is described.

The gas path component models include volume dynamics and heat soakage effects. Component models employing tabular maps (such as compressors and turbines) include deterioration, variable geometry and Reynolds effects. For the turbine, there is a blade cooling model.

Compressor and turbine map table format is compatible with the GasTurb [34] map format. This allows the use of the SmoothC/SmoothT programs [23] for editing and smoothing maps.

6.9   Custom component models

Sometimes, components are required with application specific properties and characteristics. This may be when detailed analysis into specific phenomena inside a gas turbine is required or for analysing the effects of specific engine control logic (e.g. non-linear, multivariable control, specific Full Authority Digital Electronic Control or 'FADEC'). These custom components require code development outside the GSP development scope, but compliant to the GSP component class rule set. They are provided in separate custom libraries that can be runtime-loaded by GSP as Borland Programming Library (BPL) executable files, which are similar to DLLs (Dynamic Link Libraries). With limited understanding of GSP's architecture, custom components can easily be derived from the standard component models

using object inheritance (see section 6.3). Many custom components have been developed and applied. The 'Lift-fan driven by afterburning turbofan engine' application described in section 16.3 gives a good example of custom component development.

6.10   Conclusions

The GSP gas turbine simulation environment is a tool for gas turbine system performance analysis. The architecture has proven its benefits in terms of flexibility with a variety of applications. The object orientation has facilitated numerous rapid developments of application specific custom components requiring relatively small effort.

GSP's standard modelling capabilities are continuously being extended based on user demands. Many of those are rather specific and result in custom components inheriting from the standard ones, in order to prevent unnecessary complexity (too many features) in the standard and generic components.

Chapter 7   Gas properties, combustion and emission formation models[4]

7.1   Introduction

With the increasing attention to gas turbine exhaust gas pollution, a need has emerged to predict gas turbine exhaust gas emission levels at varying operating conditions. On the manufacturers side, the processes in the combustor are modelled in detail (i.e. with CFD) in order to develop new technologies to reduce emissions, such as LPP and RQL combustion [35]. On the operational side, there is interest in how to minimize emissions by optimizing operating conditions such as engine condition, aircraft flight procedures, fuel type and water/steam injection. The latter two variables mainly relate to ground based gas turbines, using natural gas, hydrogen or fuel obtained from gasification of coal or bio-mass. However, it must be noted that liquefied natural gas and hydrogen fuels for aircraft are being considered [36].

Several R&D programs have been directed at more accurate assessment of gas turbine exhaust gas emissions and their effects on the environment, using test-bed and in-flight measurements [37] and prediction with models. For developing accurate models to predict emissions at deviating operating conditions, accurate measurement methods are required for validation.

An effective approach to analyse operating condition effects on emissions is to integrate emission models in gas turbine performance models like the Gas turbine Simulation Program GSP. A lot of work has already been done modelling the processes in the combustor in order to predict the major exhaust gas emissions NO_x, CO, UHC and smoke, ranging from simple relations between engine performance parameters and emission levels (0-dim parametric models [38, 39] to complex CFD computations [40]. Especially the more simple, often empirical, models require some sort of calibration to a reference condition before they can be used for sensitivity analysis, so they can be referred to as "off-design" or "ratio" models [41]. For accurate direct prediction of emissions without any reference data, CFD calculations will be required. It must be noted that best results with combustion CFD modelling still are suffering from relatively large uncertainty.

Ratio models can easily be implemented in an engine performance model in order to provide a tool to directly relate operating conditions (via combustor

---

[4] This chapter is based on: [33]   W. P. J. Visser and S. C. A. Kluiters, "Modeling the Effects of Operating Conditions and Alternative Fuels on Gas Turbine Performance and Emissions", RTO-MP-14, presented at the RTO-AVT symposium on "Gas Turbine Engine Combustion, Emissions and Alternative Fuels", Lisbon, Portugal, 1998.

operating condition) to emission levels. However, the potential of the single equation ratio models to analyse a large variety of effects is very limited.

In order to obtain better insight in effects of using other fuels, deviating air properties, water injection etc. a more detailed model is required. Yet, integration of CFD computations in GSP was not considered feasible due to the disproportional complexity and computing power requirement of CFD in relation to the 0-dimensional GSP model.

A compromise between the CFD models and the simple empirical models are multi-reactor models, which apply a limited degree of spatial differentiation inside the combustor. Multi-reactor models usually include separate flow and chemical models and offer a means to calculate a number of intermediate temperatures along the combustion process such as primary and dilution zone temperatures.

The simplest *combustor flow models* employ "well-stirred" reactors, assuming immediate mixing of separate user defined reactant flows. Explicit modelling of the distribution of cooling flows and the mixing processes involves a significant increase in complexity (e.g. multi-dimensional models).

Simple *chemical models* assume complete combustion in each reactor (no dissociation). Higher fidelity is obtained when calculating chemical equilibrium and best 1-dimensional detail is obtained when calculating chemical kinetics [42, 43].

A considerable number of publications suggest the value of multi-reactor models for prediction of especially NO_x emissions [42, 44]. These models include detailed fuel and gas composition data and NO_x formation kinetics.

This approach was considered as the best trade-off between model fidelity, complexity and computing power requirements, and has been employed in the work described below. An important presumption was that the model would primarily be used to calculate deviations of emissions from predefined reference values at reference engine conditions.

7.2   Gas model

A first improvement necessary to be able to model the combustion process in GSP in more detail is a gas model including detailed accounting of gas composition, and the implementation of the equations for chemical equilibrium to calculate dissociation effects and effects of evaporation of injected water. This, combined with a detailed specification of fuel composition provides a means to calculate effects of fuel and gas composition and water or steam injection on gas turbine performance.

The resulting gas model is now used throughout the entire GSP engine cycle calculation and currently includes the following species: CO_2, CO, O_2, Ar, H_2O(gas), H_2O(liquid), H_2, CH_4, C_2H_6, C_2H_4, C_3H_8, C_4H_{10}, O, H, OH, NO, N_2O, N_2.

For the gas path stations outside the combustor components, chemical equilibrium is calculated for the CO_2-CO-O_2-H_2O-H_2 system:

$$2CO_2 \leftrightarrow 2CO + O_2 \qquad (7.1)$$

$$2H_2O \leftrightarrow 2H_2 + O_2 \qquad (7.2)$$

For water, also the vapour-liquid equilibrium is calculated.

In the combustor, a more detailed gas model is used, calculating equilibrium for CO_2, CO, O_2, O, H_2O, H_2, H, OH, NO, N_2O, N_2. Because of the (usually) high combustion temperatures all water is assumed to be vaporized.

7.2.1   Determination of the equilibrium composition

An efficient algorithm was developed to calculate the equilibrium using the equilibrium constants method [45, 46] thereby avoiding explicit solution of the Gibb's equations like in the NASA CEA program [47, 48]. For typical cycle simulations involving large numbers of engine operating points, this meant a substantial reduction in computation time.

As explained more extensively in the GSP Technical Manual [29] a system of five or (for combustion) more equations has to be solved to find the unknown fractions of the equilibrium composition at a given temperature. Solving this system is achieved by guessing one fraction and then calculating the other fractions for this guess. A new value for the O_2-fraction results from the other fractions again. The deviation between the new value and the guess is used to iteratively find the correct value for the guessed fraction and therefore the correct equilibrium composition. The guessed fraction must be a non-zero fraction and this makes the O_2-fraction suitable for this purpose, Since the calculation is required inside many iteration loops in GSP, an efficient algorithm has been developed for rapid convergence towards equilibrium. However, because of the limited precision of the numerical calculations on a computer, this will give problems if the O_2-fractions becomes smaller than about 10^{-15}. Normally, this will not be a problem, because this only happens in (very) rich mixtures and lower temperature in combustion chambers. However, within combustors fuel-rich zones can be present. Usually, the equivalence ratios corresponding to O_2-fractions lower than 10^{-15} are above (approximately) 1.7. This means that except for special cases with extreme rich mixtures, the equilibrium composition can usually be found.

7.3 Combustion heat release model

The combustion process is simulated assuming instantaneous attainment of chemical equilibrium. This can be justified by the fact that hydrocarbon reactions generally are rapid (see [49] and 48]) and therefore the error in the heat release prediction will be negligible in most cases.

For the combustion reaction and chemical equilibrium calculation, formation and reactant enthalpies must be calculated for both the combustion products and all reactants entering the combustor including the fuel. The *reactant enthalpy* is the enthalpy change, required to heat or cool the reactant to the chemical reference temperature 293.15 K. *The formation enthalpy* is the internal enthalpy level corresponding to a specific chemical composition. During a chemical reaction, the change in the sum of formation enthalpies of the begin- and end products, corresponds to the *reaction enthalpy* or, for combustion, heat release.

The conservation of energy then dictates that the sum of reactants and formation enthalpies remains the same as shown in the next equations:

$$h_{reactant_{in}} + \Delta h_{reaction} = h_{reactant_{out}} \tag{7.3}$$

$$with \ \ \Delta h_{reaction} = h_{formation_{in}} - h_{formation_{out}} \tag{7.4}$$

or

$$h_{reactant_{in}} + h_{formation_{in}} = h_{reactant_{out}} + h_{formation_{out}} \tag{7.5}$$

The enthalpies in the equations above are all functions of gas composition and temperature. As the combustion product composition is at chemical equilibrium which is depending on the combustor exit temperature, an iterative procedure is required. The equilibrium composition is repeatedly calculated as a function of the varying exit temperature. The result is a combustor exit composition and temperature at chemical equilibrium, also meeting the equations above.

The combustion process is simulated as adiabatic. Heat transfer and volume dynamics effects (see 5.6) are calculated afterwards and applied to the exit conditions followed by a final chemical equilibrium calculation.

Combustion efficiency can be specified to represent losses that reduce the heat release. These may represent heat loss and/or losses due to unburnt fuel.

For more details, see the GSP Technical Manual [29] (chapters 4 and 5).

7.4 Fuel specification

In order to maintain proper bookkeeping of the composition downstream of the combustor, specification of fuel composition is required. Therefore GSP was extended with a flexible user interface module for fuel properties with either:

- specification of hydrogen/carbon (H/C) ratio and heating value or
- explicit specification of composition.

For fuels with many different species like jet fuels, specification of all specie concentrations is unpractical and the H/C ratio option is used with the heating value specified. The resulting combustion gas composition is calculated using the H/C ratio and heating value is converted to formation enthalpy. Liquid fuels are represented by the properties of $C_{12}H_{23}$.as in the NASA CEA program [47, 48] with an enthalpy polynomial for methane for the specific heat c_p (for the reactant enthalpy calculation). This polynomial is converted by a factor 12 for the difference in mole mass.

For fuels with a limited number of species, the composition can be specified explicitly (per specie) and the heat release can directly be calculated from the heat of reaction (changes in formation enthalpies) and the enthalpies of the reactants, using the NASA CEA program data. This option enables the user to specify exotic fuels such as those generated with bio-mass gasification and allows for detailed analysis of effects of alternative fuels on performance and emissions, taking the effects of deviations in combustion gas properties fully into account.

Other fuel properties to be specified include pressure and temperature and data to calculate fuel pump compression power.

The two methods can also be mixed. For this purpose the 'virtual' $C_xH_yO_z$ specie has been added to the gas model species set described in section 7.2. A fuel can be specified using a number of fractions for specific species plus a residual $C_xH_yO_z$ fraction of hydrocarbons with unknown composition but known H/C and O/C ratios, specific heat c_p (i.e. the assumed average value between fuel temperature and chemical reference temperature 293.15 K) and formation enthalpy.

As a result, reactant and formation enthalpies, required for the combustion heat release and exit conditions calculation, can be obtained by summation of the values of the $C_xH_yO_z$ fraction and the other species.

The fuel properties described above are also used to calculated fuel compression power for either liquid or gaseous fuels. Especially in the case of gaseous, high-temperature and/or low calorific value gas fuels (such as bio gas in some cases), fuel compression power levels become substantial.

7.5   Emission formation model

For gas turbine performance and emission prediction, the combustor model must accurately calculate both heat release and combustor exit gas composition. Heat release is calculated assuming the combustion ends with chemical equilibrium, as calculated with the gas model described in the previous sections.

If the chemical equilibrium equations include terms for NO_x, CO, and UHC emission species, then the equilibrium emission values in a combustion process can

be calculated. However, due to the rapid variation of gas conditions (temperatures etc.) in the combustion process, the formation of these emissions is highly subject to chemical kinetics, resulting in emissions significantly deviating from equilibrium, like "frozen" NO_x after rapid cooling of hot gas. Thus, the model should include kinetics to calculate the emission reaction rates.

In order to account for different reaction rates in the different combustor zones, the multi-reactor approach is required.

7.5.1 Generic multi-reactor model

A generic reactor model was developed, allowing the calculation of both chemical equilibrium and kinetics between reactor entry and exit (see Figure 7.1).
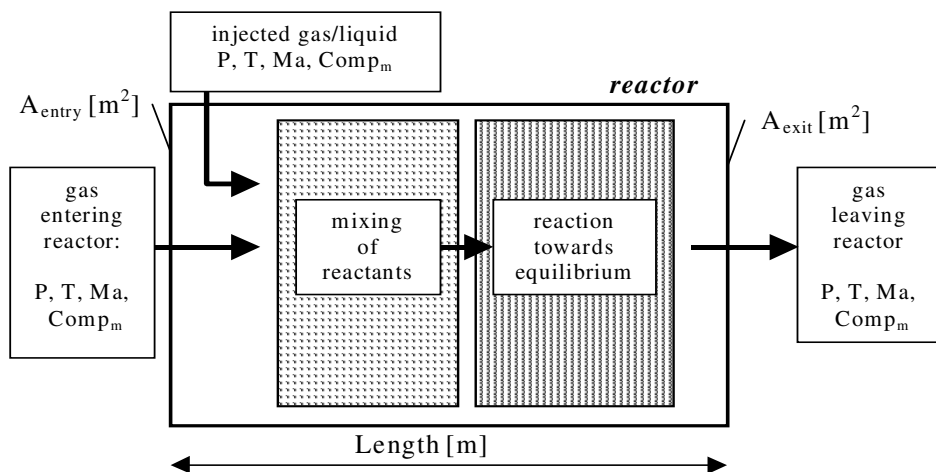
Figure 7.1 Generic 1-dim reactor model

The reactor receives the gas from a preceding reactor and exits into a successive reactor (the first and the last reactors will usually connect to compressor discharge and turbine entry instead, as shown in Figure 7.2). A second reactor entry permits the injection of fuel, cooling air, gas, water or other matter to be mixed or combusted in the reactor.

By stacking a number of reactors, a multi-reactor model is obtained simulating the subsequent processes of flow-dividing, combustion, secondary combustion, mixing and, if desired, the injection of other species such as water or steam.

Any number of reactors, each with specific characteristics, can be specified. For a conventional combustor the first reactor would represent the primary combustion zone followed by one or two reactors for the secondary or tertiary (mixing) zones (as in the two-reactor model shown in Figure 7.2). For detailed analysis of emissions or for multi-stage combustors, more reactors can be added.
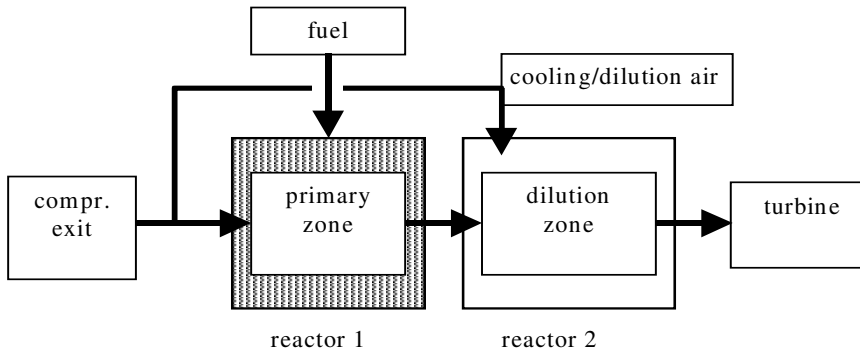
Figure 7.2 Simple multi-reactor configuration for a conventional combustor

7.5.2 Flow model

The flow model represents the distribution of the flows over the different reactors defined for the combustor. Mixing is assumed to occur instantaneously (i.e. *well-stirred reactors*). The detailed combustor data necessary to determine flow distribution often are hard to obtain. For a fixed operating point of a conventional combustor model, a reasonable estimate can be made of the portion of total compressor air flow entering the primary combustion zone (i.e. the first reactor), which determines the primary zone equivalence ratio. However, to predict how this ratio will change with changes in power setting or other operating conditions is difficult and requires advanced experimental methods or CFD models. It has therefore been decided to use fixed user defined ratios in GSP at this stage. Future research will be directed at an attempt to find relatively simple 1-dim models for this effect using parametric models of the aerodynamics of the cooling flows (e.g. using equations suggested by [50]).

The limitation of user defined fixed flow ratios implies that validity of the model may well degrade with large deviations from the reference operating point.

7.5.3 Emission formation kinetics

For the exact determination of the combustor exit composition and the emission fractions, the instant equilibrium model cannot be used. This is demonstrated in [51] where application of kinetic schemes were compared with an equilibrium model, showing significant differences.

Emission calculations

The formation of all four emissions of interest (NO_x, CO, UHC and Smoke) is modelled using the same generic approach, assuming two separate mechanisms. The first mechanism is "prompt" emission formation in a flame in an infinitely short time. The second mechanism is the subsequent change in emission concentrations due to chemical reactions during the flow through the successive reactors. This way

of modelling reaction kinetics (the *kinetic scheme*) implies the integration of reaction rates, calculated at the reactor intersections. The reaction rates are calculated depending on the type of emission.

Kinetic schemes

An approach was chosen using average reaction rates at the reactor entry and exit planes. By (trapezium rule) integration of these rates across the reactors, a 1-dim kinetics model is obtained.

For a number of species, relations between reaction rate, gas composition and conditions can be derived. With known gas conditions, flow rates at the reactor intersections and reactor lengths, reactor residence times can be calculated and used for integration.

The kinetic scheme reaction rates are functions of temperature and concentrations of species (including radicals) participating in the reaction. Kinetics of radical formation are neglected and equilibrium radical concentrations are assumed. Due to the rapid radical reaction rates relative to residence times in the combustion zones of interest, this is expected to be a good approximation.

Heat release is assumed not to be affected by emission formation itself. Normally, this is a good approximation because exhaust gas emission concentrations are very low.

The generic reactor model algorithm allows easy implementation and adaptation of equations for reaction rates of any specie. For the current multi-reactor model, kinetics calculations are only applied to the emission species NO_x, CO, C_xH_y and Soot (smoke). All other species are assumed to correspond with the chemical equilibrium composition.

Overall emission concentrations result from integration over the reactors.

7.5.4 NO_x

A NO_x prediction method is used similar to the methods described in [42, 52, 53] and extended with extra chemical reactions and equations. NO_x concentration is defined as the sum of NO and NO_2. NO_2, if existent, easily reacts to NO at high temperatures. In the flame zone, a portion of NO_2 may remain as a result of sudden chilling [46, 54]. In a combustor dilution zone, NO_2 may also be formed due to a shift of the equilibrium towards NO_2. However, in most cases, the portion of NO_2 is relatively small. Therefore, the sum of NO and NO_2 concentrations is represented by a single NO concentration in the chemical and kinetics models.

N_2O concentration is calculated as an intermediate specie in the NO formation reactions. At the end of the combustor N_2O is only present in very small (calculated equilibrium) concentrations.

All four significant NO_x formation pathways are modelled: prompt, fuel and thermal NO_x and formation via N_2O. Fuel and prompt NO_x formation is assumed instantaneous in the flame zone because both mechanisms are very rapid and

involve radicals that are only present in the main fuel reaction zone. This is consistent with the assumption that the combustion process reaches equilibrium instantaneously (see section 7.5.3).

Prompt NO$_x$

An equation for the prompt NO$_x$ mole fraction is used suggested by [55]

$$[NO]_{prompt} = X_{CH} f(\phi) \sqrt{p} [NO]_{eq.stoich} \tag{7.6}$$

where: X_{CH} = mole fraction of hydrocarbon species in fuel,
         $f(\phi)$ = a function of equivalence ratio ϕ (see Figure 7.3),
         p = static pressure (bar),
         $[NO]_{eq.stoich}$ = stoichiometric equilibrium NO fraction.
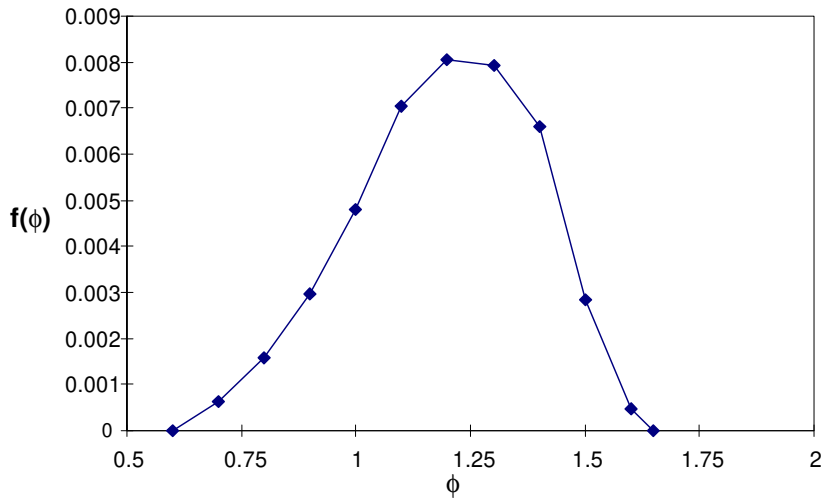
Figure 7.3   Prompt NO$_x$ factor function

The empirical equation predicts prompt NO$_x$ formation at combustion of hydrocarbon fuels according to the following reactions:

$$C_2 + N_2 \rightarrow CN + CN \tag{7.7}$$

$$C_2H + N_2 \rightarrow HCN + CN \tag{7.8}$$

$$CH + N_2 \rightarrow HCN + N \tag{7.9}$$

$$CH_2 + N_2 \rightarrow HCN + NH \tag{7.10}$$

The radicals formed by reactions (7.7) through (7.10) may subsequently oxidize to NO_x.

Prompt NO_x formation via the Zeldovich mechanism with super-equilibrium O and OH radical fractions and the N_2O mechanism is neglected. This is a good approximation because in flames, super-equilibrium O and OH fractions are usually only present at temperatures too low for the Zeldovich mechanism [54].

The contribution of the N_2O mechanism to prompt NO_x formation is also neglected because it only becomes significant at conditions where total NO_x emissions are very low [46]. An empirical function f(ϕ) (Figure 7.3) is determined using measurement data described in [56] and assumes negligible prompt NO_x formation at equivalence ratios below 0.6 and above 1.65.

Fuel NO_x

Fuel NO_x formation is specified with the *conversion fraction*, i.e. the fraction of total fuel bound nitrogen that is actually converted to NO_x. [46] and [57] indicate that the conversion fraction seems independent of the way nitrogen is chemically bound in the fuel, but it strongly depends on the combustion environment (e.g. equivalence ratio and fuel composition). Experiments by [57-60] indicate large differences in conversion fractions depending on many different factors. It was therefore decided to apply a user specified conversion fraction for the model at this stage. The fraction of fuel-bound nitrogen in the fuel is also user-specified.

Thermal NO_x

For both the thermal and N_2O mechanisms, a reaction scheme is used to derive an equation for NO formation rate, required for integration across the subsequent reactors. Thermal NO_x formation rate is predicted according to the extended Zeldovich mechanism:

$$N_2 + O \leftrightarrow NO + N \tag{7.11}$$

$$N + O_2 \leftrightarrow NO + O \tag{7.12}$$

$$N + OH \leftrightarrow NO + H \tag{7.13}$$

N_2O mechanism

For the N_2O mechanism's contribution to the NO_x formation rate the following reactions are included:

$$N_2O + M \leftrightarrow N_2 + O + M \tag{7.14}$$

$$N_2O + O \leftrightarrow N_2 + O_2 \tag{7.15}$$

$$N_2O + O \leftrightarrow NO + NO \tag{7.16}$$

$$N_2O + H \leftrightarrow N_2 + OH \tag{7.17}$$

$$N_2O + H \leftrightarrow NO + NH \tag{7.18}$$

$$N_2O + CO \leftrightarrow NO + NCO \tag{7.19}$$
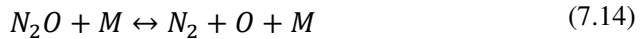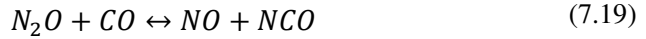
In reaction (7.14, M is a non-reacting collision partner (also called third-body specie) for N_2O. It is only important at low pressures, where the reaction behaves like a second order reaction while at pressures higher than 10 bar it behaves like a first-order reaction, so that M is omitted. Between the high-pressure and low-pressure case, there is a gradual change between first order and second order reaction, described by the so-called Lindemann fall-off rate [46]. For simplicity this gradual fall-off is ignored here. N2 is assumed to be the collision partner.

The NO_x formation rate equation is derived similarly to [53] with slightly different reaction mechanisms. All the species are assumed to be in equilibrium, except for NO, N_2O and N.

One-way equilibrium reaction rates [52] represent the forward and backward reaction rates of reactions (7.11) through (7.19) when equilibrium is assumed. For reaction r, with on the left of the reaction equation, n species with concentrations $[X_1]$ to $[X_n]$, the (one way) equilibrium reaction rate is:

$$R_r = k_f \prod_{i=1}^{i=n} [X_i]_{eq} \tag{7.20}$$

k_f is the *forward* specific reaction rate constant (Arrhenius law):

$$k = AT^B e^{-\frac{E_a}{RT}} \tag{7.21}$$

A, B are constants, E_a is the activation energy and R is the gas constant. The equilibrium reaction rate R_r can also be calculated using the concentrations on the *right* of the equation and the *backward* specific reaction rate constant. As described above, the reaction rate $R_{7.14}$ for reaction (7.14) depends on the pressure level.

The factors α, β and γ are defined to represent the deviation from equilibrium of the *actual* NO, N and N_2O concentrations at a time t during integration:

$$\alpha = \frac{[NO]}{[NO]_{eq}} \tag{7.22}$$

$$\beta = \frac{[N]}{[N]_{eq}} \tag{7.23}$$

$$\gamma = \frac{[N_2O]}{[N_2O]_{eq}} \tag{7.24}$$

From the above equations and the equilibrium reaction rates for equations 7.11 through 7.19 the following equations for the reaction rates can be derived:

$$\begin{aligned}
\frac{d[NO]}{dt} &= R_{7.11} + \beta(R_{7.12} + R_{7.13}) + \gamma(2R_{7.16} + R_{7.18} + R_{7.19}) \\
&\quad - \alpha(\beta R_{7.11} + R_{7.12} + R_{7.13} + 2\alpha R_{7.16} + R_{7.18} + R_{7.19})
\end{aligned} \tag{7.25}$$

$$\frac{d[N]}{dt} = R_{7.11} + \alpha(R_{7.12} + R_{7.13}) - \beta(\alpha R_{7.11} + R_{7.12} + R_{7.13}) \tag{7.26}$$

$$\begin{aligned}
\frac{d[N_2O]}{dt} &= R_{7.14} + R_{7.15} + R_{7.17} + \alpha(\alpha R_{7.16} + R_{7.18} + R_{7.19}) \\
&\quad - \gamma(R_{7.14} + R_{7.15} + R_{7.16} + R_{7.17} + R_{7.18} + R_{7.19})
\end{aligned} \tag{7.27}$$

The N and N_2O concentrations may well assumed to be in steady state [44, 61]. With this assumption, the left-hand sides of equations (7.26) and (7.27) are zero, and β and γ become functions of α and the relevant one-way equilibrium reaction rates. After substitution of β and γ in equation (7.25), the following equation is found for the NO formation rate:

$$\frac{d[NO]}{dt} = 2\left(1 - \alpha^2\right) * \left\{ \frac{R_{7.11}}{1 + \alpha \dfrac{R_{7.11}}{R_{7.12} + R_{7.13}}} + \frac{R_{7.16} + \dfrac{R_{7.18} + R_{7.19}}{2(1+\alpha)}\left(1 + \dfrac{\alpha R_{7.16}}{R_{7.14} + R_{7.15} + R_{7.17}}\right)}{1 + \dfrac{R_{7.16} + R_{7.18} + R_{7.19}}{R_{7.14} + R_{7.15} + R_{7.17}}} \right\} \tag{7.28}$$

Equation (7.28) can directly be used in the integration in the reactor model. The one-way equilibrium reaction rates can directly be calculated from gas conditions and equilibrium composition, and α results from the actual NO concentration as calculated in the previous integration step.

The first term between the curly brackets represents thermal NO_x formation, while the second term relates to the N_2O mechanism.

Because the one-way equilibrium reaction rates can be calculated using either the forward or backward reaction, the number of equilibrium concentrations to be calculated can be limited to only the NO and N_2O equilibrium concentrations.

7.5.5   CO

For the carbon monoxide emission calculation, the assumption is made that during combustion, fuel first reacts to all CO and water. After this initial and instantaneous step, CO further reacts to CO_2 depending on reaction rates calculated in the reactor models. This approach is based on the fact that oxidation to CO is very rapid relative to oxidation from CO to CO_2, [49, 51, 62]. The reaction scheme is used for CO emission calculation only and does not affect heat release. Also the CO formation rate still depends on equilibrium temperature level.

The reaction to CO_2 is assumed to take place according to the dominant mechanism at CO oxidation [62, 63]:

$$CO + OH \leftrightarrow CO_2 + H \tag{7.29}$$

[64] proposes the following equation for the rate of carbon monoxide oxidation assuming H and OH equilibrium concentrations and a separate conservation of carbon atoms for this mechanism:

$$\frac{d[CO]}{dt} = -k_{29f}[OH]_{eq} * \left\{ 1 + \frac{[CO]_{eq}}{[CO_2]_{eq}} \right\} ([CO] - [CO]_{eq}) \tag{7.30}$$

In Equation (7.30) k_{29f} is the specific forward reaction rate constant of equation (7.29). It represents the effect of rapid reaction towards equilibrium CO concentrations at relatively high temperatures and also to simulate the effect of frozen high CO concentrations due to sudden quenching. In the latter case, the reaction rate constant will suddenly decrease to a very low value, thereby preventing further rapid CO oxidation. The equation is integrated across the combustion chamber reactors similar to the method for NO_x.

7.5.6 UHC

To predict the emission levels of unburned hydrocarbons, reaction rates are integrated starting at an initial concentration corresponding with the fuel flow entering the reactor. Two different reactions are used. Jet-A fuel may well be represented by $C_{12}H_{23}$ [47, 48] which initially reacts according to:

$$2C_{12}H_{23} + 12O_2 \leftrightarrow 24CO + 23H_2 \tag{7.31}$$
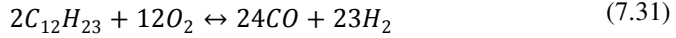
Other jet and diesel fuels are assumed to react according to this reaction also. In [65], the following equation is proposed for the rate of this reaction:

$$\frac{d[C_{12}H_{23}]}{dt} = -10^{11.5}\left(\frac{p}{p_0}\right)^{-0.815} * e^{\left(-\frac{12200}{T}\right)}\left[\frac{9T}{10^4} - \frac{1}{2}\right]\sqrt{[C_{12}H_{23}]}[O_2] \tag{7.32}$$

For natural gas and other hydrocarbon gas fuels, the flow of hydrocarbons entering the combustion chamber is converted to a concentration of methane assuming that the molar mass of the hydrocarbons is the same as the methane molar mass. The burning rate of methane is taken from [63]:

$$\frac{d[CH_4]}{dt} = -10^{10.2}e^{\left(-\frac{48400}{RT}\right)}[CH_4]^{0.7}[O_2]^{0.8} \tag{7.33}$$

The UHC level is found by integrating either equation (7.32 or (7.33 depending on the fuel type.

7.5.7 Smoke

The smoke emission model is based on a number of properties described by [66]. It appears that the soot formed in flames only weakly depends on the conditions where it is formed. For example, the soot formation is hardly affected by the type of flame (premixed or diffusion). Soot primarily contains carbon, although also hydrogen and oxygen can be present. Concerning structure, soot particles are roughly spherical and grouped together in a "necklace-like" fashion. The smoke model again utilizes the assumption of instantaneous formation followed by subsequent oxidation according to the kinetics mechanism in the generic reactors. The formation model is derived from an empirical equation taken from [39] predicting both formation and oxidation. The equation's term for oxidation is omitted resulting in the following equation for formation:

$$S = 0.0145 \cdot \frac{\phi \cdot FAR_{stoich} \, p_3^2}{W_{ox} T} \left(18 - H\right)^{1.5} \tag{7.34}$$

p_3 = burner pressure [kPa], W_{ox} = oxidant mass flow [kg/s], T reaction end temperature [K], H = fuel hydrogen mass [%]. The term for fuel air ratio is replaced by the equivalence ratio multiplied with the stoichiometric fuel air ratio. This results in a more generic representation of the fuel air ratio relative to a stoichiometric mixture and allows for oxidants and fuels other than pure air and jet fuel.

Equation (7.34) is based on measurements in diffusion flame combustion chambers and because the soot formation process is relatively poorly understood, it can only be roughly predicted with this equation.

The soot oxidation process is much better understood and can be modelled using equations for the overall specific surface reaction rate developed by [67]:

$$\omega = 12x \left[\frac{k_A p_{O_2}}{1 + k_Z p_{O_2}} \right] + k_B p_{O_2} \left(1 - x\right) \tag{7.35}$$

with:
$$x = \frac{1}{1 + \dfrac{k_T}{p_{O_2} k_B}} \tag{7.36}$$

$$k_A = 20 \, e^{\left(-\frac{30}{RT}\right)} \tag{7.37}$$

$$k_B = 4.46 \cdot 10^{-3} \, e^{\left(-\frac{15.2}{RT}\right)} \tag{7.38}$$

$$k_T = 1.51 \cdot 10^5 \, e^{\left(-\frac{97}{RT}\right)} \tag{7.39}$$

$$k_Z = 213 \, e^{\left(\frac{4.1}{RT}\right)} \tag{7.40}$$

ω in equation (7.35) is specific surface oxidation rate [g/cm^2/s], p_{O2} is partial pressure [atm] of O_2. For validation and explanation of these semi-empirical equations refer to [66].

The smoke calculation procedure is as follows. First, the smoke (mass) formation calculated with equation (7.34) is converted into a number of spherical smoke particles per unit of combustion gas. This number depends on a user specified initial radius of the spheres, which usually should be around 40 nm. The smoke particles are then oxidized in the subsequent reactors. The smoke surface oxidation rate is calculated using equation (7.35). Applying a constant average soot density of 1800 (kg/m^3), this surface oxidation rate is converted into a rate of radius change. At the end of the combustion chamber the number of spherical particles and their radii are used to find the "particulate mass loading" (for the smoke number). In the case where new particles are emitted in subsequent combustion stages (e.g. in multi-stage combustors), particles with different radii would exist. In that case, a weighted averaged radius is used to continue calculation.

7.6   Considerations for building a model

For application of GSP's new combustor model to predict emissions the following issues need to be considered:

- In general, it is best to use the model corresponding to GSP's general way of use: i.e. as a sensitivity analysis tool instead of a direct prediction tool. Accurate analysis can be made of effects of a large variety of operating conditions on emission levels.

- For off-design analysis, reference emission data are required as well as combustor data.

- The emission model can be tuned to the reference data using unknowns like geometric reactor data (determining residence times), flow distribution factors and a number of other parameters depending on the emission type.

- At this stage, flow distribution is specified with constant factors. Until a combustor operating condition dependent flow distribution model is available, the implications of this limitation must be considered for large deviations from the reference combustor flow conditions.

- CO, UHC and smoke emissions are to a large extent caused by effects that cannot be easily simulated with one-dimensional models (e.g. combustor liner cooling, atomization etc.). Therefore "temperature tuning factors" have been added to represent deviations from equilibrium temperatures at the reactor intersections. These factors will typically be used to represent effects like cooling flow films on average temperatures. Temperature factors may be set for all emission types at every reactor intersection and can also be

used for NO_x. A temperature factor of 1 indicates unmodified equilibrium temperature is used.

- Specific attention must be paid to the multi-reactor configuration. With only two reactors, the combustor processes can only be simulated to a very limited extent. With a large number of reactors, several effects like varying dilution ratios, residence times, temperatures etc. can be calculated accurately.

- Direct prediction of emissions is possible if limited (geometric) combustor data are available but will only provide reasonable estimates for NO_x emission levels.

- Accurate simulation of combustor operating conditions is required for deriving the correct relation between engine operating conditions and emissions. This requires a validated GSP thermodynamic model.

- The model may be particularly valuable for coupling detailed CFD calculation results to general gas turbine performance models. In this case combustor CFD results must be transformed into an accurately tuned GSP multi-reactor model.

7.7   Demonstration

Extensive validation of the models will be the subject of future work, requiring the acquirement and analysis of detailed gas turbine data. However, the new model has been applied to a number of gas turbine engines to demonstrate the analysis of a variety of problems.

7.7.1   Deterioration in a large turbofan engine

First, the ability of the model to predict emissions of a large turbofan engine (GE CF6-80C2) was tested. Emission data from the ICAO databank [68] and (especially low power setting) test bed measurement data were used for validation. The combustor was modelled with three reactors (Figure 7.4). The data required at the intersections are given in Table 7.1.

Initial soot radius was set to 50 nm. Little was known about the flow distribution within the combustor and therefore stoichiometric primary zone (first reactor) fuel-air ratio was assumed for the design point (sea level static rated thrust) at this stage. Limited tuning with temperature factors (see section 6) was applied for the NO_x and UHC emissions.

Figure 7.4 shows fuel-air ratio (FAR), temperature, emission concentrations and soot radius as calculated at the 4 intersections along the axial in the design (reference) operating point.
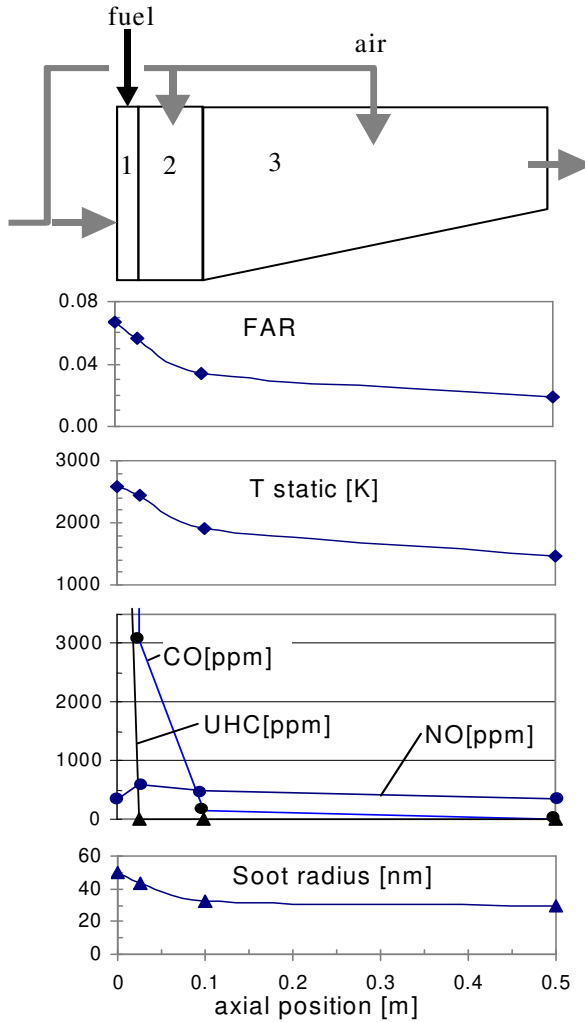
Figure 7.4   CF6-80C2 3-reactor combustor model and design point results

Table 7.1   CF6-80C2 combustor model data

Zone	Flow area (m^2)	reactor length (m)	Air inflow fraction
Flame front	0.360		0.28
Primary	0.360	0.025	0.05
Secondary	0.360	0.074	0.22
Dilution	0.1653	0.4	0.45
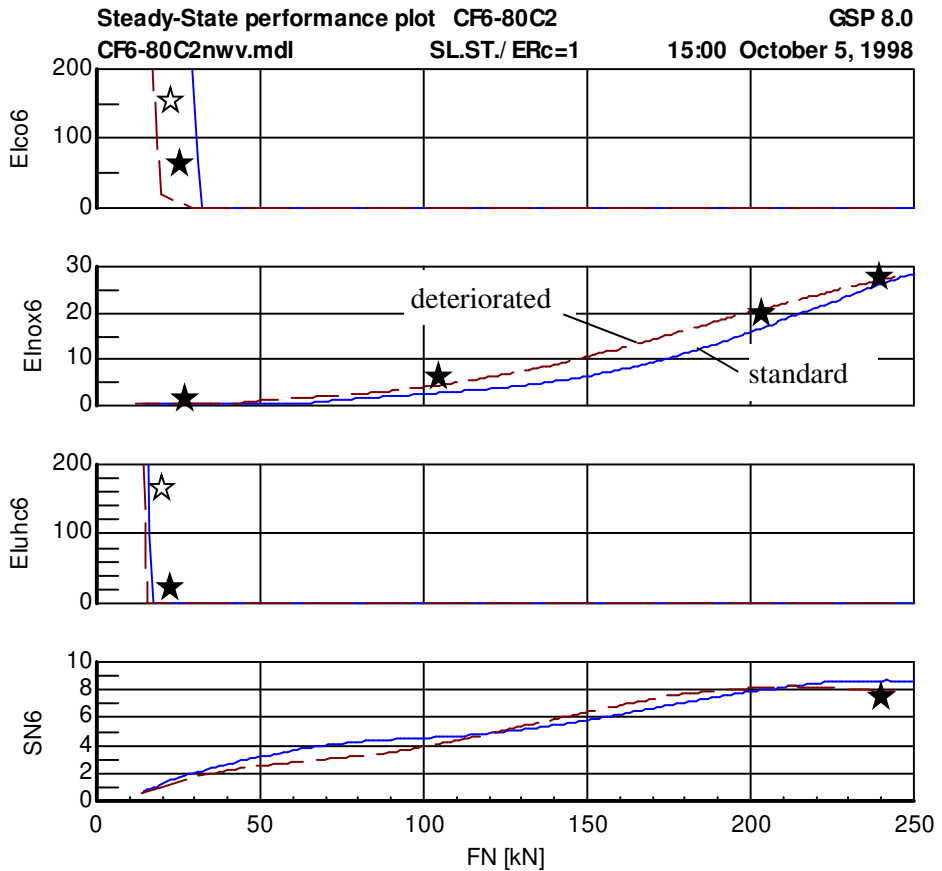
Figure 7.5   CF6-80C2 emission results and deterioration effects

In Figure 7.5 emissions calculation results are presented for standard conditions (solid curves) and for the case of a deteriorated high-pressure turbine (dashed line) to demonstrate typical use of the model. Turbine deterioration is represented by a 4% lower isentropic efficiency combined with a 2% increase in flow. The solid lines should correspond with data from the ICAO databank (solid stars) and with test-bed measured data (open stars, for the low power settings). The NO_x prediction matches the data along the operating range. UHC emissions only become significant in a narrow low power range, which is well predicted by the model. Significant CO emissions are predicted to occur at slightly higher power settings than those of the reference data. The single smoke number (SN6) value that was available could accurately be matched.

The effects of turbine deterioration are as expected: due to higher combustor temperature levels, higher NO_x and lower CO and UHC emissions. Note that at high

power setting, the NO_x increase becomes smaller due to the richer primary zone with a deteriorated turbine. Other results with rich (instead of stoichiometric) primary zone mixtures (in the design point) even indicated a fall in NO_x with turbine deterioration, resulting from the then dominant effect of decreasing combustion temperatures with equivalence ratios increasing beyond 1. Smoke number values could only be validated against the take-off power value (i.e. 7.1) from the ICAO databank.

7.7.2 Alternative fuel for an industrial gas turbine engine

A second application is the analysis of the effect of low calorific fuel (LCV, 15.6% CO_2, 8.8% CO, 24% steam, 7.4% H_2, 5.2% CH_4, 0.3% C_2H_6, 1.1% C_2H_4, 37.6% N_2) obtained from a bio-mass gasifier at Delft University of Technology [69, 70], if used for a GE-LM2500 natural gas (NG)-fuel industrial turboshaft engine.
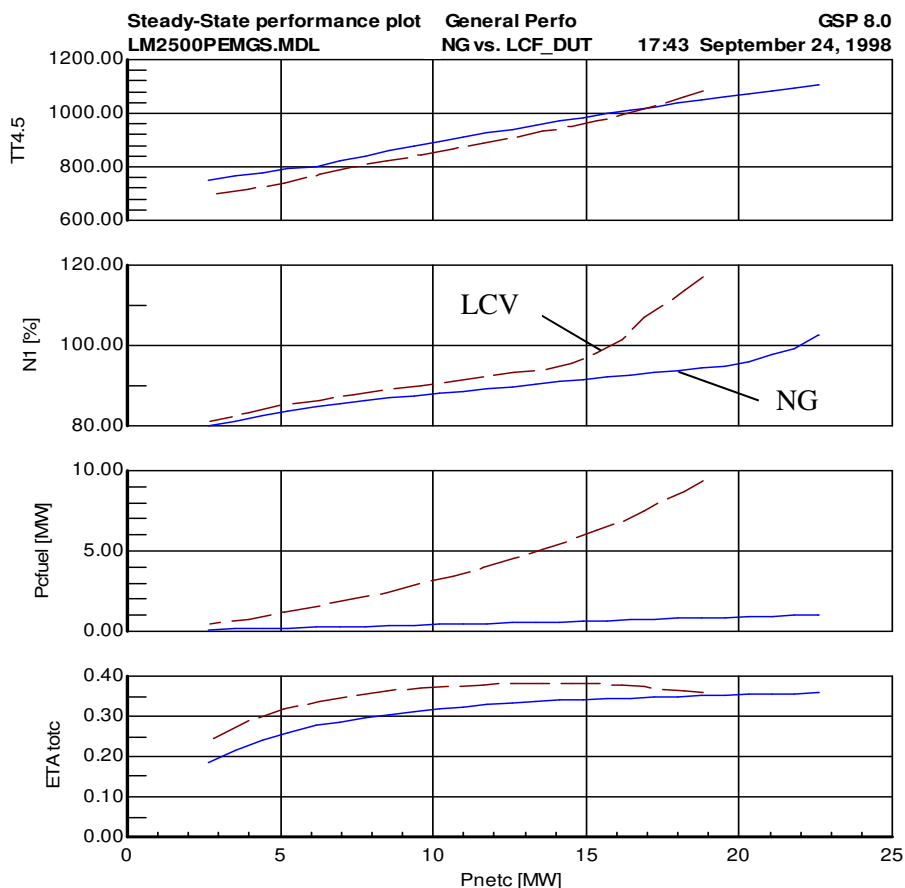
Figure 7.6   Effects of LCV fuel on LM2500 gas turbine performance
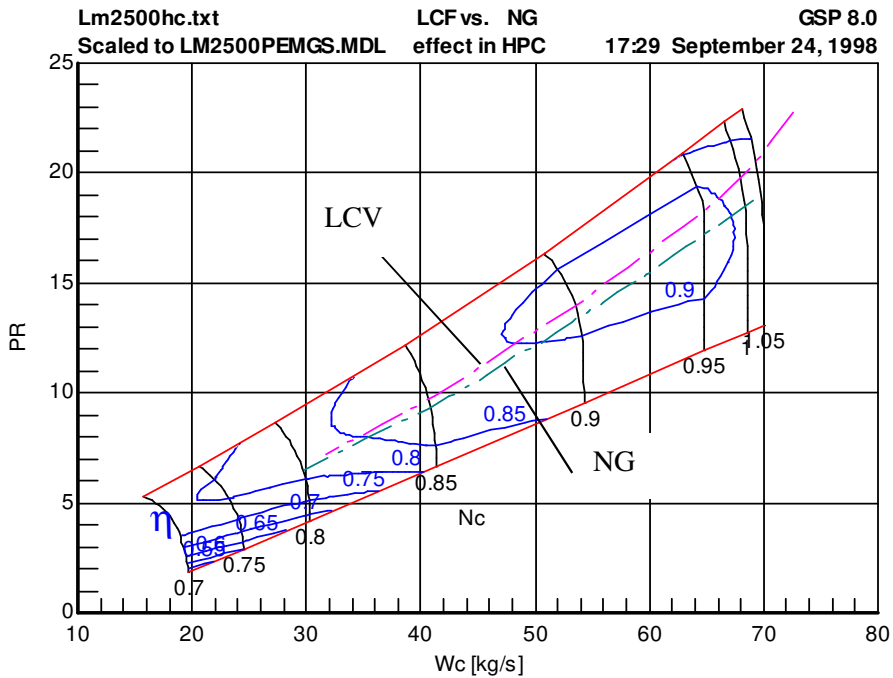
Figure 7.7 LCV vs. NG fuel HPC operating lines

The gasified fuel heating value is only about 1/10 of the NG heating value, delivery pressure is 5 bar and temperature is 1073 K. Separate compressors are assumed to compress the gasifier air and fuel gas for injection into the combustor. With the large amount of (hot) fuel gas this requires a considerable quantity of power to be taken from the power turbine drive shaft, leaving Pnetc as net power output[5]. The effect on both thermodynamic performance and emissions was calculated (LCV=dashed curves) and compared to normal operation with NG (solid curves). In Figure 7.6 the effect on performance is presented with net power output Pnetc on the X-axis. The third graph shows the high LCV fuel compression power Pcfuel. The TT4.5 power turbine entry temperature curves indicate similar turbine temperature levels for both fuels.

An important outcome is that nominal power cannot be obtained without exceeding the compressor speed (N1) limit. This is due to the mismatch between compressor and HP turbine power resulting from the large fuel mass flow injected into the combustor. Unless compressor load is increased (e.g. by taking compressor bleed air to feed to the gasifier) or major hardware modifications are applied

---

[5] This case may not represent an optimal configuration but only serves to demonstrate the potential of the model.

(turbine flow capacity), lower net power output must be accepted. It should be noted that with a fixed power turbine (i.e. a single shaft engine) this problem will not occur; but then stall-margin problems are likely to emerge instead. Total efficiency (ETAtotc, corrected for required fuel compression power) shows favourable values at partial power levels, but this may well have to be corrected with extra power required for the gasifier.

Figure 7.8   LCV vs. NG fuel exhaust gas emissions

A major concern will be how the compressor operating line will be affected. Figure 7.7 shows the expected shift towards the surge line, possibly resulting in implications with regard to (turbine) hardware modifications.

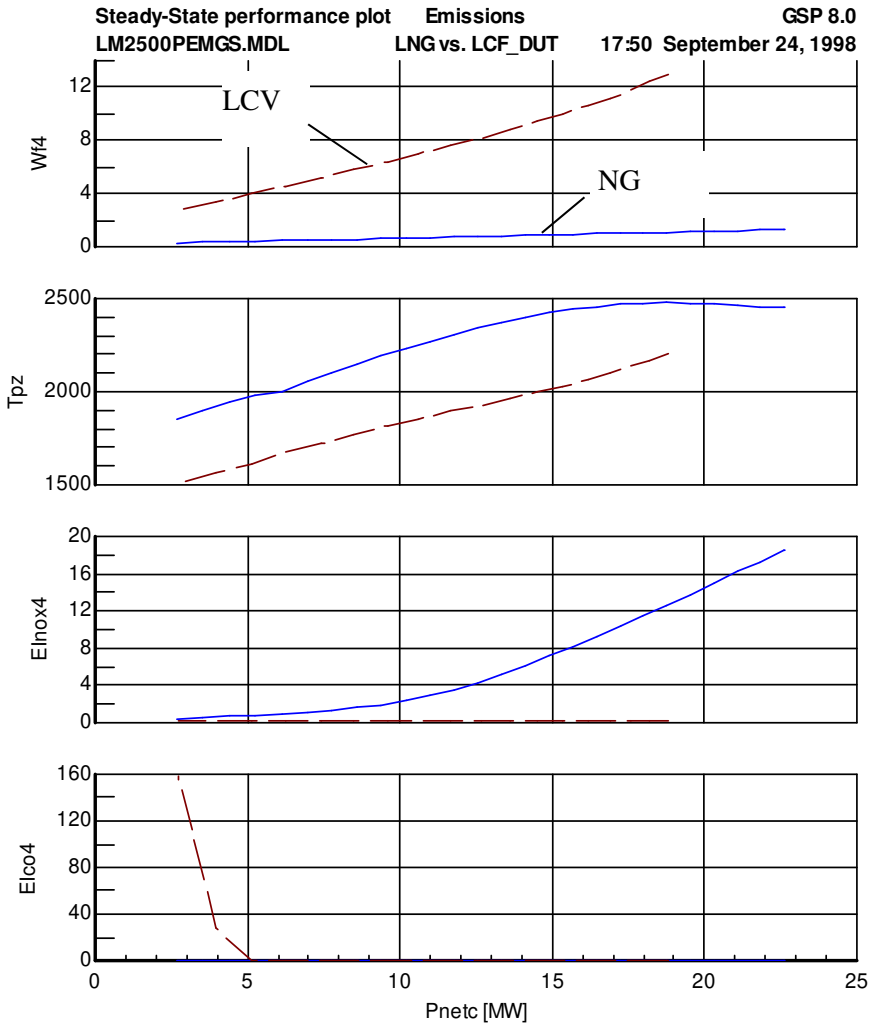Finally, the effects on emission levels are predicted using the multi-reactor emission model with similar characteristics as those of the above-mentioned CF6-80C2 model, assuming similar global combustor geometry.

The top graph in Figure 7.8 shows the large LCV fuel mass flow Wf4 (to be multiplied with the EI indices for total emission output by mass). The next graph shows the much lower primary zone temperature T_{pz}, causing virtually no (thermal) NO_x emission with LCV at equal power levels (as compared to NG fuel, 3rd graph in Figure 7.8).

The lower T_{pz} values with LCV fuel are due to the large portions of N_2, CO_2 and H_2O in the LCV fuel "cooling" the combustion process, resulting in a low adiabatic flame temperature. Finally, the high CO emission at low power (4th graph in Figure 7.8), only with LCV, is due to the low CO reaction rate at lower temperatures.

7.8   Conclusions

With the chemical gas model including gas composition calculation on all engine stations GSP is able to accurately predict effects of alternative fuels on performance and emissions.

The new multi-reactor combustor model is a generic structure in which 1-dim kinetic models can be implemented for formation of various species including the major exhaust gas emissions.

For NO_x, CO, UHC and Smoke, models have been developed for instantaneous formation in the flame zone and subsequent formation or reaction according to multi-reactor kinetics schemes.

It should be noted that in general these models are best used as sensitivity analysis tools, i.e. to calculate effects on performance and emission parameters relative to reference values.

A useful application of the new gas model has been demonstrated in the analysis of the effect of low calorific gas from a bio-mass gasifier on various performance parameters and emissions. This type of performance analysis may well be used to support decisions concerning engine hardware modifications.

The emission models have also been demonstrated on a large turbofan engine. The results corresponded with measured emission data and with expected operating condition effects on emissions. With the NO_x model best accuracy was obtained. The accuracy of particularly the CO, UHC and Smoke formation models may be improved by adapting the multi-reactor model to allow for modelling of effects such as film cooling and other effects not covered by a one-dimensional model. In particular, a flow distribution model depending on a variety of conditions in the

combustor must be developed to allow for large deviations from the reference conditions.

More work needs to be done to validate results using detailed combustor data of a variety of engines and operating conditions. The generic set-up of the model allows easy implementation of improved emission models.

Interesting future applications include performance analysis of LH_2 and NG fuelled aero-engines and a variety of alternative fuel solutions for land based gas turbines.

Chapter 8   Schedulers and limiters

8.1   Introduction

GSP version 11 was developed following extensive customer requirements for enhancing usability, flexibility and extensibility for control over the equations and model and simulation results data management. In this chapter, an overview of the new functionalities is given, including the numerical and software implementation and architecture approach. For details, refer to the GSP User and Technical manuals [28, 29].

8.2   Scheduling equations

In section 5.5 it has been explained that many operating condition input parameters imply extra equations to be added to the NDE's described in section 5.9. There are many cases where this is required. For example, power setting is often specified in terms of shaft power, torque, turbofan N1 rotor speed, engine pressure ratio EPR or thrust and corresponding fuel flow has to be calculated.

The GSP Scheduling and Power Control component libraries have been developed to include components for setting relations among parameters that are automatically added as equations to the system set of NDE's. The extra equations 'force' the engine to operate at specific operating points or within specific limit schedules. The use of the scheduling components implies that other parameters need to be assigned as free states (unknown in the equations) in order to maintain a number of states equal to the number of equations. When specifying jet engine thrust as input for an OD simulation for example, usually fuel flow becomes a free state. Naturally, the free state variable must be independent and its value must affect the new equation in order to avoid a singular Jacobian matrix. It must therefore be carefully selected.

Also design point (DP) simulations may require extra equations imposing a specific relation to the model. For an engine sizing study for example, design inlet air flow can be calculated for a given design turbofan engine thrust.

The Power Control components include pre-configured equations for setting rotor speed, thrust or EPR for jet engines. More comprehensive components allow specification of complex tabular relations between a power setting input variable and user specified performance parameters schedules. There is also an afterburner control component to add an equation to relate some afterburner related parameter to the engine power setting variable.

For simulations where the control laws still need to be defined or are not available or when 'ideal control scheduling' is required, relations among several

performance parameters can be defined using the following components which are available in the GSP 'Scheduling' component library:

- 1-D Lookup Table Scheduler
- 2-D Map Scheduler
- Equation Scheduler
- Generic Schedule Control
- Limiter
- Design Point Equation Control

In the following sub section these components are described.

8.2.1 Table and equation schedule control components

The first four controllers all are able to specify relations among parameters using 1-D or 2-D tables, expressions or combinations of tables and expressions, for both design point (DP) and off-design (OD) simulations. The user has to assign a free state parameter (e.g. fuel flow) that the solver may adapt to make the engine system model match the schedule.

8.2.2 Limiter component

The Limiter component is a special component that interferes with an OD simulation, only if some user specified limit schedule has been exceeded. Here the concept of deactivating equations is required (see section 8.3). The Limiter adds an equation for the limit schedule that initially is deactivated. A power setting component input (e.g. fuel flow, or N1 rotor speed control) has to be assigned that must be used to 'throttle up or down' if necessary to stay within bounds. After an initial OD simulation has converged, a switch is set indicating whether the limit schedule (e.g. a burner pressure P3 maximum value) has been exceeded. If it has, the limit schedule equation is activated and a second simulation is performed. Now the power setting input is adapted by the solver toward the value at which the P3 limit value is exactly matched. If it has not, the second simulation can be skipped.

The Limiter component is especially useful to generate unknown schedules for control parameters that make sure limits of other parameters will not be exceeded, by specifying the other parameter's limit schedule, and making the control parameter the unknown. Subsequently a series of steady-state points is often calculated sweeping all operating envelope variables. The limiter usually will only become active in limited parts of the operating envelope.

In Figure 8.1 a common example is given of the application of the Limiter component for calculation flat rated performance of a micro turbine. The power setting is expressed in turbine exit temperature TT5, which is set to 1070 K. Ambient temperature (Tamb) is varied from -20 to 40 $^{\circ}$C. Ambient pressure is varied from (ISA standard) 101325 Pa by -200, -100, 0, +50 Pa deltas. The Limiter component limits the generator power PW_gen to a maximum of 3700 W. At lower

ambient temperatures, the TT5 setting has to be reduced in order not to exceed the 3700 W limit. Note that using TT5 as power setting variable also implies the addition of a scheduler component to schedule TT5 with fuel flow Wf_b (i.e. the addition of an equation with unknown Wf_b). Note that ETA_PW_gen is cycle efficiency based on PW_gen and PW_gen includes a small electric loss.
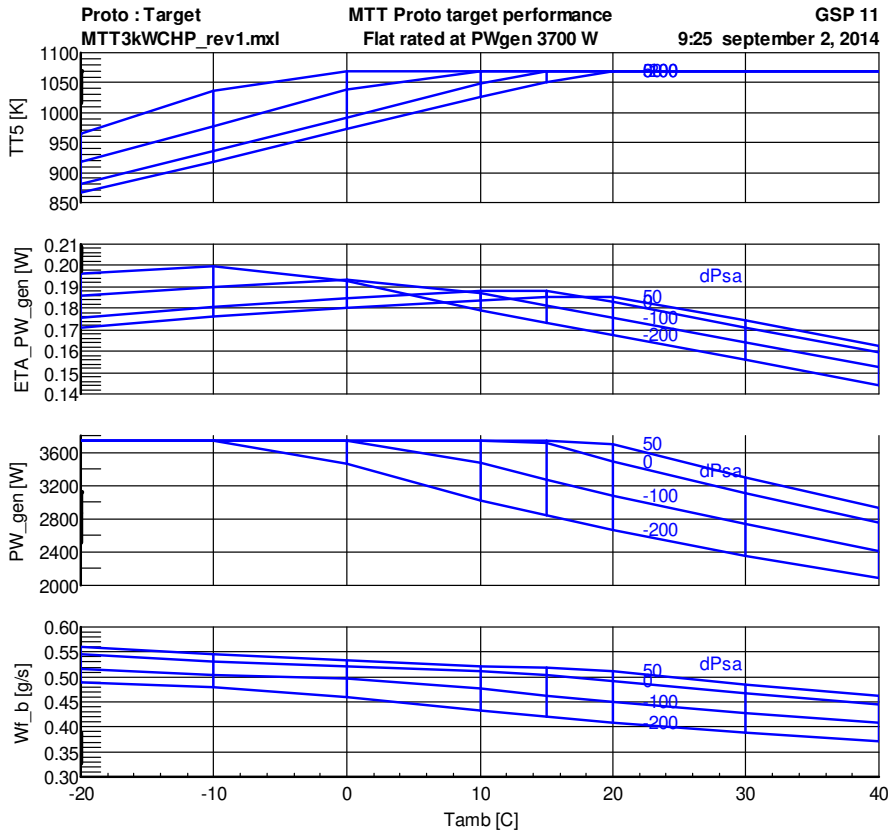
Figure 8.1 Flat rated performance of a 3kW micro turbine

8.2.3   Design point equation control component

The Design Point Equation Control component is dedicated for design point (DP) simulation only. In case an implicit relation between design parameters is needed, usually one or two DP Equation control components are used, such as a fixed DP thrust for a range of user specified TIT values and unknown inlet air flows to be calculated by the simulation for example. This practice is often required during conceptual cycle design studies where optimal design parameters are yet to be found. An interesting example is given in Chapter 18.

8.2.4   Schedule parameters

The parameters to be scheduled can either be *simulation output parameters* or component model *properties*.

The output parameters are determined after every calculation pass through the cycle during the Newton-Raphson iteration. Thereby they add an implicit relation and therefore they always require an additional equation and the assignment of an extra free state variable.

Component model properties are internal parameters that may optionally be scheduled directly. This only works if the model user is certain that the relation between schedule and property is explicit and the schedule is calculated prior to the point where the property is used in the cycle calculation pass. In other cases also an extra equation and free state are needed.

8.3   Activating/deactivating equations

Essential for simulation of gas turbine performance, including effects of control systems scheduling and limiting, is a method to activate and deactivate the associated equations during simulation. This is not a straightforward task. Changing the actual number of equations and states during simulation involves a complex series of procedures involving storing of the states prior to (de-)activation, redefining the new set (and different number) of equations and states, restarting the simulation and then later reversing the process.

In GSP 11 a more elegant method has been implemented. The equation sets to be solved by the Newton-Raphson iterations are not redefined. Instead the equation is deactivated by breaking the connection of the state variable with the model parameter and changing the equation terms. The active schedule equation i would be represented by

$$F_i(\bar{S}) - L(\bar{S}) = 0 \qquad (8.1)$$

with F_i as the non-linear function of model state $\bar{S}$ returning the actual value of the scheduled parameter, such as P3 from the above example. L returns the schedule value that usually comes from a table or expression of only a limited subset of $\bar{S}$ elements. Upon deactivation, the equation is changed to

$$1 - S_i = 0 \qquad (8.2)$$

with S_i as a 'dummy' state not connected to a model parameter. The transition between the active and deactivated equations is done only after convergence (i.e between successive steady-state or quasi-steady-state transient simulations). The number of equations and states remains the same and when deactivated, S_i will

simply converge to 1 in order to satisfy equation (8.2) while the rest of the equation set (see section 5.9) is solved yielding a valid state $\bar{S}$ not affected by the schedule.

Scheduler component equations can be (de-)activated manually by the user, for example halfway a transient or series of steady-state point simulations. With a Limiter the equation always initially is inactive and only becomes automatically active in case the Limit schedule is exceeded (see 8.2.2).

Chapter 9   Thermal effects modelling[6]

9.1   Introduction

The temperatures in the gas path of a gas turbine may vary significantly with power setting and operating conditions, especially in the hot section parts such as the combustor and turbines. As the casings around the gas path separate the hot gas from the normally much cooler environment outside the engine or inside engine internal compartments, there will be heat transfer between the casing material and the gas or air.

9.2   Steady-state heat loss

In fully stabilized steady state engine operation there usually is a constant heat transfer from the hot gas through the casing to the external surroundings. However, except for very small engines or engines with relatively large volume hot section components, this heat loss is usually very small and can be ignored in many cases. Therefore, there was only a very simple provision for this effect in terms of a user specified heat flux in the gas path component models of earlier GSP versions.

The application of GSP for very small gas turbines (see Chapter 18) prompted the need to implement more detailed thermal effect models. In small gas turbines, heat transfer effects become significant due to the high surface-to-volume ratios [72, 73]. A more advanced modelling capability was required to simulate steady state heat transfer among components and heat loss to the environment.

9.3   Heat soakage effects

In large engines, steady state heat loss effects often are negligible and only heat soakage effects affects transient response in some cases. However, with the high surface-to-volume ratios in small gas turbines, apart from steady-state, also transient (heat soakage) effects become significant. Thermal inertia of the gas turbine hardware around the gas path has an effect on transient performance. For example, during an acceleration of a gas generator from low speed and relatively low temperature levels in the gas path, to a fully stabilized steady-state high speed high temperature operating point, heat is lost heating up the material around the hot sections of the gas path. This heat loss affects performance and the acceleration

---

[6] This chapter is based on [71] W. P. J. Visser and I. D. Dountchev, "Modeling Thermal Effects on Performance of small Gas Turbines", GT2015-42744, to be presented at the ASME IGTI Turbo Expo 2015, Montreal, Canada, 2015.

response. It may be compensated to some degree by burning extra fuel, especially at cold start-up.

In earlier versions of GSP, this effect can be simulated to a limited extent using the Heat soakage effect option in the gas path components that is described in the Technical Manual [29]. In the next sections, a method is described with a much more extensive thermal effects modelling capability including heat transfer *among* components and heat loss to the environment. As a result, with GSP 11, the old Heat soakage functionality is obsolete and only retained for backward compatibility in older GSP projects and models.

9.4   Generic thermal network modelling

A generic thermal network approach was developed, allowing the simulation of the following heat transfer types:

a) Convective and radiative heat transfer between the bulk flow and the gas path wall.
b) Conduction heat transfer through the gas path wall and adjacent material.
c) Convective and radiative heat transfer from gas path wall to the exterior.
d) Conductive heat transfer among different component hardware elements.
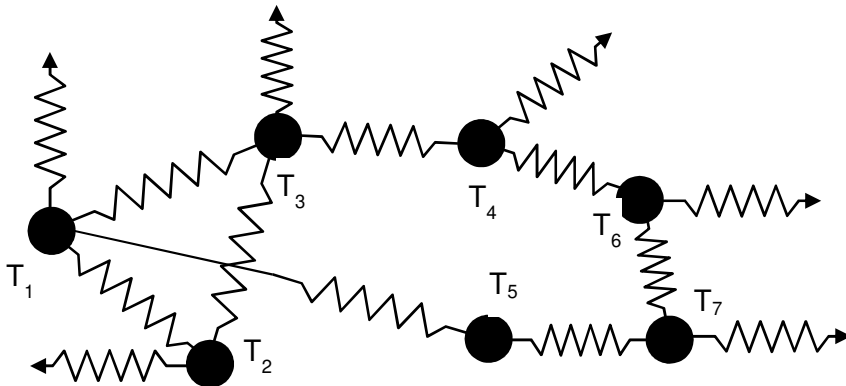
Figure 9.1 Thermal network nodes connected by heat transfer links

A 0-D or parametric thermal network consist of a number of heat capacities or *heat sinks* that allow heat transfer of some sort among each other and to the exterior. In Figure 9.1 a graphical representation is shown of an example thermal network with 7 heat sinks (the solid nodes). The 'resistors' in the figure represent heat transfer coefficients that may be calculated by more or less complex models depending on the heat sink temperatures and other parameters, using theory from textbooks such as [74]. The heat sinks each have uniform (average) temperatures

($T_1..T_7$) that are the unknowns in a system of NDEs (Non-linear Differential Equations). The NDEs represent the conservation of heat for each heat sink. Equation (9.1) shows the NDE for a heat sink i (with temperature T_{hsi}, mass M_{hsi} and specific heat c_{phsi}) that is connected to a total of n other elements with corresponding n heat fluxes Q_j.

$$\sum_1^n Q_j - M_{hs_i}.c_{p_{hs_i}}.\frac{dT_{hs_i}}{dt} = 0 \tag{9.1}$$

The heat fluxes Q_j are depending on the adjacent heat sink temperatures (i.e. the states in the NDE set) and the specific heat transfer model specified for that connection. Elements in the model that are considered to have infinite heat capacity such as the ambient air or very large masses do not require heat sink nodes since these will have temperatures that are constant or at least independent of the others. Heat transfer to these external elements is indicated by the arrows in Figure 9.1. Both steady-state and transient simulations can be performed. For steady-state, the time derivative in Equation (9.1) is equal to 0.

Figure 9.2 GSP heat sink component heat transfer model

This concept can be efficiently integrated into GSP as follows. Heat sinks are represented by non-gas path component models. They can be added to the model configuration, assigned a mass and specific heat for the heat capacity. They will automatically add a state and an error equation corresponding to Equation (9.1), to
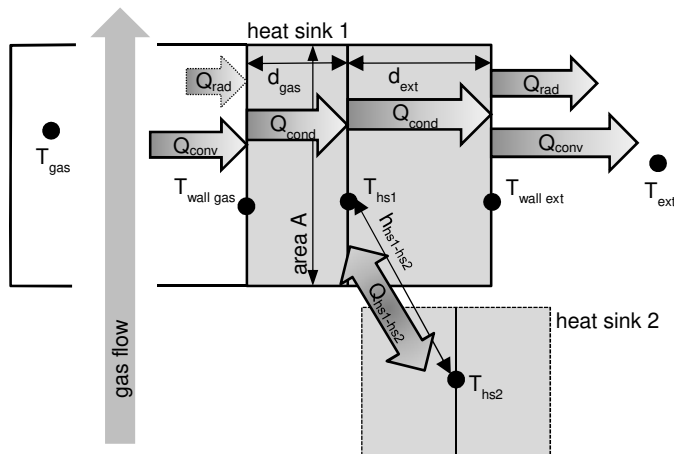
the modelling system as described in 5.9 and also Chapter 11. In all gas path components, the user can assign an unlimited number of heat transfer links to one or more heat sink components. The user can specify the heat transfer model using his own expressions for Reynolds and Nusselt numbers for convection, emissivity for radiation heat transfer and conductivity and characteristic thickness for conduction inside the heat sink. The heat sink components themselves can be connected to ambient conditions or an alternative user specified external condition. Also, heat sinks can be interconnected with single expression based heat transfer models.

In Figure 9.2 the different heat transfer elements that may be active in a GSP heat sink model are shown. A second heat sink (heat sink 2) is added to show the heat transfer among heat sinks. Given are gas path temperature T_{gas} and external temperature T_{ext}. T_{hs1} is the temperature of heat sink 1, as determined by a state in the modelling system.

9.4.1 Conduction

Conduction between the wall of the heat sink and its 'core' is calculated with

$$Q_{cond} = (T_{hs} - T_{wall}) * \frac{k_m \cdot A}{d} \qquad (9.2)$$

In the 0-D parametric thermal network model, the heat sink is assumed a point mass m. However to account for heat flux resistance represented by the heat sink material, a characteristic length (or thickness) d is specified through which the heat has to be conducted. As a result, the outside temperature T_{wall} of the heat sink is different from the core temperature. For simplicity, still the heat content of the heat sink is proportional to T_{hs} as in equation (9.1). A is the equivalent cross section area though which conduction can take place and k_m is the conductivity of the material. It is up to the user to specify A and d to represent the thermal effects of some structure and mass near the gas path with best possible accuracy.

9.4.2 Convection

Convection heat transfer between the heat sink wall and the gas path or the exterior on the other side is calculated using:

$$Q_{conv} = (T_{gas} - T_{wall}) * A * h_{conv} \qquad (9.3)$$

For the exterior side, replace T_{gas} by T_{ext}. Area A is the same as A in equation (9.2). The convective heat transfer coefficient h_{conv} depends on the boundary layer and flow conditions outside the wall. This dependency is characterized by the Nusselt number Nu and h_{conv} relates to Nu according to

$$h_{conv} = \frac{Nu.k}{D} \qquad (9.4)$$

D is some characteristic length, such as hydraulic diameter of a duct or diameter of a rotating element (in case of a rotating GSP component). k is conductivity of the gas. Nu is usually calculated as a function of Reynolds number Re and Prandtl number Pr as follows.

$$Re = \frac{\rho.v.D}{\mu} \qquad (9.5)$$

$$Pr = \frac{\mu.c_p}{k_g} \qquad (9.6)$$

$$Nu = a.Re^b.\Pr^c \qquad (9.7)$$

Here, ρ is density of the gas, v is gas mean velocity (or wall velocity in case of a rotating element) and μ dynamic viscosity of the gas. C_p is specific heat of the gas and k_g conductivity of the gas. The constants a, b and c are user specified and typically are selected based on Nusselt relations given in literature for specific cases. In the application to micro turbine development described in 18.7 for example, a heat sink is used to represent the radial turbine casing heat capacity and for the internal convection from the gas flow inside to the internal wall, the values 0.023, 0.8 and 1/3 are used for a, b and c respectively.

Although usually, the general form of equation (9.7) is used, the user is free to use any relation or constant for Nu in the GSP heat sink models. This is convenient in case Nu has been determined from other analysis outside GSP.

9.4.3   Radiation

Radiation may have a significant contribution to heat transfer at high temperatures. Equation (9.8) represents the radiative heat transfer between the heat sink wall and the surrounding gas and other objects when they have a uniform temperature T_∞.

$$Q_{rad} = \varepsilon \cdot \sigma \cdot A \cdot \left(T_{wall}^4 - T_\infty^4\right) \qquad (9.8)$$

ε is user specified emissivity of the wall surface, A the wall area (same as A in equation (9.2)) and σ the Stefan-Boltzmann constant.

If the temperature of the surrounding gas and other objects is indeed close to T_∞ (relative to the difference T_{wall} - T_∞) then equation (9.8) will not introduce large error. This would apply to radiation by the *outside* walls of hot gas path components to the exterior or to engine compartments for example.

For the *inside* walls of a hot gas path duct radiation cannot be calculated with equation (9.8) since the internal diameter is usually much smaller than the radiation free path length in the gas, virtually making the gas inside optically transparent, even if the radiating/absorbing species CO_2 and/or H_2O are present (pure air is fully transparent). In that case, the walls will merely exchange radiation heat with the opposite sides without affecting the gas in-between. Instead, convective heat transfer will be dominant and radiation effects can usually be considered negligible.

9.4.4 Combined overall heat transfer

For the heat sink model shown in Figure 9.2, all heat transferred via convection and radiation has to be conducted from the heat sink wall to its core, so

$$Q_{cond} = Q_{rad} + Q_{conv} \tag{9.9}$$

This applies both to the heat transfer from the heat sink to the gas with given temperature T_{gas} and to the exterior with given temperature T_{ext}. Q_{cond}, Q_{rad} and Q_{conv} are all functions of the unknown wall temperature T_{wall}, so for calculating the terms in equation (9.9), it first must be solved for T_{wall}. Substituting equations (9.2), (9.3) and (9.8) into equation (9.9) and some rearranging yields:

$$T'_{wall} = \frac{h_{cond} \cdot T_{hs} + h_{conv} \cdot T_{gas} + \sigma \cdot \varepsilon \cdot \left(T_{wall}^4 - T_{gas}^4\right)}{h_{cond} + h_{conv}} \tag{9.10}$$

Equation (9.10) is for the gas side, for the exterior side replace T_{gas} by T_{ext}. It can be repetitively calculated until the solution is found where T'_{wall} is equal to T_{wall} (within a certain accuracy tolerance).

If radiation is not taken into account, the model is simplified and T_{wall} does not need to be calculated. Instead, the heat transfer with the heat sink is equal to both the conduction and convection heat transfer and can be directly (without iteration) calculated with equations (9.11) and (9.12).

$$Q_{cond} = Q_{conv} = \left(T_{hs} - T_{gas}\right) \cdot A \cdot U \tag{9.11}$$

With the overall heat transfer coefficient U [W/K/m^2]:

$$U = \frac{1}{\left(\dfrac{1}{h_{conv}} + \dfrac{d}{k}\right)} \tag{9.12}$$

Heat transfer among heat sinks in a gas turbine model often is primarily conduction through structures that are joined together. However, as principally it can be of any kind, a simple heat transfer model with a heat transfer coefficient in which several heat transfer types are lumped together is used according to equation (9.13).

$$Q_{hs1-hs2} = (T_{hs2} - T_{hs1}) \cdot H_{hs1-hs2} \tag{9.13}$$

9.4.5 Effects on gas path component performance

With simple gas path components such as ducts, heat transfer is simply added or taken from the enthalpy at the component exit, affecting exit temperature. For turbomachinery, it is a bit more complicated. Heat transfer has an effect on power absorbed or delivered in respectively compression and expansion processes. Since this effect is generally small and the heat transfer model depends on empirically determined constants, the power is corrected assuming part of the heat (equal to R_q) is transferred before and the rest after the compression or expansion. The following corrections for compressor and turbine power can be derived using the customary methods to calculate adiabatic compression or expansion enthalpy change with isentropic efficiency:

$$\text{for the compressor: } PW_{corr} = \left(\frac{h_{out}}{h_{in}} - 1\right) \cdot \frac{Q}{\eta_{is}} \cdot R_q$$

$$\tag{9.14}$$

$$\text{for the turbine: } PW_{corr} = \left(\frac{h_{out}}{h_{in}} - 1\right) \cdot Q \cdot \eta_{is} \cdot R_q$$

PW$_{corr}$ is added to adiabatic compression or turbine power which is calculated using

$$PW = (h_{out} - h_{in}) \cdot w \tag{9.15}$$

Then, with heat transfer Q, the output enthalpy h$_{out}$ has to be recalculated using

$$h_{out} = \frac{(h_{in} \cdot w_{in} + Q + PW + PW_{corr})}{w_{out}} \tag{9.16}$$

The factor R_q is user specified. The default value is 0.5, meaning half of the heat is transferred before and half after the process. Note that in the actual GSP component models, more corrections are implemented, depending on the turbomachinery type, such as bleed and cooling flows that are not discussed in this thesis.

9.4.6   Application examples

A typical application would be the modelling of thermal effects with a reverse flow combustor configuration as shown in Figure 9.3, where compressor and hot section are close together.

Figure 9.3 Reverse flow combustor gas turbine configuration

In Figure 9.4 an example is shown of a corresponding GSP thermal network scheme. A compressor component is connected to a heat sink representing the heat capacity of its casing and a turbine component is connected to two heat sinks, one for the casing and one for another part that absorbs heat from the hot gas (e.g. the combustor casing). The objective is to simulate the heat transfer from the hot section to the compressor air flow, which has a negative effect on compressor performance.
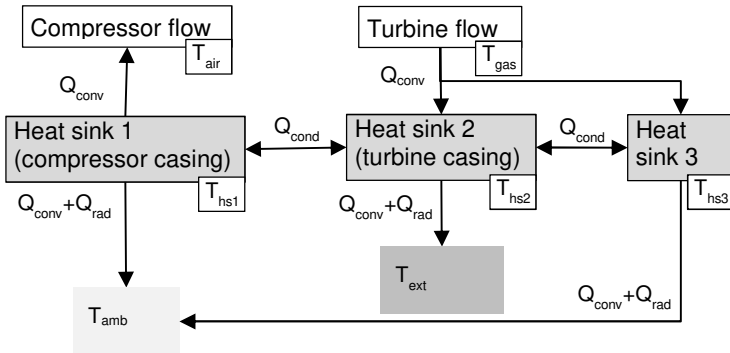
Figure 9.4 GSP example thermal network

Heat is transferred via convection from the hot gas into Heat sink 2. We assume there is no radiation effect inside the gas path so equation (9.11) can be used. Equation (9.2) is used to calculate conductive heat transfer to the other 2 heat sinks. In addition there is convective and radiative heat transfer from Heat sink 2 to some

exterior with T_{ext} calculated using equation (9.9). Heat sink 3 is similar to Heat sink 2, but with heat transfer to the ambient environment with T_{amb}. Heat sink 1 is heated up by the conduction from Heat sink 2 and in turn heats up the compressor air by convection heat transfer. In addition, there is some convective and radiative heat transfer from Heat sink 1 to ambient. With 3 heat sinks in the GSP model, 3 extra model states (heat sink temperatures) and equations (equation (9.1)) are automatically added to the system model set of equations.

It is up to the user to configure the model using heat transfer theory to specify the Nusselt expressions and emissivity values. Geometric and material data can be used to specify values for conductivity, heat sink wall thickness d and area A. Finally, 'synthesis by analysis' must be used to tune the model such that it best matches performance measurements and associated energy balances. In section 18.7.5 heat loss analysis using a detailed thermal network model for a micro turbine is described.

Figure 9.5 Effect of heat transfer from hot section to compressor

In Figure 9.5 the effect on performance of a micro turbine is shown. Between the compressor (Heat sink 1) and hot section (Heat sink 2) convection heat transfer elements, a conduction 'bridge' with cross area A_Qcbridge is specified. By

increasing A_Qcbridge heat transfer to the compressor Qhsink_c (Q_{cond} in Figure 9.4) is increased up to about 600 W. Qhsink_c is distributed over the compression process with R_q=0.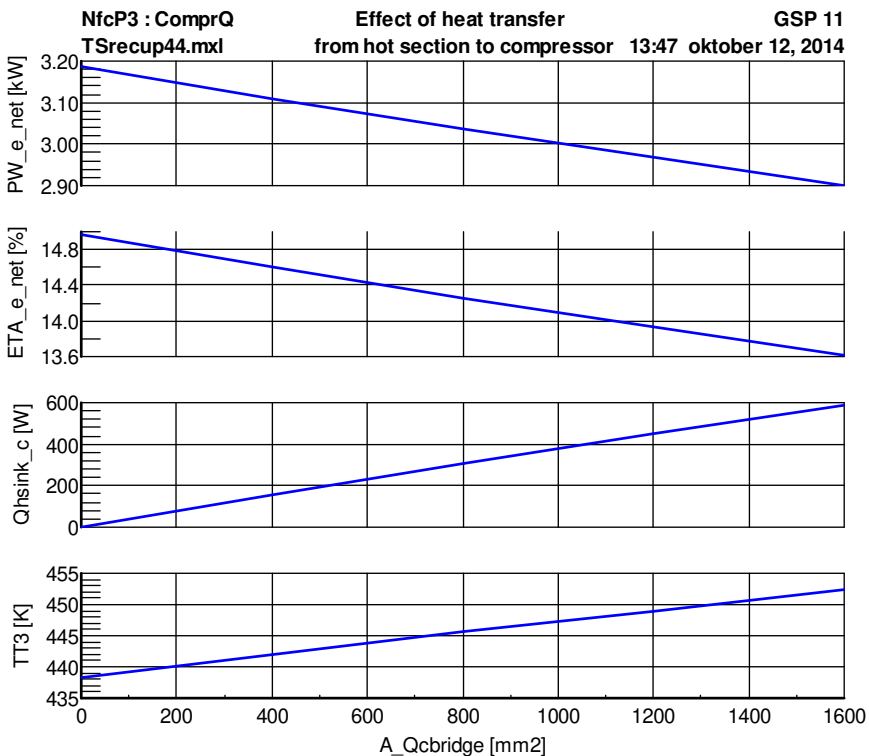5 (see equation (9.14). This significantly affects required compression power. As a result, end compressor temperature TT3 is increased and power and efficiency decreased.

Another application is described in section 18.7.5 where the model is used to predict recuperator heat loss effects on performance.

9.5   0-D thermal recuperator model

The recuperator in a recuperated gas turbine cycle usually introduces a very large thermal inertia effect on transient performance. Thermal steady-state is reached only after the recuperator is fully warmed-up and this usually takes a lot of time compared to the responses of the other parameters such as spool speeds. The thermal energy stored in the recuperator is in many cases even able to 'keep the engine running' even after fuel shut-off, which may present a hazardous situation (uncontrolled overspeed) in case of a load shed event for example. This makes an accurate transient system simulation of recuperated gas turbines including thermal effects essential for design of efficient and safe systems.

The standard GSP recuperator component model is inherited from the generic heat exchanger model. The heat exchanger model includes a heat sink representing the material heat soakage effect during transients. This effect is dominated by the material between the hot and the cold side of the recuperator (i.e. the heat exchanger *matrix*). The modelling method is similar to the heat sink model above, using convective-conductive-convective heat transfer respectively, from the hot gas, through the separating wall in the heat exchanger matrix, to the air on the other side. However, instead of a single state for the average temperature of the heat sink between the gas flows, two states are added for the heat transfer rates on both sides of the wall with the air and gas. Two equations are added requiring these heat transfers to equal the heat transfers calculated from an average material temperature. This material temperature depends on a user specified time constant characterizing the first order nature of the heat sink temperature response.

For relatively small recuperator heat capacities and mild transients, the model accurately simulates heat soakage effects. However, with large thermal inertia and sudden temperature changes the model easily becomes unstable due to failure of the 0-D approach to capture the variation of thermal effects along the recuperator gas path (see section 9.6). The instability manifests itself as severe overshoots of heat transfer rates between the gas flows and the matrix.

More information on this model can be found in the GSP Technical Manual [29]. Note that this model has more or less become obsolete with the much more accurate 1-D thermal recuperator model described in the next section.

9.6   1-D thermal recuperator model

9.6.1   Introduction

An important limitation of the 0-D thermal recuperator model described in section 0 is the fact that thermal effects active along the length of the counter flow gas paths cannot accurately be described with a 0-D model. The temperature profile in the wall between the gas paths may be very peculiar, depending on the transient history, especially during transients with rapid power setting changes and relatively high thermal capacities of the wall. This is illustrated in Figure 9.6 showing results of the 1-D model described in this section: the gas (i.e. hot fluid) inlet temperature (at location 1) drops rapidly after a sudden power setting drop. However, due to the heat soakage effect of the wall in between, the hot gas is now initially heated up instead of cooling down, resulting in an increase in gas temperature instead of a decrease, as would be the case in steady state.
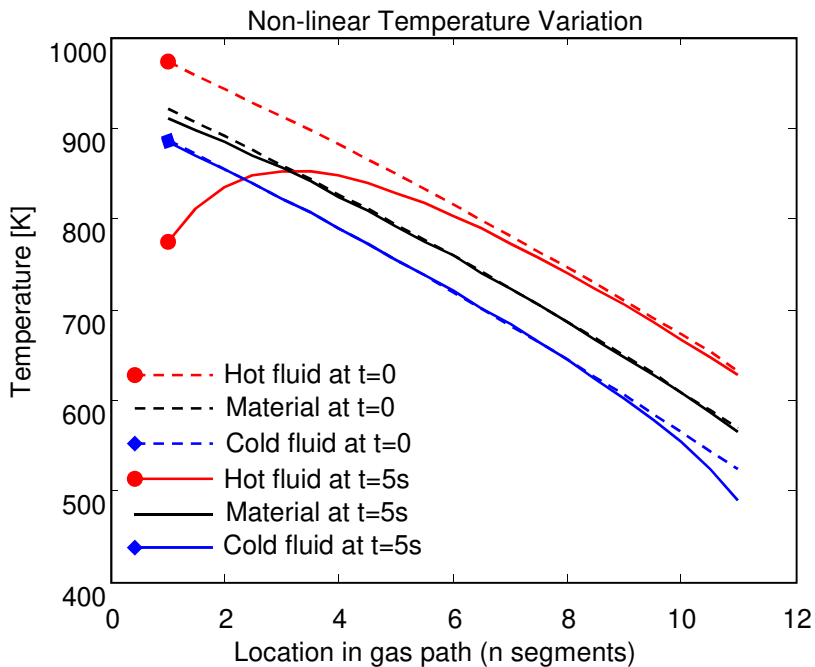
Figure 9.6   Transient temperature profiles along recuperator gas path after rapid turbine entry temperature decrease

9.6.2   1-D modelling approach

Clearly, the effect shown in Figure 9.6 can never be captured with a 0-D model so a 1-D approach was followed to develop an improved recuperator thermal model. A 1-D differentiation was applied along the counter flow gas paths, breaking up the heat transfer process into a number of n *segments* as depicted in Figure 9.7.

Each segment in Figure 9.7 consists of an air side cell (with length dx) into which air enters and exits after some heat is exchanged with the wall element (with length dx, width y and thickness d) in the middle, via convection and conduction. The wall segments act similar to the 0-D heat sinks described in section 9.4. On the other side, the wall exchanges heat with a gas segment cell. The wall element has a mass M_{matrix}/n, with M_{matrix} as the user specified mass of the matrix.
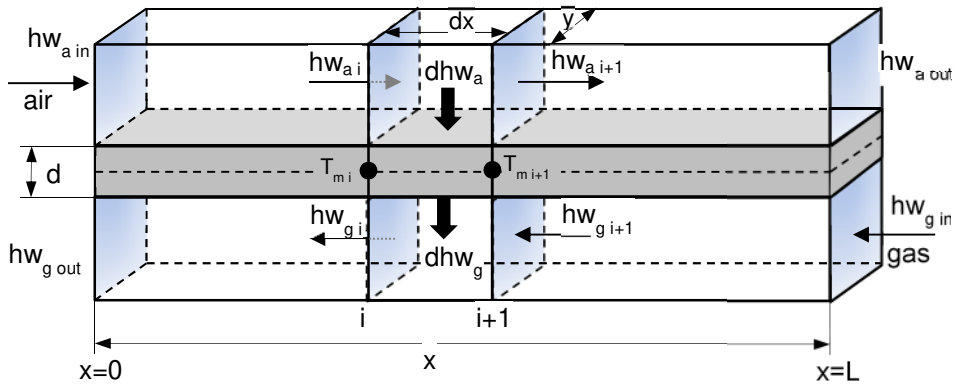
Figure 9.7   1-D counter flow heat exchanger model concept

9.6.3   Assumptions

The following assumptions must be made for the 1-D model, several of which will be explained in the following sections:

- There is no heat exchange among the segments, or with other parts of the heat exchanger. This is a reasonable assumption if the wall is very thin as is common with recuperators, since then the 'sideways' conduction heat transfer between adjacent segments will be much smaller than the conductive heat transfer with the air and gas.
- There is no heat loss to the environment.
- Heat transfer areas of the segments are all equal, both at air and gas sides
- Heat transfer coefficients are uniform along the air and gas sides.
- User specified ratio of air and gas side heat transfer coefficients.
- Transient heat transfer coefficients are determined from steady-state heat exchanger effectiveness characteristics ('quasi-steady-state' approach).

- Internal wall material heat capacity is concentrated in the centre of the wall, requiring conduction heat transfer over half the material thickness.
- Effects of gas dynamics are not taken into account.

9.6.4   Heat transfer coefficients and effectiveness

The question remains how to determine the heat transfer coefficients for the segments. If consistent with the other component models, steady-state performance is provided by a map. In case of a heat exchanger (from which the recuperator inherits most of its functionality), this is effectiveness as a function of the air and gas side heat capacity fluxes $w_a.c_{p\_a}$ and $w_g.c_{p\_g}$. If no map is available, often a constant effectiveness is used, sometimes determined during tuning of the cycle model to experimental data.

A heat transfer model for the segments is required that is consistent with the overall effectiveness. An alternative approach, modelling the heat transfer from geometrical data and Nusselt relations for example, would suffer from inaccuracy and deviate from detailed component models or test data.

The following approach is followed to derive a relation for the heat transfer coefficient from effectiveness. Effectiveness is defined as

$$E = \frac{Q}{Q_{max}} \tag{9.17}$$

For a recuperator, the maximum heat capacity flux is always on the gas side, as the gas on this side always has higher mass flow rate w and higher specific heat c_p, so

$$Q_{max} = w_a \cdot \left(h(T_{g_{out}}, GC_a) - h_{a_{in}} \right) \tag{9.18}$$

$h(T_{gas\ out}, GC_{air})$ is the enthalpy of air (gas with composition GC_{air}) at temperature $T_{gas\ out}$ as calculated by the gas properties model in GSP. Now the air and gas side recuperator exit enthalpies can be calculated from the air and gas inlet enthalpies that are given during the cycle calculation:

$$h_{g_{out}} = h_{g_{in}} - \frac{E \cdot Q_{max}}{w_g} \tag{9.19}$$

$$h_{a_{out}} = h_{a_{in}} + \frac{E \cdot Q_{max}}{w_a} \tag{9.20}$$

The steady-state enthalpy flux *h.w* on the gas side is changing along the gas path due to the heat transfer to the wall with temperature T_m according to:

$$\frac{dhw_g}{dx} = -U_g \cdot y \cdot (T_g - T_m) \qquad (9.21)$$

dx is a small increment in the direction of the gas path and y a dimension perpendicular to dx such as dx.y is the area dA of an element through which heat is transferred. U_g is the overall heat transfer coefficient between gas and the centre of the wall according to equation (9.12). For the air side enthalpy flux the equation is

$$\frac{dhw_a}{dx} = -U_a \cdot y \cdot (T_m - T_a) \qquad (9.22)$$

At steady state, the heat flux on the air side must equal the heat flux on the gas side so:

$$-U_a \cdot y \cdot (T_m - T_a) = -U_g \cdot y \cdot (T_g - T_m) \qquad (9.23)$$

After rearranging:

$$T_m = \frac{U_a T_a + U_g T_g}{U_a + U_g} \qquad (9.24)$$

Substituting equation (9.24) into equation (9.21) yields:

$$\frac{dhw_g}{dx} = -\frac{U_a U_g}{U_a + U_g} \cdot y \cdot (T_g - T_a) \qquad (9.25)$$

and into equation (9.22):

$$\frac{dhw_a}{dx} = -\frac{U_a U_g}{U_a + U_g} \cdot y \cdot (T_g - T_a) \qquad (9.26)$$

So it follows that

$$\frac{dhw_a}{dx} = \frac{dhw_g}{dx}$$ (9.27)

So obviously, the enthalpy flux at the air side and at the gas side change at the same rate, if the overall heat transfer coefficients U_a and U_g are uniform along the gas path in the recuperator. This means

$$hw_a = hw_g - C_{dhw}$$ (9.28)

Where C_{dhw} is the constant difference between hw on the air and on the gas side. C_{dhw} can be calculated easily either at the hot or cold side of the recuperator.

$$C_{dhw} = hw_{g_{out}} - hw_{a_{in}} = hw_{g_{in}} - hw_{a_{out}}$$ (9.29)

In Figure 9.8 this result is depicted. While clearly the temperature delta T_{gas}-T_{air} must change along the gas path due to the higher heat capacity flux in the gas side, the difference between hw is constant.
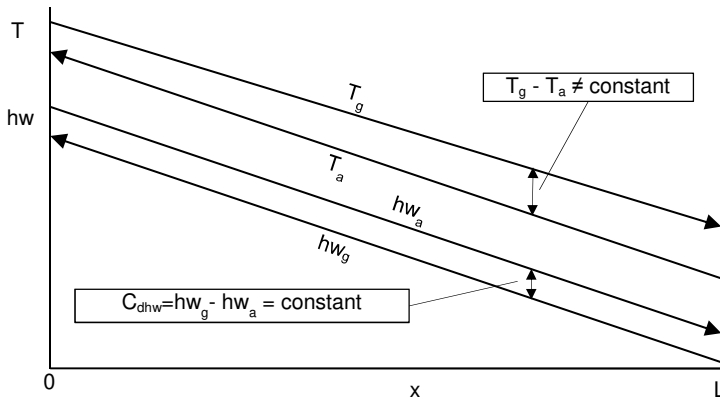
Figure 9.8   Steady-state temperature profile along recuperator gas path

Integrating equation (9.26) over the length of the gas passage through the recuperator yields:

$$\int_{L}^{0} -\frac{U_a U_g}{U_a + U_g} \cdot y \cdot dx = \int_{hw_{g_{in}}}^{hw_{g_{out}}} \frac{dhw_g}{(T_g - T_a)} \tag{9.30}$$

or

$$-\frac{U_a U_g}{U_a + U_g} \cdot A = \int_{hw_{g_{in}}}^{hw_{g_{out}}} \frac{dhw_g}{(T_g - T_a)} \tag{9.31}$$

The temperatures Tg and Ta can be calculated from the enthalpy h and gas composition GC using GSP's gas model function FT

$$\begin{aligned} T_a &= FT(h_a, GC_a) \\ T_g &= FT(h_g, GC_g) \end{aligned} \tag{9.32}$$

Also

$$h_a = \frac{hw_a}{w_a} \quad and \quad h_g = \frac{hw_g}{w_g} \tag{9.33}$$

Then with equation (9.28):

$$h_a = \frac{hw_g - C_{dhw}}{w_a} \tag{9.34}$$

Now substituting (9.34) into equation (9.31) yields:

$$-\frac{U_a U_g}{U_a + U_g} \cdot A = \int_{hw_{g_{in}}}^{hw_{g_{out}}} \frac{dhw_g}{\left(FT(h_g, GC_g) - FT(\frac{hw_g - C_{dhw}}{w_a}, GC_a)\right)} \tag{9.35}$$

Knowing, $hw_{g\ in}$ and $hw_{g\ out}$, the integral on the right side of equation (9.35) can now be simply calculated using the trapezium rule. With I_{hw} as the result of the integral we obtain

$$-\frac{U_a U_g}{U_a + U_g} \cdot A = I_{hw} \tag{9.36}$$

The constant overall heat transfer coefficients U_a and U_g can be calculated if a ratio $R_u = U_g/U_a$ is given:

$$U_g = \frac{I_{hw} \cdot (1 + R_u)}{A} \tag{9.37}$$

$$U_a = \frac{U_g}{R_u} \tag{9.38}$$

From an analysis of the heat transfer conditions at the air and gas sides a reasonable value for R_u can be specified by the user. A typical value would be 0.65.

9.6.5 Calculating the steady-state wall node temperatures

Now a method is available to obtain the overall heat transfer coefficients for a number of n discrete elements along the recuperator gas path, that correspond to a steady state operating point with known recuperator inlet and exit gas conditions corresponding to a given steady state effectiveness. A quasi steady state transient simulation approach can now be followed to calculate the heat soakage effect of the wall, i.e. the thermal inertia effect of the wall resulting in a response lag of material temperature. This lag will affect the heat transfer between the wall, gas and air, resulting in profiles such as shown in Figure 9.6. Air side, gas side and material temperatures are defined at the n+1 nodes that represent the entries and exit of the n segments.

Prior to any transient simulation, the steady-state material temperatures $T_{m\,i}$ for all nodes must be calculated and stored in order to set the initial condition of the subsequent dynamic thermal simulation. Then also the air and gas side node temperatures ($T_{a\,i}$, $T_{g\,i}$) must be calculated. Although not really necessary, the $T_{a\,i}$, $T_{g\,i}$ values are also stored to have favourable starting values for the iteration required during transient simulation.

First, the overall heat transfer coefficient (for the entire surface A) UA [W/K] from the cold to the hot flow for each segment is calculated:

$$UA_{ag} = \frac{A/n}{\dfrac{1}{U_a} + \dfrac{1}{U_g}} \tag{9.39}$$

As the entry (i=0) and exit (i=n+1) node conditions can directly be calculated, the numerical problem to be solved here is a set of n-1 equations with n-1 unknown material node temperatures ($T_{m\,1}$ through $T_{m\,n-1}$). These equations could be added to the global GSP equation set and simultaneously be solved. However, this may well lead to severe iteration instabilities, so a local iteration is used instead, satisfying the effectiveness and entry and exit conditions of the recuperator that are given during

the global model iteration. Also, instead of a Newton-Raphson approach, as simple iterative procedure is used. Starting with the first segment between i=0 and i=1, for each successive segment, the segment exit temperatures T_{g_i} and T_{a_i} are recalculated until the drop in enthalpy over both the gas and air side of the segment corresponds to the heat transfer according to UA_{ag} and the average temperatures in the segments and so $Q_{err} = 0$:

$$Q_{err} = dhw_{g_i} \cdot w_g - UA_{ag} \cdot (T_{g_i\,avg} - T_{a_i\,avg}) \qquad (9.40)$$

with

$$T_{a_i\,avg=} \frac{(T_{a_i} + T_{a_{i-1}})}{2} \quad and \quad T_{g_i\,avg=} \frac{(T_{g_i} + T_{g_{i-1}})}{2} \qquad (9.41)$$

and

$$dhw_{g_i} = \left[FH(T_{g_i}, GC_g) - FH(T_{g_{i-1}}, GC_g)\right] \cdot w_g \qquad (9.42)$$

For the air side similarly:

$$dhw_{a_i} = \left[FH(T_{a_i}, GC_a) - FH(T_{a_{i-1}}, GC_a)\right] \cdot w_a \qquad (9.43)$$

Note that for steady-state:

$$dhw_{a_i} = dhw_{g_i} \qquad (9.44)$$

FH is GSP's function calculating enthalpy as a function of temperature and gas composition.

While $Q_{err} \neq 0$ in equation (9.40), T_{gi} is corrected using:

$$T_{g_i} = T_{g_i} - \frac{Q_{err}}{w_g \cdot FCp(T_{g_i}, GC_g)} \qquad (9.45)$$

With FCp being the GSP function to calculate specific heat from temperature T_{gi} and the gas composition. From the corrected T_{gi} a new value for the enthalpy drop dhw_{gi} across the segment can be recalculated and then the new T_{ai} can be recalculated from equations (9.43) and (9.44). Repeating this procedure results in stable convergence towards a solution for segment i within a user specified tolerance after which the iteration is started for the next segment.

After completion at segment n, the gas and exit temperature of segment n is compared to the already given exit temperatures of the recuperator. Any residual deviation (due to error accumulating with the successive segment iterative calculations) is used to correct the air and gas node temperatures proportionally.

With the now calculated steady-state gas and air node temperatures, the wall node temperatures can be calculated using the notion that the ratio of overall heat transfer coefficients U is inversely proportional to the ratio of temperature deltas between the gas/air and the wall:

$$R_u = \frac{U_g}{U_a} = \frac{T_m - T_a}{T_g - T_m} \tag{9.46}$$

After rearranging, an expression for the node temperatures T_{mi} can be derived:

$$T_{m_i} = \frac{R_u \cdot T_{g_i} + T_{a_i}}{R_u + 1} \tag{9.47}$$

After calculating all material node temperatures using equation (9.47) the 1-D thermal steady-state of the recuperator is fully determined. Although not required for a steady-state cycle simulation as such, this procedure is executed for every steady-state simulation in GSP so as to make sure that always an initial condition is available for a successive transient simulation.

For more detailed information on the numerical procedures, refer to the code of the GSP 1-D recuperator model.

9.6.6   Transient simulation

For the transient simulation also an iterative procedure is followed, but this time separately for the heat transfer between the air and the wall and the wall and the gas. Clearly, the overall heat transfer coefficient (for the whole area A) UA_{ag} cannot be used anymore since there is no steady state heat transfer anymore.

For every segment, the heat flux Q_i is calculated for the gas and air sides using:

$$Q_{g_i} = U_g \cdot \frac{A}{n} \cdot (T_{g_i\,avg} - T_{m_i\,avg}) \tag{9.48}$$

$$Q_{a_i} = U_a \cdot \frac{A}{n} \cdot (T_{m_i\,avg} - T_{a_i\,avg}) \tag{9.49}$$

with

$$T_{m_i\,avg} = \frac{(T_{m_i} + T_{m_{i-1}})}{2} \tag{9.50}$$

From Q_i then the next node enthalpies $h_{g\,i}$ and $h_{a\,i}$ and thus the temperatures $T_{g\,i}$ and $T_{a\,i}$ can be calculated:

$$T'_{g_i} = FT\left(h_{g_{i-1}} - \frac{Q_{g_i}}{w_g \cdot FCp(T_{g_i}, GC_g)}, GC_g\right) \qquad (9.51)$$

$$T'_{a_i} = FT\left(h_{a_{i-1}} + \frac{Q_{a_i}}{w_a \cdot FCp(T_{a_i}, GC_a)}, GC_a\right) \qquad (9.52)$$

The temperatures T'_{gi} and T'_{ai} must equal the temperatures T_{gi} and T_{ai} used to calculate the average temperatures in equations (9.48) and (9.49).

The calculation of equations (9.48) is iteratively repeated, correcting T_{gi} and T_{ai} using

$$T'_{a_i} = \frac{T'_{a_i} + T_{a_i}}{2} \qquad (9.53)$$

$$T'_{g_i} = \frac{T'_{g_i} + T_{g_i}}{2} \qquad (9.54)$$

until $T'_{gi} = T_{gi}$ and $T'_{ai} = T_{ai}$ within a certain tolerance.

This process is executed for nodes i through n-1. The sums of all segment heat fluxes on the gas and air sides are calculated to calculate the transient overall heat transfer of the wall with the air and gas flows through the recuperator.

$$Q_g = \sum_{i=1}^{n} Q_{g_i} \qquad (9.55)$$

$$Q_a = \sum_{i=1}^{n} Q_{a_i} \qquad (9.56)$$

Next the temperature time derivatives of the material node temperatures are calculated, using the averages of the heat fluxes calculated for the adjacent segments i and i-1:

$$\frac{dT_{m_i}}{dt} = \frac{\frac{(Q_{g_i} + Q_{g_i-1})}{2} - \frac{(Q_{a_i} + Q_{a_i-1})}{2}}{c_{p_m} * \frac{M_{wall}}{n}} \qquad (9.57)$$

Equation (9.57) is used for nodes 1 through n-1. At nodes 0 and n+1 there is only a segment on one side and then the following equation is used:

$$\frac{dT_{m_i}}{dt} = \frac{Q_{g_i} - Q_{a_i}}{c_{p_m} \cdot \frac{M_{wall}}{n}} \tag{9.58}$$

The time derivatives of the material node temperatures calculated with equations (9.57) and (9.58) are integrated at each time step of the GSP global model transient simulation, resulting in a wall material response deviating from the steady-state profile and also resulting in values for Q_g and Q_a deviating from the values that correspond to the given steady-state effectiveness. As a result, the overall recuperated gas turbine transient response will also be affected. In 18.7 an application is described of the 1-D recuperator model.

9.6.7   Application example

In Figure 9.9 the 1-D thermal recuperator model is demonstrated showing the heat soakage effect of varying recuperator mass on 0 to 100% fuel (Wf/P3) step response transients of a recuperated micro turbine. The results of these simulations are used for system identification required for control system design and also to analyse the effect of weight reductions of the recuperator on transient performance and start-up times.

The figure shows the response during the first 5 minutes. Tmat_0_rec1 and Tmat_10_rect1 are the (internal wall) material node temperatures at the hot and cold entry/exit sides of the recuperator respectively. Thermal steady state is reached only after at least 30 minutes. The response curves of the 25 kg recuperator correspond with measured responses of the 3kW MTT recuperator micro turbine described in Chapter 18. With increasing mass, the system requires significantly longer time to warm up. The figure clearly shows that, depending on the recuperator mass, the electric efficiency (ETA_PW_gen) and power (PW_shaft_net) only become positive after a period up to 1 minute and then slowly increase towards steady state. With the cold material temperatures during warm up, extra fuel can be added by the fuel control (without risk of overheat) to compensate for the effect and shorten warm up time, but this also results in lower efficiency.
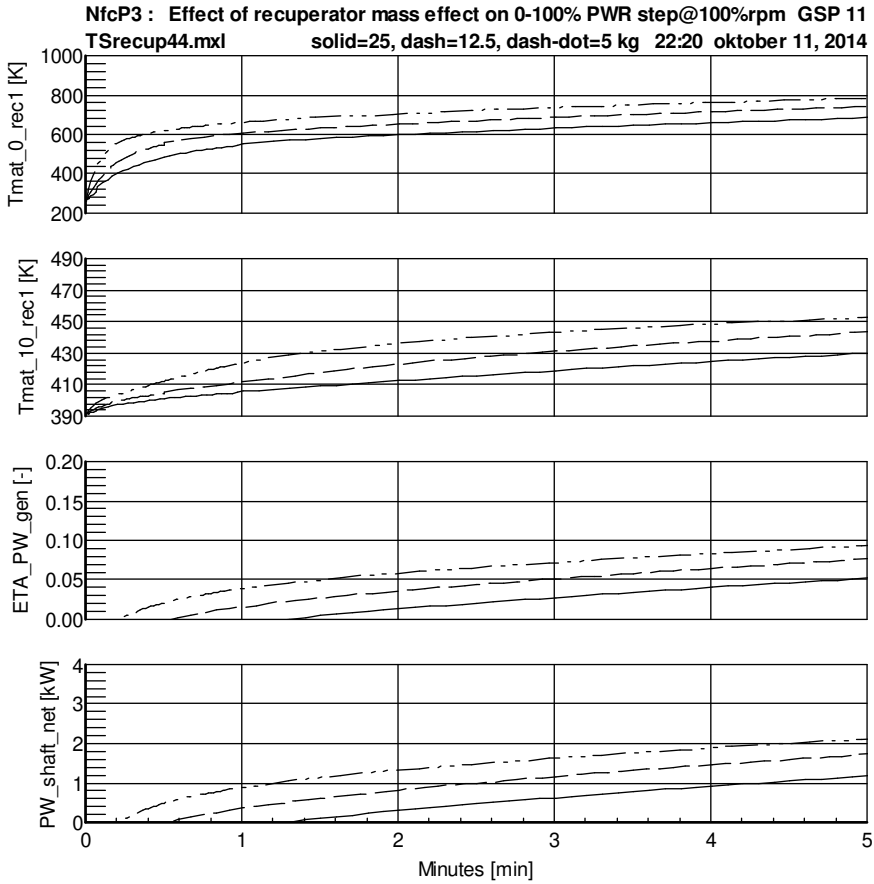
Figure 9.9   Example of 0-100% power (Wf/P3) step transient response with varying recuperator masses (5, 12.5, 25 kg).

Chapter 10 User interface and data storage

10.1   Introduction

The user interface design and software engineering of gas turbine system simulation tools such as GSP is a field unrelated to the physical and numerical modelling and simulation issues. However, it is an essential element for making it efficient and effective for performance analysis tasks. Therefore, this chapter describes the most important user interface elements of GSP and their relation to the modelling and simulation functions.

Tools with a poor interface often do not see application beyond a small circle around the developer himself, leading to a waste of resources and duplication of development efforts if new scientists and engineers enter the performance analysis arena. A good user interface can only be designed from a thorough understanding of gas turbine modelling theory and applications. In the case of GSP, the user interface has been designed to meet the requirement for generic nature of GSP and can easily be extended and adapted to changes in the simulation system.

10.2   Model editing interface

GSP's graphical user interface fully reflects the object-oriented architecture for the gas turbine system and component models, as is depicted in Figure 10.1. The main window mainly manages the model and library windows. A model window forms the 'work bench' on which a number of component icons are arranged to form a valid gas turbine configuration. It further includes all items necessary for a system simulation. GSP's context sensitive on-line help enhances user-friendliness.

Icons representing the component models are copied from component library windows onto the model window. The drag-and-drop interface allows the copying of multiple instances of components between models, enabling the user to build his own specific component repositories and save them as a generic model.

GSP offers a variety of flexible tabular and graphical input and output formats. For the model window these include ambient/flight conditions, a variety of simulation control options, result tables, result graphs, data export formats etc. Each component type has its own specific interface with design data, control system inputs, graphical component maps with operating curves, deterioration and variable geometry data etc. Off-design input includes tabular time functions for transient response calculations.
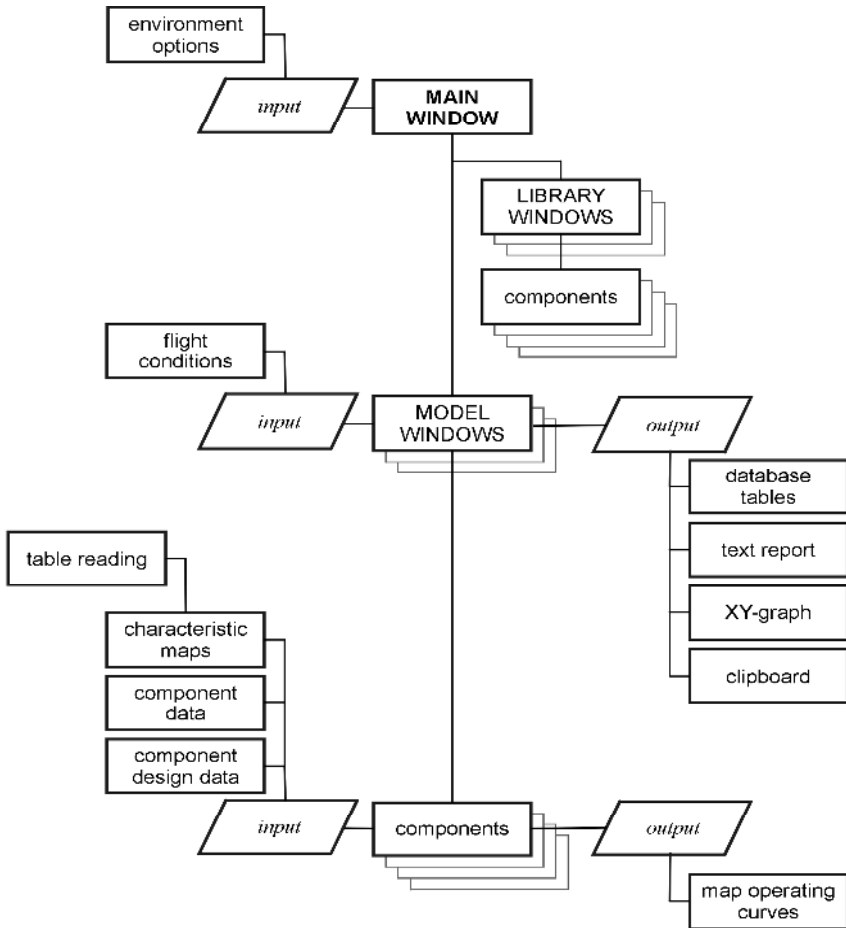
Figure 10.1   Interface architecture

10.3   Model data storage

The model data that are specified by the user must eventually be accessed by the model algorithms and also by the code saving and loading models to and from data storage devices such as hard disks. For model data storage in relation to the user interface several alternative approaches are possible.

10.3.1   Data storage format

The most obvious way to store model data is in a database, consisting of one or more tables that have specific relations. With the tables having columns and rows however, model data from an unknown number and variety of component models cannot be efficiently stored. As a consequence, a more flexible storage method has

to be used, not using tables with fixed records. Several existing simple text format concepts can be used such as Windows ini files for example. A more powerful and also modern industry standard for storing polymorph data is XML (Extensible Markup Language). For GSP 11, a flexible object oriented data storage concept using XML has been developed capable of storing data for any model configuration of various component models. In section 10.5.1 it is explained that GSP models are stored in XML files including one or more model configurations and run cases.

10.3.2 Run time model data

At run time of GSP 11, model data are read from XML files into run time XML memory, manipulated and optionally save back in XML files. Before simulation, the run time memory XML data are read into the actual component model parameter data fields which are directly accessed by the simulation algorithms.

10.3.3 Relation with the user interface

The component model parameter data fields can be either kept separate from the user interface or shared with the user interface data. The former option has the advantage of flexibility in terms of user interface: the same simulation code may be controlled by a different user interface of a different computer platform. With the latter option (model data and interface data fields are the same) however, significant benefits in code development efficiency and maintainability can be obtained.

For the GSP development environment the latter (shared data fields) option has been chosen and a special (object oriented/virtualized) data component library has been developed [75] that automatically reads and writes user data from the component data entry windows to and from the model data (i.e. XML, see section 10.5.1 below). This way, the developer never needs to worry about the data reading and writing process after adding new data entry fields in components. Note that without this concept, the developer would have to write separate code for storing and retrieving values between the user interface element and the run time data, every time a new component or system model parameter is needed.

A drawback of this method is the fact that all the model's user interface elements need to remain instantiated while running the model. With older Windows version this may pose a problem with very larger models or several models opened simultaneously in view of the limited number of window handles in MS Windows®. In future GSP updates, the concept will be adapted so that the window handles can be released when not used, while retaining all the code development benefits.

For more information on the model control user interface design, refer to the GSP documentation [28-31].

10.4   Configuration and case management

10.4.1 Introduction

Prior to GSP version 11, GSP models were stored as separate files and represented only a single gas turbine system configuration and also a single simulation input setting. However, except for very simple projects, usually a simulation exercise involves several changes in the system configurations and also many different run cases (design point, off-design and transient) with different inputs (different operating conditions). This means that the management of the various models (model files), run cases and results, becomes a complex task. From this notion the idea was born to extend GSP 11 with a *configuration* and *case management* capability. Instead of individual model files, GSP 11 would work with project files including (and saving) several *configurations* and *run cases*. Naturally, instead of just keeping unrelated models and cases inside the project, mechanisms were required to provide logical relationships among configurations and cases and avoid data duplication.

10.4.2 Inheritance

An optimal concept for the above described requirement is an inheritance mechanism for cases and configurations. From a single reference configuration, child configurations can be derived inheriting all properties from the parent and with a limited number of additions of modifications. When the configuration 'knows' its parent, only the data that are different need to be stored, avoiding duplication. *Configurations* can have both child-configurations and/or child cases. Configurations cannot be run themselves. Only *cases* (or 'run cases') represent elements in the inheritance tree that can be actually run as simulations. Therefore, only cases allow user specification of simulation input data such as gas turbine operating conditions (see sections 2.6 and 5.5). Naturally, cases cannot have child configurations.

Using this approach, the user can systematically build up his project, starting with a single root element configuration with components and elements common to all child configurations. Sub-configurations will be added for specific configuration variations. Then finally, the sub-configurations will have case children to represent the various run cases. If necessary, cases may have several sub-cases to concentrate specific simulation inputs in a single parent case, again avoiding duplication and enhancing overview. If this is done properly then a project may include all possible configurations and run cases to produce simulation results consistently, without repeatedly specifying inputs.

Using the inheritance concept, modelling and simulation projects can be managed very efficiently, but it requires analysis and planning up front before the configuration and case inheritance structure is built. If the mechanism is well understood and projects are carefully built after analysis of the modelling and

simulation objectives, very efficient set-ups can be made. A well-organized project inheritance structure offers a very efficient and user friendly environment for many modelling and simulation tasks. New cases and/or configurations can be easily added as sub-nodes and with minimal data entry efforts, simulations can be run and results analysed.

10.5   GSP project tree
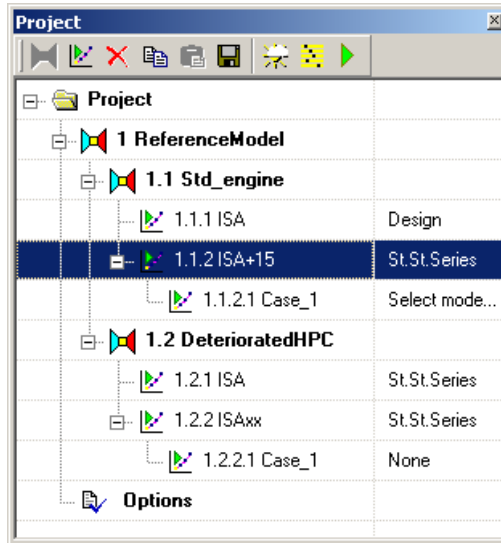
Figure 10.2   Example of a GSP project in the user interface

Figure 10.2 shows an example of the GSP project tree as seen in the user interface. Under the ReferenceModel node, two configurations are added named Std_engine and DeterioratedHPC. Under these configurations, several cases and sub_cases are added (ISA, ISA+15 etc.). The user can select a node in the tree to activate it. Then the configuration and/or case data are accessed using the model editing interface (see section 10.2).

In the right column, the *run case type* is indicated which determined the simulation mode. The following case types are available:

- Design   a single DP (design point) calculation
- Design series   a series of DP calculations with varying design parameters
- Steady-state   a single steady state off-design (OD) simulation
- St.St. Series   a series of OD calculations with varying OD input parameters
- Transient   a transient simulation calculating the response to user specified input functions of time

10.5.1 XML storage format

XML (Extensible Markup Language) is a widely accepted standard for storing and organizing digital data of any form. It provides an excellent format to implement the inheritance concept described above for storing and managing GSP project data including model configurations and cases. The *Reference model* represents the single root in the project from which adapted configurations are derived and saved as child nodes in the project tree. For a child node, only the data that deviate from the parent are stored. This means data storage size is minimized, data duplication avoided and loading and saving speed maximized. The following main elements are found in the project tree:

- Project root node with optional project name
- Project Options
- Reference Model
- Configuration
- Case

Figure 10.3 shows an example of the XML inheritance data tree. Under a single Project root node, there is always the Reference model child node and also a node for Project options. Project options are all settings on the overall project level and are edited in a separate data entry window. The number of sub-configuration and case nodes under the Reference model node is unlimited. In this example, the Reference model node has two sub-configuration nodes (named `Config`). The first `Config` node is expanded to show its own data and also two child Case nodes.

When created/added underneath a parent, a child configuration initially is an exact copy of that parent and when saved, no XML data are actually stored. Instead, all data are inherited. Only after adaptations, either directly by the user or indirectly by GSP as a result of other user actions, XML data identified as deviating from the parent are stored.

The deviating data can be seen in the Details panel view of the project window (the default location is next to the Model panel).

As there are two data storage layers between a case and configuration, the user can easily revert to a state prior to editing. Also the inheritance mechanism can be used, reverting to parent and thereby undoing all changes in a child configuration or case. Results from different cases can easily be compared since the output tables and graphical output can be fed from different cases [28].
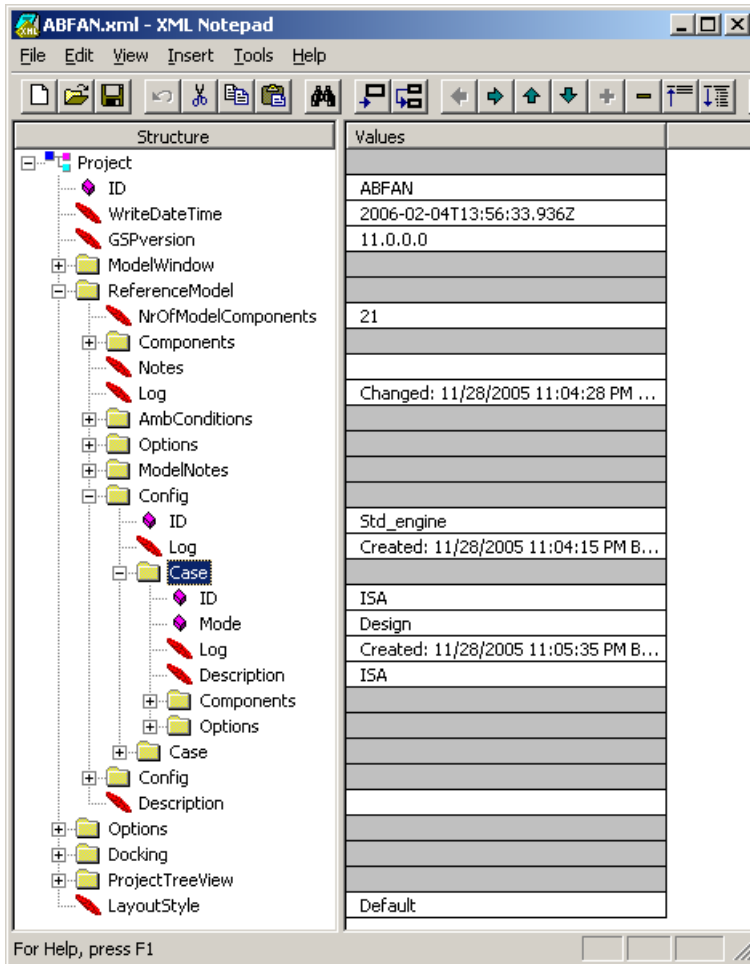
Figure 10.3   Configuration and case inheritance in XML

10.5.2   XML data controller and parser

For the configuration and case management inheritance mechanism to work, efficient algorithms have been developed for linking the model data to the XML data in the project tree. Upon activation of a configuration or case in the project tree, a local copy is made of the XML data that may be saved by the user to the overall project after completing data specification. When moving to (or creating a new) configuration or case, the local XML copy, if changed may be saved first, and then filled with data from the new selected node.

The special WVCOMPS14 [75] data entry components (see also section 10.1) automatically read and write model data to and from the XML data. A parser has

been developed to convert between the GSP model data and the XML data stored in the project files.

A particular challenge lies in the question of how to determine whether configuration or case data are equal to those in its parent or not. When saving a configuration or case, first all model data are stored in the local XML structure. However, data that are equal need not be stored in XML and instead must be inherited. To accomplish this efficiently, a fast recursive algorithm (procedure calling itself repeatedly) has been developed comparing node data (including all sub-node data) to its corresponding parent that deletes the node if found equal. So after saving all data, this algorithm is always called to 'clean' the XML from all data that is 'obsolete' because it is equal to that in its parent.

In large projects with many configuration and case levels, this process may take quite some computation time (leaving the user waiting when switching cases) so improvements to the algorithms may be considered for the future.

Upon reading configuration or case data, an algorithm has been developed that, in case no XML data are found for a model component, starts 'climbing' up the inheritance tree until it finds corresponding XML data.

10.6   Consistent data entry rules

The project tree concept with separate nodes for configurations and cases that may also inherit from parents requires a number of rules to prevent the user from entering conflicting data. Major rules include:

- Configuration input data (gas turbine configuration, model components, design parameters, input that affects the model NDE set etc.) can only be edited in Configurations.
- Simulation input data ('run case data') can only be entered in Cases.
- Cases can only have cases as children.
- When editing data in configurations or cases that have children,
    - Checks must be made whether adaptations have been made in the corresponding data in the children,
    - If this is the case, the user must be warned and asked whether or not to overwrite the data in the children with the new data specified in the parent.
    - This means the user may decide whether or not to propagate changes in a configuration into all children configuration and cases.

Detailed information on data entry rules is given in the code [75, 76] and documentation [28-31].

Chapter 11 Numerical processes in a GSP modelling and simulation session

11.1   Introduction

The following sub-sections describe the internal processes in GSP during a simulation session. The TJET.MXL simple turbojet model shown in Figure 11.1 (used also in the 'Quick start basics' tutorial in the GSP User Manual [28]) is used here as an example. The 'external' process that is visible to the user is not extensively described here since this is best shown by simply using the tutorial itself. Also, the GSP Technical Manual [29] describes the internal processes inside GSP to a limited extent.
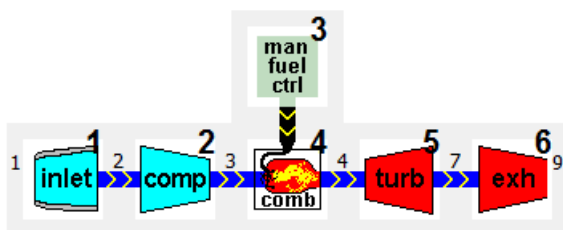
Figure 11.1 GSP turbojet model configuration

Note that GSP version 11 is used here, which has a case and configuration management layer on top of the model structure, explained in sections 10.3 and 10.5. As such, a GSP model is a *configuration* in a GSP 11 *project* and a *case* represents the specific set of conditions at which to run the simulation.

11.2   Model creation

Although in most cases an existing model is used as a template for a new model, one can start from scratch and build a model by copying component models from the GSP component libraries to the *Reference configuration* in the project tree. Later, child configurations with model adaptations or extensions can be added. The components can be linked together by the user corresponding to the desired gas turbine system configuration. GSP will prompt the user to specify station numbers. Next, the component date entry dialog windows can be opened to configure the components by specifying design point data and off-design data such as maps. After completion, a case can be added as a child of the configuration and simulation input specified after which a simulation can be run. Finally, the case and configuration

can be saved in the project, which in turn can be saved to hard disk for later retrieval and reuse, for example further extending the model and running additional simulations.

Note that the component objects are *instantiated* (see section 6.5.1) upon creation of the model in the particular *configuration* or *case*. In the following flow charts (Figure 11.2 through Figure 11.6) the grey background elements indicate components and data that are instantiated during runtime upon model initialisation (corresponding to the *Model elements* on the left in Figure 6.3). The white background elements are data and procedures in the overlaying model that is controlling the simulation process (corresponding to the *Model procedures* on the right in Figure 6.3).

For the turbojet model example the user will have to only add an Inlet, Compressor, Combustor, Turbine, Exhaust nozzle and Manual Fuel control component as shown in Figure 11.1. Next he will have to specify design point data, assign the same shaft to both compressor and turbine, so they are coupled and also assign the shaft speed as being a free state variable.

11.3   Model initialization

Before any Off-Design (OD) simulation, a Design Point (DP) simulation is required to define the engine design as described in section 2.6.4. Consequently, DP simulations are run both for design point analysis and for initializing a model for OD performance analysis. Prior to a DP calculation, the model is initialized and then the following checks are made:

- Are all component gas path interfaces linked?
- Are all external and control inputs linked?
- Are all required component data specified?
- Is the model configuration consistent (no circular references and impossible gas path links)?
- If design point calculation equations are used, are the number of states and errors equal so a Newton-Raphson iteration can be performed?

If no problems are found, the *component calculation order* will be determined. This means an algorithm is run, arranging the components in an order suitable for subsequent calculation of the thermodynamic, control and other calculations in each component. Usually, a number of simple non-gas path components come first (e.g. defining operating point constants, control inputs, scaling and user defined constants), and then gas path components starting with the (sometimes more than one) inlets and ending with exhausts. Finally, post processing components are added. For some cases, the user is able to control the order, for example the non-gas path component calculation order and, in the case of multiple inlets, the inlet with which to start. Also in the case of a splitter or fan, which of the two downstream gas

paths is handled first, can be user specified. The rest of the gas path components are automatically arranged in the correct order.

In our example turbojet model of Figure 11.1 the order automatically becomes: Inlet – Compressor – Manual Fuel Control – Turbine – Exhaust nozzle. Component control components such as the Manual Fuel Control always are calculated just before the component that is controlled by it (in this case the Combustor).

11.4   Design point simulation

If initialisation errors or problems are detected, the simulation is aborted and errors are reported. If not, a DP simulation starts and runs as depicted in Figure 11.2. A top level system model simulation procedure ('`CalcDesign`') will call all component simulation routines ('`Calc`' virtual methods with component specific implementations) in the order specified in the initialization phase. For a simple DP calculation with no equations, only a single pass is sufficient to generate the design point.

Special *DP equation components* can be added to the configuration to define user defined relations among DP parameters and corresponding free states. For example, a certain design thrust level may be specified with inlet design mass flow as a *free state variable*. If there are DP equations, a Newton-Raphson iteration (see 11.5 and 11.6) starts and the series of component `Calc` routines will be run repeatedly to generate error variables as a function of state variables until convergence has been reached within a predefined tolerance (for example: iterate DP inlet mass flow towards a value that results in a required thrust level).

In the default case with no DP equations, there is no iteration and the simulation only involves a single pass through the `CalcList`.

To speed up calculation, there are two 'fidelity modes' (in code the `TDetailLevel` type): a Low fidelity mode for rapidly iterating towards the solution, using simple gas relations (omitting chemical equilibrium calculations). Then after convergence and obviously very close to the solution, the iteration is continued in high fidelity mode (chemical equilibrium and more accurate but time consuming methods) until 'high fidelity' convergence has been reached. This simple loop is not shown in the flow charts.

Finally, DP performance output parameters are calculated in a post-processing routine.

In many cases, series of DP simulations are run with one or more design input parameters varying over user specified ranges. These 'Design series' or 'DP parameter sweeps' are controlled by outside loops not shown in the flow charts.
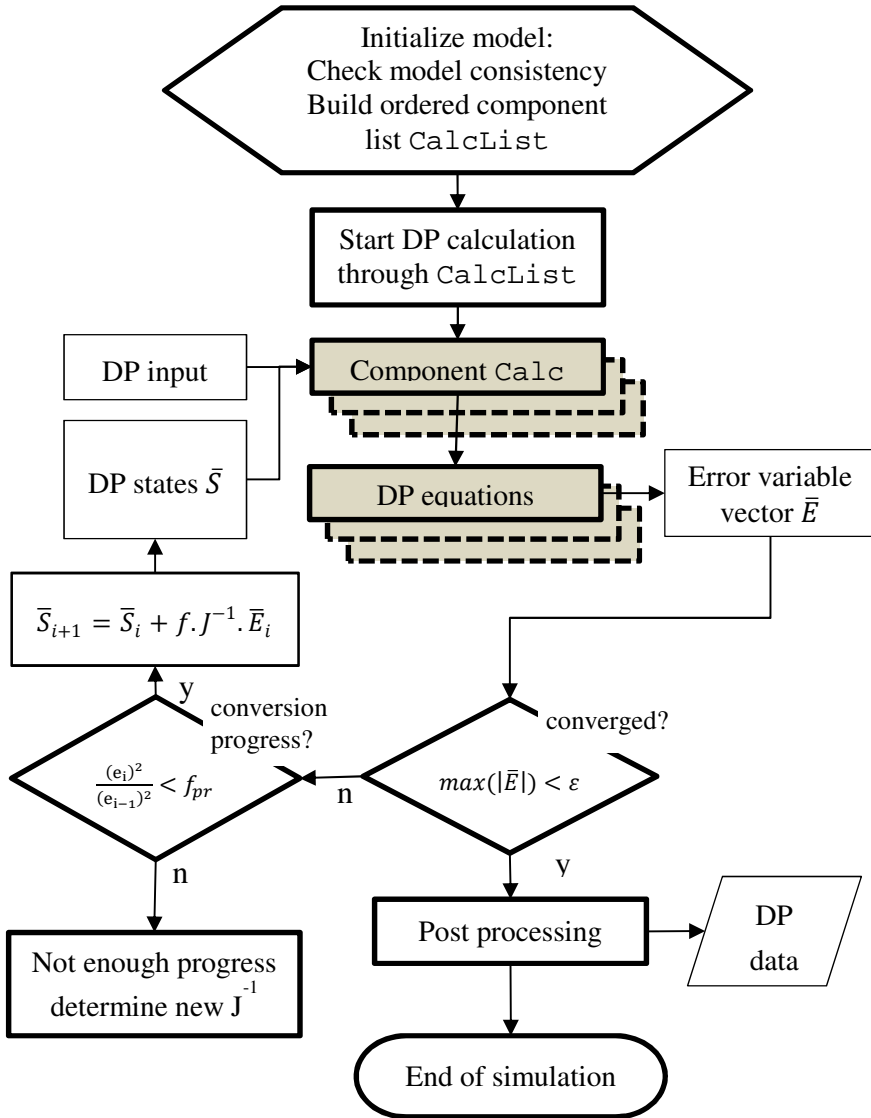
Figure 11.2 Generic GSP Design Point calculation procedure `CalcDesign`

In our example turbojet model of Figure 11.1 there are no DP equations and the DP cycle is simply calculated from inlet to exhaust with a user specified design fuel flow specified in the Combustor as shown in Figure 11.3. The Manual Fuel Control is for OD fuel control specification only. Inlet conditions are specified in the Design Flight/Ambient conditions data entry window.
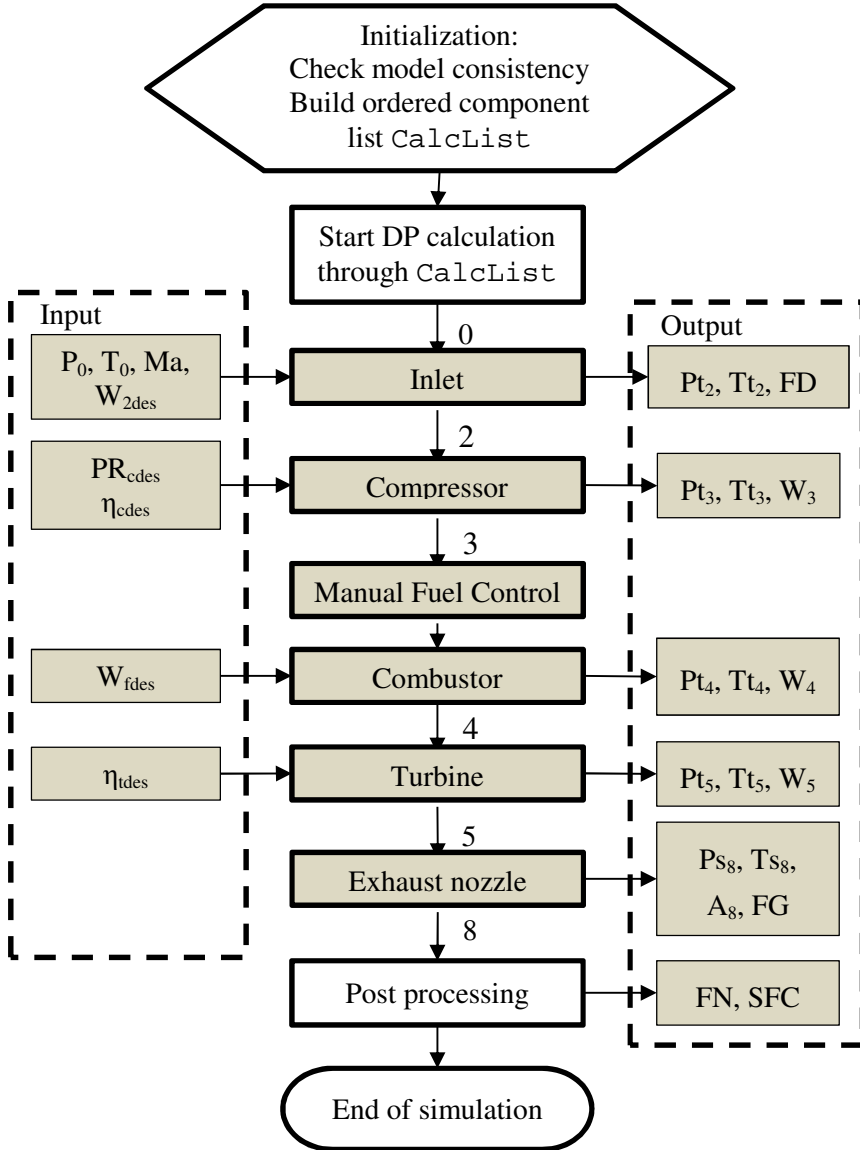
Figure 11.3 GSP Design Point calculation procedure in TJET model

11.5 Newton-Raphson iteration

In section 5.9 the Newton-Raphson method for solving gas turbine model non-differential equations is explained. In GSP, as shown in Figure 11.2 and Figure 11.5, the iteration updating $\bar{S}$ using an inverse Jacobian matrix continues until all elements in the error vectors are smaller than the user specified normalized

accuracy ε which has a default value of 0.001. As the iteration step updates of $\bar{S}$ are truncated using the program controlled factor f (see equation (5.14)), usually many steps can be made with the same inverse Jacobian J^{-1}. Progress is tested evaluating whether the reduction per step of the sum squared $\bar{E}$ is at least corresponding to the ratio f_{pr}. f_{pr} is user defined with a default setting of 0.9. If there is not enough progress, the iteration is aborted and a new inverse Jacobian calculation started.

11.6   Inverse Jacobian calculation

Figure 11.4 shows the calculation procedure of the inverse Jacobian matrix J^{-1} that is required for the Newton-Raphson iteration as explained in section 5.9. The Jacobian J is calculated by first calculating the error vector $\bar{E}$ for state $\bar{S}$ (the starting point for the subsequent iteration steps) and then for i=1..n the vectors $\bar{E}_i$ for states $\bar{S}_i$ where I denotes the element in $\bar{S}$ with a small perturbation Δs. Δs is a user specified constant with a default value of 0.001 which means a 0.1% perturbation relative to the DP state vector with all elements equal to unity (since the state variables are normalized to DP values). After successful inversion using LU decomposition, J^{-1} is passed back to the Newton-Raphson iteration.

The enhancements to the GSP Newton-Raphson method mentioned in section 5.9.1 are not shown here as they are not changing the primary methodology.

11.7   Steady state OD simulation

In Figure 11.5 the OD simulation process is depicted. First, OD state and error parameters are assigned, depending on the user specified configuration of the components. Note that as opposed to the DP equations whereby components generate user defined equations with states and error variables for the DP simulation (see section 11.4), the OD states and error for the gas path conservation laws are set up automatically by GSP. User equations with user specified OD relations such as control schedules and limits etc. can be specified which subsequently add additional states and errors. The state variables are normalized to 1 by dividing it by the design value ('des' suffix) of the particular parameter.

The OD simulation executes the components ordered in `CalcList`, generating error variables (vector $\bar{E}$) as a function of the state variables in $\bar{S}$. This is repeated with the same inverse Jacobian J^{-1} until either the convergence criterion is met or convergence progress is not sufficient as described in section 11.5 after which a new inverse Jacobian has to be calculated as described in 11.6.

New J^{-1} required

$$\bar{S} = \begin{pmatrix} s_1 \\ . \\ . \\ . \\ s_n \end{pmatrix}$$

Calculation at state $\bar{S}$ through CalcList

Components

Error $\bar{E} = \begin{pmatrix} e_1 \\ . \\ . \\ . \\ e_n \end{pmatrix}$

for i:=1 to n do

$$\bar{S}_i = \begin{pmatrix} s_1 \\ . \\ s_i - \Delta s \\ . \\ s_n \end{pmatrix}$$

Calculation at state $\bar{S}_i$ through CalcList

Components

$$\bar{E}_i = \begin{pmatrix} e_{i1} \\ . \\ e_{ij} \\ . \\ e_{in} \end{pmatrix}$$

$$\Delta \bar{S}_i = \begin{pmatrix} \Delta s \\ . \\ . \\ . \\ \Delta s \end{pmatrix} \qquad \Delta \bar{E}_i = \begin{pmatrix} \Delta e_{i1} \\ . \\ \Delta e_{ij} \\ . \\ \Delta e_{in} \end{pmatrix} = \begin{pmatrix} e_1 - e_{i1} \\ . \\ . \\ . \\ e_n - e_{in} \end{pmatrix}$$

$$J = \begin{pmatrix} \frac{\Delta e_{11}}{\Delta s} & . & \frac{\Delta e_{i1}}{\Delta s} & . & \frac{\Delta e_{n1}}{\Delta s} \\ . & \square & . & \square & . \\ \frac{\Delta e_{1j}}{\Delta s} & . & \frac{\Delta e_{ij}}{\Delta s} & . & \frac{\Delta e_{nj}}{\Delta s} \\ . & \square & . & \square & . \\ \frac{\Delta e_{1n}}{\Delta s} & . & \frac{\Delta e_{in}}{\Delta s} & . & \frac{\Delta e_{nn}}{\Delta s} \end{pmatrix} \text{ in } \Delta \bar{E} = J . \Delta \bar{S}$$

Invert J using LU decomposition

Success ?

n → Abort, report error
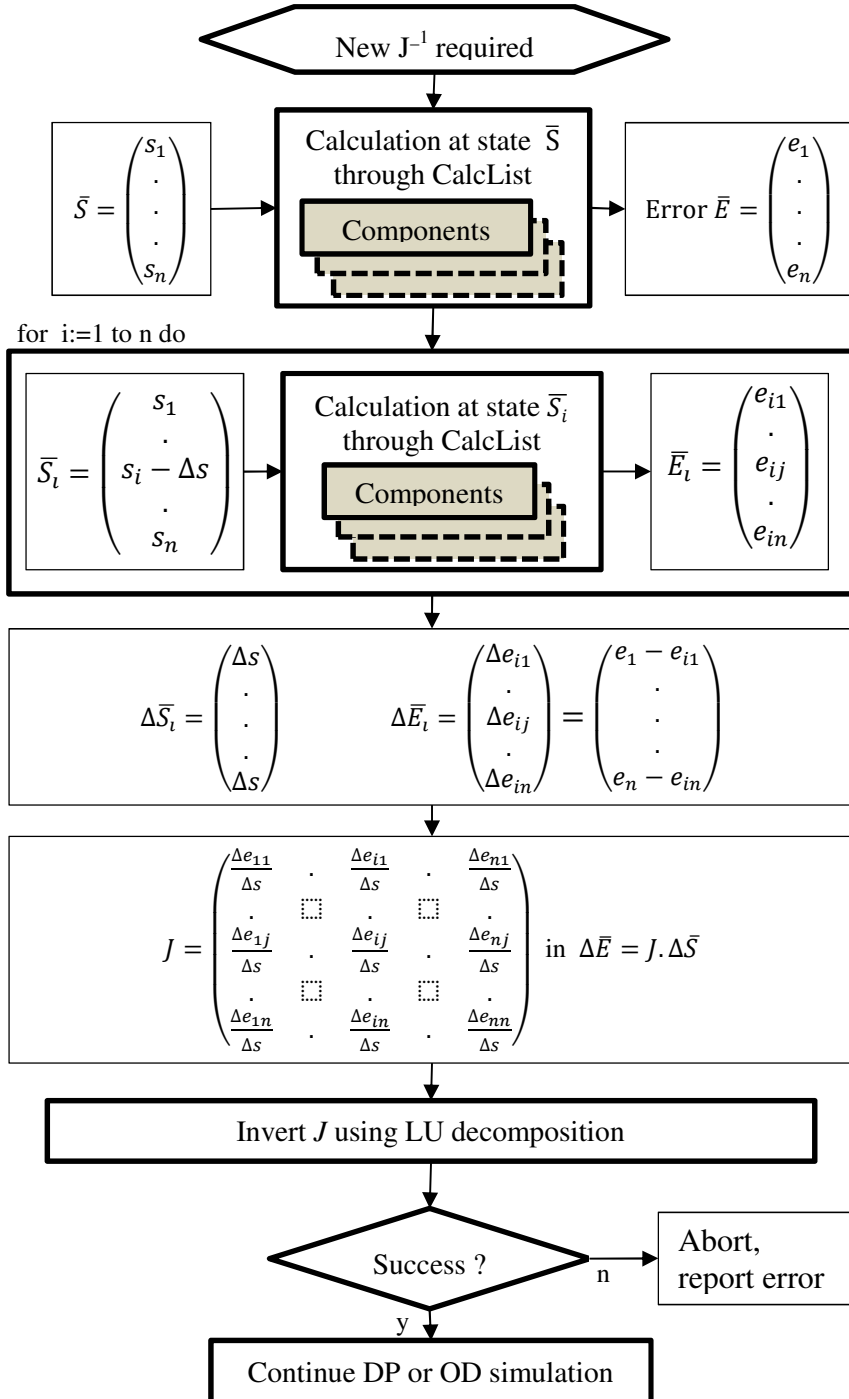
y

Continue DP or OD simulation

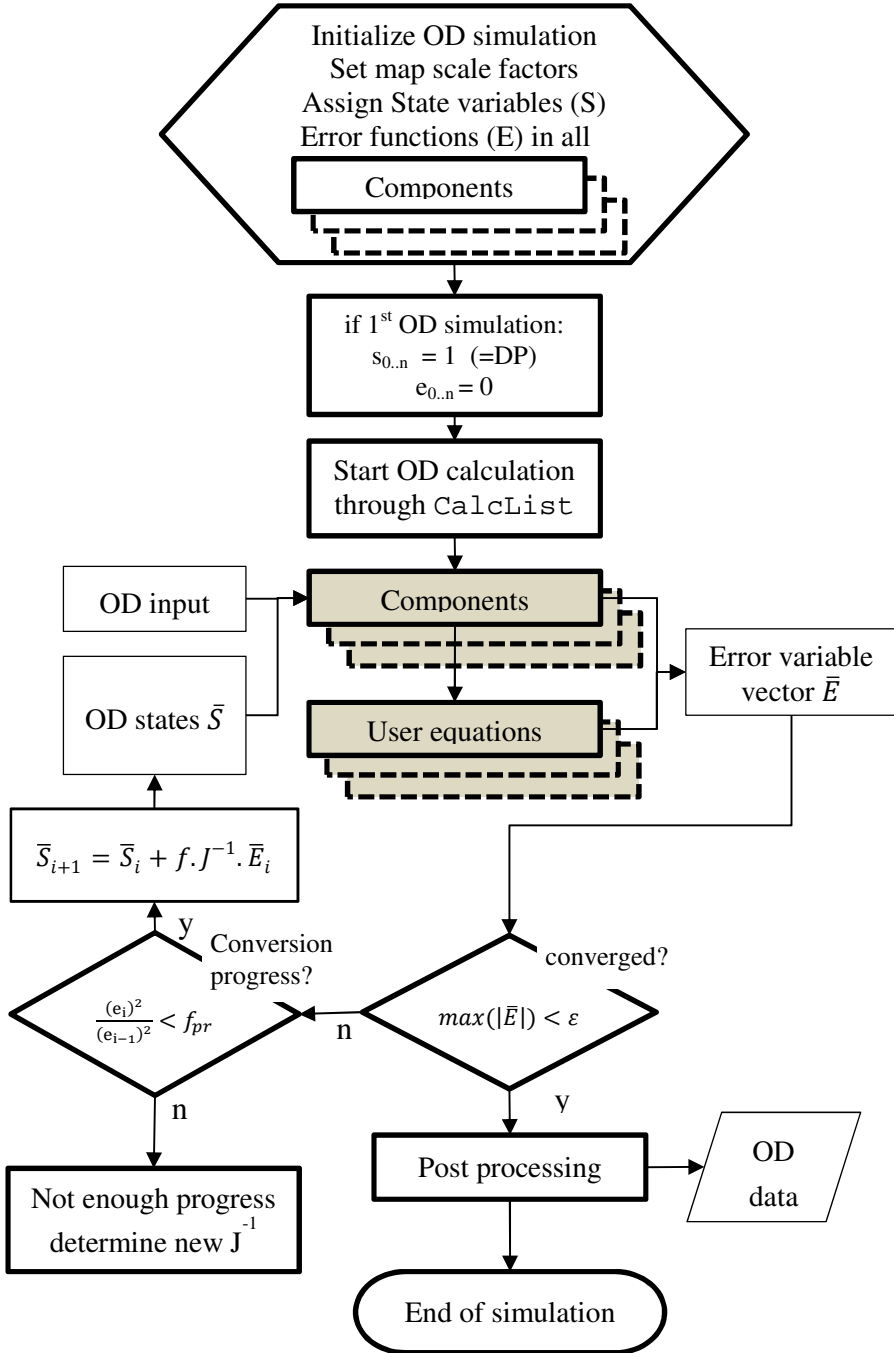*Figure 11.4 Inverse Jacobian J^{1} calculation*

Figure 11.5 Generic GSP Off-Design calculation procedure

In many cases, series of OD steady-state simulations are run with one or more input parameters varying over user specified ranges. These 'parameter sweeps' or 'steady-state series' calculations are controlled by outside loops not shown in the flow charts.

In Figure 11.6 the OD steady-state calculation procedure for the TJET example is shown. First, the following states and errors are defined automatically. Note that all states and error variables are normalized to unity in the design point by dividing by the DP value:

- *The Inlet always adds an OD state variable for the mass flow to the equation system. In this case it is the first state variable S[1]. Inlet exit corrected mass flow $W2_c$ (at station 2 in Figure 11.1) is used as it results in best stability at varying operating conditions:*

$$S[1] = \frac{W2_c}{W2_{cdes}} \tag{11.1}$$

- *The Compressor requires 2 states to define its operating point: S[2] for the rotor speed N and S[3] for compressor map Beta (the extra polar coordinate used in the MTU map format for better iteration stability [23]. In addition the compressor adds an error variable to maintain the conservation of mass: E[1] = compressor inlet flow – mass flow according to the map:*

$$S[2] = \frac{N}{N_{des}} \tag{11.2}$$

$$S[3] = \frac{Beta}{Beta_{des}} \tag{11.3}$$

$$E[1] = \frac{W2 - W2_{map}}{W2_{des}} \tag{11.4}$$

- *The Combustor does not require separate states as it depends only on fuel flow and the compressor operating point which determines the inlet air flow.*
- *The Turbine also requires 2 states to define its operating point: S[4] for turbine map β (extra coordinate in the MTU map format corresponding to pressure ratio) and rotor speed, which is S[1], shared with the compressor and thus already defined. Two error variables are added: E[2] for the power balance (conservation of energy) on the shaft and E[3] for conservation of mass: turbine inlet flow W4 - mass flow according to the turbine map $W4_{map}$:*

$$S[4] = \frac{Beta}{Beta_{des}}$$ (11.5)

$$E[2] = \frac{PW_t * \eta_m - PW_c}{PW_{tdes}}$$ (11.6)

$$E[3] = \frac{W4 - W4_{map}}{W4_{des}}$$ (11.7)

- *The Exhaust nozzle component adds the final error variable for conservation of mass: the exhaust inlet mass flow W5 minus the exhaust nozzle exit flow as calculated from inlet gas conditions and nozzle area W8:*

$$E[4] = \frac{W5 - W8}{W8_{des}}$$ (11.8)

In this example, the user defined station numbers are used to identify the parameters (e.g. 2 for inlet exit in W2) for the sake of clarity to the reader. Internally in GSP, the parameters are not identified by station numbers but related to the inlets, exits or shaft numbers of the component. As such, every GSP component 'knows' when and how to add states and errors to the equation system automatically. The states and errors are expressed in parameters that are defined *within the scope of the particular component class*. This approach is essential for a truly generic component stacking architecture offering ultimate flexibility in terms of gas turbine model configurations. The components only link with their 'outside worlds' *dynamically* (i.e. during program execution) at model initialization, when relations with the global state and error vectors $\bar{S}$ and $\overline{E}$, shafts and other component objects and secondary airflows are defined in program memory. Component inlet and exit gas conditions (flow, P, T and gas composition) are shared with adjacent gas path components using special gas path interface object classes.

Several rule sets and checks are built in the component drag-and-drop interface to guarantee a consistent set of states and errors (equal number of states and errors). Gas paths always must start with inlets and end with exhausts nozzles, gas path and control connectors must always be linked to a corresponding component.

Although in most cases with customary gas turbine configurations there is no need for the user to interfere, the user has some control over the states and error building for special cases. If then the equation system becomes inconsistent (number of errors and states not equal) an error is reported.

Initialize:
set map scale factors,
assign State variables (S) and Error
functions (E). determine first J^{-1}

Input

P_0, T_0, Ma

Start OD calculation
through `CalcList`

0

$S[1] \rightarrow W_{c2}$

Inlet

2

$S[2] \rightarrow N$
$S[3] \rightarrow \beta c$

Compressor

$E[1] = \dfrac{W_2 - W_{2map}}{W_{2des}}$

3

$W_{f\,OD}$

Manual Fuel Control

Combustor

4

$S[2] \rightarrow N$
$S[4] \rightarrow \beta_t$

Turbine + map

$E[2] = \dfrac{PW_t * \eta_m - PW_c}{PWtdes}$

$E[3] = \dfrac{W_4 - W_{4map}}{W_{4des}}$

$\bar{S}_{i+1} = \bar{S}_i + f.J^{-1}.\bar{E}_i$

5

Exhaust nozzle

$E[4] = \dfrac{W_8 - W_5}{W_{8des}}$

8

y

$\dfrac{(e_i)^2}{(e_{i-1})^2} < f_{pr}$

$max(|\bar{E}|) < \varepsilon$

n

n

y

Post processing

OD performance
FN, SFC etc.

Not enough progress
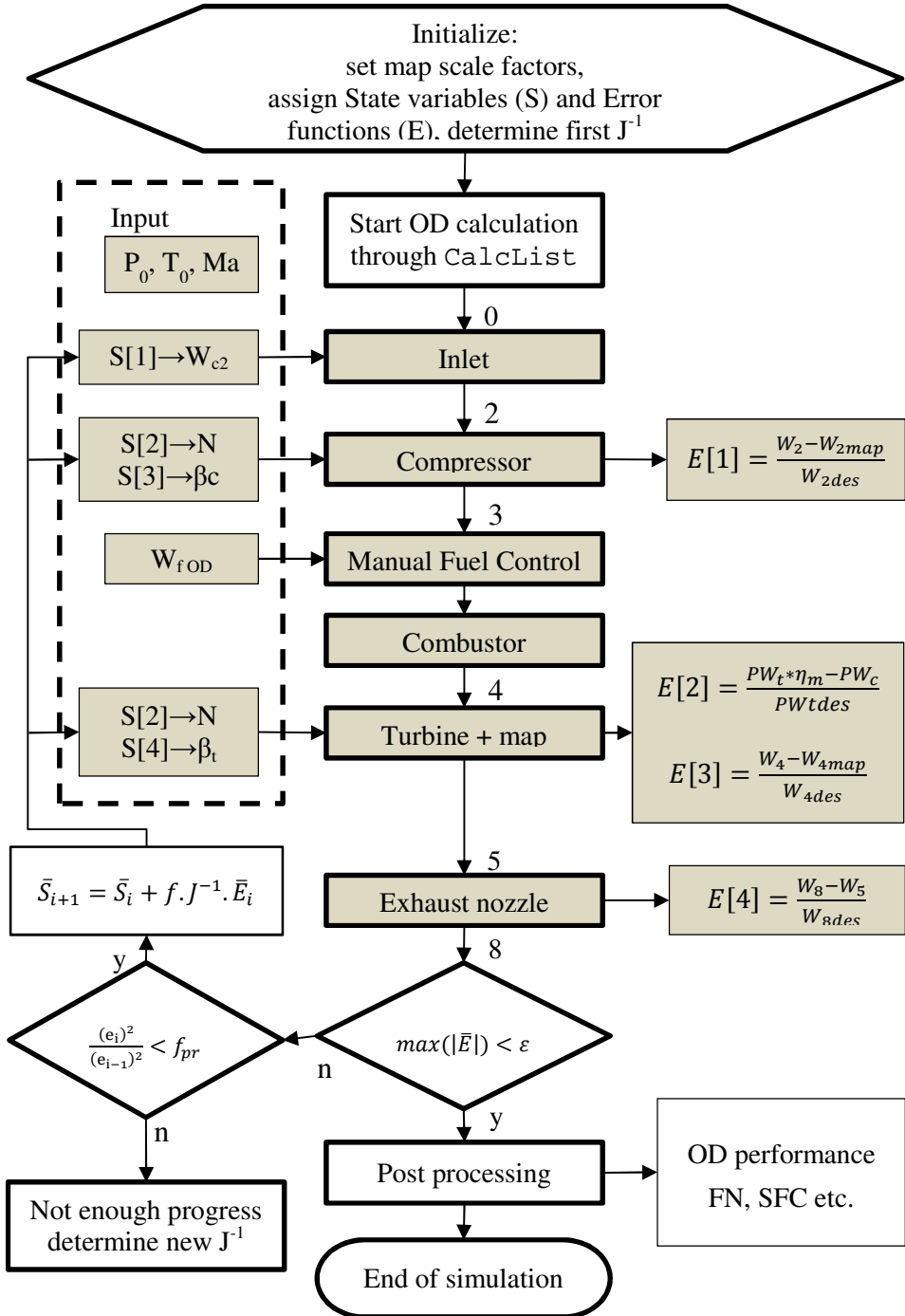determine new J^{-1}

End of simulation

Figure 11.6 GSP Off-Design calculation procedure in TJET model

If the states and errors are specified such that a singular Jacobian matrix would result, an error is reported when inversion of the Jacobian is attempted. A singular Jacobian would result for example if a state is defined that has no effect on any of the error variables, or an error variable is insensitive to all states.

The state and error adding procedures are virtual. This means state and error manipulation is handled in virtual ancestor components where possible, so code duplication of is avoided and object orientation benefits used optimally. The compressor for example inherits its shaft state variable from its ancestor Turbomachinery component class which includes all code common for turbomachinery (see section 6.4 and Figure 6.2).

11.8   Transient simulation

The OD simulation procedure is used for either a steady-state or a transient simulation. In the latter case the time derivative terms in the conservation equations (see section 5.6) become active and subsequent quasi-steady state operating points are calculated for successive time steps. As such, the internal procedure for transient simulation is technically the same as for steady-state.

11.9   Analysis of results

Simulation output can be presented in various ways. Single *operating point reports* in text format can be generated that show the engine state at the point where the simulation stopped. Often however, series of operating points are generated and then the table output is more convenient from which graphs can be plotted in many forms. With transients, separate transient output tables are used with an extra column for the time variable.

11.10   Inside the GSP code

GSP is developed in the Delphi© software development environment, offering excellent overview of code, embedded documentation options, debugging capabilities and other features. It is based on Object Pascal which offers clear code readability and compiler checking functions (superior to C/C++) while retaining the flexibility of the widely accepted C/C++ language as a standard.

As a result, for further information on the internals of GSP, the code with embedded comments can be used along the GSP documentation [29-31].

Chapter 12 A Generic Approach for Gas Turbine Adaptive Modelling[7]

12.1 Introduction

The last few decades have provided gas turbine performance engineers with increasingly powerful modelling tools. At an early stage, the opportunity was identified to use simulation models for test analysis and diagnostics purposes, requiring modelling of deterioration and fault effects. Much focus was put on gas path analysis (GPA) methods, linking measured gas path parameter deviations to engine condition. A large number of publications show the development of different GPA approaches including linear GPA [77-79], non-linear GPA including adaptive modelling [80, 81], neural networks [82-86] and genetic algorithms [87-90]. Linear and non-linear GPA often employ cycle models to calculate deterioration and fault effects.

An effective GPA method is adaptive modelling (AM). Adaptive models have an inherent capability to generate deterioration and fault data by adapting to measured engine performance data. The adaptation is done by adjusting component characteristics such as compressor and turbine maps. Measured engine performance is compared to baseline performance providing performance deviation data. The AM calculation translates this information into a change of the component model characteristics, which is required to match the measured data. This change is a measure for component condition relative to a reference level (for example due to deterioration) and thus represents diagnostics information as shown in Figure 12.1.

Several parameters can be used to represent component condition, depending on the type of component. Usually, the focus is on the turbomachinery components and then mass flow capacity (i.e. corrected mass flow) and efficiency are very suitable. 'Map modifier' parameters are used to represent the deviation from reference map mass flow and efficiency and as such are the unknown condition indicators in an AM calculation.

Most efforts to apply adaptive modelling GPA for diagnostics have resulted in engine type specific tools [80, 81, 91, 92]. This is due to the fact that many cycle models used as a starting point already are engine specific. Moreover, the optimal configuration of an adaptive model in terms of measured parameters and unknown condition modifiers depends on engine type [91, 92]. As a result, development of gas path analysis tools this way has required excessive implementation efforts.

---

[7] This chapter is based on: [27] W. P. J. Visser, O. Kogenhop and M. Oostveen, "A Generic Approach for Gas Turbine Adaptive Modeling," *ASME Journal of Engineering for Gas Turbines and Power,* vol. 128 GTP-04-1039, 2004.
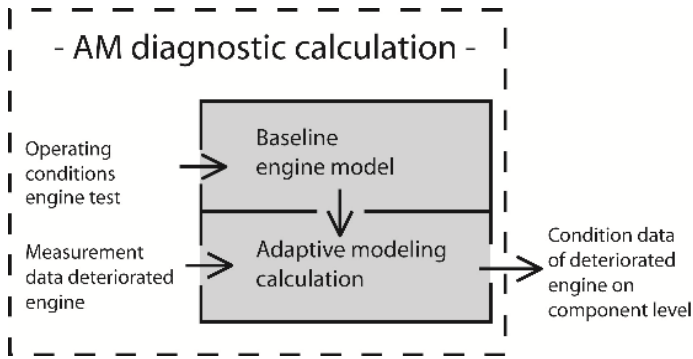
Figure 12.1 GSP Adaptive Modeling GPA

The Gas turbine Simulation Program GSP, with its built-in flexibility, offers an opportunity to develop GPA tools much more efficiently and without requiring extra coding. It has successfully demonstrated the capability to model virtually any gas turbine configuration [12, 93]. With the need for improved diagnostics capabilities in many gas turbine operational environments in the Netherlands, a research program was conducted to develop a *generic* GPA capability inside GSP. The objectives of this research program funded by the Netherlands Agency for Aerospace Programmes NIVR were to be able to:

- Turn any existing GSP model into an adaptive model.

- Rapidly configure an effective diagnostics tool for any engine type.

Although GSP was used as the environment for implementation, the concept presented can be used in any program with a flexible and generic structure.

12.2   Approach

There are two approaches to turn a gas turbine system model into an adaptive model. One approach is to use a numerical loop outside an existing model, iteratively adapting condition parameters until the model output matches the measurement. A Newton-Raphson or similar iteration then adapts the condition parameters based on model output deviation from the measurement. The advantage of the external numerical loop is that no interference is needed with the internals of the engine model

Another approach is to extend the internal equation set of the gas turbine model with equations that enforce the match with the measurement data, by adapting an extra set of unknowns in the equation set corresponding to the condition deviations. The advantage is that the absence of external iteration loops provides optimal stability, convergence speed and no additional complexity. However, the AM capability must be integrated in the numerical heart of the engine model.

In GSP, the advantages of both approaches are combined using the second approach extending the internal equation set. As a result, GSP can rapidly turn any GSP engine model into an adaptive model using an 'AM control module'.

12.3   Adaptive model equations

Gas turbine cycle models normally calculate steady state or transient off-design operating points by solving sets of non-linear differential equations. The equation set represents the conservation laws that apply for the specific engine. Truly generic modelling tools such as GSP must automatically build up the equation set during model initialization [12]. The individual gas turbine component models must then be able to add any equation and free state variable to the set that is processed by a separate generic solver. An adaptive model can be represented numerically by just adding a number of equations equal to the number of measurements to adapt to. To obtain a 'square' equation set with a single solution then also an equal number of unknowns must be added representing various engine or component conditions such as efficiency and mass flow deltas or 'map modifiers'. Naturally, the condition parameter set must include realistic deterioration modes and/or faults with identifiable effects on performance via the gas path.

12.4   Object oriented implementation

Object orientation provides an efficient means to implement functionality common to different modelling elements in a simulation environment (see section 6.4). This allows the implementation of capabilities required for adaptive modelling in a single (*abstract*) component model class, common to all gas path components. The capabilities added are:

1. a list of measurement values corresponding to component performance parameters,
2. a list of condition factors to be multiplied with condition parameters such as efficiencies and map flow rates,
3. an interface to have the user select the measurements and condition factors that are active during 'adaptive simulation' mode (the user must be able to quickly change parameter selections in order to evaluate and optimize the adaptive model configuration),
4. user interface elements to present results, such as bar charts to visualize deltas on performance and component condition parameter values.

Although not essential, object orientation clearly provides significant advantages over alternative approaches to implement generic adaptive modelling functions.

12.5 Numerical methods

As explained in the previous sections, the numerical solution of the set of adapted condition factors is simply found by adding the corresponding equations to the equation set that represents the reference engine. In equation (12.1) the complete set of equations for an adaptive model is shown. The upper left section represents the reference engine: f_1 through f_n are the n error equations based on the conservation laws with the unknown states s_1 through s_n. ε represents the relative equation tolerance (convergence criterion for the conservation equations) and should be very close to zero (typically 0.0001). f_{m1} through f_{mm} represent the m additional equations added in adaptive modelling mode and simply require a model output parameter to be equal to a specified measurement value. s_{c1} through s_{cm} are the scalars representing the unknown condition factors that need to be solved for. ε_{m1} through ε_{mm} represent the separate tolerances for the adaptation to the measurement parameters.

$$
\begin{array}{ccccc|ccccc}
f_1(s_1)+ & \cdots & f_1(s_n)+ & & f_1(s_{c1})+ & \cdots & f_1(s_{cm}) & = & \varepsilon \\
\vdots & & \vdots & & \vdots & & \vdots \\
f_n(s_1)+ & \cdots & f_n(s_n)+ & & f_n(s_{c1})+ & \cdots & f_n(s_{cm}) & = & \varepsilon \\
\hline
f_{m1}(s_1)+ & \cdots & f_{m1}(s_n)+ & & f_{m1}(s_{c1})+ & \cdots & f_{m1}(s_{cm}) & = & \varepsilon_{m1} \\
\vdots & & \vdots & & \vdots & & \vdots \\
f_{mm}(s_1)+ & \cdots & f_{mm}(s_n)+ & & f_{mm}(s_{c1})+ & \cdots & f_{mm}(s_{cm}) & = & \varepsilon_{mm}
\end{array}
\tag{12.1}
$$

A more compact notation for equation (12.1) using vectors is

$$
\overline{F}(\overline{S}) \leq \overline{\varepsilon}
\tag{12.2}
$$

with $\overline{S}$ including both the s and s_c elements and $\overline{\varepsilon}$ including elements equal to the conservation equation tolerance ε and measurement tolerances ε_m. The equations representing the adaptation constraints for a measurement i are

$$
f_{mi} = P_{i\,mdl} - P_{i\,meas} \leq \varepsilon_{mi}
\tag{12.3}
$$

with $P_{i\,mdl}$ and $P_{i\,meas}$ the adapted and measured values of parameter P_i respectively.

A Newton-Raphson based (or other) solver can be used to iterate towards the solution and at this stage there are no further numerical additions required. The absence of outside iteration loops provides optimal stability and minimal complexity.

12.6   Reference models

The objective is to extend an existing gas turbine model with an adaptive modelling capability, without having to interfere with the model itself. In GSP, this can be simply done by drag-and-drop of the adaptive model control component icon (top-left in Figure 12.2). With adaptive mode turned off, the model represents the reference or baseline engine.
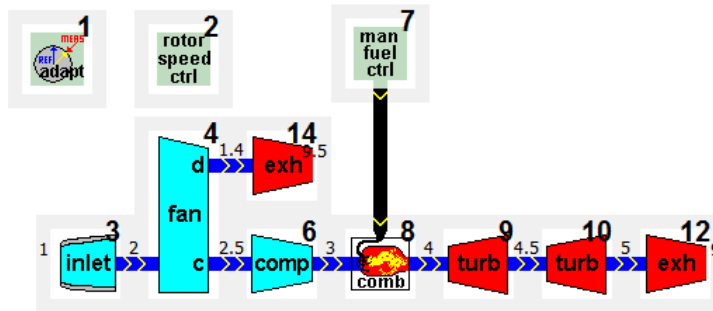

Figure 12.2 GSP model with (top-left) adaptive model control icon

The reference model must be tuned to performance data in order to obtain an accurate baseline. This means matching the model design point to a specific engine operating point data set, usually at high power levels at standard conditions such as maximum take-off thrust for a turbofan engine. If necessary, model parameters can be further fine-tuned to improve the match with available off-design data. Even if component maps are not available and must be scaled from similar public domain maps, errors can be kept small as long as the operating point stays close the design point. This is the case for example with gas path analysis diagnostics on maximum take-off power engine pass-off tests at KLM engine overhaul facility Amsterdam (see the case study addressed in section 12.13).

The accuracy of the reference model match (with reference engine performance data) affects the adaptive model simulation process. Reference engine model errors will interfere with the adaptive modelling numerical solution. Therefore, 'calibration factors' f_c are introduced, compensating the adaptive model numerics for model errors. Equation (12.4) shows how a model parameter $P_{i\_mdl\_raw}$ is calibrated using the ratio of the design point measured and model parameter values.

$$P_{i\,mdl} = P_{i\,mdl\,raw} \cdot f_{ci}$$

$$f_{ci} = \frac{P_{i\,meas\,des}}{P_{i\,mdl\,des}}$$

(12.4)

Normally, if an accurate design point match has been obtained, the f_c factors are very close to 1. The f_c factor calibration method was found to have a significant effect on adaptive model stability and results, even if the f_c factors only deviated 1% from unity.

Another important consideration is the source of the data for tuning the reference engine model design point. This source is optimally the same engine test bed under the same calibration settings. Data from a single engine test, well corresponding to the average (new or overhauled) engine performance, are usually sufficient to be used for an entire engine fleet and this approach has been used for the case study at KLM. Even better results would be obtained if a range of engine tests would be used and averaged to eliminate measurement scatter effects. Ultimately, the best but also most laborious approach would be to match models to every new engine at the start of its service life (or time between overhaul) and keep the model for diagnostics for the particular engine. Then engine to engine variation is eliminated and performance deviations will be due to deterioration or faults only. This approach may well be applied in the future in on-wing or remote-wireless continuous engine monitoring systems [94-98]. With the adaptive model continuously running on-board in the FADEC, more interesting opportunities emerge, such as adaptive control logic [99].

12.7   Selection of parameters

The 'square' equation set with an equal number of measurements and conditions parameters is the most straightforward approach. However, the number of condition parameters and especially measurements may vary among engine types and applications. Ideally, a large number of accurate measurements is available, covering the gas path conditions at most engine stations, and exceeding the number of condition parameters. In that case, the solution of the 'over-determined' equation set would be a minimization problem, for example using a weighted least squares method [77, 100]. In most cases however, the number of measurements is limited and often smaller than the number of condition parameters required for a complete representation of engine health including all deterioration and failure modes. Several solutions have been proposed to handle the case of fewer measurements than condition parameters, including multi-point [87, 89, 101], adding constraints or equations derived from knowledge of the (relations among) deterioration modes

[102] or working with optimized selections of condition parameter 'sub-sets', equal to the number of measurements. With the latter approach, methods proposed by [87, 91, 103] can be used to define a measurement and condition parameter set that is best able to isolate specific problems. A method suggested by [103] is used in the case study described in section 12.13.

Different sets can be used to identify different fault- or deterioration cases. With an adaptive modelling tool that can be rapidly configured, this approach is attractive and therefore has been used in the GSP diagnostics module at this stage. As will be explained in the following sections, the GSP diagnostics component includes a powerful generic GUI, allowing rapid configuration of adaptive models for any GSP modelled gas turbine engine. Results with different sub-selections of both the measurement and condition parameters can be quickly analysed.

12.8 Measurement uncertainty

The measurement tolerances ε_{ml} through ε_{mm} are independent of conservation law inaccuracy ε and represent measurement specific tolerances for the adaptation equations. The ε_m values are separately user specified corresponding to measurement uncertainty data. Normally, the ε_m values will be larger than ε and can be tuned to obtain optimal results.

With large ε_m values, solutions may be found at the extremes of ε_m margins, which are unrealistic in a sense that the deviation from the reference engine parameter value is 'ignored' by the solution. In the future, additional methods may be applied to account for statistical probability distribution of measurement error using weight factors for example. This will allow better representation of measurement error and provide solutions with maximum probability with larger measurement uncertainty margins.

12.9 Standard and adaptive simulation modes

The engine simulation tool only needs to solve the additional equations during adaptive modelling mode. The adaptation of the model can simply be deactivated by replacing the f_m equations (Equation (12.3)) by

$$f_{mi} = s_{ci} - 1 \qquad (12.5)$$

The result will be a solution with all condition scalars being equal to 1, representing the case of the healthy reference engine. Every adaptive simulation must be preceded by a standard (non-adaptive) simulation to determine the reference engine baseline performance and deltas at the particular operating point. In GSP this is done automatically.
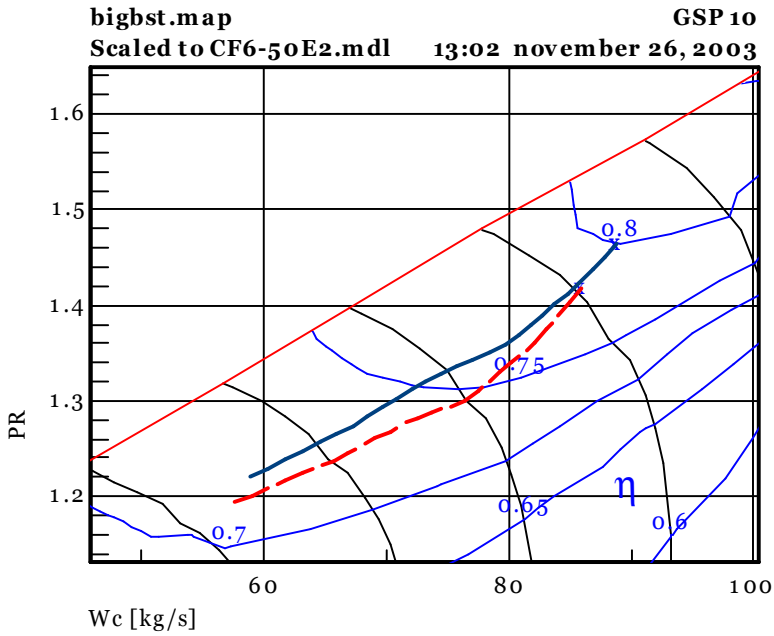
Figure 12.3 Booster running lines for reference (solid) and deteriorated (dashed) engine (case 1).
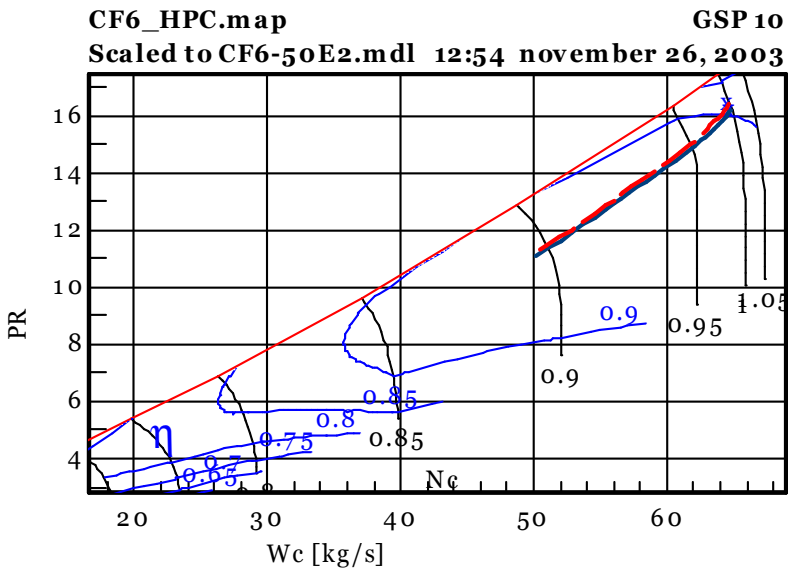

Figure 12.4 HPC running lines for reference (solid) and deteriorated (dashed) engine (case 1)

Obviously, the ability to use the same model for both performance analysis with the reference engine model and adaptive simulations and diagnostics in the same session, is very convenient. Following a diagnostics session, the performance of the adapted model can be analysed and directly compared with the reference engine by plotting curves for varying power setting for both cases in simple X-Y graphs and compressor maps for example. See Figure 12.3 and Figure 12.4 for example (representing results of the case study discussed later in this paper).

12.10 Model stability

Large measurement errors may well result in attempts to find engine operating points that are impossible, even with extreme component condition variations. In such cases the conservation equations for mass and energy can simply not be satisfied while simultaneously matching the measured performance parameters. In this case widening the ε_m tolerance margins may help to a certain extent, but with large measurement uncertainty (especially scatter) it is often better to omit the particular measurement from the measurement set.

Another problem is multiple solutions. Especially with a small measurement data set the model may adapt with unrealistic condition factors such as very high efficiencies. A slightly different measurement then may have totally different results, indicating there are multiple solutions for the condition vector $\bar{s}_c$. In this case more measurements are required to 'more tightly' capture engine performance.

In the case study with the twin spool turbofan described later in this paper, at least six parameters were required to obtain realistic results pointing in the right direction. As described in the case study section, the low-pressure section behaves more or less independently from the gas generator. If only a few parameters such as fan duct pressure and fan duct side efficiency are added, results become unstable. It appeared that either the low-pressure (fan and LPT exit) parameters must be fully omitted or sufficient measurement parameters must be added to unambiguously determine fan and LPT performance.

12.11 User interface

A major challenge is to develop a graphical user interface (GUI) capable to effectively control adaptive models based on any model configuration. For application to virtually any working cycle configuration, a highly flexible concept is required. Several examples of GUIs for GPA exist [92, 97] but these usually are engine specific, so a new approach was required.

Generic component based simulation environments usually have a GUI with separate data entry windows for individual component models. In GSP for example, these are accessed by double-clicking the component icons shown in Figure 12.2. This approach can easily be used for the adaptive modelling capability. However,

for adaptive modelling, the focus is on the engine as a system and therefore a separate single interface is required to control all adaptive modelling functions on the system model level. A concept using a tree-view with multiple columns was chosen as the best solution for this.
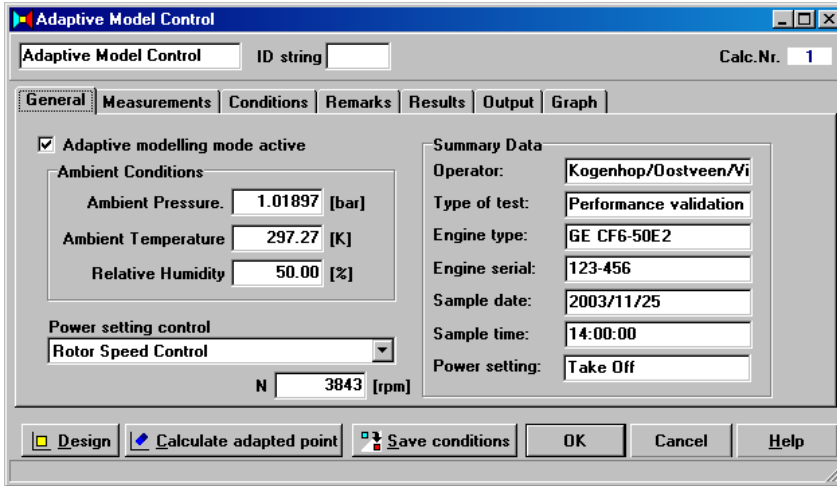

Figure 12.5 GSP adaptive model control component window

In GSP, an interface component was inherited from a 'model control component' object class that has access to all other component models. Tree-views are used including all component models as top level elements. The resulting adaptive model control window is accessed via the top left adaptive model component icon in Figure 12.2 and includes the tab-sheets shown in the following figures with screenshots.

Figure 12.5 shows the general configuration tab sheet for specification of engine and session reference data, ambient conditions and engine power setting. Depending on the model configuration, rotor speeds, fuel flow, thrust or other parameters can be specified for power setting. Two tree-views are defined, one for measurements (Figure 12.6) and one for the condition parameters (Figure 12.8).

In the Measurements tree (Figure 12.6), each component in the tree has sub-elements representing the individual performance parameters that can be used for adaptive modelling. The parameters listed depend on component type. For each parameter, measurement values can be entered and these are compared with reference model calculation results. The check boxes are used to select the set of parameters to adapt to (i.e. the parameters used in the f_m equations). Note that Figure 12.6 shows the tree-view with an option activated making the unchecked parameters invisible for user convenience. For each parameter, the reference model calculated value, the user specified measured value and tolerance for adaptation

(ε_m), the calculated delta (reference–measured), the calculated adapted value (should be within tolerance range of measured) and the error (adapted–measured, should be close to zero) are shown. Not displayed are the columns for the design point calibration factors f_c of equation (12.4). By scrolling to the right 3 columns with model design and measured design values and the calibration factors are shown.

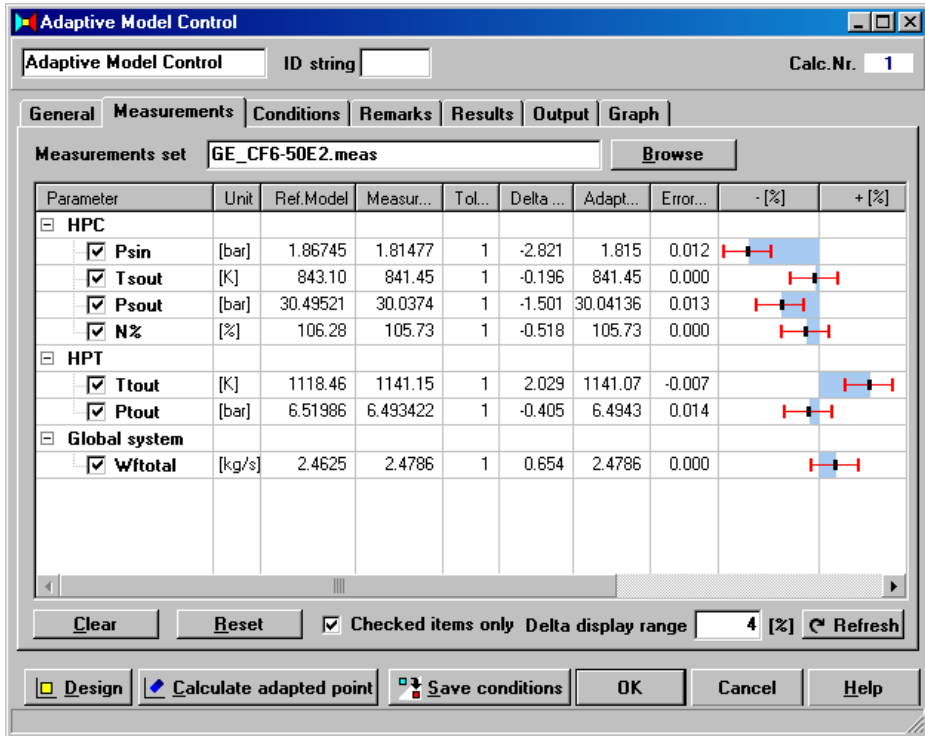*Figure 12.6 Measurements tab sheet*

Figure 12.7 Detail of Measurement tab sheet

The horizontal bars (see detail in Figure 12.7) indicate measured performance delta (solid blue bar), tolerance for adaptation ε_m (red range indicator) and the

calculated adapted value (black dot). The latter value must be in the red tolerance range for the modelling system to be accepted as a valid adapted operating point.
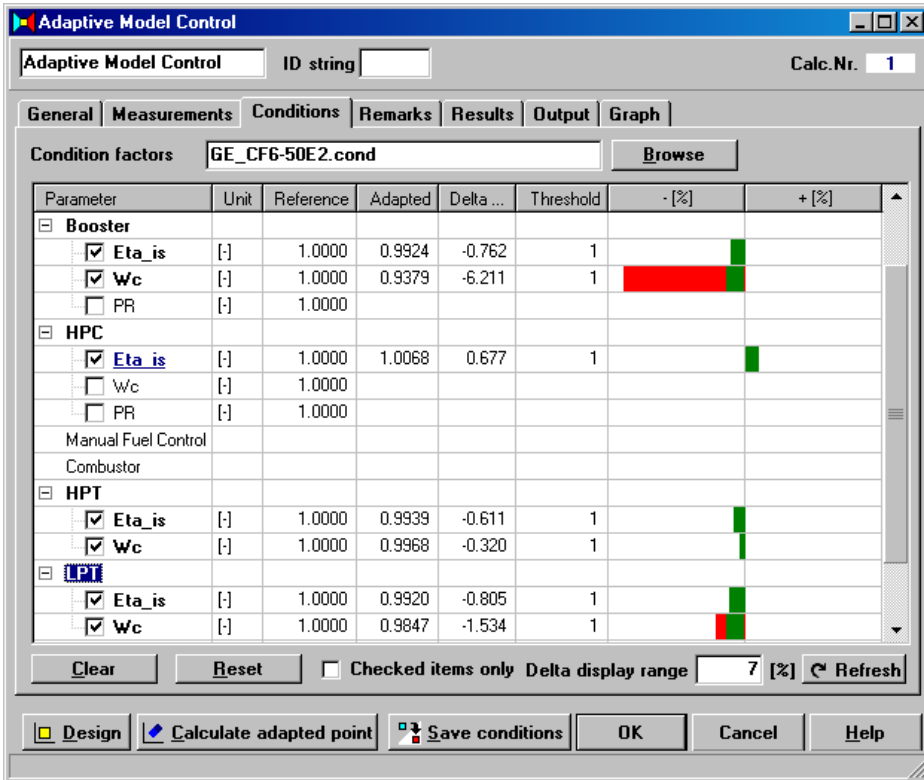

Figure 12.8 Conditions tab sheet

In Figure 12.7 a result was found exactly matching the measurement value so the black dot is in the middle of the tolerance range.

In the Conditions tree (Figure 12.8) each component has sub-elements representing the individual condition parameters (s_c) that are adapted to match measured performance. The parameters listed depend on component type. The check boxes are used to select the subset of parameters that are allowed to be adapted (i.e. represent the $\overline{s}_c$ vector). Figure 12.8 shows the tree-view with all possible condition parameters visible (the scroll bar must be used to scroll up and down to cover all components). The horizontal bars indicate the deviations of the condition parameters, thereby providing the gas path diagnostics information. Individual threshold values can be specified to indicate levels beyond which the condition parameter deviation is considered significant. Beyond the thresholds, the bars turn red. The chart can optionally be normalized to the threshold values.

Figure 12.9 shows the graphical report output of the results with both the performance and the condition parameter deltas.

The information described above can be assembled in a comprehensive diagnostics report to be printed or digitally stored for later reference. Also, event logs are kept to store settings, user comments and results generated during the diagnostics session. The resulting GUI and reporting functions enable the deployment of GSP models as user-friendly diagnostics tools.

12.12 Results

During development, the adaptive modelling component has been tested and experimented with a variety of engine models for which measurement data were available. It was found that results (stability and realistic result data) are sensitive to both model and measurement inaccuracy. The model accuracy can be improved by better tuning to known data and the use of accurate component maps (rather than maps scaled from generic ones) if available. With the addition of the user measurement tolerance and the design point calibration factors, stability and results were significantly improved.

The user interface was evaluated by several engineers and, after an evolution via several designs, approved as a tool that can be pre-configured to an effective diagnostic aid. The ultimate test was an industrial application as described in the following section.

12.13 Case study

A case study has been performed on an application that is very suitable for gas path analysis diagnostics. At KLM Royal Dutch Airlines CF6 engine maintenance facility, CF6 family engines are overhauled and finally submitted to a 'pass-off test' before being returned into service. GPA is one of the techniques used to diagnose problems indicated by deviating or unacceptable test bed measurement results. Costs could be significantly reduced if more accurate GPA tools than those currently used were available. Therefore, the GSP tool was tested on a number of cases with CF6-50 engines to assess its potential. Two cases will be described in this section.

First a baseline model was developed and tuned to data measured on an average healthy turbofan engine. This data point corresponds to the GSP design point. In the adaptive model component, the residual design point deviations are stored in the design point calibration factors, to be later used for adaptive modelling mode. Note that the GSP design point is at arbitrary ambient conditions. Power setting in GSP (and on the test bed) is represented by a particular N1 fan rotor speed using the GSP rotor speed controller.

Next, the measurement data of the problem engine under consideration are entered in the particular measurement column in the data entry window shown in Figure 12.6. In this case either fuel flow or N1 rotor speed can be used to specify power setting (i.e. represent an input parameter). If N1 is chosen, then fuel flow can be defined as a measurement parameter and vice versa.

To obtain an optimal measurement set, the parameter offset method as suggested by [103] was applied. This method provides a ranking of measurement parameter sensitivities to (1%) component condition parameter offsets. A cycle simulation tool such as GSP can be used to determine the individual sensitivity values. The parameter set should be selected from the top of the sensitivity ranking order. In Table 12.1 the ordered lists of the 9 measurement parameters available are shown for the two alternative power setting parameters available.

Table 12.1   Measurement parameter sensitivity rankings

	Wf = control parameter	N1 = control parameter
1	Ps2.5	Pt4.5
2	Pt4.5	Ps2.5
3	Ts3	Wf
4	N1	N2
5	N2	Tt4.5
6	Ps3	Ps3
7	Tt4.5	Ts3
8	FN	FN
9	Pt1.3	Pt1.3

Although the power setting parameter has an effect on the ranking, the diagnostics end results are not significantly affected by the power setting selection, as may be expected. For the case study, N1 was chosen as power setting parameter since N1 is also the test bed power setting indicator.

Condition parameters were selected using engineering judgement and trial and error. With the powerful GUI, many combinations can be tested very rapidly.

Best results were obtained with the top 7 measurement parameters from Table 12.1 including Ps2.5 (booster exit), Ps3, Ts3, N2, Tt4.5 (EGT), Pt4.5 and Wf. Extending the set with the remaining number 8 or 9 parameters FN and Pt1.3 did not generate stable and realistic results with any combination of condition parameters. Using 9 parameters including both Pt1.3 and FN prevented the model from finding a solution at all. This is due to the strong correlation between FN and

Pt1.3. As a result, the set could not be extended to include fan conditions at this stage due to the limited data for the low pressure system performance. It is expected that with additional measurements such as hot exhaust (station 5) pressure and/or temperature this could well be improved. This will be the subject of future research.

Case 1

With the 7 parameters described above, a diagnostics session was performed on a CF6-50 engine with a low EGT margin. The engine test indicated an EGT of 23 K over the expected value for a healthy engine but still within acceptance limits. For GPA this means a more difficult case due to the relatively small performance deviation.

Condition factors chosen for this case were booster efficiency and mass flow, HPC efficiency, HPT efficiency and flow capacity and LPT efficiency and flow capacity. As explained above, this set is mainly focused on booster and gas generator health and will not be able to identify fan problems.
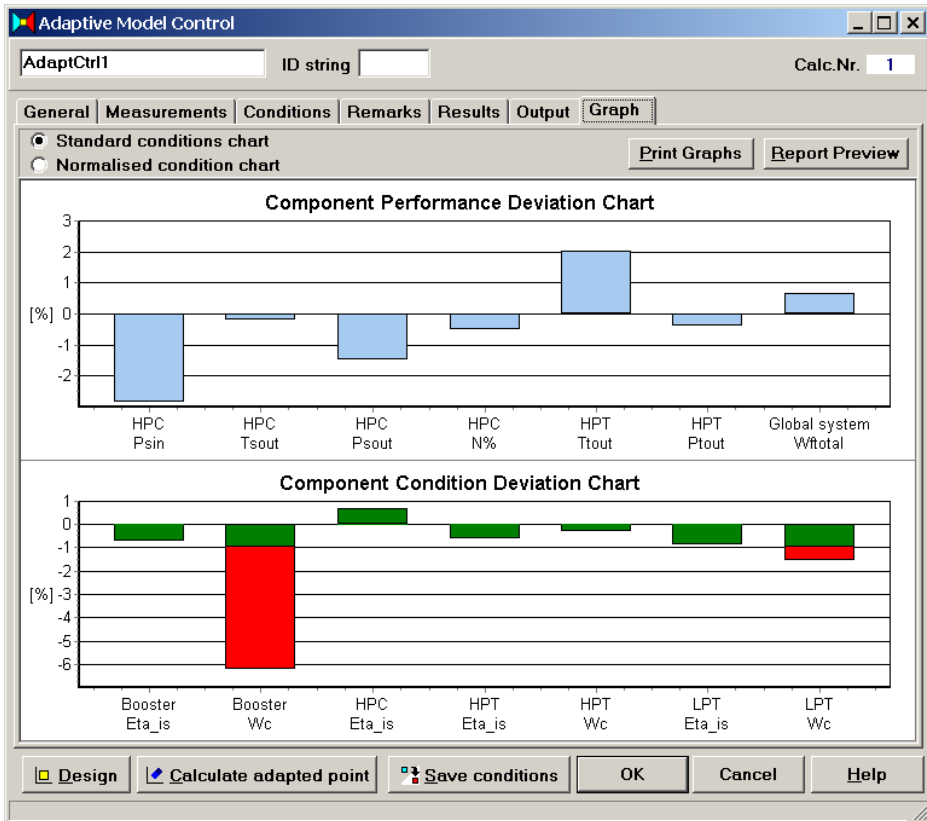

Figure 12.9 Gas path analysis results chart window, case 1

Results are shown in Figure 12.9 depicting a screenshot of the 'Graph' tab sheet of the adaptive model control window. The upper part of the figure depicts the performance deviation relative to the reference engine. The lower part of the figure shows the adaptations needed to fit the base model to the measurement set. As stated above, the performance delta is small, i.e. within 3% for all 7 parameters (including the 23 K EGT delta). The adaptive model calculation indicates the booster to be responsible for the poor performance due to a flow capacity problem. Since the booster has no variable geometry, VSV mis-rigging is ruled out as a cause, leaving at least blow-off valve leakage or tip clearance as candidates for further investigation. This outcome was confirmed after further analysis at KLM, proving the accuracy of the GSP adaptive model to identify engine problems on component level.
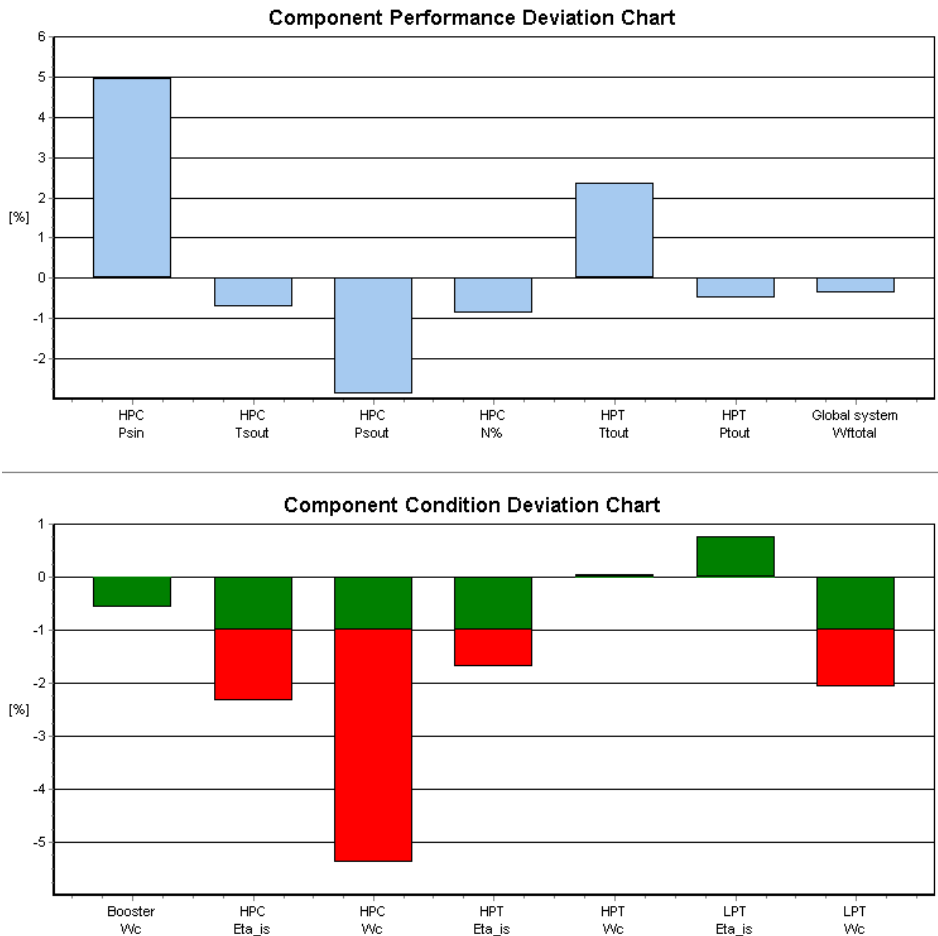
Figure 12.10 Gas path analysis results case 2

After a valid diagnostics result has been found the resulting adapted engine model performance can be analysed. The deterioration deltas are stored in the model and adapted (deteriorated) versus reference engine performance can be compared at various other operating conditions and power settings.

Figure 12.3 (earlier shown in this paper) shows the calculated booster running lines for the case 1 reference and deteriorated engine in the booster map. A significant shift away from the stall limit is shown as may be expected from the deteriorated booster flow capacity. Figure 12.4 shows the HPC running line is not significantly affected as may be expected if only the booster condition has changed.

Case 2

In a second case, an engine was analysed that was rejected at the performance test after overhaul. The performance test was eventually passed after replacement of the HPC during a second shop visit, although this was not recommended by the available conventional diagnostic methods. However, the GSP adaptive model indicated an HPC mass flow deficiency (Figure 12.10), thereby clearly proving its capability to effectively isolate component faults.

Note that the condition set is different from case 1 and includes HPC mass flow instead of booster efficiency. The case 1 set was used first but did not generate realistic results, which was caused by the absence of the condition factor responsible for the engine problem. Case 2 demonstrates the benefit of the ability to rapidly evaluate results with different condition parameter sets.

12.14 Conclusions

Generic gas turbine simulation environments can be extended to generic adaptive modelling tools for diagnostics and gas path analysis of deteriorated engine performance. Critical elements for the extension are

- modelling structure,
- flexibility with regard to the model equations and numerical methods and
- graphical user interface (GUI).

With the flexible object oriented architecture of GSP an efficient implementation has been realized and demonstrated. It allows automatic addition of the necessary equations for the model adaptation to measurement values.

A tree-view based GUI has been developed that adapts to any gas turbine model. Different combinations of measurement and condition parameter sets can be rapidly evaluated and optimized for specific engines and deterioration types. The different sets can be saved and later activated on request to verify different hypotheses and assumptions with regard to the engine problem.

Component faults were successfully isolated in a number of test cases with a high bypass turbofan engine. The GSP adaptive model control component turns

existing GSP models into adaptive models that can be rapidly configured to become powerful user-friendly GPA (gas path analysis) tools.

The adaptation function can be applied to new GSP component models derived from existing using object inheritance. Condition factors and measurement equations can be added for any component model. This means other system models including additional systems such as load compressors and combined cycle components can be included for GPA diagnostics.

The user-friendly GUI enables the deployment of GSP models as diagnostics tool for maintenance engineers. The user can pre-configure the adaptive model and quickly optimize gas path diagnostics capability using experimentation with field data. The tool is being used by KLM engineers on a routine basis [104, 105].

Future work is planned to enhance GSP's adaptive modelling and diagnostic tool capabilities, including:

- application to cases with more measurement data (i.e. including exhaust gas pressure and/or temperature),
- adding a numerical minimization option for cases with more measurements than condition factors,
- exploration of feasibility of multi-point GPA,
- additional methods to compensate measurement uncertainty (constraints on and relations among condition parameter variations),
- separate GSP adaptive modelling versions with optional hiding of model configuration data entry items to provide a secure and user friendly diagnostics tool at flight line or test bed.

Chapter 13 Real-Time Gas Turbine Simulation[8]

13.1   Introduction

Real-time simulation of gas turbine engine performance is used in a variety of aerospace applications. For simulation of propulsion system performance in flight-simulators, fidelity requirements become increasingly stringent. Significant improvements in simulation fidelity can be obtained when using thermodynamic models instead of the customary (piece-wise) linear real-time models. However, real-time thermodynamic models require sophisticated methods to efficiently solve the model equations on a real-time basis with sufficient speed.

The 'Turbine Engine Real-Time Simulator' (TERTS) is a component-based real-time modelling environment for gas turbines developed at the Dutch National Aerospace Laboratory NLR. With TERTS, real-time thermodynamic models of any type of gas turbine configuration can be developed by establishing specific arrangements of engine component models. Applications include analysis of effects of malfunctions of control systems and other sub-systems on performance, in pilot-in-the-loop simulations. Since NLR is presented with a wide variety of gas turbine performance problems, simulation tools with a high degree of flexibility are required. As with the Gas turbine Simulation Program GSP described in the previous chapters, TERTS was developed to allow rapid adaptation to various configurations, rather than being dedicated to a specific engine. TERTS is implemented in the Matlab-Simulink[9] environment, offering excellent means to develop separate component and subsystem (especially control system) models. From Simulink, C-code can be generated for direct implementation of the model in the NSF simulation environment.

Following the rapid increase in computing power, today also GSP is considered to be extended with a real-time simulation capability (see section 14.3). However, for platforms other than MS Windows® such as with pilot in the loop simulations, TERTS remains the best option in terms of simplicity and compatibility.

13.2   Real-time gas turbine simulation methods

With transient simulation, *off-line* models may accept undefined calculation times for iteration towards a transient operating point solution in a single time step.

---

[8] This paper is based on [106]   W. P. J. Visser, M. J. Broomhead and J. v. d. Vorst, "TERTS, A Generic Real-Time Gas Turbine Simulation Environment", 2001-GT-0446 presented at the ASME TURBO EXPO, New Orleans, Louisiana, USA, 2001.

[9] Registered trademark The MathWorks, Inc.

However, *real-time* models must employ special numerical methods to guarantee sufficient convergence at every time step within a predefined execution time.

Customary methodology of real-time gas turbine simulation is creating linear models obtained from system identification. Often 'piece wise' linear models are used where a series of separate linear models is used to cover the highly non-linear state space. Separate linear models are then determined for separate operating conditions (e.g. rotor speeds). This method is widely applied for flight simulators and control system design [107]. However, since this method is principally empirical, all operating condition effects on performance (such as failures, installation losses and deterioration) need to be implemented explicitly. For analysis of every new effect, additional code needs to be developed. Especially for research purposes where a large variety of effects is analysed, this is unpractical.

Thus, instead of empirical models, higher-fidelity physical (thermodynamic) models are required in which most effects on performance are implicitly included in the model equations. These optimally are real-time derivatives of the customary 0-D component based engine models such as GSP in which the equations for the conservation of mass, energy and momentum are solved for each component.

These models may use several methods to solve the non-linear set of equations representing a valid (quasi steady state) engine operating point during a transient [108, 109]. Often, a Jacobian matrix is used to represent a linearized model (the sensitivity of the equation errors to the state deviations) in a particular operating point. The solver methods include Newton-Raphson based schemes such as also used in GSP (see section 5.9.1), the Broyden Jacobian update method [24], and also different transient integration methods.

During iteration, new inverse Jacobians need to be determined to represent successive linearized models used to iterate towards the solution, due to the highly non-linear nature of a gas turbine system. Many pitfalls exist that can prevent successful solution, such as oscillation around the solution, ill-conditioned or singular Jacobians or dwelling in areas in the state space where most of the equation errors have a minimum. Stable, reliable convergence is hard to obtain, especially with generic engine simulation systems, where engine specific 'fixes' cannot be used.

The requirement of a limited execution time per time step for real-time simulation introduces an additional problem, since the execution time for the iteration is unknown in advance. A general approach here is "truncated iteration": after a limited number of iteration steps (within maximum execution time per time step) the iteration is stopped and the accuracy accepted. It is assumed that succeeding time step iterations will further reduce any inaccuracies. This assumption is reasonable if the engine simulation involves high transient rates only at short intervals. In between where the engine runs "relatively steady", any

remaining errors in the equations are eliminated. This is normally the case, even with rather "violent" aircraft gas turbine operation.

Still, truncated iteration with re-determination of Jacobians during the simulation remains risky in unknown operating conditions. Extensive testing in all possible modes of operation is required to determine accuracy and execution speed requirements. Especially with complex thermodynamic engine models, the operating conditions are determined by so many variables that all combinations can never fully be tested.

13.3   Model description

13.3.1 Numerical method

With TERTS, the approach to avoid recalculation of inverse Jacobians during simulation is applied. It was recognized that a single inverse Jacobian is able to represent engine behaviour in a limited part of the operating envelope, implying that a multiple of inverse Jacobians could represent the entire envelope. With many different variables defining the operating envelope however, this would be unpractical. An attempt was made to find a limited set of variables able to represent the engine envelope using dimensionless and reduced engine parameters.

Analysis of the inverse Jacobian indicated that corrected gas generator speed is the main factor responsible for deviations in the inverse Jacobian. This only applies if the Jacobian is determined for dimensionless and normalized state parameters. For a fixed corrected gas generator speed level, engine operation may well be simulated using a single Jacobian inverse (i.e. a single linear model, sufficiently able to provide convergence to various non-linear operating points). This would mean the entire operating envelope can be covered with a series of inverse Jacobians J^{-1} as a function of corrected gas generator speed N_{ggc}:

$$J^{-1} = F(N_{ggc})$$
(13.1)

For a real-time simulation this would entail pre-calculation and storage of an array of inverse Jacobians, while during simulation an inverse Jacobian is obtained by interpolation with gas generator speed. Hence, no inverse Jacobians need to be recalculated. To minimize the equation errors $\overline{E}$, one or more iteration steps per time step i can be performed for the states $\overline{S}$ using the interpolated inverse Jacobians:

$$\overline{S}_{i+1} = \overline{S}_i - J^{-1}.\overline{E}_i, \qquad i = 1 ...$$
(13.2)

If time step size is small enough (see section Stability), explicit Euler integration can be used:

$$\overline{S}_{t+1} = \overline{S}_t + \Delta t.\left[\frac{\partial \overline{S}}{\partial t}\right]_t \tag{13.3}$$

An important observation with gas turbine simulation is that rotor inertia is a major factor determining transient performance. The high frequency dynamics of thermodynamic states in the components (pressures, temperatures, flows etc.) only have small effects on rotor dynamics. This means the rotor speed dynamics can be 'de-coupled' from the component thermodynamics: with the explicit Euler integration, rotor speed states can be updated using the spool power errors for acceleration. The iteration updating the state at each time step therefore does not need to be applied to the rotor speed states. With a turbojet for example, 4 states and 4 errors would suffice to describe the engine system: one state represents rotor speed and therefore only 3 states need updating, requiring a 3x3 Jacobian.

Another issue is the limitation of the state update. With accurate off-line models where new Jacobians occasionally need to be re-determined and inverted repeatedly during single time steps, the state change often is limited for the linearization to remain valid. With single iterations per (small) time steps this limitation is unnecessary: the test models showed that best results (i.e. lowest equation errors and high stability) were obtained with state updates based on the full (unlimited) result of the product of J^{-1} and the error vector $\overline{E}$.

13.3.2 Stability

The stability of a TERTS model can be assessed using eigenvalues of the non-linear system. Real eigenvalues show state variables inhibiting first order behavior, while complex eigenvalues refer to at least second order responses of state variables. A stable system has eigenvalues with only negative real parts. Linearizing the non-linear system around an equilibrium point (a standard function in Matlab) allows determination of the eigenvalues. For a range of steady state operating points determined in advance, the stability of the system for small disturbances in input can be obtained. Figure 13.1 for example indicates the stability of a turboshaft engine model.

With the explicit Euler method, time step size must be minimized in order to obtain maximum stability [20]. This implies a single iteration step per time step, as was found from test runs evaluating different iteration/integration schemes.
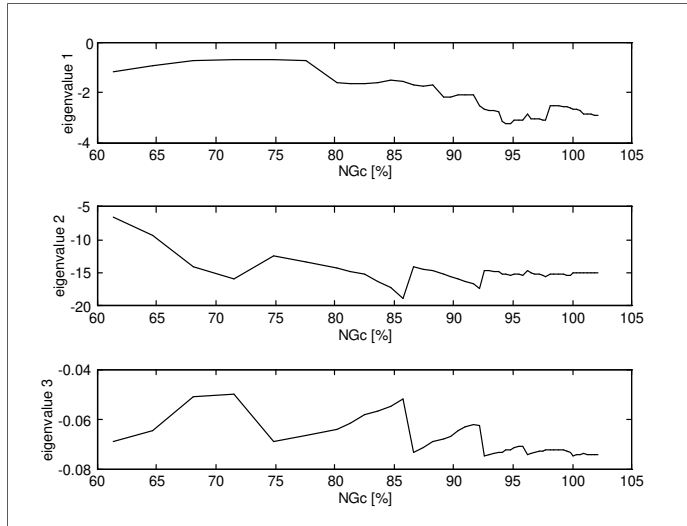
Figure 13.1 Eigenvalue analysis example

Some simple models were developed to test stability of the concept including a turbojet and a turboshaft. To improve the solver iteration stability, states and errors have been normalized. Best results were obtained with a single iteration step (state update) per integration time step at the smallest time step. At least 0.0333 (30Hz) is required to keep equation errors below 5%. With more complex models, the time step requirements become more stringent: with the AB Turbofan model, at least 60 Hz is required to maintain accuracy with the afterburner control modelling. Figure 13.6 shows the equation errors during slam accels / decels. Stability was maintained at all conditions tested while the equation errors remained below 2% in most cases. With more computing power available, the best way to increase accuracy and stability is to just reduce time step size.

13.3.3 Accuracy

Both the equation errors and deviations of the thermodynamic model from known data affect accuracy of the simulation results. The previous section showed that the equation errors can be minimized by applying small time steps. Even if optimally tuned, the thermodynamic model has limitations in the 0-D component models. During (the quasi-steady state simulated) transients, the steady state component maps may not accurately represent component performance. If detailed control system simulations are involved, simulation time step size should correspond to (be at least smaller than) the smallest control update time step.

In some cases convergence (rate at which the equation errors disappear) is relatively slow, even during stable steady state. This is due to deviation of the Jacobian from the actual linear model in the particular operating point. In the
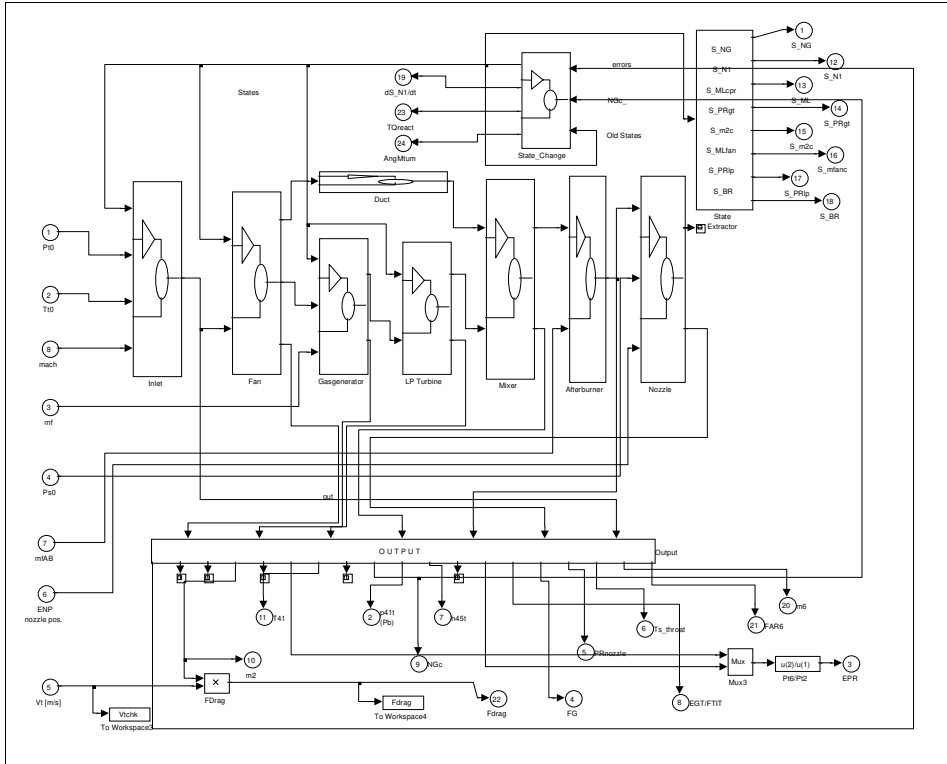
example application at the end of this paper this is visible at IDLE power (Figure 13.6): the errors stay in the order of 1% for several seconds. Although this is sufficient for most applications, adding dimensions in the inverse Jacobian function for more precise representation of the entire state space can further improve convergence. This may well be required for simulations of particular failure effects, significantly affecting component performance. Adding T4/T2 (TIT over inlet temperature) as parameter representing the gas generator load would be the next step in this direction. Then the equation for J^{-1} would change into:

$$J^{-1} = F(N_{ggc}, T4/T2) \qquad (13.4)$$

Additional errors in the thermodynamic model can be evaluated by comparing steady state performance results and errors minimized by fine-tuning the model. Finally, evaluation is required for transient performance, although often only limited transient data are available. In the AB Turbofan application example some validation data will be given.

Figure 13.2   TERTS top-level model of an afterburning turbofan

Figure 13.3 TERTS afterburning turbofan - thermodynamic model level

13.3.4 Architecture

TERTS models are composed of configurations of component models similar to off-line 0-D gas turbine cycle models. Off-design transient gas turbine performance is calculated, relative to a reference operating report, usually the design point.

Matlab-Simulink offers the ability to decompose complex systems into smaller functional subsystems. A basic similarity between TERTS and GSP is therefore applicable and used to derive TERTS models from GSP. However, of the three object-oriented principles (encapsulation, inheritance and polymorphism), only encapsulation is supported by Matlab-Simulink.

13.3.5 User interface

TERTS employs the Simulink graphical user interface and reflects the component-based architecture for the gas turbine model. The main window manages the top-level model (Figure 13.2) and simulation, while lower level models (Figure 13.3) are accessed by zooming in on a system through double-clicking.

Input is provided in files listing input variables, off-design component maps, control schedules, etc. These files are simply accessed by any text file editor. Using scalable maps and control functions and dimensionless parameters, most component models are generic.

Matlab-Simulink's powerful graphical output features enable efficient presentation of results in many forms (see Figure 13.6 through Figure 13.9).

13.3.6 Component models

Calculation is performed on component level, using relations between component entry and exit gas properties based on component maps and thermodynamic equations. All component models are non-dimensional.

To enable real-time simulation, any component detail not having a significant effect on operation or response of the system may be eliminated. Therefore, gas path component models generally do not include volume dynamics or heat soakage effects and for thermodynamics a "quasi steady state" method is applied. Exceptions are large volumes such as afterburners: the application example indicates volume effects are significant during AB light-up for example where relative large equation errors emerge (see section Validation, Figure 13.6).

The component models allow for simulation of secondary airflows, turbine cooling and variable (compressor) geometry if required for higher fidelity or accuracy. This often applies to high-performance engines where large turbine cooling flows have a significant effect on performance. All components are modelled using the GSP algorithms, except for the turbine, which employs:

- a simplified efficiency model based on a parabolic function of the loading parameter $\Delta H/U^2$,
- a rotor speed independent flow capacity map (function of pressure ratio only).

If higher fidelity is required (volume and heat soakage effects, turbine model etc.), component models can easily be adapted at the cost of execution speed but without affecting the overall simulation concept.

13.4   Applications

TERTS has been used in several applications:

- The T700 turboshaft engine model [110]
- The EUROPA (European Rotorcraft Performance Analysis) tool, a common European helicopter performance prediction computer program [111]. The EUROPA code determines the dynamic performance of helicopters by simulating manoeuvres, such as offshore platform take-offs and landings. By simulating engine failures at the most critical time during the manoeuvre, the helicopter's safe maximum operating mass can be

determined. A TERTS model of a small Allison 250 class turboshaft has been implemented in EUROPA.

- An afterburning turbofan engine model including detailed control system models. This more complex model is selected for demonstration of TERTS in the next section.

13.5   Twin-spool afterburning turbofan model

The engine used in this example is a twin-spool, afterburning turbofan with a low bypass ratio, a maximum thrust of approximately 110 kN and an overall pressure ratio of 25. Separate models are added for the electronic engine control (DEEC), the nozzle control and actuation, and the afterburner fuel control (Figure 13.2). Figure 13.3 shows the model one level deeper: i.e. the thermodynamic model that obtains inlet conditions and fuel flow from the top-level model. Many more sublevels exist for detailed simulation of components and subsystems.

In TERTS, a twin-spool afterburning turbofan engine model employs 8 states and 8 errors:

8 state variables representing:

- S_{N2} gas generator speed state
- S_{N1} fan speed state
- $S_{ML,3}$ compressor pressure ratio state
- $S_{PR,hpt}$ high pressure turbine pressure ratio state
- S_{m2c} inlet flow state
- $S_{ML,fan}$ fan state
- $S_{PR,lpt}$ low pressure turbine pressure ratio state
- S_{BPR} bypass ratio state

8 error variables calculated from:

- Fan entry corrected flow and map corrected flow
- Compressor entry corrected flow and map corrected flow
- HPT power and compressor power
- HPT entry corrected flow and map corrected flow
- LPT power and fan power
- LPT entry corrected flow and map corrected flow
- Mixer duct-to-core static pressure ratio
  (for conservation of momentum, constant duct-to-core entry flow static pressure ratio is assumed)
- Nozzle entry flow and exit flow

13.5.1 Validation

Steady state performance of the model was evaluated using engine manufacturer installed performance data (N1, N2, thrust and fuel flow across the entire flight envelope).

Figure 13.4 shows one of the validations at MIL power. In the relevant part of the flight envelope the errors remain within a 5% margin (beyond Mach 1.2 @ 0 ft, a large deviation occurs due to omission in the model of special control laws in that region).

Inaccuracies in the order of 5% were accepted at this stage, since the focus was put on a demonstration of the modeling concept. With additional fine-tuning using more engine data (obtained from off-line GSP models) the accuracy can be improved (see Accuracy section).

TERTS determined thrust was also compared with steady state reference data during a test session in the NSF to assess inaccuracy during a typical F-16 mission simulation. The thrust-time history is displayed in Figure 13.5. Since the altitudes during the test session did not exactly match the reference data altitudes, the reference thrust data have been corrected for differences in pressure altitude. Results indicate a match well within 5% inaccuracy.
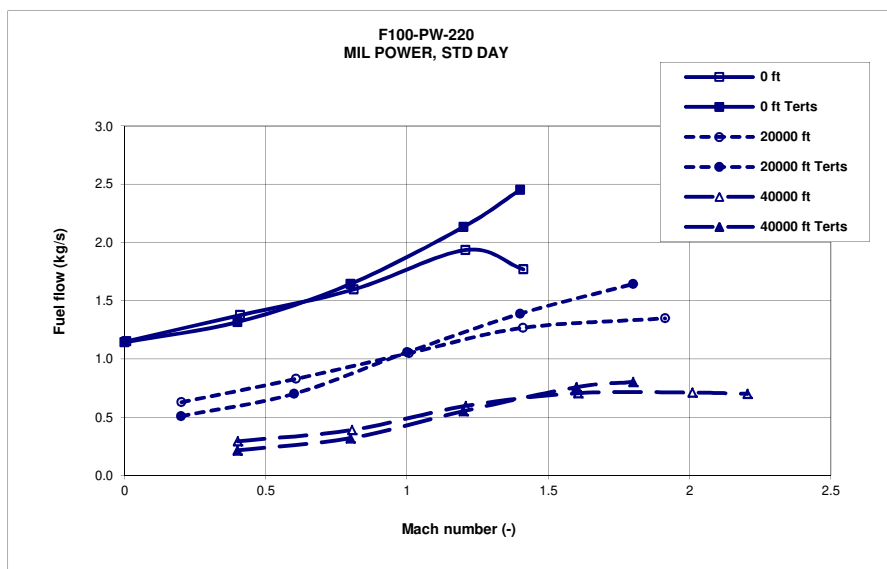

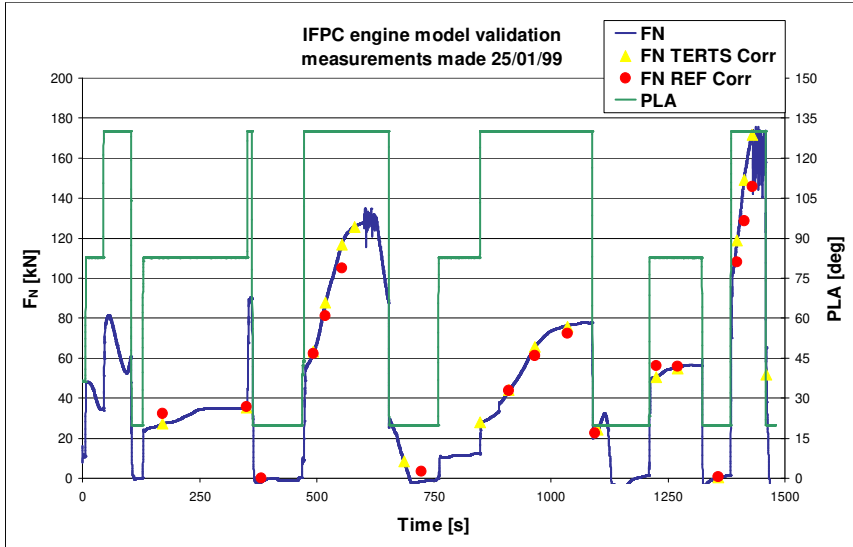*Figure 13.4 Validation of steady state fuel flow at MIL power*

Figure 13.5   Validation of net thrust at all throttle settings
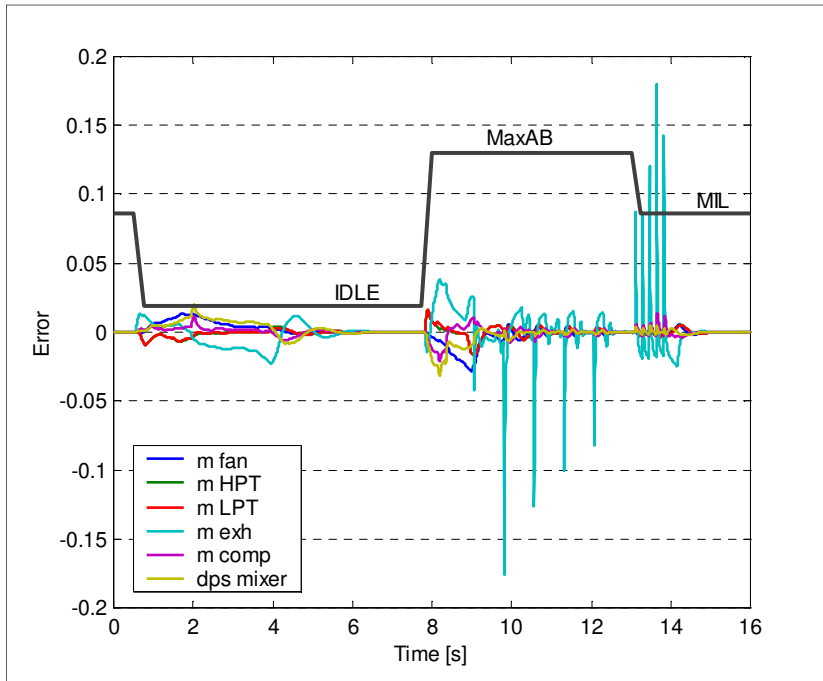

Figure 13.6   AB turbofan equation errors during accel/decel

The oscillations in the thrust curve are the result of imperfections in implementation of afterburner permission control, which have been corrected after the test session.

Figure 13.6 shows the response of the equation errors during slam decels and accels, also indicating the stability of the model. The errors remain within 4%, also during the accels. During stabilizing intermediate periods, the errors remain within 2%. During AB segment light-ups the exhaust mass flow error briefly exceeds 10%, which is corrected after a single time step and does not affect the performance parameter responses significantly as can be seen in Figure 13.7.

During IDLE (2–8 s), convergence (although complete and fully stable) is rather slow (Figure 13.6: visible errors between 2-6 s). This effect is due to the limitations of the pre-calculated Jacobian approach and can be reduced by adding more dimensions to the inverse Jacobian function (see section Accuracy).

13.5.2 Transient performance

Transient performance has not been evaluated with test bed data at this stage. However, transient performance was found to correspond sufficiently with GSP calculated transients and with the test pilot experience in the NSF in all regions of the flight and engine power setting envelope.

Figure 13.8 shows transient thrust response results for a MIL to MAX-AB slam accel (at ISA Static). The thrust shows the typical peaks at subsequent AB segment light-ups. These thrust peaks correspond to undesired pressure peaks that may cause fan stall. In practice, these must be avoided by adjusting the timing of change in exhaust nozzle position.

Figure 13.9 shows an IDLE - MAX-AB transient response (at ISA Static) of the fan rotational speed N1 and compressor rotational speed N2. Again the afterburner segment light-ups are visible through the effects of the pressure peaks on the fan rotational speed N1.

More validation work needs to be done to improve accuracy of both steady state and transient performance of the AB turbofan model. Apart from fine-tuning the present model, this may involve extending fidelity of component models (control system models, afterburner volume dynamics). This task can be performed using the existing TERTS component model library.

13.6   Real-time execution speed

Using Matlab-Simulink's C-code generator, the AB turbofan model described was implemented in the NSF flight-simulator and used for Integrated Flight Propulsion Control (IFPC) and pilot-in-the-loop thrust vectoring concept research. For this purpose, flight control logic was integrated with engine control (not covered in this paper). At 100Hz (0.01s time steps), the engine model used up to about 20% of the available computing power (a 4-processor Silicon Graphics

Challenge L computer, 180 Mwhetstones). Together with the aircraft model, this was well within the computing speed limitations.
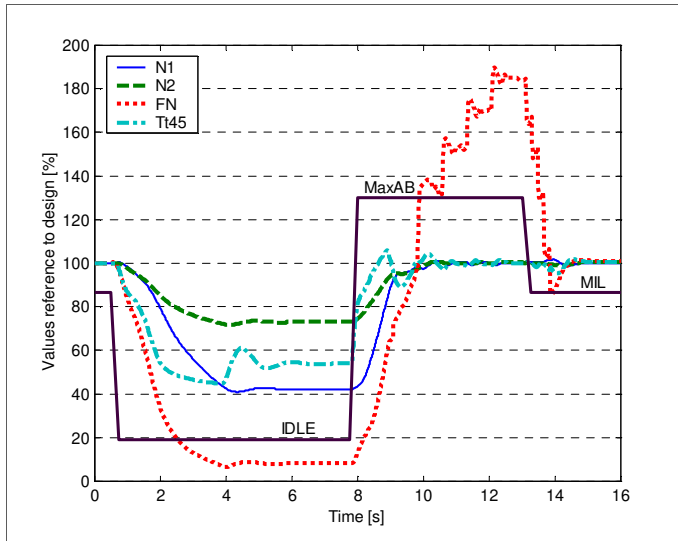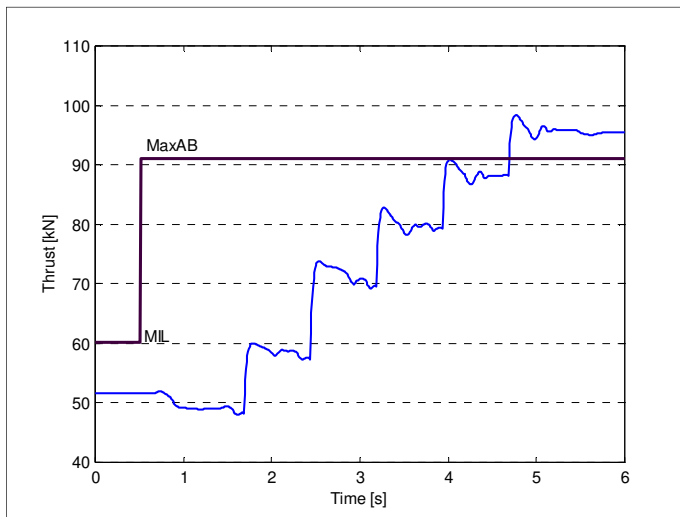

Figure 13.7 Transient response example

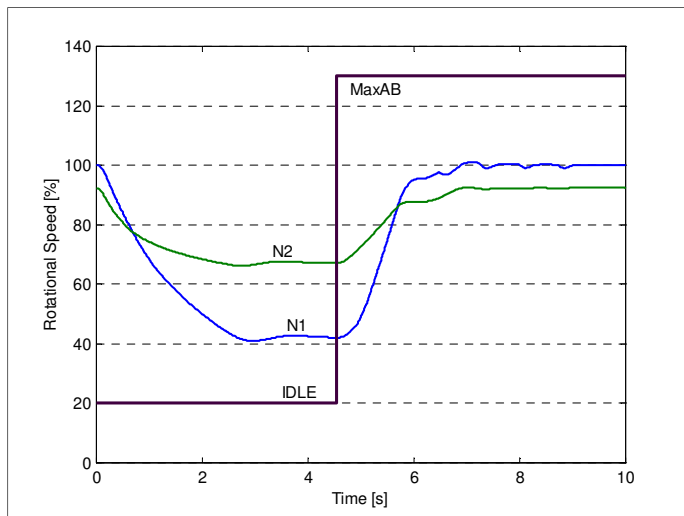*Figure 13.8 MIL to MAX-AB thrust response*

Figure 13.9 IDLE to MAX-AB engine N1 and N2 response

13.7   Conclusions

The TERTS real-time gas turbine simulation environment is a powerful tool for development of high-fidelity thermodynamic (gas turbine) propulsion system performance models integrated in both off-line and pilot-in-the-loop flight simulation models.

The TERTS numerical method using pre-calculated inverse Jacobian functions provides high stability and accuracy, and minimizes execution time, even for complex models such as military afterburning turbofan engines.

The Matlab-Simulink environment offers efficient means to create new and adapt existing models using the component-based approach and Simulink's powerful control system modeling features.

With Matlab-Simulink's C-code generation tool, TERTS models are easily ported and embedded in aircraft modeling environments such as pilot–in-the-loop flight simulators.

TERTS provides the best option to develop a physical real-time engine model where compatibility with the Matlab-Simulink environment is required and the GSP alternative with the MS Windows$^{©}$ or the GSP Application Programmers Interface (API, see section 14.3) cannot be used,

TERTS has been successfully demonstrated in NLR's National Simulation Facility (NSF) as part of a project demonstrating Integrated Flight Propulsion Control (IFPC) and thrust-vectoring (TV) concepts.

TERTS flexibility will prove valuable to future applications such as detailed simulations of complex STOVL/TV propulsion systems, tilt-rotor and compound helicopter propulsion systems, integrated in research flight simulators.

Model inaccuracy of the current system is well within 5%. Further improvement is possible through:

- Obtaining more validation data, especially transient response data.
- Adding extra parameters such as T4/T2 to the inverse Jacobian function, thereby further reducing the equation errors.
- Extending the level of detail of the component models (e.g. the turbine).
- This would require more computing power while the numerical concept can be maintained. This exercise is the subject of future research.

Chapter 14 Future of GSP

14.1   Introduction

From the large GSP user community, there is a continuous flow of new requirements, ideas, suggestions and also bug reports. These are categorized, prioritized and addressed by the GSP development team. Some may be urgent (i.e. bugs) and obtain high priority, some may be saved for major updates. Many new requirements emerge during application such as the thermal network model described in Chapter 9 that was developed during the application of GSP to micro turbine simulation (18.7). Finally, also the GSP team itself continuously identifies areas for improvement. The object oriented architecture of GSP (Chapter 6) enables rapid implementation of new simulation functionality and usually does not need adaptation.

In the following sections, the major areas with requirements or ideas for improvement are listed and specific improvement items described.

14.2   Fidelity

The *fidelity* of GSP models is its capability to accurately represent the performance and processes in the gas turbine engine to a specific level of detail. The 0-D modelling approach sometime fails to capture the detail necessary for accurate simulation of system performance. A good example is the 0-D recuperator model that fails to properly represent transient effects and led to the development of the 1-D recuperator component model described in section 9.6.

Future improvements will include more 1-D component models, both for heat transfer and aerodynamics. Other fidelity improvement may simply be obtained by using more detailed performance maps. Examples are compressor maps including variable geometry parameters.

A important area where fidelity can be improved is the gas model described in Chapter 7. A future update is envisioned where the Gibb's equations are solved without the current 'short-cut' method solving for the equilibrium oxygen fraction, which will not work with oxygen fractions very close to zero. Then also over-rich mixture combustion can be simulated. In addition, more species can be added to the gas model.

14.3   Application Programmer's Interface (API)

GSP has an application programmer's interface (API) for controlling a GSP simulation from another application. The API consists of a number of *Dynamic Link Library* (DLL) files containing procedures that can be executed from outside the

GSP environment. A typical GSP API application example is running GSP simulations from Matlab$^{®}$ which has a capability to call procedures from DLLs.

The API works well for steady-state and off-line transient simulations. However, for real-time transient simulation, the API requires additional functionality w.r.t. synchronizing with time and the calling application.

14.4   Real-time simulation

In 2001, the TERTS real-time simulation tool was developed with a notion of computation speed limitations. GSP's method of solving sets of very non-linear equations including many lengthy internal iterations within the gas model (chemical equilibrium) was not considered suitable for real time execution on the platforms considered. However, computation speed has grown substantially since then. In addition, todays multi-core processors allow multi-threading concepts that can be employed to perform parallel processing. These developments make real-time transient simulation in GSP feasible. Together with the API (section 14.3) this would enable GSP to provide engine performance data real-time to aircraft performance simulations.

14.5   Multi-disciplinary simulation

GSP model projects can easily be expanded to cover different tasks such as performance prediction, gas path analysis and diagnostics, lifing analysis etc. However, GSP is primarily focused on 0-D aero-thermodynamic performance, which is only one of the many disciplines involved in engine design and development. Coupling with models from other disciplines such as high-fidelity multi-dimensional models and structural models, is an important requirement for multi-disciplinary optimization (MDO) applications. Model based MDO is becoming increasingly important for the engine design process. This means GSP must facilitate coupling with simulation environments of the other disciplines.

In [17] an application is described coupling GSP with a lifing model using GSP's standard output data formats. The coupling here is 'off-line' and GSP performs a single step in a sequential process involving several types of models.

One step further is to include a GSP simulation in an automated iterative process towards an optimal aerodynamic design (coupling with multi-dimensional CFD) or an optimal structural design (coupling with a FEM model) for example. Then an interface is required to couple the simulation to the other models. This is facilitated by the GSP API described in section 14.3.

14.6   Automatic optimization

Along with the development of MDO capabilities, requirements emerge to automatically optimize multiple operating points. For aero-engines for example,

usually performance requirements are specified for take-off, end-of-climb and cruise performance. Currently, the user must select a single DP (or Cycle Reference Point CRP, see 2.6.4) and optimize this point simultaneously with one or more OD points, which requires a time consuming manual iteration process. Numerical solutions will be sought to have GSP help the user with this process, ultimately providing automatic iteration functionality.

14.7   User interface

The GSP 11 user interface is significantly enhanced with the configuration and case management functionality described in Chapter 10. Although many small improvements are and will be made on a routine basis following user suggestions, significant changes in the GSP user interface concept are not anticipated.

PART III

APPLICATIONS

Chapter 15 Application areas

Until the development of GSP 7, applications were focused on jet engines for research and engineering projects at NLR. During the development of GSP version 7 up to version 11, the number of applications has grown rapidly, including a wide variety of aero-engine, power generation and other gas turbine related studies and projects. These were performed at NLR, Delft University and many international companies, institutes and universities. The application areas include:

- Aircraft engine design and performance prediction
- Aircraft engine failure analysis
- Industrial gas turbine alternative fuel effects on performance issues
- Gas turbine maintenance support
- Gas turbine diagnostics, gas path analysis
- Aero-engine lifing studies
- Integrated gas turbine – bio-mass gasifier design studies
- Exhaust gas emission studies
- Recuperated gas turbine control issues
- Micro turbine development and test analysis
- Micro turbine sizing study for an electric vehicle range extender application
- Power generation application studies
- Micro turbine based Combined Heat Power system simulation

In the following chapters, GSP's capabilities are demonstrated by descriptions of a variety of applications. In Chapter 16 a number of application examples are given with varying complexity. In the subsequent chapters applications to gas turbine R&D programs are described.

Chapter 16 Application examples

16.1 High-bypass turbofan engine simulation

A relatively simple example of using GSP is the analysis of off-design performance of a typical flat rated high-bypass turbofan engine represented by the GSP demo model configuration 'BIGFAN', depicted in Figure 16.1. Generic component maps are used scaled to the BIGFAN design point.

Let us assume we are interested in sea level take-off performance at varying ambient temperatures and compressor bleed flows. This implies the calculation of steady-state points at a series of different ambient temperatures, with the engine running at either maximum total turbine inlet temperature TIT (Tt4) or maximum burner pressure Ps3 (i.e. the flat rated limitation in this example). If we assume a flat rated temperature FRT at 288 K which is also the design point (DP) ambient temperature, then the engine is at both maximum TIT and Ps3 at DP (FRT is the ambient temperature where both maximum TIT and the flat rated limit are reached).
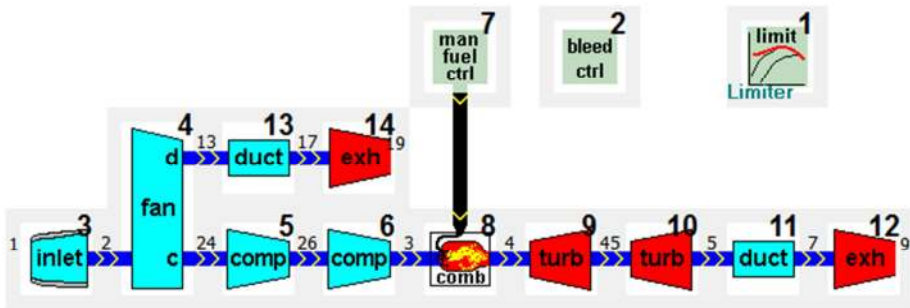

Figure 16.1   BIGFAN model window

A limiter component is added, limiting Ps3 to the design point value of 28.9 bar by reducing fuel flow if necessary (see section 8.2.2 on the limiter component model). First, a design point calculation with a TIT of 1554 K (i.e. Take-off T/O power) is executed. Next, an ambient temperature 'parameter sweep' from 253 K (ISA-35) up to 323 K (ISA+35) is performed, while maintaining the 1554 K TIT unless the flat rated limit is reached and the limiter reduces TIT. The parameter sweep is performed both for no bleed and for 5% compressor bleed. The results in Figure 16.2 show the typical turbofan trends for fan speed N1, Ps3, net thrust FN and TIT at ambient temperatures both below and above FRT. As expected, with 5% HPC bleed, the flat rated limit is only reached at very low ambient temperatures.
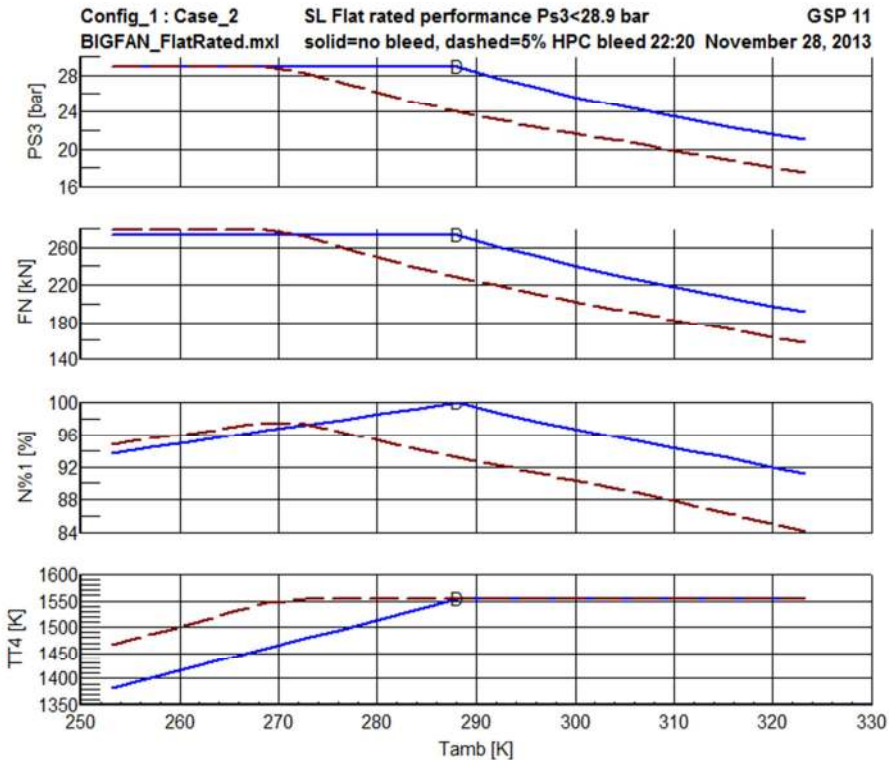
Figure 16.2 Effect of compressor bleed on take-off performance

The procedure can be easily repeated for other parameter variations such as at different pressure altitudes, deterioration conditions, power off-take values etc. instead of the customer bleed flow variation as shown in this example.

16.2   Recuperated turboshaft engine simulation

The simulation of a recuperated turboshaft gas turbine demonstrates GSP's flexibility for building a model. The model depicted in Figure 16.3 is simply derived from an existing turboshaft engine model. Using GSP's drag-and-drop interface for adding a simple recuperator (heat exchanger HX) model and some 'link bars' to make the proper gas path connections, a gas turbine is extended with a recuperator.

Next, the user can redefine the design point with a new (lower) fuel flow, additional pressure losses in the recuperator and modified control schedules in the power turbine (PT) speed control component. The latter task is complicated due to the relatively unstable nature of the recuperated cycle. An effective and stable control system design (maintaining constant PT speed with torque variations)

requires separate attention to optimize the PID control system gains. With GSP, effects of different gains can be analysed combined with acceleration and deceleration schedules.
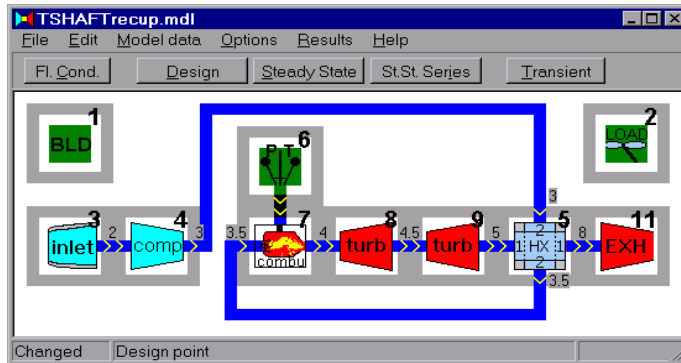

Figure 16.3   Recuperated turboshaft model

Important issues are the volume and heat soakage effects of the recuperator. When these are substantial, accurate PT speed control is hard to achieve. With GSP, these effects can be analysed in detail with several kinds of transient response simulations.
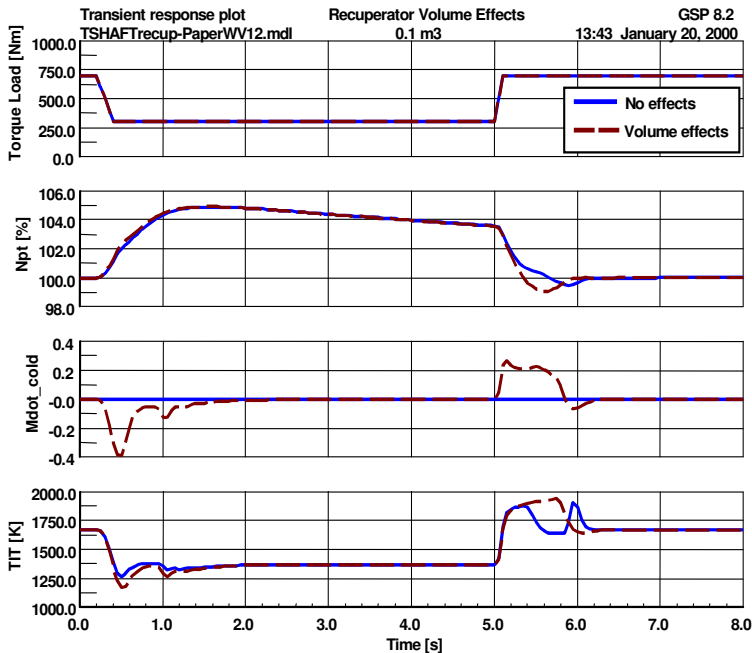

Figure 16.4 Analysis of recuperated turboshaft volume effects

Figure 16.4 shows recuperator volume effects on engine response (the dashed line is with 0.1 m^3 volume for both hot and cold flow passages, the solid line is without recuperator volume). Mdot_cold shows the rate of mass content change in the cold flow passage volume.

Note that Figure 16.4 shows the response of a non-optimized control system. During acceleration, the nominal Tt4 is exceeded, especially when including the volume effects. Also, the PT rotor speed Npt dip (down to 99%) is entirely due to the volume effects. The solid curve (no volume effects) indicates virtually no dip at all.

16.3   Lift-fan driven by an afterburning turbofan engine

An interesting problem requiring a high degree of flexibility is the integrated simulation of an afterburning turbofan engine driving a lift-fan through a clutch, engaging and disengaging the lift-fan driveshaft from the fan shaft while the engine is running. GSP offers the flexibility to model such a complete system, enabling thorough analysis of its performance, including lift-fan-engine interaction, optimizing control logic, drive shaft rotor dynamics and torque loads. The lift-fan will only require minor modelling effort since it can inherit most of its code from the compressor or fan component. For the clutch, new relations must be implemented for transmitting torque between engine and lift fan, depending on the clutch engagement schedule.

One of the challenges modelling the lift-fan was to make GSP able to handle rotating turbo-machinery components at zero speed levels. The lift fan model and the numerical solver required some adaptations to allow model states at zero (zero speed and mass flow).
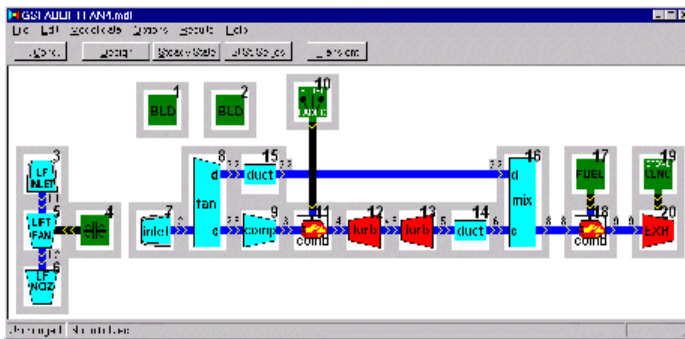

Figure 16.5   Model of AB turbofan driving lift-fan

In Figure 16.5, the model of the afterburning (AB) turbofan driving a lift-fan is shown. A lift-fan model and a simple clutch model are added to an AB turbofan model. The turbofan has 85 kN (max dry) rated thrust, 100 kg/s airflow, an overall

pressure ratio PR of 39 and a maximum Tt4 of 2050 K. The lift-fan has 47 kN thrust at 100% speed (fully engaged at full turbofan speed) and 130 kg/s air flow.

The engine system design point can either be specified with engaged or disengaged lift-fan. In this example a disengaged fan is used at design so as to have a customary AB turbofan configuration as the design point reference.

The AB turbofan has a Full Authority Digital Electronic Control (FADEC) model controlling fan speed with fuel flow and engine pressure ratio EPR with exhaust nozzle area. With the lift-fan engaged, power is obtained from the fan shaft. Fan speed can be maintained by increasing fuel flow but this may well result in an unacceptable increase of Tt4 and compressor speed N2. Increasing exhaust nozzle area offers a means to increase fan shaft power without this problem.

The turbofan exhaust nozzle and additional roll-rate control air bleed nozzles will also provide vertical thrust during lift-fan operation. Although this affects system performance and may well be modelled using GSP also, this aspect is not addressed in this example. Also AB operation is not used in this example.

A very important aspect is how to control engagement and disengagement of the clutch. With GSP, effects of different (dis)engagement turbofan speed windows, engagement duration times, clutch maximum torque capacities, detailed clutch characteristics and lift fan variable geometry on system performance can be analyzed. Important parameters then are maximum lift-fan drive shaft torque levels, clutch friction heat production rates, clutch total engagement heat production, clutch slipping time durations, fan speed and lift fan speed responses, Tt4 response, turbofan exhaust nozzle thrust response and system control stability.

For the lift-fan AB turbofan system 6 custom components had to be derived from the existing GSP standard classes: a lift-fan component inherited from the compressor component class, a clutch component derived from the abstract control component class, a lift-fan inlet component derived from the standard inlet, a lift-fan nozzle derived from the variable nozzle class, a FADEC fuel control derived from the generic fuel control component class and a variable exhaust nozzle control derived from the generic nozzle control class, interfacing with the FADEC. These components all have functionality added specific for this type of configuration. The component user interfaces have been extended to enable quick adaptation of control logic, gains and schedules, and clutch and lift-fan characteristics. This enables quick analysis of the effects of numerous variations in the configuration. When detailed specific characteristics are known and available (such as detailed digital control logic), these can easily be implemented in extended custom component classes.

In Figure 16.6 to Figure 16.10, responses of subsequent lift-fan engagement and disengagement are shown for two cases. The solid curves represent the case with a 14000 Nm maximum (fully engaged) static torque capacity clutch. The dashed

curves represent a clutch with 28000 Nm maximum static torque capacity (maximum dynamic torque capacity is somewhat lower).

The turbofan engine initially runs at 100% speed without the lift-fan engaged, thus the lift fan speed is 0. The control is simplified, with N1 control using customary fuel flow/burner pressure schedules. Furthermore, a PID controller was defined, maintaining scheduled EPR combined with a separate open loop nozzle schedule for lift-fan operation using the exhaust nozzle area.
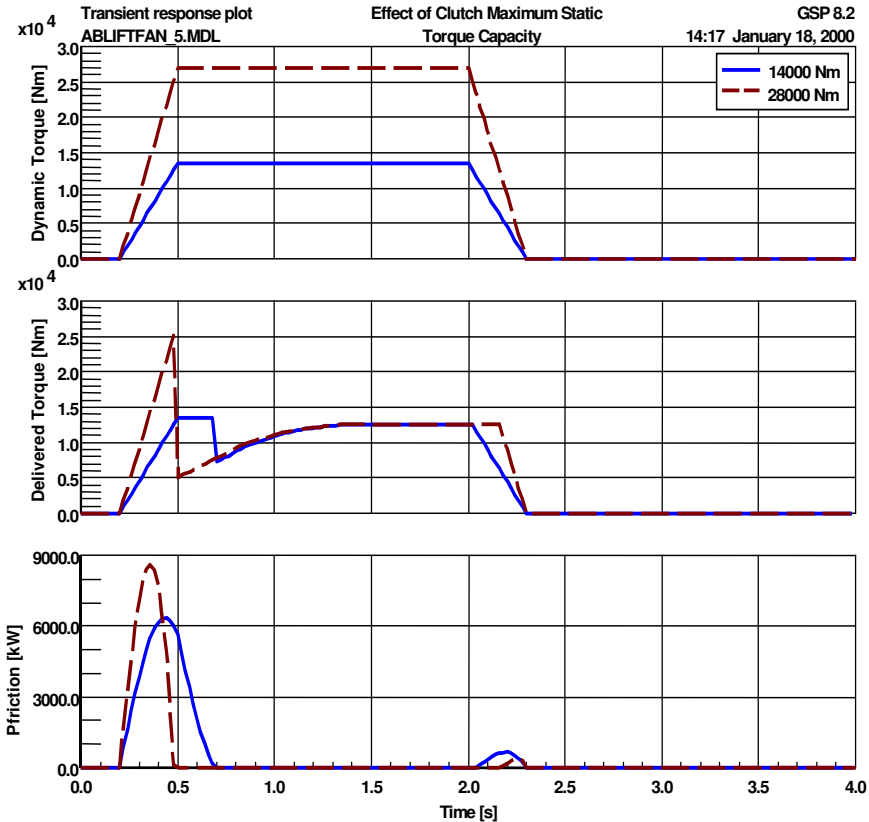

Figure 16.6   Lift-fan (dis)engagement clutch response

Figure 16.6 shows clutch parameter responses versus time for lift-fan engagement (starting at 0.2 s) and disengagement (starting at 2 s). The top graph shows clutch engagement in terms of (dynamic friction) torque capacity. Next actual torque delivered to the lift-fan and the heat dissipation (Pfriction) during clutch slipping are shown.

Figure 16.7 shows the rotational speeds of the lift-fan and the engine fan in a single graph, effectively summarizing rotor speed and clutch performance histories.
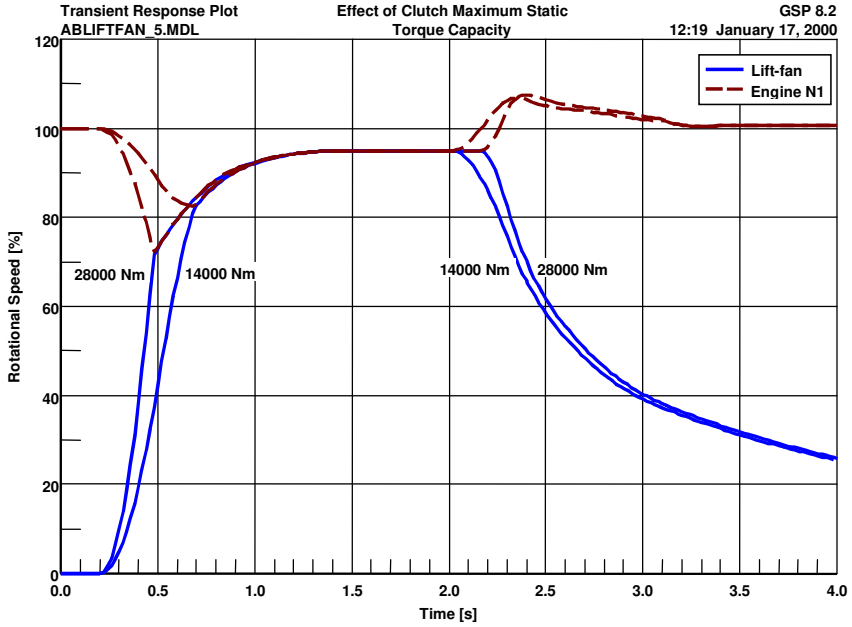
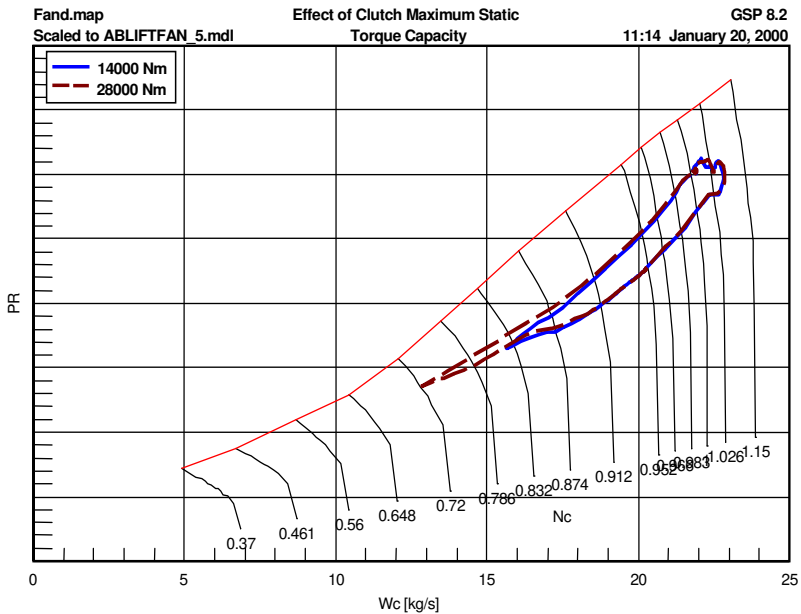*Figure 16.7   Lift-fan (dis)engagement & N1 response*

Figure 16.8   Lift-fan (dis)engagement in fan duct map

Figure 16.8 shows the transient operating curve in the fan duct map and Figure 16.9 shows thrust and turbofan nozzle and N2 responses. Note that the solid curves in Figure 16.6 indicate quite a long engagement (slipping) time of the clutch, which may be favourable in terms of smooth engagement but unfavourable in terms of friction heat rate. The dashed curves show the same response with a higher clutch maximum static torque capacity, which reduces the locking time (and friction heat production) significantly. However, the N1 response now shows an increased dip as displayed in
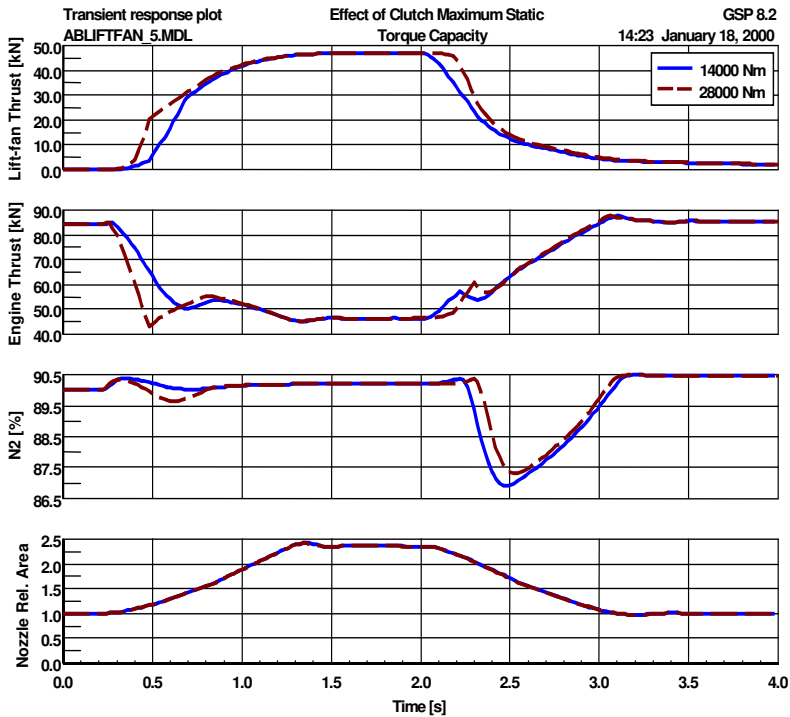
Figure 16.9   Lift-fan (dis)engagement engine response

Figure 16.10 shows the results for a more optimized control system (dashed curves), incorporating a higher nozzle actuator rate and a lower maximum acceleration schedule. The higher nozzle actuator rate allows the engine control to better maintain EPR, while the lower maximum acceleration schedule better limits Tt4 to acceptable levels.

Figure 16.10 Lift-fan (dis)engagement response with faster nozzle actuator and lower maximum acceleration fuel

PART III   APPLICATIONS

Chapter 17 Experience with GSP as a Gas Path Analysis Tool[10]

17.1   Introduction

There is an increasing focus on optimizing gas turbine availability and maintainability while minimizing operating costs. Accurate engine diagnostic methods have the potential to improve performance check accuracy and also reduce costs related 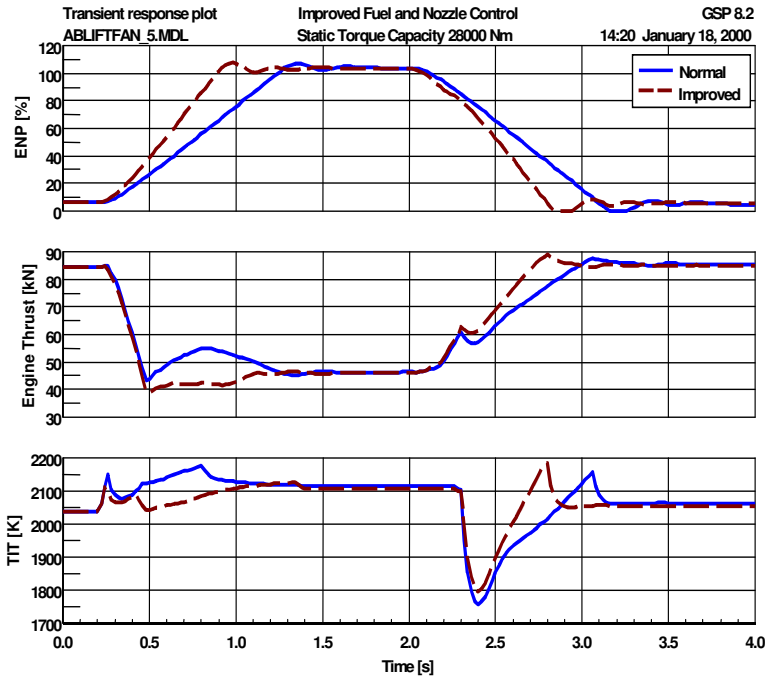to the labour intensive inspections of components. Gas Path Analysis (GPA) is a method to diagnose the components in the gas path using performance measurements.

The last few decades, GPA methods have evolved, from linear methods to non-linear methods including adaptive modelling and more empirical methods such as neural networks and genetic algorithms.

17.2   GSP Adaptive Modelling method

In Chapter 12 the development of the GSP adaptive modelling (AM) functionality is described that can be used on any GSP gas turbine performance model. The method was successfully demonstrated in the Gas turbine Simulation Program GSP on the CF6-50 engine.

17.3   Towards a practical GPA tool

The next step was to test the GSP GPA capability on other engine types and implement the methodology into a tool for industrial application. For this purpose, improvements in diagnostic accuracy, analysis capability and user friendliness were required. In this paper the new developed methods and functionality are described and demonstrated in a case study.

The new developed tool was applied on other engine types in an industrial environment. The objectives of these exercises were:

- to investigate applicability of the tool to other engines and associated performance measurement sets,
- assessment of the additional functionalities developed to make the tool more user-friendly and robust for use in a maintenance shop or test-bed environment.

---

[10]This chapter is based on: [112]   W. P. J. Visser, H. Pieters, M. Oostveen and E. v. Dorp, "Experience with GSP as a Gas Path Analysis Tool", ASME GT2006-90904, presented at the ASME TURBO EXPO 2006, Barcelona, Spain, 2006.

Although the tool was kept as generic as possible, some of the new functionalities had to be made engine-specific, such as test-bed data import functions etc. These exercises provided valuable insight in how to optimize the tool, by developing concepts of user configurable set-ups to easily adapt to different specific engine performance measurement/test-bed environments.

17.4   Requirements

The following major requirements for an industrial GPA tool were identified:

- Accurate diagnostics over a wide operating range.
- Effective diagnostics with limited performance data.
- User-friendly.
- Accumulation and trending analysis of GPA results.

In the following sections the requirements and associated solutions will be discussed.

17.5   Accuracy

The accuracy and stability of the adaptive model calculation strongly depends on model accuracy. Deviations between model and engine measurement data interfere with the adaptive model iterations. In the original version described in 0 this effect was compensated by calibrating the model in the design point, which gave accurate results close to the design point only. However, deviations between modelled and measured performance may change as a function of the power setting (see Figure 17.1). This is usually due to increasing model deviations when departing from the design point into off-design operating regions. These off-design model errors usually are related to inaccurate component maps, but may also have their origin in small secondary effects that are not covered by 0-D gas turbine models. Component maps are often not available from the engine manufacturer and then usually 'scaled' maps of similar components are used [113]. Moreover, sensors may generate different values of bias at different operating points.

17.6   Multi point calibration

In Chapter 12, a method was described, calibrating the GSP engine model design point to a measured reference engine operating point. This was to eliminate the effects of deviations between reference model and reference engine (i.e. the actual engine measurement data set appointed as reference for condition deviations). The single set of calibration factors was applied to various AM sessions around the design point, thus suffering from 'second order' model deviations (i.e. model errors varying with operating conditions, particularly power setting).

It was realized that with a variable calibration factor depending on power setting, inaccuracy and reliability could be significantly improved. This 'multi point' calibration method proved an efficient method to have the reference model exactly match the measured reference performance over a wide power setting range. This means the operator is not limited anymore to analysis of engine operation close to the design point. Moreover, by comparing and averaging analysis results of an engine test at different operating points, the effect of measurement uncertainty can be reduced.

Calibration functions had to be derived from measurements at a series of operating points. These functions can principally depend on several operating condition parameters, including inlet conditions, power setting and installation effects such as power off-take and compressor bleeds. To avoid complexity, a calibration function of only a single parameter was used. Power setting parameters such as gas generator rotor speed or turbine inlet temperature corrected to inlet temperature can cover most of the 'calibration envelope'. For the GEM42 engine discussed below, corrected Nh (Nhc, corrected HP compressor rpm) was used (see Figure 17.1).
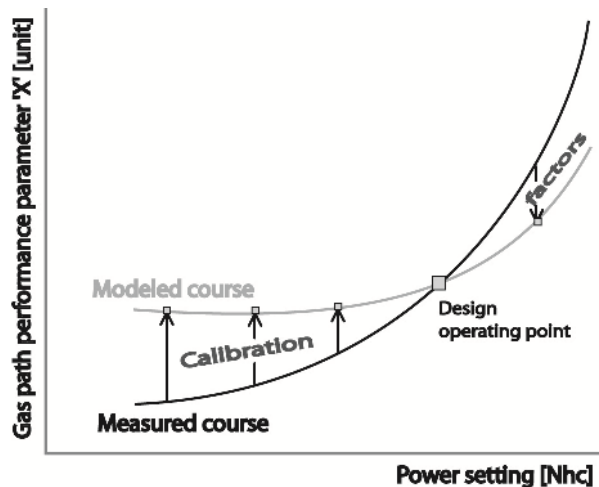
Figure 17.1, schematic representation of multi point calibration

For smooth interpolation polynomial fits are used. This way, the 1st derivative of the calibration function is kept continuous, which enhances adaptive model iteration stability.

17.7   Limited Performance data

An AM calculation requires an equal (or larger) number of independent measured performance parameters and condition variables in order to find a unique

solution for the set of model equations. Generally, only a limited number of performance variables are measured.

In the GEM42 test facility of the Royal Netherlands Navy for example, 8 independent performance parameters are measured. This implies that in a single AM calculation a maximum of 8 condition parameters can be calculated. The GEM42 engine however consists of five turbomachinery components, implying determination of at least 10 condition indicators as shown in Figure 17.2.
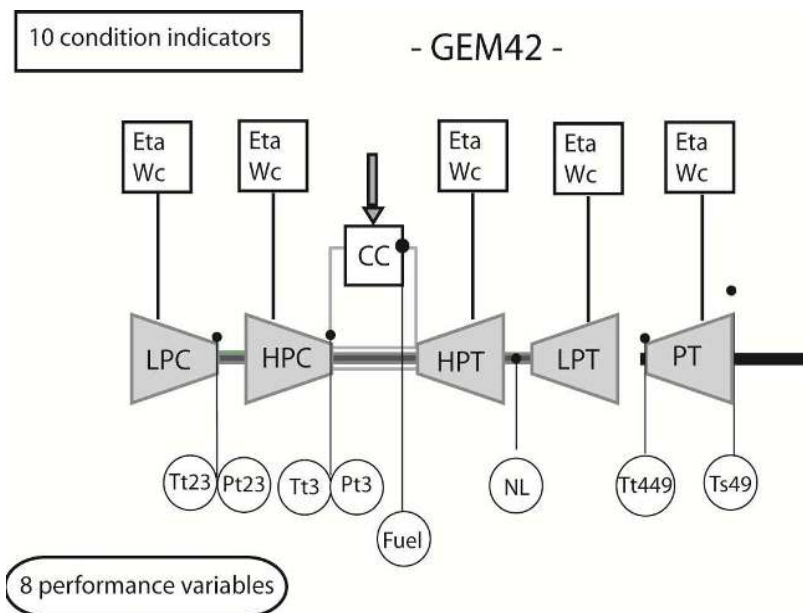
Figure 17.2 Example case: 10 condition vs. 8 measured parameters

The previous project (0) was concerned with a GSP GPA tool for the CF6 turbofan engine. Also in this engine the number of measured independent performance variables was limited. The number was too small to determine values for the condition indicator parameters of all components. However, in case of a turbofan engine it is a reasonable option to leave the entire fan module out of the AM analysis. Justification for this exclusion is that the physical condition of the fan can partly be assessed by means of a visual inspection. For analysis of the turbofan gas generator only, the number of measured performance variables was therefore sufficient.

In other cases, such as with the GEM42 engine this is not an option. Its configuration does not allow an easy visual inspection of any of the turbo machinery components. It is therefore desirable to use GPA to establish all 10 condition parameters.

17.8   Extending the diagnostics capability

A solution to generate a number of condition indicators higher than the number of measured parameters is presented using the 'dominant trend' that root cause condition indicators (the actual condition defects in the particular engine being analysed) show in the analysis results. The approach has similarity with the method described in [102]. Multiple AM calculations are performed with different sub-sets of condition indicators. A condition indicator with a 'dominant trend' persistently shows similar values independent of the sub-sets of condition indicators selected in the AM calculation. Numerical experiments with a large number of 'artificial measurement sets' (obtained from performance models) were performed to analyse the dominate trends in the AM results.

Another approach to extend the diagnostics capability is true multi-point GPA where an AM solution is calculated simultaneously on multiple engine operating points [87]. However, at this stage this method has been rejected as not suitable for a generic tool approach due to complexity and stability problems.

17.8.1 Condition indicator sub-sets

Using a GSP GEM42 model, engine component deterioration effects (map modifiers) were introduced to calculate the effects on engine performance. These deteriorated engine performance data represent the artificial measurement sets.

With a total of n condition indicators and a maximum of k indicators that can be calculated in a single AM calculation (k measurements), in theory $\begin{pmatrix} n \\ k \end{pmatrix}$ subsets of different combinations of condition parameters can used in an AM calculation. For example, for the GEM42 case with 10 indicators and a maximum of 8 in an AM calculation this would result in 45 combinations. It is generally not possible to derive a solution for all possible combinations, since the system of equations can be ill conditioned for some of them. This is also observed in [102]. The reason is that the AM model requires at least some variation of condition indicators around components with measurements at both entry and exit.

By analysing the thermodynamic relations between measured parameters and the condition indicators, the condition indicators that must be in any AM configuration, can be identified. For the GEM42 for example this means that the compressors always need variable conditions parameters in order to have the model match the temperature and pressure values that are available at all compressor entries and exits.

Figure 17.3 shows the 8 well-conditioned AM systems that were obtained for the GEM42 example. The condition parameters that are not included in a subset are indicated with a cross.

	LPC		HPC		HPT		LPT		PT	
	Eta	Wc	Eta	Wc	Eta	Wc	Eta	Wc	Eta	Wc
subset 1							X	X		
subset 2								X		X
subset 3								X	X	
subset 4					X		X			
subset 5							X		X	
subset 6							X			X
subset 7					X				X	
subset 8					X					X

Figure 17.3 GEM42 predefined condition indicator subsets

17.8.2 Numerical experiments

After having defined a number of AM subsets, the condition of the AM equation system can be verified with numerical experiments. With each GEM42 artificial measurement set, 8 subsequent AM calculations were performed, one for each of the 8 condition indicator subsets.

In Figure 17.4 results are shown of an experiment with an artificial measurement set obtained with an imposed deterioration of a 3% increase of corrected mass flow in the HPT (Wc_{HPT}) and a 3% decrease of efficiency, also in the HPT (Eta_{HPT}). Only the map modifiers of six condition parameters of the three turbines are shown; for the values of the remaining four parameters no significant condition deviations were calculated. The condition parameter subsets 1, 2, 3, 5 and 6 all include both root cause condition parameters (Eta_{HPT} and Wc_{HPT}). The values calculated for the corresponding map modifiers are -3% and +3% respectively, whereas the map modifier values of the remaining condition parameters are equal to zero.

The results obtained with subset 4, 7 and 8 only contain the condition parameter Wc_{HPT}. The values for Wc_{HPT} still are large, but not equal to 3%. Moreover, the values of the remaining condition parameters are much larger then zero. As a result, it is concluded that the dominant trend of the root cause condition parameters Wc_{HPT} and Eta_{HPT} is distinct. Similar results were obtained with other artificial measurements.
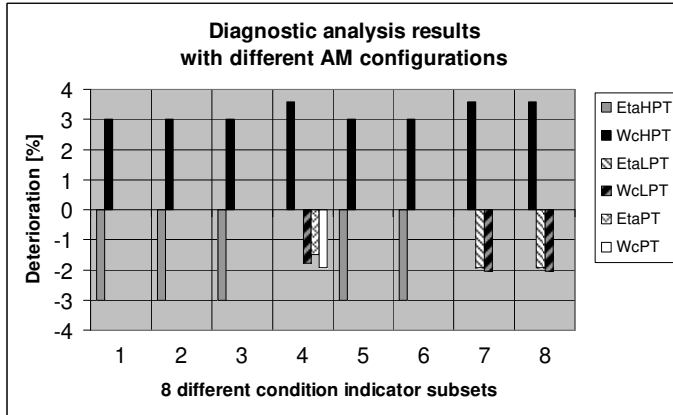
*Figure 17.4 Analysis results of 8 different subsets with known deterioration
(EtaHPT and WcHPT)*
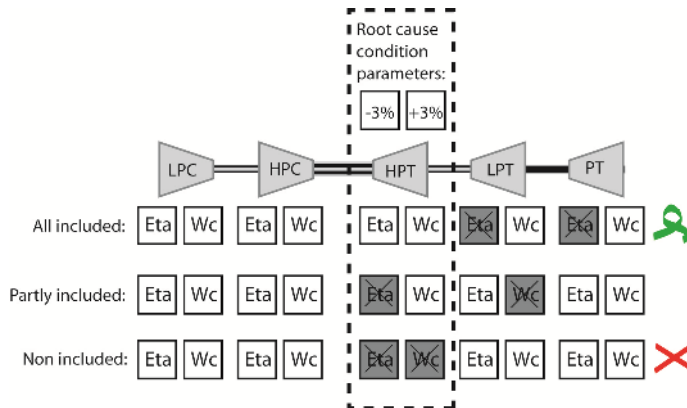
*Figure 17.5 Three different subsets with respect to included root cause
parameters*

Three different situations with respect to the condition parameter subsets were distinguished (Figure 17.5):

1. All root causes included in the condition indicator sub-set. In this case the AM calculation rapidly converges. Moreover, the exact condition indicator values are calculated for the root cause parameter and the non-root cause indicators remain zero.
2. Root causes partly included. In this case the root cause condition indicators deviate somewhat from the actual values but only to a limited extent. The non-root cause indicators are not zero anymore but alternate between positive and negative values, depending on the condition parameters in the subset selection. The latter can be explained by the fact that since the

missing root cause indicators cannot be adapted, some other non-root cause indicator must be adapted instead in order to maintain the conservation laws in the gas turbine cycle (and compensate the missing root cause effect).

3. No root causes included. In this case the conditions indicators in the set may have any value. However they often must alternate between positive and negative values again to maintain the conservation laws.

The actual deterioration will always persistently exert in the results of any selection of 8 condition parameters. The condition parameters not representing actual deterioration may show significant deviations from some reference cases (where the condition parameters corresponding to the actual deterioration are not included), but never in all selected cases. The observation of a dominant trend in true root cause components is confirmed in [102].

The logical next step is to automate the identification of the dominant condition indicators, which ultimately must represent the diagnostic information. Several approaches may be adopted with different criteria for validity or reliability of the values of a particular condition indicator, depending on its variation with different condition indicator sub-sets.

17.8.3 Averaging analysis results

The observation of the dominant trend of root cause condition parameters, and positive-negative alternating behaviour of the non-root cause indicators suggest that averaging the results of different analysis cycles provides a good first estimate for an engine condition diagnosis.

The averaged results, including all 8 analysis cycles, are represented by striped bars in Figure 17.6. After averaging, the condition indicators remain close to the actual values, while the non-root cause indicators are significantly smaller. The solid bars represent results when all condition indicators are included in the sub-set.
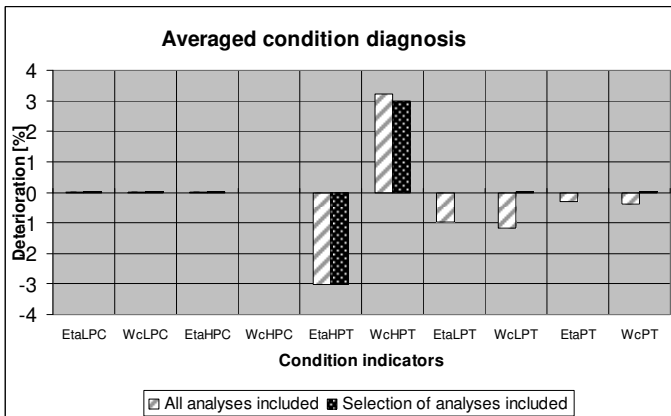

Figure 17.6 Averaged condition diagnosis

In the analysis tool described below, averaging results is used for a first automatic suggestion to eliminate suspected non-root cause condition indicators. This suggestion may then be reverted and corrected by the tool operator.

17.8.4 Eliminating invalid results

The averaging of results has the risk that results from sub-sets that do not include all root cause faults 'contaminate' the averaged end result. One approach can be to eliminate the sub-sets that indicate that they do not include all faults, leaving only the sub-sets that include all faults for averaging. When using a GPA tool with a suitable user interface this process can be rapidly performed manually. It may also be automated with algorithms that can identify the 'include-all' sets.

Another approach is to develop algorithms that automatically eliminate results from sub-sets that do not include all root causes or that eliminate condition indicators from all sets, because they do not show a dominating trend. In this case still all subsets are processed. In the analysis tool described below the concept of a 'validity index' is introduced, that is a function of alternating behaviour. The validity index will then suggest or automatically eliminate suspected invalid results. At this stage however, this concept has not been fully developed yet.
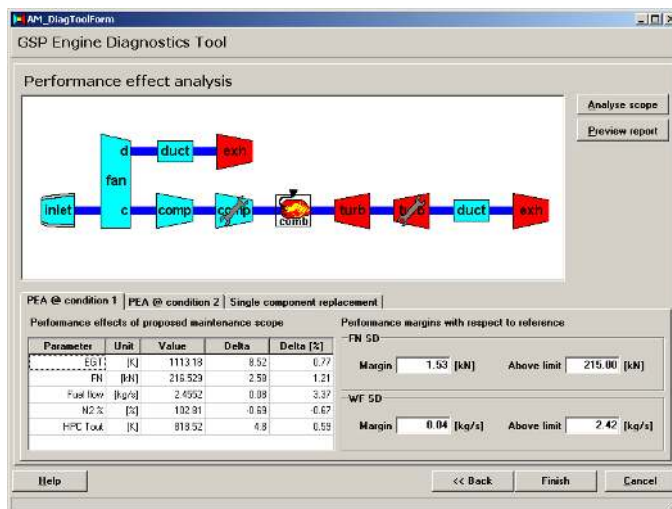
Figure 17.7   Work scope effect prediction tool user interface

17.8.5 Analysing effects of overhaul work scope

The tool was extended with an option to calculate the effect on performance of different overhaul 'work scopes'. Using the user interface in Figure 17.7 the engineer can select one or more components in the GSP model that are reverted to reference condition (indicated by the spanner shown on top of the component icon).

This functionality allows rapid prediction of the extent to which engine performance will be restored after applying a certain work scope (i.e. replace of refurbish certain components). This functionality offers valuable decision support with performance testing in a gas turbine overhaul facility.

17.9   Generic GPA database system

Accumulation of the GPA data in a database system provides the possibility to analyse performance on a fleet of engines. Individual engine condition history can then be analysed and also analysis and statistics can be applied to data from multiple engines to obtain insight in the engine fleet condition and engine deterioration processes.

For this purpose the GSP GPA tool for the GEM42 has been extended with a database system that can file analysis results of an entire fleet. Figure 17.8 shows a screen shot of the interface that allows the user to select (a number of) engines to be displayed and trended in a graph. Apart from all condition indicators, the interface also allows displaying of a subset of condition indicators, to e.g. focus on the condition trending of a specific component.
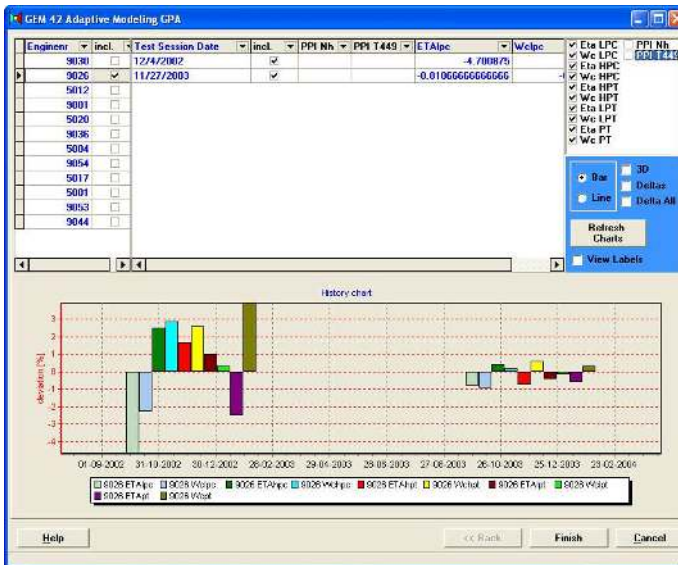

Figure 17.8   Engine fleet analysis window

The database system forms a start for the development of the engine fleet analysis tool. Additional functionalities such as statistical analysis and data mining are opportunities for the future.

17.10   Case study: A GSP GPA tool for the GEM42

17.10.1 Description

The new GPA tool was demonstrated on the GEM42 turboshaft engine installed in the Westland Lynx helicopter. Figure 17.2 shows a schematic lay-out of the GEM42 engine. Test data were obtained from the GEM42 engine test facility of the Royal Netherlands Navy. The requirements for an industrial GPA tool that were defined above could be met as follows:

- The reference model accuracy was improved over a power range of 450-780 kW using the previously described multi point calibration method. This allows analysis of off-design operating points.
- For the GEM42, the GSP GPA tool was configured to automatically perform 8 subsequent AM calculations, each with a different condition indicator subset (see Figure 17.3). The 8 sets of analysis results as well as the averaged values are displayed, providing a good first estimate of the root cause condition indicators.
- The new diagnostic validity index (DVI) function was used. The DVI is calculated by an algorithm that indicates whether an analysis result is within a realistic range. It forms a guideline in the assessment of which cycle analysis results should be included and which should be excluded from the final averaged diagnosis.
- All engine data, including rough measurement data, analysis results and final engine condition diagnosis are stored in a database. This allows trending of the analysed data
- A GUI 'wizard' could now be used, guiding the maintenance engineer stepwise through an entire GPA session. This means minimal training is required for the end user of the tools.

17.10.2 Results

The accuracy of the GSP GPA tool developed for the GEM42 was evaluated by analysis of existing test data and comparison of the obtained diagnostic results with the overhaul notes. The analysis results presented here show the condition history of a single engine, analysed over a period of 3 years. During this period the engine was tested 4 times in the GEM42 test facility of the Royal Netherlands Navy. GSP GPA analysis sessions were performed on all 4 tests results. For the 3 intermediate periods, the changes in component condition values were calculated using the GPA 'delta mode' (where only the changes in condition indicators before and after a period are shown) and presented in the next figures[11]. Now, the GPA results can be evaluated by comparison with information on engine usage and maintenance.

---

[11] Note that the individual GPA results on the 4 test points that indicate conditions relative to the reference engine are not shown here.
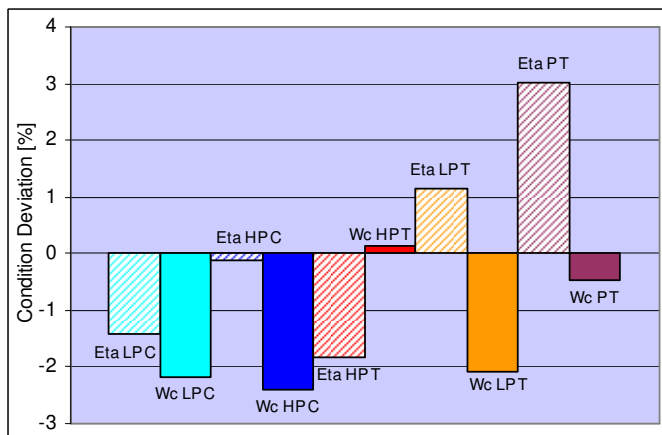
Figure 17.9   Condition change September 2000 - February 2002

Figure 17.9 shows the difference in component conditions of a single engine, tested in September 2000 and February 2002. The bars indicate the condition delta relative to the first test. Shortly before the second test was performed the power turbine (PT) was replaced. In the graph the condition of the PT is represented by the purple dashed bar (Eta_{PT}) and the purple solid bar (Wc_{PT}) on the outer right.

Apart from relatively small conditions changes that can be attributed to normal deterioration and data scatter, Figure 17.9 clearly shows an improvement in PT performance, corresponding to the PT replacement.

The overall engine performance however had not improved sufficiently with replacement of the PT. Therefore, after the February 2002 test the engine was returned to the work shop.

After rejection of the engine in February 2002 it was decided, based on experience, to replace the engine's hot section module. The hot section consists of the HPC (Eta_{HPC}, Wc_{HPC}), the combustion chamber and the HPT (Eta_{HPT}, Wc_{HPT}). The engine was tested again in March 2002. Figure 17.10 shows the engine condition change between the February 2002 and March 2002 tests.

The GPA results confirm the decision to replace the engine's hot section after the February 2002 test is the right one. The diagnostic results of the March 2002 test show a significant improvement of the hot section performance. The improvement in HPC flow capacity (Wc_{HPC}) is over 8% (note that this is from an about -4% to +4% deviation from the reference engine, these results are not shown here) and the Eta_{HPC} improves with 3%. The HPT flow capacity Wc_{HPT} has decreased by 6% indicating the HPT nozzle guide vanes of the HPT that was replaced must have been significantly corroded or otherwise deteriorated. The performance improvement was also confirmed by an improved PPI value.
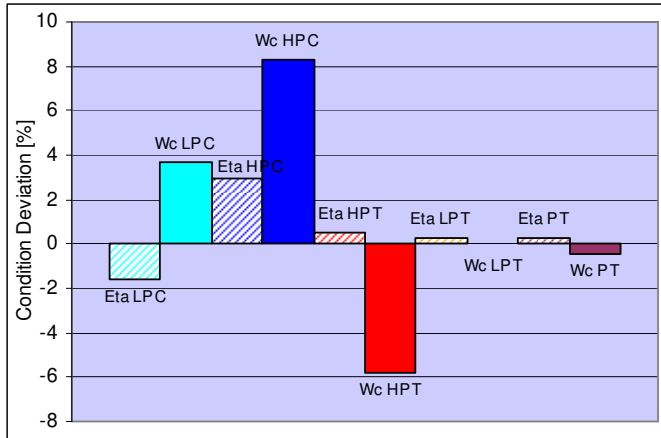
Figure 17.10 Condition change February 2002 - March 2002
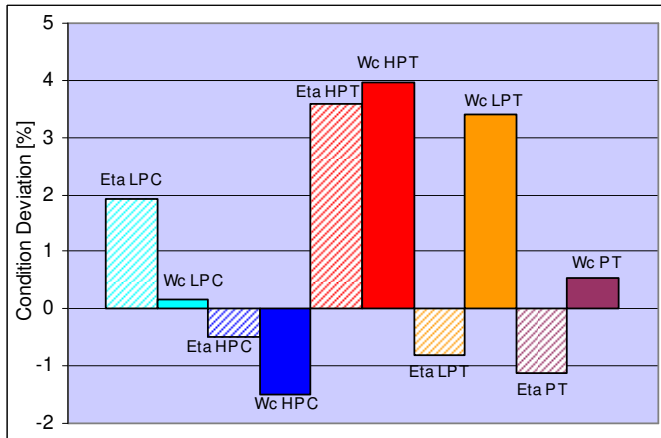
Figure 17.11   Condition change March 2002 - August 2003

Figure 17.11 shows the condition change between the tests carried out in March 2002 and in September 2003, almost 1.5 years later. Based on experience it was decided to replace the LPT module in order to improve the overall engine performance. The test of September 2003, performed after this overhaul action, indicated that the engine's PPI value had decreased instead of improved. Replacement of the LPT turned out not to have been an effective maintenance action.

The results in Figure 17.11 indicate that the performance of the newly placed LPT is indeed worse than the LPT performance analyzed 1.5 years earlier. This all indicates this LPT was in a poor condition.

Moreover, the results indicate a further deterioration of HPC (lower Eta and Wc) and PT (lower Eta and higher Wc). The HPT performance that especially the performance of the PT is unsatisfactory. The large negative value of Eta_{PT} and very large positive value of Wc_{PT} indicate a very low efficiency and an increased cross flow area, both signs of significant condition deterioration of the PT. Changing the PT instead of the LPT probably would have been more effective. In this situation, assistance of the GSP GPA tool in planning the work scope would have paid!

Based on the information available from inspections and 'overhaul notes', one part of the diagnostic result cannot be explained. Figure 17.11 shows in August 2003 an improved LPC efficiency with respect to March 2002. Such a large improvement of component efficiency, without any performed maintenance action, is very unlikely. It is probable that a compressor wash was carried out just before August 2003. Compressor washing is regularly carried out to remove fouling from the compressor blades and usually significantly improves performance. However, this suggestion could not be verified due to limited access to the maintenance records.

17.11 Conclusions

- The GSP Adaptive Modelling method is able to effectively identify component deterioration of different types of gas turbine engines, even with limited accuracy and availability of measured performance variables.
- Multi-point calibration of the reference model provides a significant improvement of GPA accuracy and stability.
- The method using *multiple analysis cycles* on different condition indicator sub-sets successfully generates values for all condition parameters in cases with fewer measurement parameters than condition indicators and where measurement data are unreliable. However, a minimum of accurate measurement data, depending on the engine configuration, is essential to effectively apply GPA.
- The dominant trend of root cause condition indicators can be effectively used to determine valid condition indicators.
- Several methods can be applied to eliminate invalid sub-sets and/or condition indicators including averaging the *multiple analysis cycle* results and manual or automatic elimination of invalid results using the validity index concept.
- A tool has been developed that enables rapid application of the method to any GSP gas turbine model.
- The method has been successfully demonstrated on the GEM42 turbo shaft engine. A number of case studies have shown GPA results corresponding to available maintenance notes and inspection data.

- The extension of the tool with a function to predict maintenance work scope effect on engine performance offers valuable decision support with performance testing in a gas turbine overhaul facility.
- The extension of the GSP GPA tool with a database system provides a useful tool for analysing engine history and comparison of analysed component conditions throughout the fleet. When a large number of analysis data is stored in the database, statistical analyses, trending and data mining can be performed.
- The automatic processing of *multiple analysis cycle* GPA results (eliminating invalid results) can be improved in order to minimize manual effort of the GPA engineer to obtain valid and accurate diagnostics results.
- The *genericity* of the tool can still be improved, allowing end-user configuration to any type of gas turbine measurement set-up.
- At the current stage, the database system only has limited analysis functionality. Additional extensions are required for powerful analysis of GPA data on engine fleet level.
- Although from a numerical point of view it is clear that the integral AM iteration in GSP is more efficient than a separate AM outside iteration loop, an interesting study for the future would be to compare performance with external loop AM solutions.

Chapter 18 Micro Turbine Research and Development[12]

18.1   Introduction

During the last few decades, several attempts have been made to develop micro turbines with efficiency levels close to those of larger gas turbines. Various interesting applications have emerged for both aircraft propulsion and power generation. Particularly for micro turbines below 100 kW, many developments have failed to obtain sufficient efficiency, reliability and cost effectiveness to be successful for the market.

The turbomachinery dimensions for rated power levels lower than 10 kW become very small. When using the Balje [117] design rules for characteristic rotor speed and diameter, a 3 kW gas turbine optimal radial compressor would have a diameter in the order of 30-40 mm and a speed of several 100,000 rpm. The major technical factors that challenge micro turbine development programs are the small-scale effects:

- low Reynolds numbers in the turbomachinery flow passages causing relatively high viscous losses,
- relatively high tip clearances due to manufacturing tolerances and bearing limitations,
- large area-to-volume ratios resulting in high heat losses and inadvertent heat transfer to the compressor; and
- relatively high auxiliary system losses due to the low power output level.

Another factor is cost. Development of efficient turbomachinery optimized for a particular cycle is very expensive and, in the micro power generation market, can only be justified with very large production volumes. An interesting opportunity to get around this cost problem is to use automotive turbocharger technology. During the last decade small turbocharger turbomachinery has become sufficiently efficient for gas turbine cycles, and cost price is low due to the very large production volumes.

---

[12] This chapter is based on 3 different publications:

[114] W. P. J. Visser, S. A. Shakariyants and M. Oostveen, "Development of a 3kw Micro Turbine for CHP Applications," *Journal of Engineering for Gas Turbines and Power,* vol. 116, 2011.

[115] W. P. J. Visser, S. A. Shakariyants, M. T. L. d. Later, A. Haj Ayed and K. Kusterer, "Performance Optimization of a 3kW Microturbine for CHP Applications", GT2012- 68686, presented at the ASME Turbo Expo 2012, Copenhagen, Denmark, 2012.

[116] A. J. Head and W. P. J. Visser, "Scaling 3-36kW Microturbines", ASME GT2012-68685, 2012.

At MTT (Micro Turbine Technology b.v., Eindhoven, the Netherlands) a preliminary sizing study indicated that with the smallest off-the-shelf turbocharger turbomachinery, a 3kW recuperated micro turbine with a thermal efficiency of at least 16% could be developed. If this concept could be mass produced at low prices corresponding to automotive parts, a competitive opportunity would emerge in small scale CHP (Combined Heat and Power) applications.
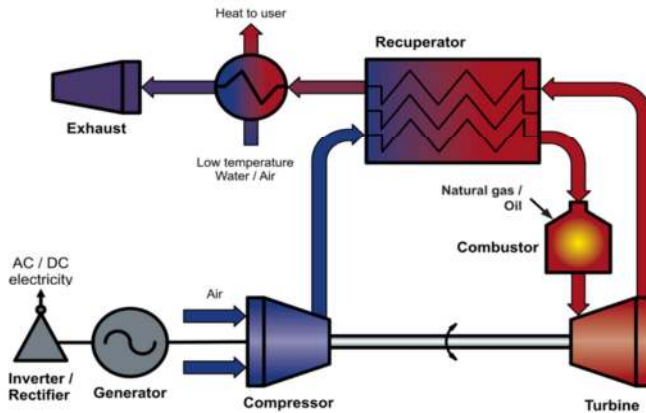
Figure 18.1 Recuperated micro turbine based CHP system

18.2   CHP application

Figure 18.1 shows the process of a recuperated micro turbine based CHP system. CHP concepts for small scale distributed power generation offer significant potential for saving energy and reducing CO2 emissions. Micro turbines are an interesting candidate for small CHP systems with advantages in terms of performance, size, noise and costs.

At MTT, a development program focuses on a heat demand driven micro CHP system to replace heating boilers for households and small businesses. During the development, large attention is given to cost price, reliability and low maintenance costs. Domestic micro CHP offers significant energy saving potential. Projected CO_2 savings per installed system are up to 6 tons per year.

While natural gas is the initial fuel of choice for the domestic micro CHP application, liquid fuels such as heating oil or diesel are required for micro CHP at locations without access to a natural gas distribution grid. A separate development program has started for the development of a clean combustor for liquid fuels that will comply with future emission requirements.

18.3   Conceptual design

As written in section 18.1, the 'off-the-shelf available' turbocharger technology offers an interesting opportunity to develop low-cost micro turbines. The compressor, turbine and sometimes bearing unit can be selected and matched without much modification. With the addition of a combustor, fuel system and control unit, a simple turbojet engine can be built. This concept is used for very small aircraft such as model planes. With a generator coupled to the shaft, a turboshaft engine is obtained for producing electrical power instead of thrust. With a recuperator, the efficiency of a turboshaft engine can be significantly increased, especially at the low cycle pressure ratios of turbocharger-based micro turbines. This is due to the consequent relatively high turbine exit temperature providing good opportunity to recover heat. Turbochargers are available off-the-shelf for both petrol and diesel engines with rated air flows down to 30 g/s.

Lab condition tests have indicated turbine inlet temperatures up to 1000ºC are feasible with the customary Inconel 713 material [118]. With advanced materials such as MAR-M247 TIT can be raised up to 1050ºC [119]. With these TIT levels for a typical small turbocharger based micro turbine rated at 35-45 g/s air flow, a power output of 2 to 3 kW is achievable. The heat input depends on the efficiency. For simple cycle it would be around 35-40 kW. With a recuperator the heat input reduces to around 15 kW due to the much higher efficiency. Equivalence ratios are around 0.35 (simple cycle) and 0.15 (recuperated) respectively.

A study has been performed on the performance potential of a case with off-the-shelf turbocharger components rated at 45 g/s. A development program has been defined including demonstration of a recuperated micro turbine design driving a 3kW generator, based on off-the-shelf turbocharger turbomachinery. The next phase is the development of a micro turbine optimized for a 3kWe turbogenerator in a domestic micro CHP system, replacing conventional boilers in environments such as larger houses and small offices, for which 3kW of electric power makes an optimal business case. At a target net turbogenerator efficiency of 16.5%, about 15 kW is available for the heating system and hot tap water functions.

18.3.1 Component efficiencies and losses

Modern small turbocharger turbomachinery performance has been significantly improved over the last decades. A simple survey of performance maps publicly available on the internet shows that, despite the small scale, isentropic compressor efficiencies of 75% and turbine efficiencies exceeding 65% are now state of the art. There is room for more improvement by optimizing the turbomachinery for the gas turbine application:

- The compressor impeller and/or diffuser design which is commonly optimized for a wide flow range [120] can be adapted towards maximum pressure ratio and efficiency. GSP cycle calculations indicate MTT micro

turbine design point power output and efficiency increase by about 2.5% per % increase in compressor isentropic efficiency at constant TIT.

- The turbine design with isentropic efficiency often peaking at lower pressure ratios for the automotive application [121] can be adapted for maximum efficiency at higher pressure ratio. Application of nozzle guide vanes does not guarantee efficiency improvement [122, 123]. Impeller redesign however can increase efficiency at high pressure ratio by a few percent. Because for the MTT turbine, total turbine power is roughly 3.5 times the shaft power output, this translates into 3.5% power and efficiency increase per % turbine efficiency increase. This has been confirmed with GSP cycle calculations.

Because turbomachinery redesign involves significant additional development efforts and also compromises the off-the-shelf advantages, the design adaptation option is kept for later study.

For the MTT micro turbine design, a component matching study has been performed resulting in a compressor driven by a turbine that in the turbocharger application would drive a larger compressor but still fits to the same off-the-shelf shaft and bearing unit. The larger turbine is required to comply with the turbine inlet conditions that are different from the automotive application.

For the conceptual design, component efficiencies and losses as listed in the reference case column of Table 18.1 have been assumed using the OEM specifications (where available), literature and engineering judgment. This case is expected to have the highest probability of matching the real performance, assuming all secondary engineering problems emerging from tests have been solved (leakage, component mismatch, improper assembly, rotor dynamics problems etc.).

The best case column in Table 18.1 represents the case were component efficiencies higher than expected or OEM-specified due to overestimation of loss factors. Also, newer turbocharger component designs that become available during the project will show higher efficiencies and these effects are also included as best case. The best case is also the starting point for the 2nd phase of the development program with increased efficiencies that are considered realistic objectives for an optimization program.

Finally, also a worst case scenario has been defined for the case that component efficiencies would be less than expected.

18.3.2 Modelling

Figure 18.2 shows the MTT recuperated cycle model configuration in GSP, including station numbers. The GSP models have been used for conceptual design, component matching and test analysis.

Figure 18.3 shows the results of a cycle performance study with 4 different carpet plots showing the relation between TIT, CPR (PRc), Eff, thermal efficiency

and power. Component efficiencies have been obtained from the reference case data in Table 18.1. Note that generator and inverter losses are not included at this stage. Net power output is defined as power delivered by the shaft to the generator.

The simple cycle option clearly does not get beyond 10% efficiency. The positive effect of increasing cycle pressure ratio and TIT is clear. Yet, with the phase 1 reference limits of around 1300 K and PR = 2.4, only 6.5% can be expected.

Table 18.1 Conceptual design study assumptions for ISA reference performance, efficiencies and losses

Parameter	Unit	Phase 1 – COTS Turbocharger based		
Air flow	g/s	**35-45 depending on compressor type**		
Thermal power	kW	**Simple cycle : 35-45 / Recuperated : 10-18**		
		Worst	**Reference**	Best
PL_{inlet}	%	1	**0.5**	0.2
$\eta_{is\_compressor}$	%	60	**70**	75
$PR_{compressor}$	-	2.0	**2.4**	3.2
$PL_{combustor}$	%	2	**1**	0.5
$\eta_{combustor}$	%	99	**99.5**	99.9
TIT	ºC	977	**1027**	1077
	K	1250	**1300**	1350
$\eta_{is\_turbine}$	%	60	**65**	70
$\eta_{mech\ (bearings)}$	%	95	**97**	98
Eff_{rec}	-	0.70	**0.8**	0.9
PL_{rec_hot}	%	Eff.0.7 : 3 Eff.0.8 : 4 Eff.0.9 : 5	**Eff.0.7 : 2 Eff.0.8 : 3 Eff.0.9 : 4**	Eff.0.7 : 1 Eff.0.8 : 2 Eff.0.9 : 3
PL_{rec_cold}	%	Eff.0.7 : 2 Eff.0.8 : 3 Eff.0.9 : 4	**Eff.0.7 : 1 Eff.0.8 : 1.5 Eff.0.9 : 2**	Eff.0.7 : 0.5 Eff.0.8 : 1 Eff.0.9 : 1.5
$PL_{exhaust}$	%	0.8	**0.5**	0.2
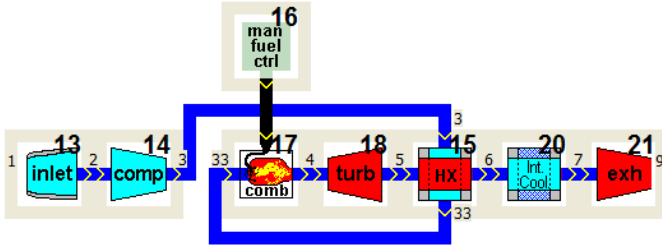
Figure 18.2 Simplified GSP model of MTT recuperated cycle
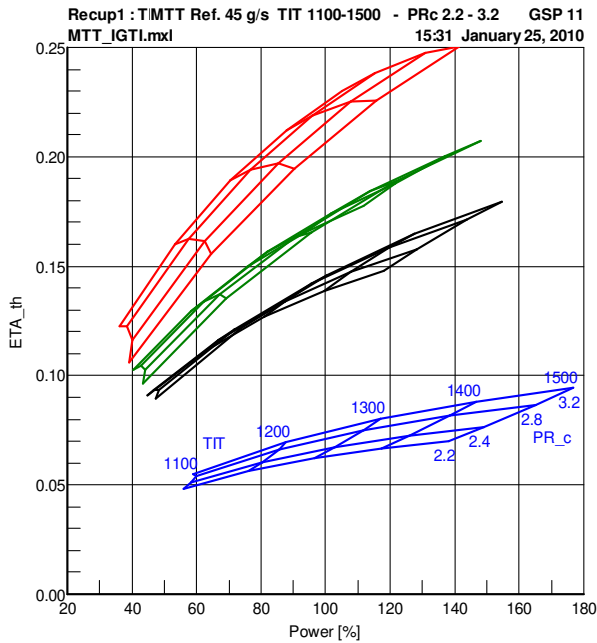
Figure 18.3 Reference case thermal efficiency as a function of PRc, TIT and Eff (blue=simple cycle, black=70%, green=80%, red=90% effectiveness)

The effect of a recuperator is significant. Already with a modest effectiveness of 70%, thermal efficiency is raised to around 13%. With the reference 80% effectiveness (green carpet plot), 15% is obtained. With the high value of 90% claimed for advanced recuperators [124, 125], thermal efficiency goes up to 18%.

Figure 18.4 shows that for a given TIT of 1300 K, recuperator inlet temperature T_{t5} is higher than today's typical limits for recuperators around 650ºC (923 K) [126, 127]. It clearly shows that if a high thermal efficiency is required combined with a low CPR, then a high temperature recuperator is required allowing inlet temperatures up to 1100 K (823ºC). It is clear there is a design conflict here and as a

consequence a multi-disciplinary optimization exercise is needed for an optimal trade-off between performance, costs and life aspects.
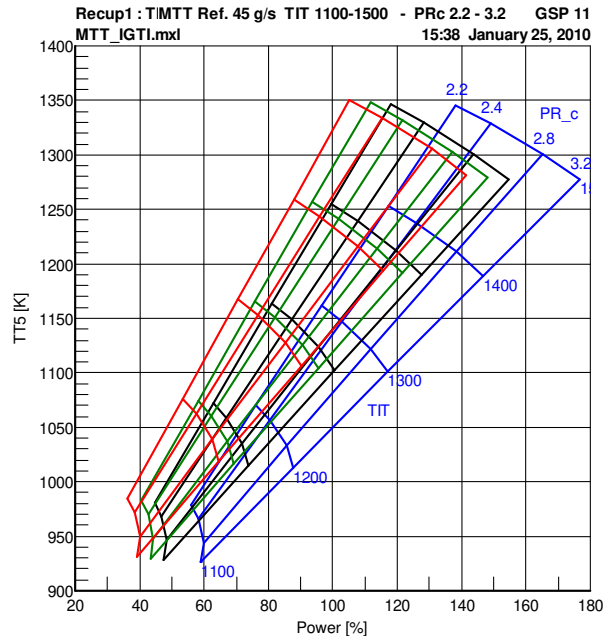
Figure 18.4 Recuperator gas side inlet temperature (blue=simple cycle, black=70%, green=80%, red=90% effectiveness)

Figure 18.5 shows that with increasing gas turbine efficiency, the combined heat-power (CHP) potential decreases due to the relatively low exhaust temperature and water vapour content as compared to CHP systems using internal combustion engines burning at close to stoichiometric conditions. This is due to the large portion of air dilution with the combustion gas in order to reduce turbine inlet temperature down to acceptable levels. Especially with a high effectiveness recuperator, the overall equivalence ratio drops down to around 0.15. As a consequence, it becomes more difficult to extract heat from the exhaust gas.

Figure 18.6 shows Table 18.1's best case performance. The increase in efficiency is dramatic. This means development effort focused on incremental increases in component efficiencies and reduction of pressure losses will be particularly effective to increase efficiency. More on this follows in section 18.7.
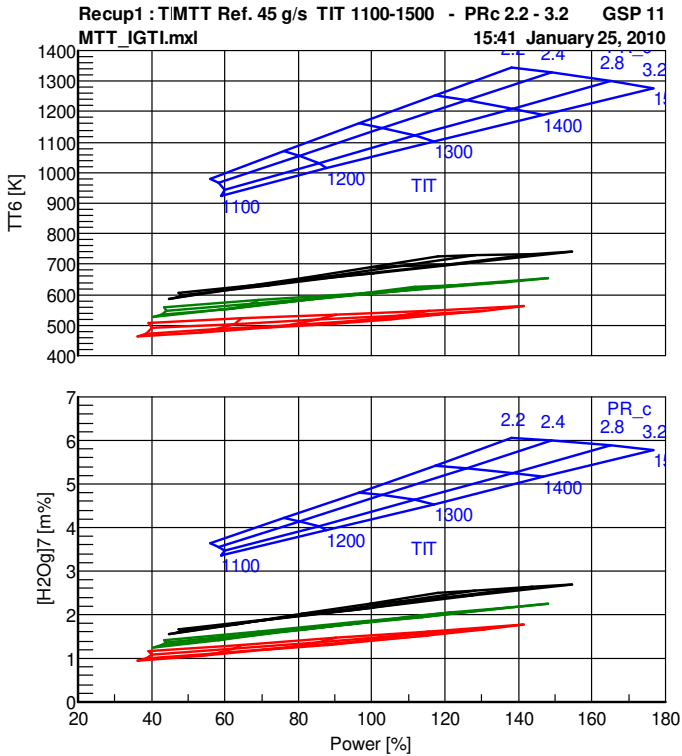
Figure 18.5 Exhaust gas conditions (blue=simple cycle, black=70%, green=80%, red=90% effectiveness)

Also the worst case of Table 18.1 has been simulated and this indicated that only a slight drop below reference case component performance already completely wipes out system performance. From this it may be concluded that only since small turbochargers have obtained efficiencies corresponding to modern small gas turbine levels, it has become possible to use these components to build micro turbines with practical efficiency levels.

18.4   Demonstrator development

The 'Mk4' demonstrator gas turbine was developed to verify results of the conceptual study. The demonstrator combines off-the-shelf components with components developed in-house at MTT. Turbomachinery and bearings are off-the-shelf turbocharger components. The radial permanent-magnet type generator is custom-designed as is the coupling with the turbine shaft. The recuperator is also a custom design of the primary-surface type. The combustion chamber and fuel control concept are developed by MTT.
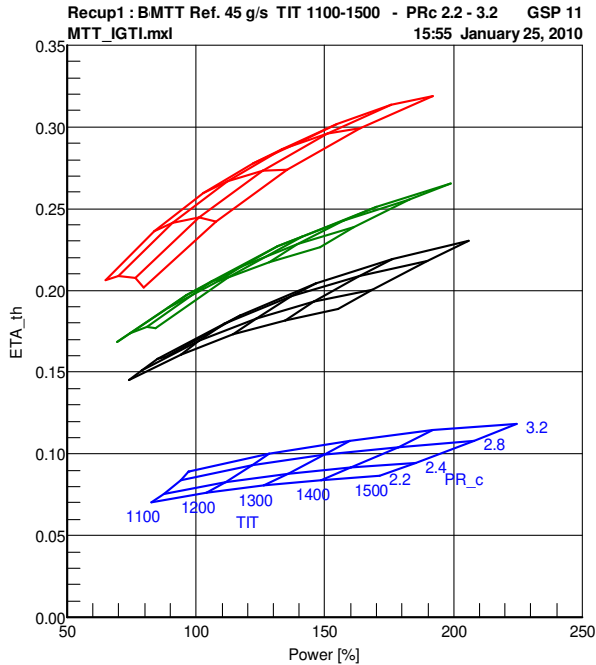
Figure 18.6 Best case performance (see Table 1) (blue=simple cycle, black=70%, green=80%, red=90% effectiveness)

The experimental program was carried out from summer 2008 until summer 2009. It included three phases during which the gas generator, the simple cycle turboshaft and finally the recuperated turboshaft configurations were tested subsequently.

18.4.1 Turbomachinery selection

The customary combinations of compressors and turbines for the turbocharger application are far from optimal for the micro turbine application which requires a higher design turbine inlet temperature and therefore larger turbine. Therefore, a turbomachinery selection study has been carried out for optimal matching of turbocharger compressor and turbine. Publicly available component performance maps from the world's leading manufacturers have been assessed and used in cycle optimization exercises.

Figure 18.7 shows the GSP generated relations between cycle design parameters and corresponding required turbine inlet corrected flow (W_{C4}) levels. With this and related model results, the optimal turbine-compressor match could be determined. For the MTT Mk4 case of 45 g/s inlet air flow, matching points are found around W_{C4}=40 g/s.
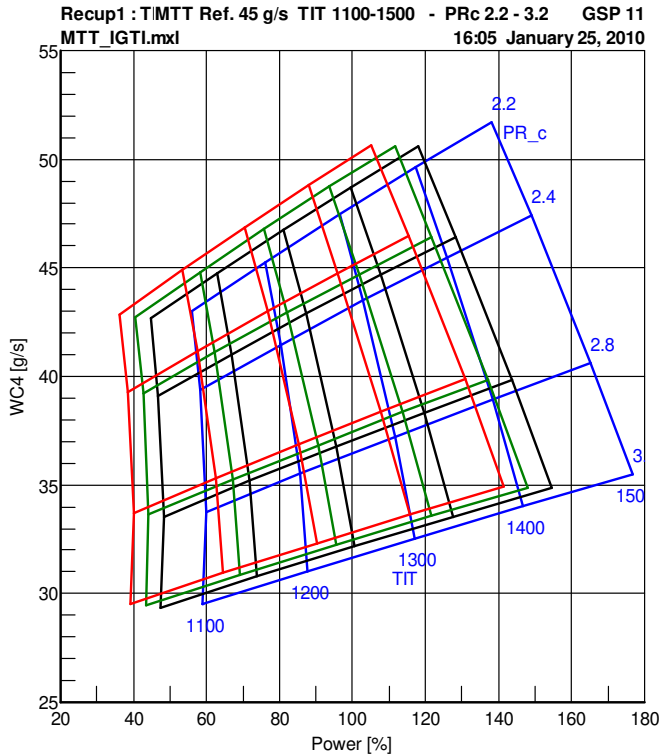
Figure 18.7 Turbine flow capacities (WC4) for various reference case cycles (blue=simple cycle, black=70%, green=80%, red=90% effectiveness)

18.4.2 Other components

In the journal article [114] the development of other components is described, including rotor, generator, bearings, combustor, recuperator and control system.

18.5   Test program

To prove the feasibility of the MTT micro turbine concept and validate the GSP model predictions, a test program was started. The final objective is 3kWe at 16% electrical efficiency for micro CHP applications. The test program included 3 phases:

- Gas generator tests using a back pressure load (a variable nozzle at the turbine exit) for proof of concept, validation of model performance predictions and component match. Objective was at least 5% equivalent efficiency.

- Simple cycle turboshaft tests to determine the optimal turbine-generator coupling configuration.
- Recuperated turboshaft tests to validate recuperated cycle model predictions and recuperator design. Objective was to obtain at least 12% electrical efficiency.

18.5.1 Test rig

A test rig was developed, suitable for the various configurations. With test data performance analysis could be performed and energy balance and losses assessed to provide the results presented in the following sections. *Analysis by synthesis* (the methodology to determine unknown parameter values by tuning the model to match measured data) was applied using GSP models.
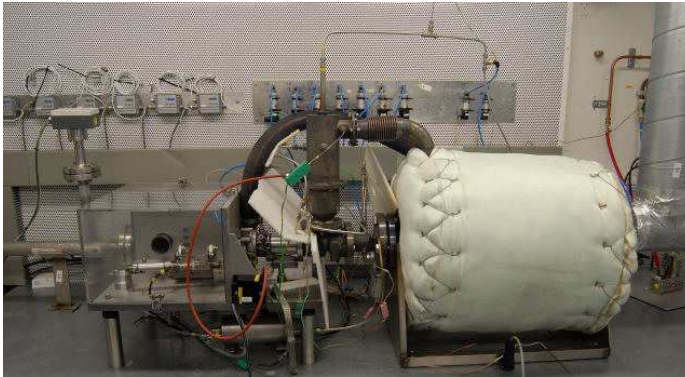
Figure 18.8 MTT micro turbine test rig

Figure 18.8 shows the test rig with the Mk4 recuperated micro turbine. On the left the inlet duct with the flow meter is located. Next the transparent plastic inlet receiver box is visible. In the middle the combustor is shown vertically connected to the turbine. The large drum on the right is the insulated recuperator which in this case is rather large since the dressing design is not optimized for minimal size.

18.5.2 Gas generator tests

For the gas generator tests, power output was expressed using 'equivalent shaft power' PW_{eq65}. PW_{eq65} represents the mechanical power that could be extracted from the gas generator exit flow with a 65% isentropic efficiency turbine and is defined as follows:

$$PW_{eq65} = 0.65 \cdot W_5 \cdot C_{p5} \cdot T_{t5} \cdot \left[1 - \left(\frac{P_0}{P_{t5}} \right)^{\frac{\gamma-1}{\gamma}} \right] \tag{18.1}$$

Equivalent thermal efficiency η_{eq65} then is defined as equivalent power PW_{eq65} over fuel input thermal power.

At the design point of 240,000 rpm and a calculated adiabatic TIT of 1369 K, 3.25 kW equivalent power with an equivalent thermal efficiency of 6.34 % was measured at almost ISA standard ambient conditions (1011 mbar and 294 K). The measurements corresponded with the GSP model predictions. Results of this test phase were used to enhance the GSP models.

18.5.3 Simple cycle turboshaft

Once the equivalent thermal efficiency was proved in the gas generator test phase, the turbine was coupled to the generator to try different coupling concepts. After various iterations the optimal stiffness/mass distribution of the shaft coupling was found. At 218000 rpm 2788 W (ISA corrected) was produced, corresponding to 6.28% electrical efficiency.

18.5.4 Recuperated cycle turboshaft

The recuperated configuration was used to demonstrate the potential for efficiencies beyond 10%. Custom design recuperators from 2 separate manufacturers were used. For the recuperator, at least 85% effectiveness and less than 4% (air + gas) pressure loss was required.

Table 18.2 Recuperated cycle measured performance

	Observed	ISA corrected	
T_0	299.3	288.15	K
P_0	1.0047	1.01325	bar
N	240,000	235,487	rpm
PW_{shaft}	2428	2983	W
Eta_{shaft}	11.84	13.5	%
PW_e	2178	2733	W
Eta_e	10.32	12.28	%
PR_c	2.69		-
TIT (T_{t4})	1334 (calc'd)	1334	K
T_{t5}	1055		K
W_2	42.21	44.4	g/s

Several different recuperators were tried in the tests with varying performance and usually total pressure loss levels exceeding 4% which means significant performance penalties. Finally, with a recuperator with about 4% pressure loss

favourable results were obtained with 2.7 kWe and 12.2 % ISA corrected electrical efficiency at 240,000 rpm. Table 18.2 lists the observed and also ISA corrected performance data.

From the test analysis with GSP, compressor isentropic efficiency could be determined: at 73.8% and turbine efficiency at 67%. These values correspond to the component maps.

The generator losses consist of bearing losses, windage losses and electrical losses. Using a torque measurement with the generator on a free-rotating cradle, losses between 250 and 300W were estimated at the operating point of Table 18.2.
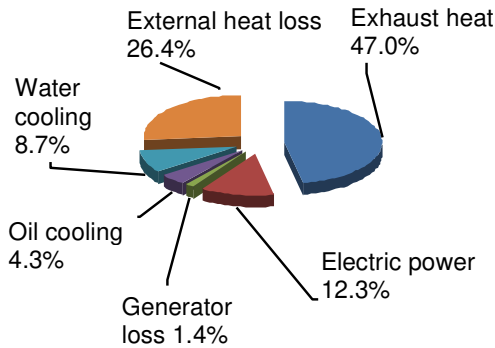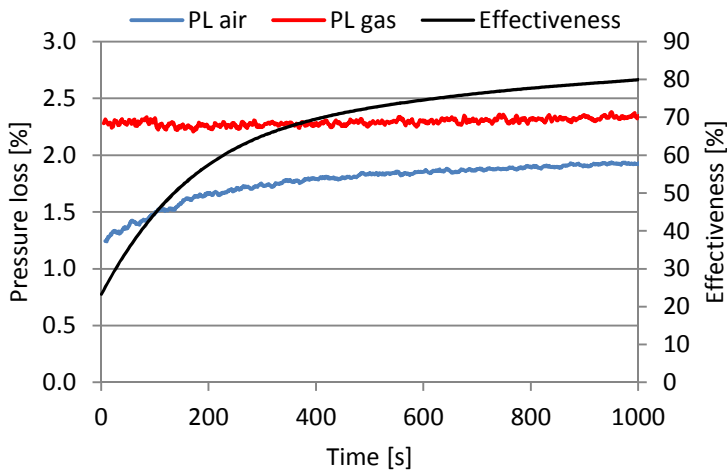

Figure 18.9 Losses overview

Figure 18.10 Recuperator pressure loss and effectiveness during warm-up

During every run the turbine lubrication and cooling flow temperatures and flow rates were measured. The associated thermal losses were in the order of 2.5 kW and depended mainly on turbine flow temperatures and to a lesser extent on input power and rotational speed. Using the GSP model and energy balance analysis the total heat loss from the hot components was estimated at 6 kW. Figure 18.9 gives an overview of all losses as a percentage of the thermal power input.

The recuperator effectiveness varied significantly with the different models used. The objective of 85% effectiveness was matched with the best recuperator after thorough insulation. The recuperators were not designed for limited size and weight for the pre-specified active volume. The resulting high heat capacity caused long warm up periods (after which steady-state effectiveness was reached) in the order of 30 minutes. Figure 18.10 shows how during warm-up effectiveness is slowly increasing towards its steady-state value due the the heat soakage effect resulting in higher fuel consumption during warm-up.

With the high sensitivity to pressure loss of the MTT cycle, the thermal effects on recuperator pressure losses are significant. During engine warm up, the pressure drop over the gas side remained almost constant. The air side pressure drop however increased signficantly as can be seen in Figure 18.10. The increase in pressure drop during warm up corresponds to a power loss in the order of 100W.

18.6   Optimal cycle pressure ratio

A GSP model of the recuperated cycle concept can be used to predict the relations among design cycle pressure ratio, efficiency, power output, recuperator inlet temperature and recuperator pressure losses. The relatively low TIT means optimal cycle pressure ratio (for efficiency) is not far above the current value of 2.69 as can be seen in Figure 18.11 (note that the recuperator air and gas pressure losses are lumped together in the PR2_rec parameter). With TIT at 1300K, the pressure ratio for optimal efficiency is about 3 with 4% pressure loss (PR2_rec=0.96). For maximum power, optimal PR_c is close to 4. When running cooler at 1250K the optimal PR levels are lower. A trade-off can be made between running at either maximum efficiency or maximum power. In any case, the efforts to increase the compressor pressure ratio beyond 3 will represent significant improvement.

Another important issue is the turbine exit (recuperator inlet) temperature TT5 which becomes very high at lower PR. Depending on the material choice (and costs) for the recuperator, a higher PR may be desired to reduce TT5 to an acceptable level. In this case TT5 is already too high for a stainless steel recuperator (with a max TT5 in the order of 650 C or 973 K) and more advanced materials such as Inconel 713C are required.
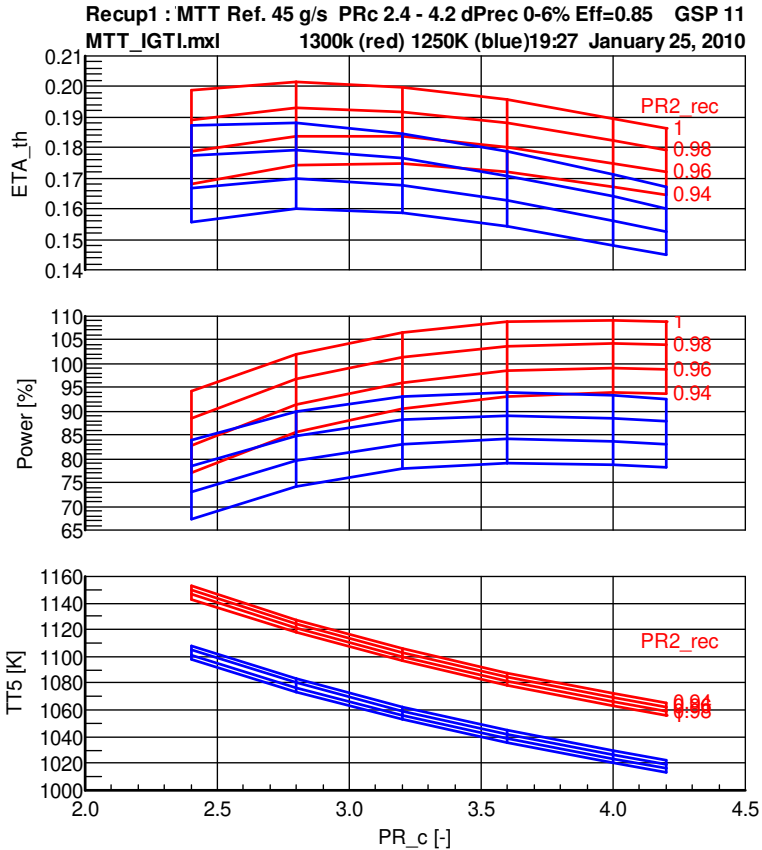
Figure 18.11 Cycle pressure ratio (PR_c) and recuperator pressure loss effects on efficiency and power output (PR2_rec=1-lumped recuperator pressure loss)

18.7   Performance Optimization

The next phase of the development program at MTT included a performance optimization program to increase the net electric efficiency to the design objective of 16.5% net efficiency η_{enet}. This corresponds to about 19.5% η_e or almost 22% shaft thermal efficiency η_{shaft}. Following an assessment of performance improvement potential, separate targets were set for of all components affecting efficiency. A detailed GSP cycle model was used to predict effects on cycle efficiency. Parallel projects were launched to work towards the overall objectives.

18.7.1 Performance optimization objectives

The 12.2% ISA electrical efficiency corresponds to 13.5% shaft (thermal) efficiency when excluding the electrical losses. An improved test turbine had been developed with a different rotor configuration, as shown in Figure 18.12.

Figure 18.12: Mk5 microturbine.

This 'Mk5' test turbine was used for further performance improvement testing and for integration in the micro CHP system prototypes shown in Figure 18.13. With the Mk5 turbogenerator and CHP system initially comparable performance as with the Mk4 was obtained.

Figure 18.13: Mk5-based CHP system prototypes in the MTT test cell.

When including all CHP sub-system losses (oil, fuel, water pumps, compressors etc.), the net electrical efficiency drops from 12.2% to about 9.5% with a power output of 2000 W. Note that this is due to several non-optimized subsystems consuming excessive power, and that many of these can be relatively easily improved substantially.

A Performance Enhancement Program started in November 2010 focused on 3kW at 16.5% net electrical efficiency with separate work packages for improving performance of the components and subsystems listed in Table 18.3.

Table 18.3   Performance enhancement objectives and status

Component/ Sub-system	Parameter	unit	Initial	Target	GSP predicted $\Delta\eta_{e\ \%}$	Oct. 2011	$\Delta\eta_{e\ \%}$
Recuperator	Δp	%	4.5	4.0	0.22	4.5	0.0
	η	%	85	88	0.8	88	0.8
Bearings	PW_{loss}	W	900	500	1.8	700	0.9
Compressor	PR	-	2.8	3.0	-	3.0	-
	η	%	70	73	1.4	75	2.0
Turbine	η	%	65	67	1.3	70	2.0
Combustor	Δp	%	1.5	1.25	0.1	1.5	
Inlet	Δp	%	1.2	0.75	0.1	1.2	
Exhaust	Δp	%	1	0.75	0.1	1	
Ducting	Δp	%	1	0.75	0.1		
Oil pump	PW_{loss}	W	75	50	0.11	75	
Fuel compr.	PW_{loss}	W	360	300	0.27	300	0.27
Heat loss	Q_{loss}	W	2500	1250			
Generator	PW_{loss}	W	317	215	0.46		
Inverters	PW_{loss}	W	465	328	0.62		
Total					7.38		6.07

Detailed GSP models were used to predict the effects of the individual improvements in Table 18.3 on electric efficiency. When the target improvements would all be realized, a net efficiency increase of 7.35% is predicted. Added to the initial 9.5% net efficiency this would result in 16.85% leaving a 0.35% margin with regard to the design objective. As of October 2011, significant progress was made on the major improvement items as shown in Table 18.3 resulting in a current net efficiency between 15 and 16%. Electric generator power efficiency η_e, reached 17.2% ISA. In the paper [115], detailed descriptions of the individual component improvements are described. Below a summary is given of the major component improvements and the predicted effects on electric efficiency calculated with the GSP model.

18.7.2 Compressor

The compressor has received specific focus for improving performance. Firstly, the pressure ratio at the design speed of 240,000 rpm and about 1300 K TIT had to be increased to the optimal values discussed in the initial development phase: In the conceptual design study (0), optimal values of cycle pressure ratio were found to be at least 3 for the optimal cycle efficiency (when assuming also 2+2% recuperator

pressure loss). Since with higher pressure ratios, recuperator inlet temperature is reduced and output power increased at the expense of only a slight reduction in efficiency, options to increase compressor pressure ratios up to 3.4 were explored by increasing tip diameter D_{tip}. Next to the reference compressor with diameter D_{tipref} and 2.9 pressure ratio, tip diameters $D_{tipref} + 1$, $D_{tipref} + 2$ and $D_{tipref} + 3$ [mm] were assessed. Prior to testing with these larger diameters, a CFD analysis was performed to assess the effect of increasing D_{tip} by up to 2 mm on performance and to identify design aspects that could be worked on to increase efficiency.

The compressor CFD analysis results (described in detail in [115]) show that it is possible to increase the total pressure ratio significantly and to maintain efficiency level by extending the impeller blades. For stationary operation an improvement of the overall compressor performance can be achieved by optimizing the blade leading edge geometry for a given operating point with regards to reduced incidence losses. Significant improvement can be achieved by reducing the tip clearance height.

The 240,000 rpm design speed is within the original turbocharger compressor and turbine structural limits and therefore no separate structural analysis was performed at MTT.

18.7.3 Turbine

The turbine used in the Mk4 test microturbine had only a moderate isentropic (and adiabatic) efficiency of 65%. This was due to both the impeller and scroll design. For the Mk5, a more advanced turbine was available with a maximum reference isentropic efficiency of around 70%. This value is obtained when an optimal scroll design is used, without application design adaptations such as the waste gate or sharp turns in the ducting causing additional pressure losses. Especially for the turbocharger waste gate, aerodynamically smooth turbine exit ducting is often sacrificed. While the Mk4 still had an off-the-shelf automotive application scroll with waste gate, the Mk5 turbine scroll design was optimized and the waste gate omitted. This, combined with the already OEM built in improvements resulted in a 5% increase in isentropic turbine efficiency which was more than anticipated. Since the turbine delivers both the compressor and generator shaft power which is around 13kW, 5% increase means 650W extra power output. However, due to the consequent lower recuperator entry temperature, recuperator heat recovery is reduced somewhat leaving a GSP predicted efficiency increase of around 2%.

18.7.4 Recuperator

The recuperator improvements described in [115] include a 3% increase in efficiency and a 0.5% reduction of pressure loss (4.5% down to 4%). With the GSP model, the effect on electric efficiency (0.8 and 0.22% increase respectively as shown in Table 18.3) has been calculated using the GSP model.

18.7.5 Heat losses

Heat losses from the hot parts due to conduction, convection and radiation are substantial if insulation measures are not thoroughly implemented. This is due to the high surface to volume ratio of the small micro turbine components. The turbine scroll surface may reach temperatures near or over 1000 °C, turning it into a red hot heat radiator. The combustor is cooler due to the cooler flow around the liner which holds the combustion process. With a recuperated cycle however, this air is preheated (in the MTT cycle up to about 720 °C) thereby increasing potential heat loss. The recuperator is relatively cool on one side and hot at the other, but has a relatively large surface.

Heat loss studies with GSP, using the thermal network modelling capability described in Chapter 9, have shown that with inorganic silicates insulation material cycle performance is significantly improved up to a thickness of 100 mm (Figure 18.14).
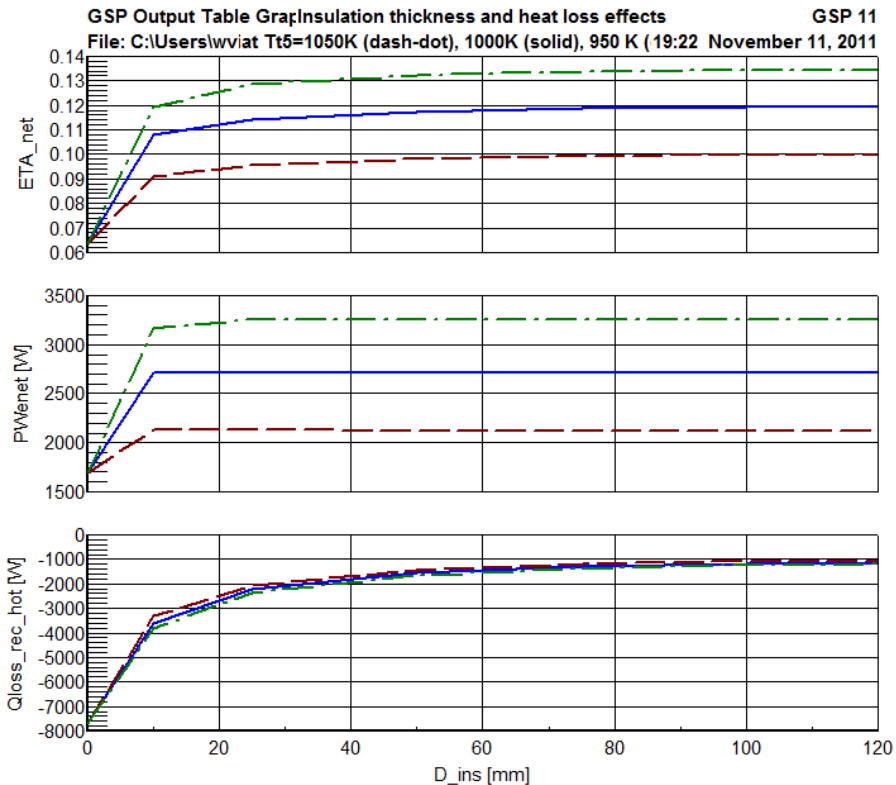

Figure 18.14: Insulation thickness effect on performance

From an energy balance calculation, the heat loss from the gas path required to meet the target efficiency is estimated around 1250 W. The latest test heat loss was still 2500 W. It is very difficult to establish an accurate energy balance, particularly around the turbine, so relatively large uncertainty margins have to be accepted. As with the pressure loss, the prototypes will have optimized insulation and are expected to show efficiency benefits from this in future tests.

While the gas path heat loss is to be minimized, the heat that is still lost should be recovered as much as possible into the CHP system heating circuit. This is done by optimal positioning of the heating water ducting near the heat loss areas. In the heat balance model, heat recovery factors are estimated to determine the overall CHP energy/heating efficiency. This includes heat lost outside the gas path from the oil and generator and bearing cooling circuits, the fuel compressor and power electronics.

An additional requirement to the heat loss is coming from the system heat management perspective. The heat loss will heat up the inside of the CHP system cabinet and to prevent overheating it must be vented to limit temperature. From a cycle calculation it shows that it is more efficient to use a separate fan for this function rather than the compressor inlet air, which, if heated up, would severely penalize microturbine thermal efficiency.

18.7.6 Test results

Following the analysis work mentioned above, tests have been performed with the improved turbine and different compressor tip diameters. Results are shown in Figure 18.15 and Figure 18.16: the performance enhancement has resulted in an increase from 12.2 to 17.2% generator power electric efficiency and 3400W power output.

The test results confirmed the CFD simulation predictions for compressor pressure ratio and efficiency (i.e. that efficiency was maintained with a small increasing in tip diameter). It is clear that with larger tip diameter and the consequent larger pressure ratio, power output increases significantly. Tip diameter D_{tipref} + 1 mm has almost the same cycle efficiency as D_{tipref}. However, beyond tip diameter D_{tipref}+1mm, efficiency drops due to the reduced heat recuperation (see Figure 18.11). From this, it is concluded that at this stage a D_{tipref}+1mm or D_{tipref}+2mm tip diameter must be selected. If during subsequent endurance tests (not covered in this paper), recuperator temperature T5 must be reduced, the (D_{tipref}+3mm) impeller can be used to further reduce Tt5.
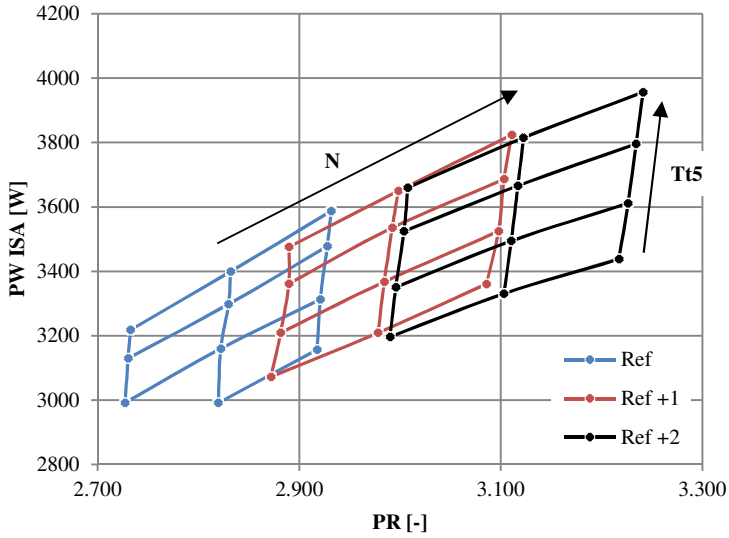
Figure 18.15: Test results: Generator power (at ISA) versus pressure ratio for different impeller diameters, rotor speed and Tt5
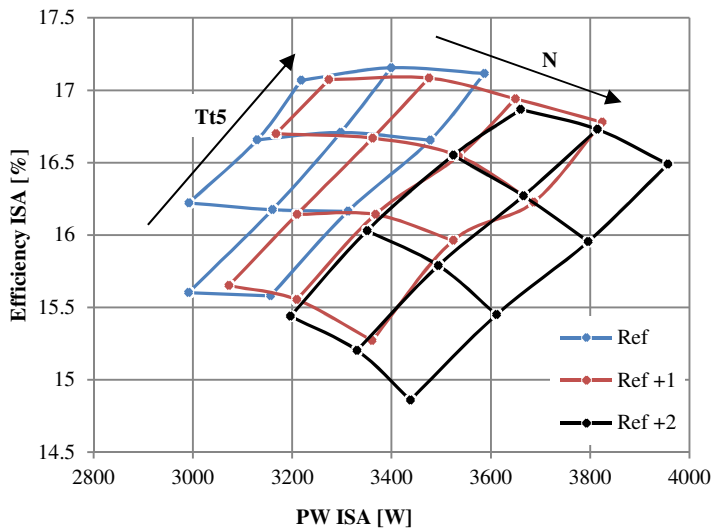

Figure 18.16 Test results: Electric efficiency vs. generator power (at ISA) for different impeller diameters, rotor speed and Tt5

18.7.7 Next steps

Significant progress has been made towards the design objectives and major component improvements have been realized corresponding to the objectives of Table 18.3. For the target net electric efficiency of 16.5%, at least 18.5% generator efficiency η_e will be required, depending on the eventual electric and other auxiliary losses. So far a η_e value of 17.2% was reached. The remaining net efficiency improvement required is at least 1.3% and can be covered for a substantial part by working on the smaller items in the table. An effective way towards a larger increase in efficiency is further improving the turbomachinery. The compressor CFD has already hinted at efficiency bottlenecks that offer potential. For the turbine also CFD models will be developed to determine design improvements. These steps will push shaft efficiency beyond 25% and then electric efficiencies of 20% come within reach.

18.8   Scaling to other power levels

18.8.1 Introduction

Microturbine performance and losses are strongly dependent on scale. Especially at very small sizes, prediction of these scale effects is important within the framework of conceptual design and sizing studies. The effects need to be accounted for in studies where the power output is varied in order to optimize the application in which the microturbine is integrated.

The scale effects can be addressed for the individual gas path and mechanical components which include turbomachinery, ducting, bearings, recuperators, combustors etc. Absolute prediction of efficiencies at the initial design stage, or at any other stage, is difficult, and the designer usually relies upon empirical loss models and correlations. Using both empirical and physical analysis, these relations can be extended to include size as a variable providing a means to predict changes of losses relative to a known reference case. An analysis is presented of size-related loss mechanisms in small turbomachinery derived from turbochargers. A microturbine cycle performance analysis has been performed in order to illuminate how these effects influence efficiency at varying design power levels. A case study is presented scaling microturbine concepts in the range of 10-36kW for an electric vehicle range extender application.

18.8.2 Correlations for scale effects

A series of empirical relationships for scale effects on performance of small radial turbomachinery, such as shown in Figure 18.17, have been analysed. Small turbomachines have lower efficiencies than larger geometrically similar machines. Several publications have presented empirical correlations that try to accurately account for scale effects.

Figure 18.17 Micro turbine rotor with compressor and turbine

These correlations can be used in cycle models to assess scale effects on gas turbine system performance. Turbomachines which are of similar geometric design (having same specific speed Ns and specific diameter Ds values (see [117]) are similar in flow mechanism. It then follows that if Reynolds is neglected the machines will have the same efficiency [117]. Therefore the effects of scale are isolated only through changing a reference geometrical design. In the study described in this paper, the effects were simulated using the Capstone C30 micro gas turbine engine as a reference. Scale effects on radial micro compressor and turbine performance and efficiency are translated into engine system performance effects. Relations between rated power and engine size and weight are also discussed. The work is focused on the application of a recuperated microturbine as an electric vehicle range extender.

18.8.3 Scaling micro turbine system performance

A preliminary micro turbine design can be drafted by scaling from an existing reference using the appropriate non-dimensional parameters. Precise prediction of component efficiencies at the initial design stage, or at any other stage, is difficult, and the designer usually relies upon empirical loss models and correlations. The predicted efficiencies are then as good as the underlying empirical loss models [117].

If the designer really wants to generate a model with significant improvements in efficiency and/or size then a fundamental aerodynamic design must be undertaken of the impeller and other essential parts. This is costly and impractical for preliminary design analysis. Therefore, in this study, an attempt is made to isolate the scaling effects to predict performance of designs scaled from proven technology such as the 30 kW Capstone turbogenerator (Capstone C30).

18.8.4 Component efficiencies and losses

The scale effects on cycle performance are composed of effects on individual components efficiencies and losses. These are generally due to Reynolds effects and gas path surface roughness, tolerances and tip clearances not scaling proportionally with size.

Empirical relations are used to account for turbomachinery component efficiency variation due to scaling. Tip clearance effects are represented separately since tip clearance does generally not scale proportionally with size and has significant effect on efficiency.

Blade thickness and throat area tolerances concern both efficiency, casting manufacturability and blade erosion. With reducing impeller diameter rotational speed must be increased in order to maintain tip speed and thereby sufficient performance and efficiency. Microturbine thermodynamic performance is therefore, size (output power) dependent, in contrast to larger industrial gas turbines [128]. The rotor/impeller sizes and clearance gaps are addressed in greater detail. Miniaturization of turbines cause large changes in Reynolds number, the geometrical restrictions related to material and manufacturing of miniaturized components become a greater concern and the heat transfer between the hot and cold components increase, which is negligible in large machines [72, 73, 129].

Steady-state heat loss effects are not considered although they become significant at smaller sizes of lower rated power levels, especially below 10 kW and if no insulation measures are taken. Heat loss effects should be assessed later once a particular design and power rating is chosen for an application.

Other gas path elements (e.g. ducts and inlets, bearings and other components) have relatively minor sensitivity to scale and are therefore neglected. Generator efficiency (including inverter losses) may well be affected by scale also but is assumed at a constant 90% at this stage of the work.

18.8.5 Scaling cycle parameters

The method to implement the equations into GSP involves defining a scaling factor "C30" for the model design power. The Capstone C30 engine is taken as reference (Pref = 30 kW) and scaled to other power levels P (equation (18.2)).

$$P = C30 \cdot \text{P}_{ref} \tag{18.2}$$

Technology level is maintained by keeping TIT and PRc constant (later these will be varied separately within each design power level in section 18.8.11). Component performance is adapted as a function of the C30 scale factor. C30 = 1 means an engine identical to the Capstone C30.

Inlet mass flow is assumed to change proportionally with rated power and thus with the C30 factor. Turbomachinery diameter D is chosen as the primary size

variable and inlet mass flow is assumed to be proportional to D^2. As a result we assume

$$P \propto \dot{m}_a \propto D^2 \qquad (18.3)$$

or

$$C30 = \frac{P}{P_{ref\,(C30)}} \propto \frac{\dot{m}}{\dot{m}_{ref\,air}} \propto \frac{D^2}{D_{ref}^2} \qquad (18.4)$$

Naturally, the above relations do not hold in reality due to the size effects themselves. Mass flow rate and P will tend to drop disproportionally with size D^2 due to increasing boundary layer and loss effects. In this exercise these effects are superimposed on the above simplified relations via efficiency drops.

18.8.6 Scaling turbomachinery efficiency

Efficiencies generally decrease with decreasing C30 according to more complex non-linear relations. Various simple corrections have been devised to allow for the effects of size (or scale) on the efficiency. One of the simplest and best known is that due to [130], also reported by [131, 132], which, as applied to the efficiency of compressors and turbines is:

$$\frac{1 - \eta}{1 - \eta_{ref}} = \left(\frac{D_{t,ref}}{D_t}\right)^n \qquad (18.5)$$

where the subscripts ref refer to the reference model, and the exponent n is in the range from 0.12 to 0.5, which is dependent on the size and design of the turbomachinery [130-132]. A comparison of field tests of large units with model tests, Moody and Zowski concluded that the best value for n was approximately 0.2 in contrary to other values used. Variations in n may well be due to different assumptions of surface roughness and its effects. It is suggested that n most likely varies with specific speed and/or b2/D2 ratio for a given size [133].

For rotor diameters smaller than 5'' (12.7cm), [134] stated that the efficiency variation with size was best represented by the following expression:

$$\frac{1 - \eta}{1 - \eta_{ref}} = \left(\frac{12.7}{D_t}\right)^n \qquad (18.6)$$

The diameter is measured in cm and the efficiency as a percentage. The examination of the test performances studied in [134], reported that the effects due to size were moderate and best represented by equation (18.5). The more significant

scale effects were best represented by equation (18.6) [134]. This correlation takes into account the cumulative effect of the deviation from complete similarity and the various types of energy losses, including hydraulic.

Figure 18.18 shows a range of tip diameters and the efficiencies and mass flow rates predicted by equations (18.5) and (18.3), which are discussed later. The Capstone C30 reference values are: $\eta_C = 75\%$, $D_C = 14.7cm$, $\eta_T = 82\%$, $D_t = 17cm$, $m_a = 0.3133\,kg/s$ [135-137].
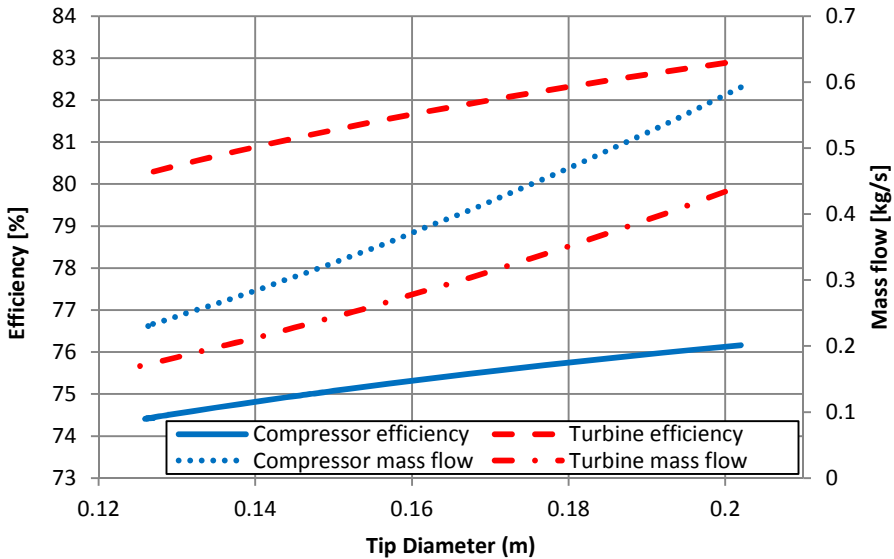
Figure 18.18 Turbine size, efficiency and mass flow trends

Other correlations try to account for scale effects in more detail with empirical relations derived for the Reynolds number effect [132]. It is very important to make the definition of the Reynolds number clear, as many authors base their correlations on different forms. This makes it hard to directly compare the correlations (directly involving Re number) that have been published [22].

The definition of the Reynolds number used is

$$Re = \frac{\dot{m}}{\mu \cdot r_t} \tag{18.7}$$

where $\dot{m}$ is the mass flow rate, r_t is the tip radius and μ is the dynamic viscosity at rotor inlet. A more generalized form of equation (18.5) as reported by [138] and [139] proposed that the overall loss be divided into viscous friction (profile and windage losses) and other losses (non-viscous losses such as mixing losses and trailing edge thickness losses) which were assumed to be unaffected by Reynolds number [117]:

$$\frac{1 - \eta}{1 - \eta_{ref}} = K + (1 - K) \cdot \left(\frac{Re}{Re_{ref}}\right)^{-n} \tag{18.8}$$

As discussed previously the exponent n depends on the compressor and turbine. It can be related to the tip diameter by

$$\frac{1 - \eta}{1 - \eta_{ref}} = K + (1 - K) \cdot \left(\frac{D_{t,ref}}{D_t}\right)^{n} \tag{18.9}$$

K is the Reynolds independent loss fraction, a constant which depends on the assumed split between the two types of loss. The values of K are between 0.3-0.4 [22, 140]. There are many values of K and n that fit available data and there is much debate over the values [133]. Casey has mentioned that values of K derived for one type of turbomachine are unlikely to be universally valid for other types [133]. The K fraction is assumed (for the rotor) to depend on the Richardson number, face clearance to diameter ratio, and the rotor blade exit angle [117]. The Kinetic energy of the exit loss is not affected by Reynolds number and therefore total-to-total efficiency is used [141]. These formulas are only used for scaling from a defined reference turbomachine (same technology level) and so therefore are suitable to be used in a design scale analysis for geometrically identical or similar machines.

Diameter roughly scales with $\sqrt{C30}$ so combining equations (18.4) and (18.9) results in equations (18.10) and (18.11).

$$\eta_t = \left[1 - 0.4 \cdot \left(1 - \eta_{ref}\right) - 0.6 \cdot (1 - \eta_{ref}) \right. \\ \left. \cdot \left(\frac{1}{\sqrt{C30}}\right)^{0.31}\right] \tag{18.10}$$

The chosen values of n and K for the compressor and turbine are based on suggested values in the literature.

$$\eta_c = \left[1 - 0.4 \cdot \left(1 - \eta_{ref}\right) - 0.6 \cdot (1 - \eta_{ref}) \right. \\ \left. \cdot \left(\frac{1}{\sqrt{C30}}\right)^{0.15}\right] \tag{18.11}$$

All the above equations do not take into account the losses due to the tip clearance nor due to high compressor pressure ratio. The relations for these are discussed below.

18.8.7 Tip clearance effects

The compressor tip clearance effects can be represented by

$$\Delta\eta_c = 0.20 \cdot \left(\frac{cl_c}{h_c} - 0.02\right) \not< 0 \tag{18.12}$$

Which appears in [134] and is similar to the form [142]

$$-\frac{\Delta\eta}{\eta} = \frac{2 \cdot a \cdot cl}{b_1 + b_2} \tag{18.13}$$

Pfleiderer [143] recommended that b1/b2=4 and a=0.5 then it reduces to a similar form of equation (18.12). The turbine tip clearance effects are represented by

$$\Delta\eta_t = 0.1\frac{cl_t}{h_t} \tag{18.14}$$

The issue still remains with finding appropriate tip clearance and corresponding blade heights for different sizes of micro turbines to assess the tip clearance effect on a single unit with decreasing size. It is inaccurate to keep the tip clearance effect constant with decreasing scale and equally incorrect to proportionally increase its influence. There is also uncertainty of values used in the Capstone C30. This has thus far restricted the authors to adequately incorporating the effects of tip clearance of both the turbine and compressor in the efficiency scaling relations. It is known that gap-to-blade height ratios increase as the engine size decreases and compressor efficiency is sensitive to small increases in tip clearance [134]. However, at this point data on scale effects on tip clearance were not available and therefore clearance effects are not taken into account. It will have to be incorporated into future more detailed analysis models once data are available.

18.8.8 Pressure ratio effects

Scale effects aren't the only causes of component efficiency losses. The fuel economy changes with optimum PR depending on parameters such as choice of fuel, TIT etc.

The decrease of compressor efficiency with increasing pressure ratio can be approximated by the empirical relationship in equation (18.15). According to [134], for small compressor designs with zero inlet air pre-rotation, a reasonable value for the 'Constant' is 0.13. R is the gas constant in $ft\frac{lbf}{lb°R}$ which is 53.3 for dry air. Small radial turbines are not prone to significant Mach number and pressure ratio penalties providing pressure ratios are lower than approximately 5.0 [134].

$$\Delta\eta_c = \frac{Constant}{\sqrt{\gamma_c R}} \cdot (PR_c - 2.0) \tag{18.15}$$

Equation (18.15) is combined with equation (18.11), resulting in equation (18.16) and is arranged to break down to the design compressor efficiency of the Capstone C30 when C30 is 1 and PR_c is 3.5. The constant value 0.02257 is the value calculated at the Capstone C30 if PR_c is 3.5, assuming gamma and R take on typical values for hot gas. In the GSP cycle performance calculations, equations (18.10) (turbine) and (18.16) (compressor) are used to account for the effect of scale and PR on efficiency. The results are graphically presented in Figure 18.20.

$$
\begin{aligned}
\eta_C = &\left[1 - 0.4 \cdot \left(1 - \eta_{ref}\right) - 0.6 \cdot \left(1 - \eta_{ref}\right) \right. \\
&\left. \cdot \left(\frac{1}{\sqrt{C30}}\right)^{0.15}\right] \\
&+ \left[0.02257 - \left(\frac{0.13}{\sqrt{\gamma R}}\right) * (PR_c - 2)\right]
\end{aligned} \tag{18.16}
$$

18.8.9 Scaling efficiency in other components

The combustor and recuperator are presented with variation in weight and volume. As already remarked the generator efficiency is relevant but was kept constant at 90%.

18.8.10 Cycle performance analysis

GSP was used to predict engine performance scale effects in terms of efficiency and power output. The thermodynamic performance of a recuperated cycle at design point conditions is predominantly a function of three parameters:

- peak cycle temperature (TIT),
- compressor/cycle pressure ratio (PR_c),
- component efficiencies and size effects.

The TIT (T4) is essentially determined by the turbine rotor alloy stress rupture and low cycle fatigue strengths, duty cycle, and rotor cooling options [72]. Likewise the recuperator inlet temperature, equal to turbine exhaust temperature (T5), is also determined by the recuperator matrix material limitations. The Capstone C30's T5 is currently limited to around 650 °C (rated full power) [135, 144, 145]. At MTT, recuperator technology is being developed for T5 values up to 800 °C [146]. Depending on the recuperator and turbine material limitations, due to the low PR_c,

either T4 or T5 may be the power limiting factor. For this study however, T4 is specified as input in the cycle calculations and T5 is a 'slave' parameter that may exceed limits of current technologies. For recuperated cycles with T4 values around 1300 K, optimal efficiency and power PR_c values are around 3 to 4. In the cycle calculations, T4 (TIT) and PR_c are varied to cover the interesting ranges of the parameters.

18.8.11 Results

GSP design point simulations were run with the turbomachinery scaling effects and pressure ratio relations implemented. Figure 18.19 shows the performance of the reference C30 design for varying design TIT and PR_c (factor C30=1). The star symbol in the middle indicates the actual C30 design point. At this point, electric efficiency η_e is 26.5% at TIT=1130 K (857 °C), $PR_c = 3.5$, T5 = 650 °C, recuperator $\varepsilon = 0.85$ (assumed), $\eta_c = 75\%$ and $\eta_t = 82\%$. Electric losses are assumed 8% of shaft power. Results with these data correspond to published C30 data [147]. PR_c varies with intervals of 0.25 from 3 (top) up to 4 (bottom) in each plot. The TIT variation is shown in the graph.
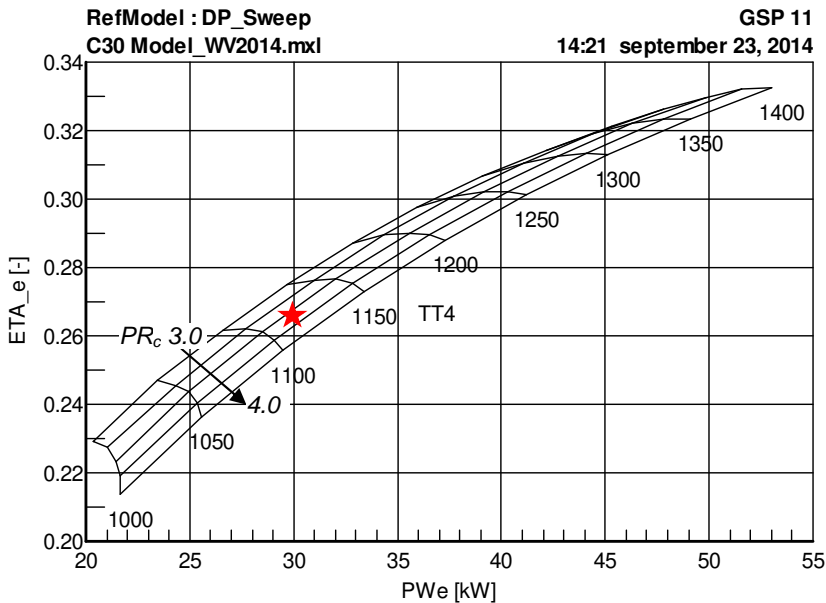
Figure 18.19 Capstone C30 scale design point carpet plot

Figure 18.20 shows the thermal efficiency carpets for varying engine power level (i.e. scale). The carpet labelled '30' is identical to the reference carpet of Figure 18.19. The carpet plots represent 6 scales, represented by power levels 3, 9, 15, 22, 30, 36kW of the cycles in the carpet plot 'centres'[13] (TIT=1130K, PR_c=3.5).

It is noted that specific speed, pressure ratio, velocity ratio change within the individual carpet plots only. *Within* every carpet plot the Ns, U/C_0 and PR_c vary in the same manner for every carpet plot (i.e. for every scale). Curves in Figure 18.20 connect points in the carpet with the same TIT and PR_c and therefore represent scale effect only with Ns, CPR and U/C_0 constant. The middle curve connects the reference design points in the middle of the carpets (TIT = 1130K, PR_c = 3.5 as with C30).
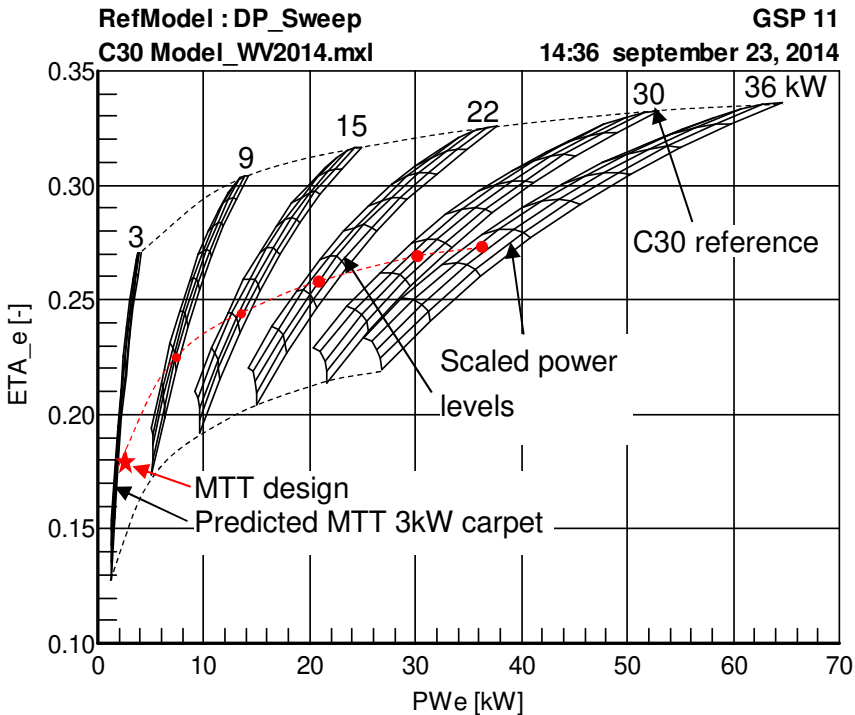
Figure 18.20 Microturbine engine scale effect simulation results

18.8.12 Validation

The 3kW MTT micro turbine design performance is used to validate the scaling model. The scaling relations predict the design performance of MTT's 3kW at

---

[13] The centres are represented by the star symbols in Figure 18.20.

21.6% and 3kW (circle symbol in Figure 18.21). MTT 3kW actual efficiency is 16.5% (generator output) at PR_c = 3, TIT = 1250-1300K, η_c = 73%, η_t = 72% [146]. Clearly the scaling model is optimistic at this small scale[14]. Presumably, the disagreement is owing to the neglected effects of tip clearance and heat loss effects on the efficiency with decreasing scale.

Still, the predictions correspond fairly well with the MTT data considering the design power changes by a factor of 10. Apart from the effect of ignoring tip clearance and heat loss scale effects, obviously, scaling prediction accuracy reduces rapidly when moving away from the reference that far. For the conceptual range extender study, the power range of interest is 9-36 kW and within this range accuracy of the current model may be assumed to be sufficient.
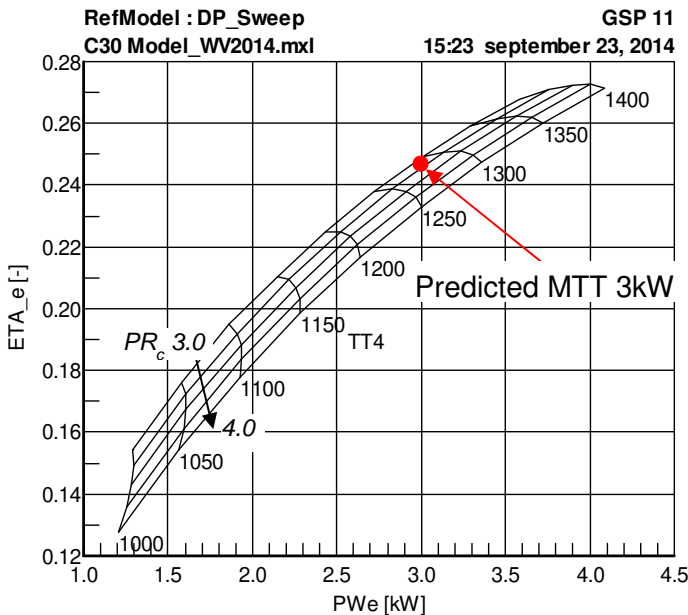
Figure 18.21 MTT 3kW performance prediction from scaling C30

18.8.13 Discussion

In Figure 18.20, the trend of efficiency with power level and scale is clearly visible. Below 3 kW efficiency rapidly becomes very low, indicating a reasonable efficiency with micro turbines below 3kW with today's technologies is difficult to realize. For accurate estimation of performance below 10 kW, adaption of equations

---

[14] Note that the MTT component efficiencies and diameters are not directly comparable to Capstone as there are geometric and operating differences such as PR. The MTT η_c = 73% differs according to tip clearance variation.

(18.10) and (18.16) is probably required, combined with a reference gas turbine chosen closer to that of the scaled one.

In reality, geometric similarity is generally not maintained when decreasing scale due to manufacturing limitations and this may well introduce additional deviations. These may be reflected in changes of:

Velocity ratio $= U_t/C_0$, ratio of rotor tip speed to theoretical spouting velocity; and Exit Flow coefficient $= C_m/U_t$ (the ratio of exit meridional velocity to tip speed).

The velocity ratio is a measure of the blade loading. The exit flow coefficient is an indirect measure of the specific speed. Turbomachinery design involves using criteria in terms of specific speed and velocity ratios [22]. Therefore, for a more in-depth analysis, the effects on performance via scale effects on specific speed and velocity ratios should be added. The subject of further research would be the effect of compressor and turbine specific speeds (Ns_T, Ns_C), U/C_0 and b2/D2 ratios[15] on component and cycle efficiency, some of which has already been shown by Casey [133].

These efficiency correlations would be curve fitted functions of pressure ratio and specific speed Ns_c for the compressor, plus U/C_0 with Ns_t for the turbine, i.e.

$$\eta_C = fnt(PR , Ns_c) \tag{18.17}$$

$$\eta_T = fnt(U/C_0, Ns_T) \tag{18.18}$$

18.8.14 Other scaling aspects

Other scaling aspects including weight and volume of the different micro turbine components, costs and vehicle model implementation issues are addressed in the paper [116]. These are outside the scope of this thesis and thus are omitted here.

18.9   Conclusions

- MTT has developed a 3kW recuperated micro turbine driving a high speed generator for micro CHP applications. The cycle optimization and performance improvement work was performed using detailed GSP models.
- The MTT Mk5 turbogenerator has demonstrated 3.4 kWe power output at 17.2% electrical efficiency.
- Further development of the current design for a micro CHP system demonstrator is focused on at least 19% turbogenerator efficiency. This will be

---

[15] The b2/D2 (Outlet width) ratio is known to be a function of Ns_c

attempted by reducing losses, adapting component characteristics and improving component efficiencies.

- Future developments of turbocharger technology will provide opportunity to focus on higher efficiencies beyond 20%.
- The relations between power level, size, weight and efficiency significantly affect the optimum power and size for a range extender application.
- The scaling model implemented in GSP proves fairly accurate in scaling performance from 30 kW down to the 3 kW MTT micro turbine indicating it is suitable for conceptual design and sizing studies in the range 9-36 kW for a range extender.
- Cycle efficiency of similar micro turbines significantly drops when scaling down from 30 kW. Below 10 kW the drop becomes very steep. For better accuracy, Reynolds number scale relations may be adapted below 10 kW.
- The scaling model can be adapted easily to represent more advanced or more moderate technology levels (with related implications on efficiency, weight, volume, cost, life etc.).
- Further work needs to be incorporated by assessing the influence of other parameters on efficiency in the scaling model such as specific speed, velocity ratio, detailed tip clearance relations and heat loss.

Chapter 19 Novel cycles and configurations

19.1   Parallel twin spool configuration with shared combustor

19.1.1 Introduction

An interesting application of GSP is the simulation of a micro turbine designed to provide pressurized air for pneumatic unloading of bulk trailer tanks. Compressed air is blown into the tank to fluidize the bulk material and for pressurization to assure positive flow to transport the material to a silo storage tank.

19.1.2 Cycle and configuration

A conceptual design study was conducted resulting in a configuration with two parallel micro turbines sharing a common combustor as shown in Figure 19.1.
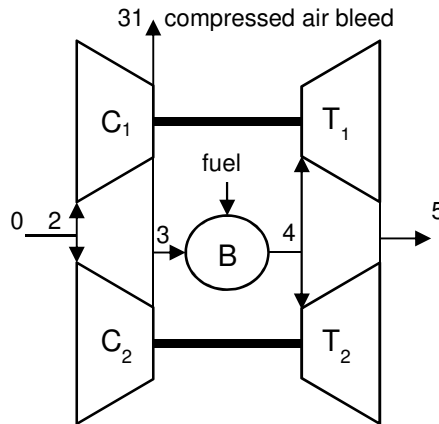
Figure 19.1 Twin shaft common combustor configuration

The configuration comprises of two parallel spools with a common combustor B. The air from compressors C_1 and C_2 is mixed before the combustor and divided between combustor entry (station 3) and air bleed flow (station 31). Combustor exit flow is divided over the turbines T_1 and T_2. An advantage is the smaller size turbomachinery which provides a large choice of off-the-shelf components. This arrangement employs equal load on both compressors and both turbines due to the mixing before the combustor, which allows two identical compressors and two identical turbines for an optimal component match. A first prototype of the micro turbine is shown in Figure 19.2. Design point data are given in Table 19.1.
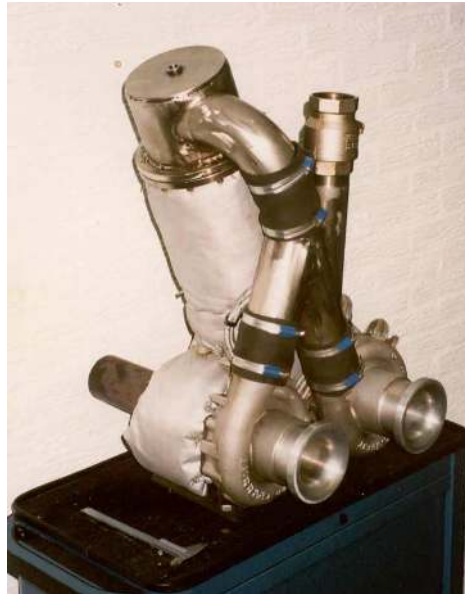
Figure 19.2 Simple cycle twin parallel shaft prototype

Table 19.1   Simple cycle design point performance

Bleed delivery pressure P_{del} (or p_{31})	3.3	bar
Delivery mass flow W_{air} (or W_{31})	0.27	kg/s
Total inlet mass flow W_2	0.84	kg/s
Fuel flow W_f	0.0084	kg/s
Exhaust gas temperature T_{exh} (or T_9)	814	K
Rotor speeds N_1 and N_2	92000	rpm
Thermal efficiency η_{th}	8	%

In addition to the simple cycle design, a recuperated version was developed for lower fuel consumption and lower exhausts gas temperature. Development target for the recuperated version was 200 K lower T_{exh} and a 12% thermal efficiency.

19.1.3 Performance simulation

GSP models were developed of both versions for analysing and comparing performance. Figure 19.3 shows the recuperated GSP model configuration.
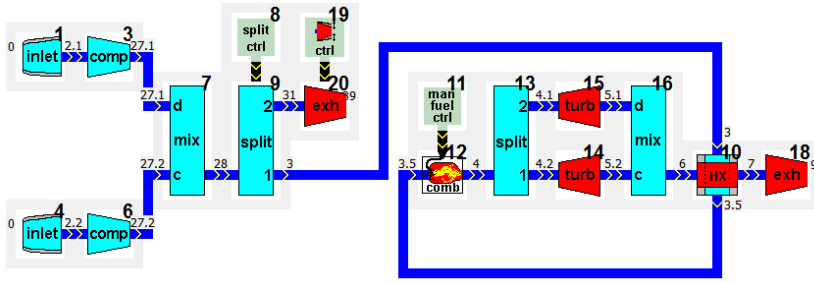
Figure 19.3 GSP model configuration

Simulations were performed with and without the recuperation and with varying recuperator pressure loss values. In GSP, the recuperator design point can be specified in terms of hot gas temperature drop. With the design target of a 200 K lower T_{exh}, an approximate 45% effectiveness is calculated for the recuperator. Fuel flow and bleed mass flow were separately varied over a wide range to cover the entire operating range. Power output is specified as *pneumatic power* PW_{air} which is defined as the maximum (isentropic) expansion power to be obtained from the compressed air bleed flow:

$$PW_{air} = W_{air}.c_{p\,air}.T_{t31}.\left[1 - \left(\frac{p_{t31}}{p_o}\right)^{\frac{1-\kappa}{\kappa}}\right] \tag{19.1}$$

Consequently, then thermal efficiency is defined as:

$$\eta_{th} = \frac{PW_{air}}{H_{vfuel}.W_f} \tag{19.2}$$

Figure 19.4 shows simulation results indicating the effect of recuperation on performance (PW_{air}, thermal efficiency η_{th}, fuel flow Wf, delivery pressure p_del and exhaust gas temperature Texh) as well as the effect of pressure losses in the recuperator. The recuperation significantly increases thermal efficiency and reduces fuel flow. With 6% pressure loss in the hot and cold recuperator passages, still significantly lower fuel consumption (as compared to the non-recuperated configuration) is obtained. An additional important outcome is that at a constant level of air compression power, pressure losses in the cold and hot recuperator passages do not affect exhaust gas temperature. This is due to the fact that for the

same P_{air}, the exhaust mass flow increases with pressure loss. This compensates the effect on T5 of the increased heat rate due to the pressure loss. In view of the strong constraints on T5 this means that the trade-off balance between (minimal) pressure loss and heat exchanger effectiveness will move towards a high-effectiveness recuperator with a relatively high pressure loss. This way a minimal T_{exh} with a reasonable fuel consumption level will be obtained.
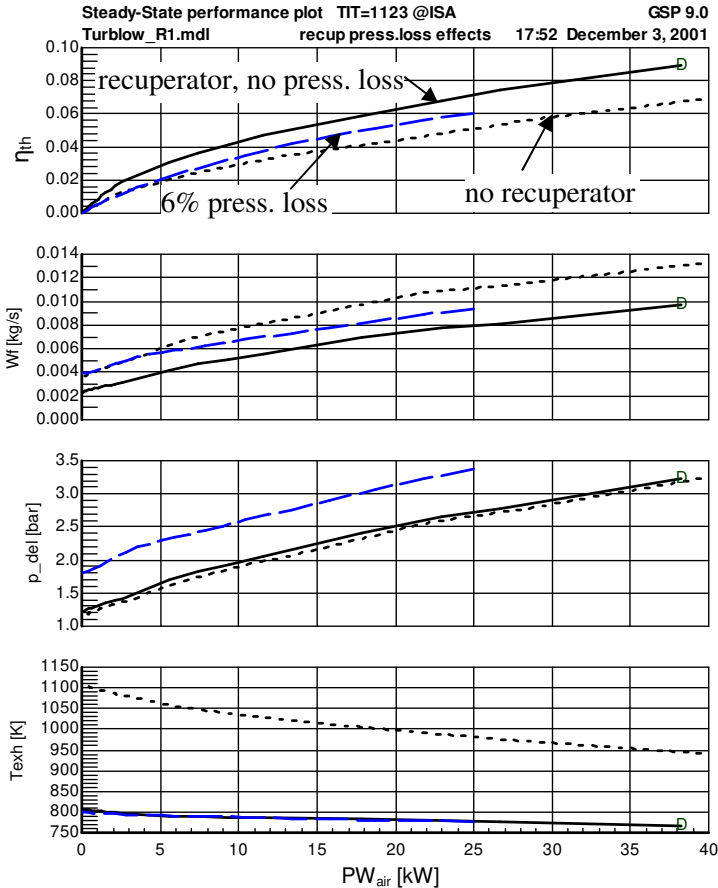
Figure 19.4 Effect of recuperator on cycle performance

Figure 19.5 shows part load performance (with '200 K recuperation') with curves for constant bleed air valve opening (0, 20..100%) and varying fuel flow. 'D' indicates the design point with full open valve. The 100% and 80% opening curves show increasing TT4 (i.e. TIT) with decreasing fuel flow W_f. This effect is due to the relatively large portion of bleed air, strongly affecting fuel air ratio. This uncommon relation between fuel flow, TT4 and power level is responsible for a

number of stability problems. This is due to the fact that multiple operating points exist for the same TT4. The problem can be avoided with a suitable control strategy using both T_{exh} and delivery air pressure as inputs.
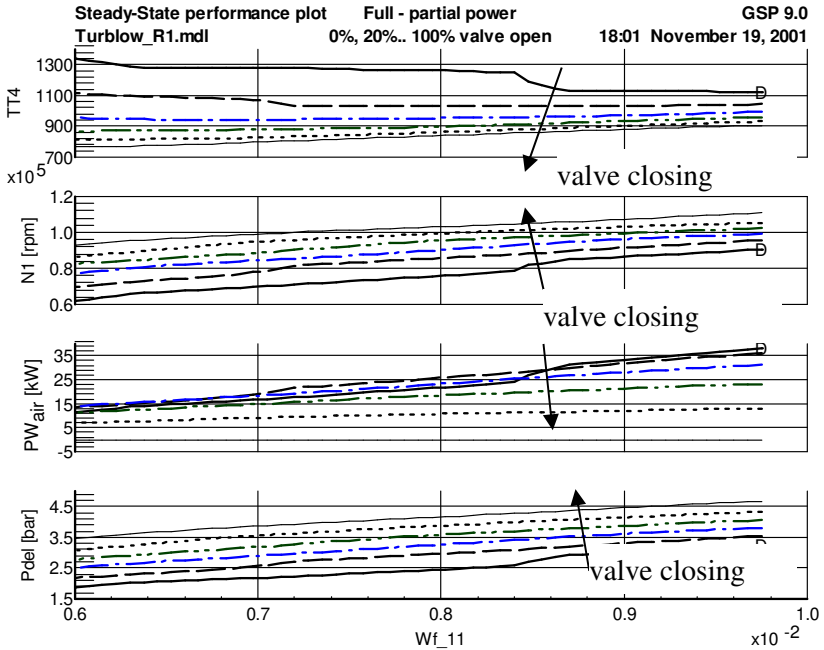
Figure 19.5 Part load performance
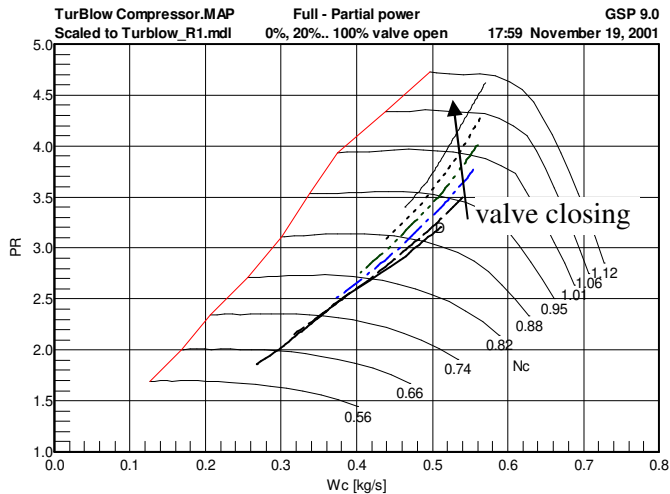
Figure 19.6 Compressor performance

Figure 19.6 shows the compressor performance corresponding to Figure 19.5 for curves with decreasing fuel flows with valve openings ranging from 0% through 100% ('D' is design point with full open valve). While there is sufficient surge margin, with a closed valve the rotor speed is nearing 112% (Nc = 1.12) indicating a risk of overspeed. Overspeed may be reduced by implementing appropriate control laws, either with or without rotor speed inputs, that limit fuel flow with valve openings smaller than 100%.

19.1.4 Transient simulations

Transient simulations of the start-up procedure were performed for control and start-up system design. A start-up sequence with given TIT and valve opening time functions was simulated. Results are shown in Figure 19.7.
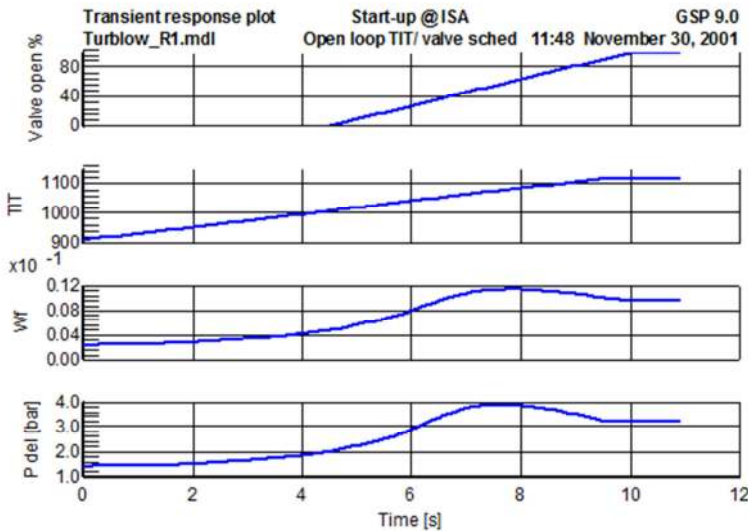
Figure 19.7 Start-up simulation results

From the resulting fuel flow Wf and delivery pressure P$_{del}$ responses, control schedules can be derived. From approximately 45% rpm the gas turbine is well able to accelerate self-sustained with an acceptable TIT level and acceleration rate. After light-off, the air valve is closed to ensure maximum turbine power, and then gradually opens again as rotor speed rises until full open position at maximum design point rpm.

Figure 19.8 shows the start-up transient in the compressor map, indicating a smooth transition to maximum power while maintaining sufficient stall margin. The simulation indicates that start-up can well be achieved using a starter motor able to accelerate the rotors up to 50% rpm. The start-up simulation also revealed the

stability problems already mentioned and indicates control logic, with at least T_{exh} and delivery pressure inputs, is required to maintain stable operation around the design point.
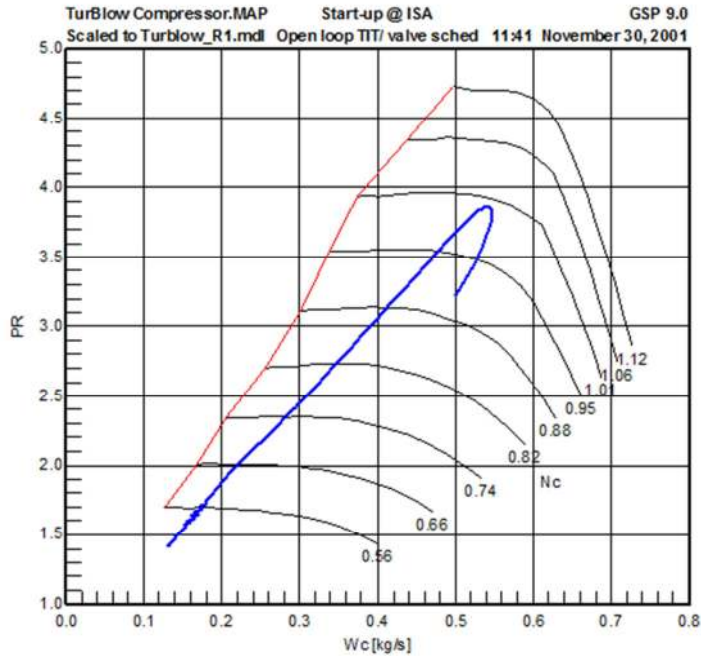
Figure 19.8 Startup transient in compressor map

19.1.5 Conclusions

The simulation of the parallel twin spool air compressor demonstrates GSP's ability to model complex and unconventional gas turbine configurations. Specific issues such as the effects of the valve opening and recuperation expressed in an exhaust gas temperature drop (instead of in effectiveness) can be accurately analysed.

19.2   Rotating combustor turbine concept

19.2.1 Introduction

Another application showing GSP's flexibility is the rotating combustor turbine concept. In this concept, a compressor impeller discharges it's compressed air into a rotating duct where heat is added by burning fuel for example. This duct is the rotating combustor and feeds the hot pressurized gas to a full reaction turbine, comprising of a number of nozzles for expanding an accelerating the gas to ambient in a circumferential direction. The reactive forces from the jets exiting the nozzles generate torque on the rotating turbine. As such, the rotating combustor turbine includes only a single rotating part, as shown in Figure 19.9.
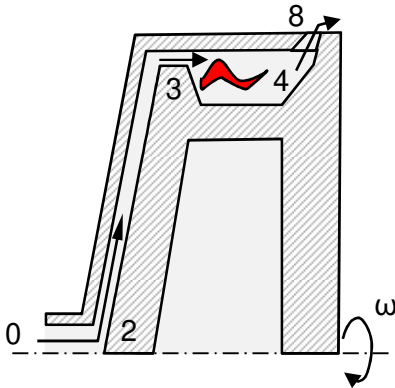
Figure 19.9 Rotating combustor turbine configuration

The rotor is rotating with rotor speed ω. Air enters the rotor inlet at station 0, flow to the compressor inlet 2, then radially flows to compressor exit 3. There is no diffuser. Between 3 and 4 the combustion takes place. From 4, the hot gas expands to ambient pressure through the nozzle throat at station 8. The jet is directed in a circumferential direction to generate torque on the rotor. This means the turbine is of 100% reaction type.

There are several patents on this and similar concepts, such as [148]. A recent research publication of the concept is [149].

19.2.2 Cycle calculation

The cycle cannot be calculated as a customary Brayton cycle. This is because the heat release to the cycle occurs in a rotating frame. There is no diffuser so the dynamic head at compressor impeller exit (station 3) cannot be converted to additional static pressure before combustion. If it is assumed that all heat is added at the radius of station 3, the conversion from static to rotating frame in a 0-D sense means a correction to the total enthalpy according to:

$$h_{t_{3rot}} = h_{t_{3stat}} - \frac{u_{hr}^2}{2} \tag{19.3}$$

u_{hr} is the velocity at the radius r_{hr} where the heat is added (heat release):

$$u_{hr} = \omega \cdot r_{hr} \tag{19.4}$$

If somehow the heat is added at a larger or smaller radius, then u at that radius must be taken. Ideal cycle pressure ratio is:

$$PR_c = \left(\frac{T_{t_{3rot}}}{T_{t_2}}\right)^{\frac{\gamma}{\gamma-1}} \tag{19.5}$$

Total temperatures T_t must be calculated from total enthalpy h_t. From the above it can be concluded that the ideal cycle has a relatively low thermal efficiency due to a pressure ratio that is corresponding to only half the specific compressor work that is equal to u^2. In effect, the cycle works at a pressure ratio corresponding to the compressor impeller exit static pressure, not the total pressure. Still the compressor requires all the work u^2 from the shaft. From the combustor heat release at the total pressure relative to the rotating frame, the cycle enters the reaction turbine. This calculation is similar to a jet engine thrust calculation. Expansion to ambient pressure at station 8 can be calculated, resulting in a jet velocity c_8 relative to the rotating frame. Then the torque per unit of mass flow is:

$$TRQ = c_8 \cdot r_8 \tag{19.6}$$

Note that results will change with changing radius r_8. The problem is that the kinetic energy of the residual velocity c_8-u_8 is lost, as with a propelling jet of a jet engine. If the concept would be integrated as gas generator in a larger system, this loss may well be recoverable using subsequent turbine stages. Alternatively, the concept could be integrated in a combined heat and power (CHP) configuration to recover the losses for heating purposes.

19.2.3 GSP simulation

GSP has been used to analyse a rotating combustor concept accounting for several losses and limitations. Figure 19.10 show the GSP model component configuration. Air and fuel are premixed in the fuel mixer component number 9, compressed in 10, then via a 'rotating duct component' 11 flowing into combustor 13. Although there is a manual fuel control component 12 linked to the combustor,

it provides no fuel since fuel is already premixed. Finally, the hot gas is flowing to the reaction turbine component 15 via a second rotating duct component 14.
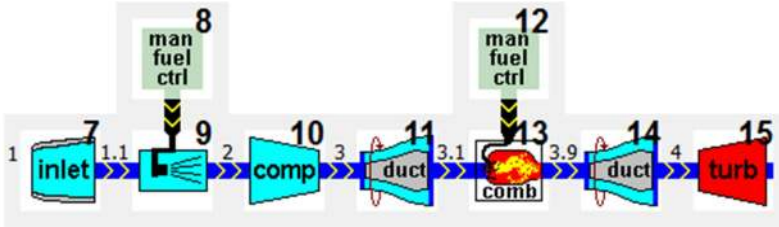
Figure 19.10 GSP rotating combustor model configuration

To simulate the processes in this cycle, custom component models had to be developed and derived from the standard components using the object inheritance described in Chapter 6.

19.2.4 Compressor component model

A special compressor component model has been derived (inherited) from the standard GSP compressor. At the exit of this custom compressor component (10) a transition is made to a rotating frame at user specified tip radius and compressor rotor speed where tip velocity is u_3. Consequently, total properties at 3 relative to the rotating frame now are corrected using equation (19.3). Isentropic efficiency can be specified for the compression process in the impeller. GSP continues calculation in the components downstream the gas path in the new frame of reference.

19.2.5 Rotating duct component model

The rotating duct component model is a child of the generic GSP duct component and inherits all its functionalities such as pressure loss and heat transfer models. Added are the user specified connection to a rotating shaft and a calculation to account for changes of the radius at which the flow rotates. For change of radius, the total properties are corrected using:

$$h_{t_{r1}} + \frac{(\omega \cdot r_1)^2}{2} = h_{t_{r2}} + \frac{(\omega \cdot r_2)^2}{2} \qquad (19.7)$$

Changes of total temperature and pressures can be calculated using the GSP functions for temperature as a function of enthalpy and equation (19.5).

The power taken or delivered to the user specified rotor shaft, resulting from the acceleration or deceleration of the flow (or change in angular momentum), is calculated using:

$$PW_{r1 \to r2} = w \cdot \frac{(\omega \cdot r_2)^2}{2} - \frac{(\omega \cdot r_1)^2}{2} \qquad (19.8)$$

In the GSP model described above, the rotating duct is used both at the compressor exit (to change from compressor exit radius to the radius at which the heat release takes place) and turbine entry (to change from combustor to turbine entry radius).

19.2.6 Reaction turbine component model

The reaction turbine component is derived from the standard GSP exhaust nozzle component. This way, all standard modelling functionality for simulation of expansion in a propelling nozzle is inherited. To convert the thrust from the rotating nozzles to torque on a shaft, a user specified shaft connection and radius for the nozzles have to be added. A jet angle can be specified to account for jets not directed in a fully tangential direction and the consequent losses. Other losses in the nozzles are inherited from the parent standard nozzle component. Torque and power can be calculated from the jet velocity using equation (19.6).

19.2.7 Simulation results

A GSP model of the ideal cycle has been used to assess the maximum performance and efficiency potential as a function of the velocity at the radius of heat release u_{hr}. As shown in Figure 19.11, velocities u_{hr}, beyond 400 m/s are required to have ideal cycle efficiencies more than 10% at a reasonable value for fuel-air mixture equivalence ratio ER. At low ER levels, efficiency will be higher but then power output lower for the same size. Power must by high to keep losses related to size (e.g. windage and bearing losses) relatively low. With 400 m/s the rotating combustor outer tip velocity will be even higher, resulting in structural stress levels requiring material properties not available today.

For the case of ER = 0.7, u_{hr}=380 m/s ideal thermal efficiency is 9.47%. Figure 19.12 shows results of a real case simulation including effects of several losses. Combustion intensity and thermal input power are strongly related to surface to volume ratio of the rotating combustor and therefore windage and heat losses become larger at smaller scales. The loss models are implemented using the GSP equation components (see section 8.2.1) and the post-processing capability (post-simulation calculated expressions) and not further described here.
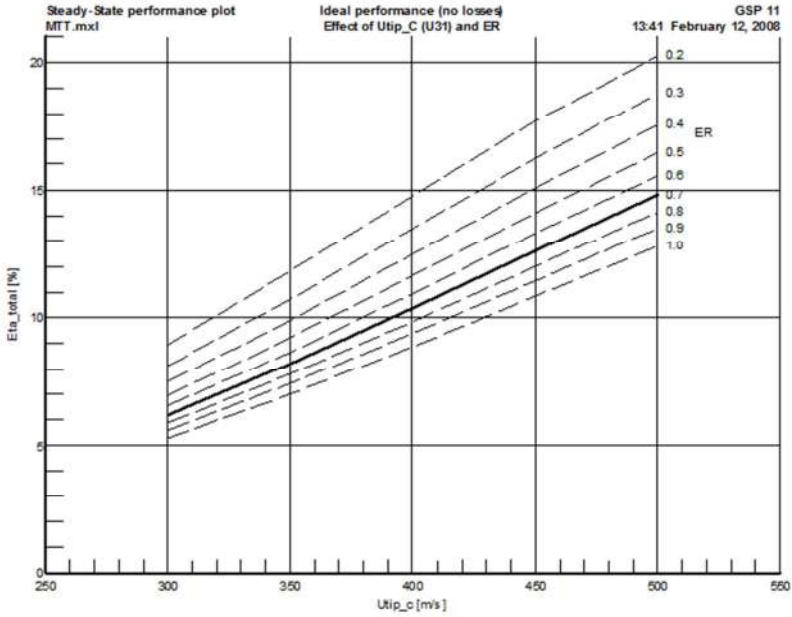
Figure 19.11 Ideal cycle performance as function of u_{hr} and ER
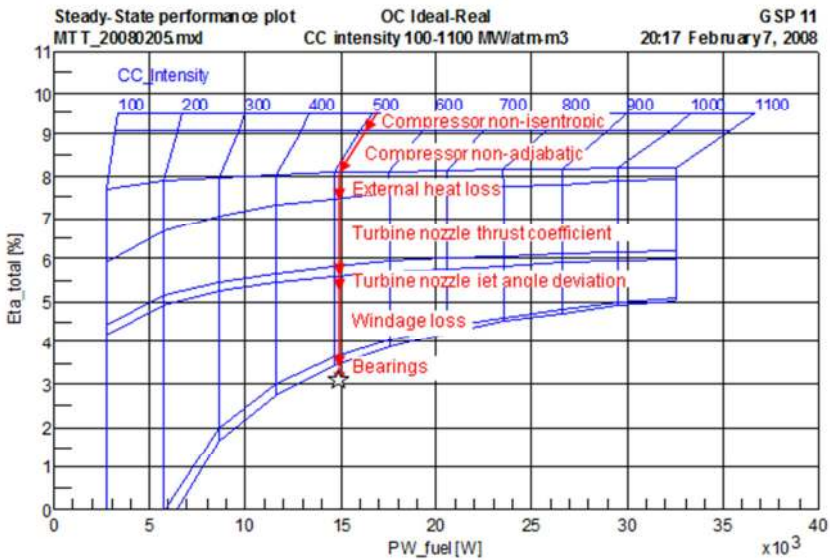
Figure 19.12 Real cycle performance as function of u_{hr} and ER
(courtesy of MTT b.v. Eindhoven, the Netherlands)

19.2.8 Conclusion

The simulation of the rotating combustor concept shows the flexibility of GSP to model any kind of continuous flow power cycle. If the standard components are not sufficient, custom components can be inherited easily from the standard gas path components to represent components with characteristics specific for novel power cycles and configurations.

19.3   Simulation of the Alstom GT26 gas turbine

In [150] a study is described focused on modelling the Alstom GT26 gas turbine. The objective is to obtain a performance analysis tool with the purpose of optimizing its operation in a large combined cycle configuration. Figure 19.13 shows the GSP model configuration of the Alstom GT26 gas turbine. The GT26 has a reheat combustor (component nr. 26 in Figure 19.13) between a first and the second turbine for operational versatility, offering options to either operate at maximum power, efficiency or minimum maintenance costs in a combined cycle configuration.
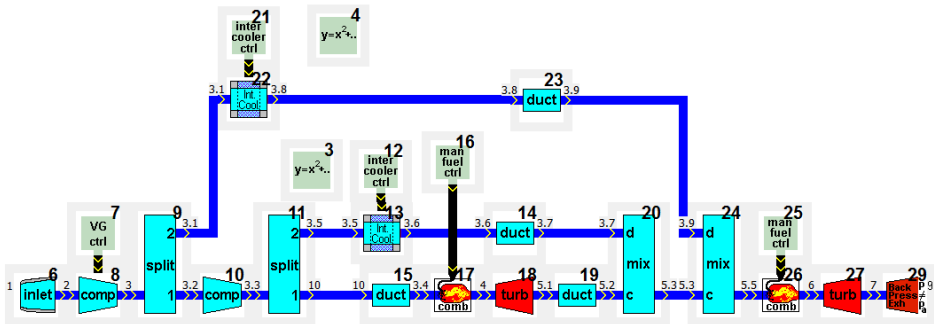
Figure 19.13 GSP model configuration of the GT26 gas turbine engine

The GT26 model clearly shows the flexibility of GSP to model unconventional gas turbine cycles and configurations. The complex air and gas flow arrangement required the use of GSP flow splitter and mixer components (components number 9, 11, 20 and 24 in Figure 19.13) and also the variable geometry control component for the compressor models (number 7). Heat exchanger components were used for the cooling stages in the process (components 12, 13, 21, 22). In addition, equation components (numbers 3 and 4) were needed to establish specific control relations among variable geometry, cooling and flow split ratio variables.

19.4   Multi-fuel hybrid turbofan engine simulation

In [151] a conceptual design study is presented on novel turbofan engine configurations with two combustors for burning different fuels simultaneously. One configuration studied is shown in Figure 19.14. The objective is to analyse the potential of concepts that optimally benefit from future fuel availability while also meeting future emission standards.
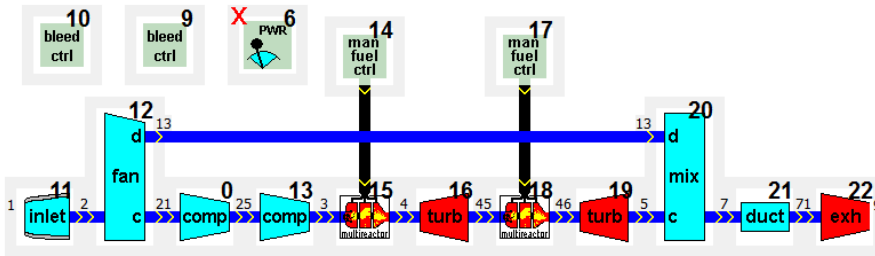
Figure 19.14 Multi-fuel hybrid engine GSP model configuration

A challenge with this model is to optimize the complex cycle for multiple flight conditions, including take-off, end-of-climb and cruise, while maintaining the specific benefits of the concept. One issue is the selection of the GSP design point DP (or cycle reference point CRP, see section 2.6.4) from these 3 flight conditions. The DP must be optimized but affects the 2 other OD points that also require optimization. The problem is to efficiently conduct the consequent iteration procedure. As explained in 14.6, future enhancements to GSP are considered to support or automate this process.

Chapter 20 Other applications

20.1 Overview

GSP has been used by all types of users that are listed in Figure 2.2 in the beginning of this thesis. This has resulted in many applications including

- cycle analysis and optimization for conceptual design,
- all kinds of off-design performance predictions,
- system identification for control system design,
- system identification for development of piecewise linear real-time models,
- emission prediction,
- failure analysis,
- structural and thermal load prediction,
- and many more...

Many applications are also demonstrated in the sample models of GSP 11 coming with installation on a PC. Below a number of more advanced applications with public references are briefly described.

20.2 Emission prediction

Following the development of the emission modelling capabilities described in Chapter 7, GSP was used for accurate prediction of cumulative exhaust gas emissions of the different phases of commercial aircraft flights [152, 153]. In addition, effects of variations in flight profiles were analysed.

In [154], GSP was used as a key element in an integral tool to optimize rotorcraft operations in terms of fuel burn, gaseous emissions and ground noise impact. See Figure 20.1 for a graphical presentation of the modelling framework.

20.3 Alternative fuels

An interesting application has been the analysis of effects of alternative fuels for industrial turboshaft engines. This capability was demonstrated in [33] and Chapter 7. This reference includes examples of the application of GSP's multi-reactor combustor model for prediction of exhaust gas emission levels.

A follow-up to this work is the development of a biomass gasifier GSP component model for performance analysis of a combined gas turbine-biomass gasifier system [155]. Here the gasifier obtains air from the gas turbine, and delivers low calorific value fuel to the gas turbine.
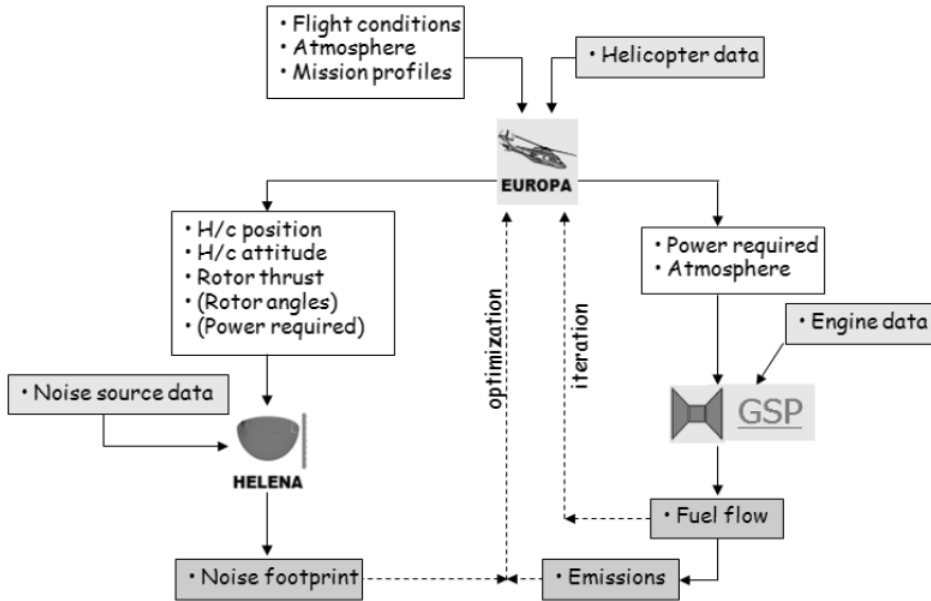
Figure 20.1 Rotorcraft emission modelling framework (from [154])

In [156, 157] results of a study on the effects of mixing low calorific value fuel with the natural gas fuel in a large combined cycle heavy-duty gas turbine are described. Limitations to the mixing ratio are analysed related to from stall margin requirements. Mitigation of the problems by adaptations of compressor variable geometry is proposed and analysed in detailed GSP models including variable geometry scheduling.

20.4   Gas turbine lifing

In [17] GSP is used as an element in a framework of models for analysis of thermal load calculation for gas turbine hot section life consumption modelling. The framework is graphically shown in Figure 20.2. A model of a military afterburning turbofan is used to accurately predict the transient thermal load history of turbine stages during an entire mission, including rapid accelerations and decelerations typical of military air combat usage. The performance history including rotor speeds and pressures combined with the thermal load history provides information to component life consumption models. Heat transfer correlations are determined with CFD simulations. The model framework was able to predict relative effects of variations in mission profile and engine usage on turbine life consumption.
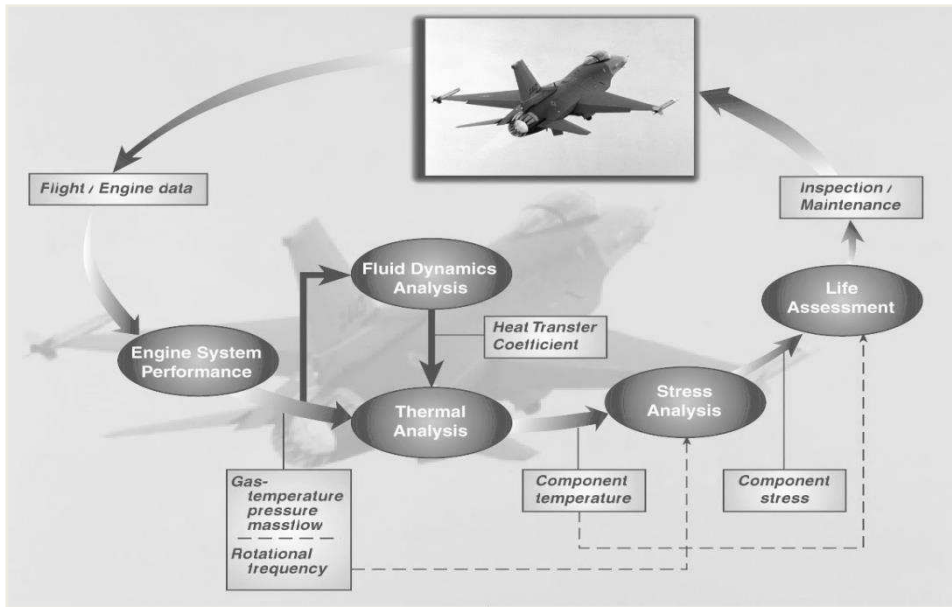
Figure 20.2 Gas turbine hot section lifing model framework (from [17])

20.5   In-flight gas path analysis

The adaptive modelling functionality described in Chapter 12 has seen continuous application as a Gas Path Analysis (GPA) tool since 2004 in the engine maintenance environment. In Chapter 17 application experiences are described as well as a number of extensions to the adaptive modelling capability including multi-point calibration, multiple analysis cycles and a simple information system concept. In [104] further developments and enhancement to the GSP GPA tool are described as well as the application to in-flight GPA. In-flight GPA offers great potential to optimize the safety, reliability, availability and the maintenance concept as engine gas path condition can be monitored continuously, either after every flight, or in case an air-to-ground data link is available, on-line during flight. It is clear that in order to obtain all these benefits optimally, comprehensive information systems are required. This subject however is outside the scope of this thesis.

20.6   Component map tuning and reverse engineering

In [105] the adaptive modelling functionality described in Chapter 12 has been used to improve the accuracy of GSP models itself. Adaptive modelling is used with on-wing turbofan performance data to fine-tune component maps. With the

adaptive modelling simulations, deviations from scaled component maps can be quantified and subsequently used to correct the map data, resulting in increased off-design simulation accuracy. In a sense, component maps can be systematically reverse engineered from engine performance data this way. The method can be used in any modelling application requiring high accuracy, provided sufficient performance data are available. In this case, the off-design simulation accuracy improvements were used to reduce in-flight gas path analysis uncertainty.

Epilogue

The development of information technology and the increase in affordable computing power of the last decades has been followed by rapid development of simulation technology. CFD tools are becoming capable of simulating fluid dynamic processes with increasing complexity and fidelity. High-fidelity CFD simulations for gas turbines however, remain limited to the component level. Generic simulations such as Matlab® tools are gradually replacing system models coded in 3rd generation (3GL) programming languages. Although these tools already cover many gas turbine modelling needs, most gas turbine system modelling work still require specific tools. Energy system simulation tools such as Aspen® and Cycle Tempo get closer but still lack many gas turbine specific capabilities. As a result, generic simulation tools for gas turbines remain essential for analysis of gas turbine performance in all areas, from the OEM developing new engines to the operator, analysing performance for maintenance purposes.

This observation has been confirmed repeatedly since the birth of GSP in 1986. Especially since the development of the object oriented version in 1996, the number of applications and users has rapidly grown. Also, the community involved in the development has expanded, including many users that actively submit requests for new functionalities.

The object oriented design has proven its value. During almost 17 years, it has provided the building blocks for an ever increasing number of component models, adaptations and extensions, without ever needing fundamental changes. Good examples are the improved chemical gas model, the adaptive modelling capability and the thermal network modelling functionality.

Initially, the GSP developers directly communicated with the users and used their feedback to extend or improve the code. In many cases, the developers and the users were the same persons. As a consequence, the developers usually were more or less controlling how GSP was used. However, if the tool is truly generic, the number of various model configurations and ways to analyse performance is virtually endless. In addition, many alternatives exist on how to post-process and present results, either graphically or in text format.

An interesting moment is when the tools start being used by anonymous professional engineers for complex modelling and simulation tasks. The surprise comes when the developers discover how remote users sometimes use their tool to build models and address performance analysis problems. The users start to discover efficient ways of using the tool the developers would never have thought of. This experience clearly indicates the developers have built a *generic tool* indeed: the user is provided with tools and gradually develops modelling skills that go beyond the imagination of the model developer. Of course, efficient solutions from

the user community are extremely valuable to the developers as these will lead to further improvements and also will be communicated to other users.

Another development is the gradual expansion of the GSP development team. Until 1999, the author of this thesis was the sole developer. But with the potential of GSP and object orientation being recognized, the generic approach was not only implemented for the GSP end user, but also for GSP developer from the start on. From 2000 onwards, the GSP development team has expanded following international customers and projects. Several of these required new capabilities, most of which were developed using the original object oriented framework and component model classes.

Most of the developers do not need to know all about the internals of the GSP *kernel* and usually focus on specific component models. Some do not code directly but only provide functional specifications or pseudo-code.

With the inheritance mechanism, the kernel developers have an extremely powerful tool at their disposal: any functional improvement in the top level component model classes propagates nicely in all child component models, in all existing models due to the fully backward compatibility.

At the time of writing this thesis, GSP has world-wide recognition as a flexible gas turbine simulation tool. It is still expanding its user base and development is also continuing. Version 12 is foreseen in 2014.

If we look further ahead, new technologies may replace today's simulation tools. With the continuous increase of computing power and development of next generations of software tools and computing platforms, modelling and simulation methods, numerical methods and user interfaces beyond our imagination may well emerge. After all, many of today's capabilities found in PC's could hardly be imagined 20 or 30 years ago.

However, as long as gas turbines and related systems will be developed and operated, there will be a need to understand their behaviour. The fundamental physics behind this will not change nor will the equations describing the processes. In that sense, GSP can be seen as a phase in the development of gas turbine modelling and simulation tools. To go one step further, maybe even the concept of modelling and simulation as we know it today will entirely change.

In any case GSP and also other tools will still be stepping stones in the development towards future methods. An interesting question is how long GSP will remain a stepping stone with many standing on it, before it is left behind for new ways. It is the author's conviction that all hard- and software technologies will one day be replaced by something new. A lot will depend on the ability of GSP and its developers to adapt to future needs and also future opportunities emerging from new computer and software technologies. So far however, GSP has proven a remarkable track record and will be around for quite a while, serving many scientists and engineers interested in gas turbine system simulation.

Nomenclature

Roman symbols

a	constant
A	area
b	blade height
b2/D2	outlet width ratio
BPR	bypass ratio
c	flow velocity
C_{dhw}	constant value of dhw (enthalphy flux) difference
cl	tip clearance
C30	scale factor relative to 30 kW power output
c_0	isentropic expansion, (spouting) velocity
c_p	specific heat at constant pressure
c_v	specific heat at constant volume
C/h	gap-to-blade-height ratio
CO	carbon monoxide fraction
CPR	cycle or compressor Pressure Ratio
d	thickness
D	diameter
D_{tip}	impeller tip diameter
Ds	specific diameter ($\frac{D.\Delta h^{0.25}}{\sqrt{\dot{V}}}$)
e_i	error vector element i
$\overline{E}$	equation error vector
Eff	recuperator effectiveness
EGT	exhaust Gas Temperature
EI	emission Index
ENP	Exhaust Nozzle Position (variable exhaust nozzle)
EPR	Engine Pressure Ratio (nozzle pressure / inlet pressure)
ETA	η, efficiency,
ETA_{TH}	thermal Efficiency
f	newton-Raphson state correction limiting factor
f_c	AM reference model calibration factor vector
F(…)	non-linear function

Nomenclature

FAR		Fuel Air Ratio
FCp(T,GC)		GSP gas model c_p function of T and GC
FT(h,GC)		GSP gas model T function of h and GC
FH(T,GC)		GSP gas model h function of T and GC
FD		Ram drag
FG		Gross thrust
FLOPS		Floating Point Operations per Second
FN		Net thrust
FRT		Flat Rated Temperature
g		gravitational acceleration constant, 9.80665 m/s^2
GC		gas composition vector
h		specific enthalpy
h		heat transfer coefficient
Had		adiabatic head
hw		enthalpy flux (h·w)
I_{hw}		Integral of enthalpy flux change
ISA		International Standard Atmosphere
J		Jacobian matrix
k		conductivity
k_f		forward specific reaction rate
L		length
L(…)		Schedule value function
$\dot{m}$, Mdot		Mass Flow
M		Mass
Ma		Mach number
M_v		Mass in a volume V
n		vector size
N	[rpm]	Rotor speed
Ns		Specific Speed ($\frac{\omega.\sqrt{\dot{V}}}{\Delta h^{0.75}}$)
N1		low pressure (fan) spool speed
N2		high pressure spool speed
Nh		high pressure spool speed
Nl		low pressure spool speed
NOx		Nitrogen Oxides fraction
Nu		Nusselt number
Δp		pressure loss
P, p		pressure or power
p_{O2}	[atm]	partial pressure of O_2 (oxygen)

266

Pcfuel	[MW]	fuel compression power
Ps		static pressure
Pt		total pressure
Pnetc	[MW]	net (fuel compression corrected) power output
Pr		Prandtl number
PR		Pressure Ratio
PL		pressure Loss
ppm		parts per million
PR2_rec		lumped recuperator pressure loss factor (1 minus both hot and cold recuperator PL)
P, PW		power
PW_{eq65}		equivalent power (expanding in a turbine with 65% isentropic efficiency)
q		dynamic head
Q		heat flux
Qloss		heat loss
r		radius
R	[J/kg/K]	specific gas constant
R_q		GSP turbomachinery inlet/exit heat transfer ratio
R_r		reaction rate
R_u		Ratio of gas/air overall heat transfer coefficients in 1-D recuperator model
Re		Reynolds number
RIT		Rotor Inlet Temperature (of turbine)
s		specific entropy
s_i		state vector element i
$\bar{S}$		state variable vector
S	[mg/kg]	soot formation concentration
SFC		Specific Fuel Consumption
SN		Smoke Number
t		time
T		temperature
Ts		static Temperature
Tt		total Temperature
TIT		turbine Inlet Temperature
TRQ		torque
U		overall heat transfer coefficient, blade velocity
U/C_0		velocity Ratio

Nomenclature

v		velocity
V		volume, recuperator matrix volume
$\dot{V}$		volume flow
W, w		mass flow
Wc		corrected mass flow
Wf		fuel flow
x		longitudinal position in 1-D recuperator model
y		lateral position in 1-D recuperator model
X		mole fraction
[X]		mole (volume) concentration

Greek symbols

α		deviation from NO equilibrium concentration factor
β		component map auxiliary coordinate (for β-lines),
		deviation from N equilibrium concentration factor
γ		ratio of specific heats
		deviation from N_2O equilibrium concentration factor
δ		functional derivative (infinitesimal change),
		ratio of pressure and standard pressure p/p_{std}
Δ		non-infinitesimal change
ε		recuperator effectiveness,
		tolerance,
		surface radiation emissivity
ε_m		measurement tolerance (adaptive modelling)
η		efficiency
η_e		electric efficiency (of turbo generator)
η_{enet}		net electric efficiency (for turbo generator with auxiliaries)
η_{shaft}		shaft power thermal efficiency
$\eta_{is,tot}$		total-to-total isentropic efficiency
θ		ratio of temperature and standard temperature T/T_{std}
μ	[N.s/m^2]	dynamic viscosity
π_{tot}		total pressure ratio
ρ		density
σ		Stefan-Boltzmann Constant (5.6703 10-8 W/m^{2}K^4)
ϕ		equivalence ratio
ω	[g/cm^2/s]	specific surface oxidation rate,
	[rad/s]	angular velocity

Subscripts

1	impeller inlet
2	impeller outlet
a	air
abs	absorbed
ag	air-to-gas
amb	ambient conditions
ad	adiabatic
avg	average
b	burner
c	corrected,
	compressor,
	cycle,
	condition (gas path analysis)
cond	conductive (heat transfer)
comp	component
conv	convective (heat transfer)
corr	correction
CH	hydrocarbon
del	delivered
D	diameter
E, e	electric
eff	effective
eq	(chemical) equilibrium
eq65	equivalent with 65% turbine efficiency
err	error in conservation equation
exh	exhaust
ext	external
EI	emission Index
f	fuel
g	gas, combustion gas
Gen	generator
Gg	gas generator
hr	heat release
hs	heat sink
hw	enthalpy flux
is	isentropic

Nomenclature

m	material,
	meridional,
	measured, measurement
m, mech	mechanical
mdl	calculated by model
meas	measured
ML	compressor map auxiliary coordinate
net	net
ox	oxidant
p	pressure
pz	primary zone
rad	radiative (heat transfer)
ref	reference
R, r, rec	recuperator
rec_hot	recuperator hot side
s	shaft
st.st.	steady-state
std	standard
stoich	stoichiometric (fuel-air ratio)
t	tip,
	total,
	turbine
th	thermal
tot	total
uhc	unburnt hydrocarbons
V	volume
∞	infinity, free stream

Abbreviations

AB	After Burner
ALM	Application Life Cycle management
AM	Adaptive Modeling
API	Application Programming Interface
BPL	Borland Package Library
CFD	Computational Fluid Dynamics
CHP	Combined Heat and Power
CRP	Cycle Reference Point
DEEC	Digital Electronic Engine Control
DLL	Dynamic Link Library
DP	Design Point
DUT	Delft University of Technology
FADEC	Full Authority Digital Engine Control
FEM	Finite Element Model
HEV	Hybrid Electric Vehicle
HPC	High Pressure Compressor
HPT	High Pressure Turbine
ICAO	International Civil Aviation Organization
GPA	Gas Path Analysis
GSP	Gas turbine Simulation Program
GUI	Graphical User Interface
HEV	Hybrid Electric Vehicle
IFPC	Integrated Flight Propulsion Control
LCV	Low Calorific Value fuel
LH_2	liquefied hydrogen
LNG	Liquefied Natural Gas
LPP	Lean Premixed Pre-evaporated combustion
LPC	Low pressure compressor
LPT	Low pressure turbine
MAX AB	Maximum Afterburner power setting
MDO	Multi-Disciplinary Optimization
MIL	Military power setting (max dry power)
NASA	National Aeronautics and Space Administration
NATO	North Atlantic Treaty Organisation
NDE	Non-linear Differential Equation
NG	Natural Gas

Nomenclature

NLR	Nationaal Lucht- en Ruimtevaartlaboratorium (National Aerospace Laboratory, the Netherlands)
NIVR	Netherlands Agency for Aerospace Programmes
NSF	National Simulator Facility (of NLR)
OD	Off Design
OEM	Original Equipment Manufacturer
ORC	Organic Rankine Cycle
PC	Personal Computer
PID	Proportional Integral Differential (control)
PPI	Power Performance Index
PT	Power turbine
PZ	Primary zone (combustor)
R&D	Research and Development
R	Specific gas constant
RC	Recuperator
RQL	Rich Quick-quench Lean combustion
RTO	Research and Technology Organisation (of NATO)
STOVL	Short Take-Off and Vertical Landing
TERTS	Turbine Engine Real-time Simulator
UHC	Unburnt Hydrocarbons
XML	Extensible Mark-up Language

Station numbering

0	ambient
1	inlet
1.3	fan bypass exit
2	compressor inlet
2.3	LPC exit
2.5	booster/intermediate compressor exit
3	compressor exit, combustor inlet
33	air side recuperator exit
34	combustor inlet
35	combustor inside
4	combustor exit/turbine inlet
4.5	HPT or inter turbine temperature
5	turbine exit/ gas side recuperator inlet
6	gas side recuperator exit
7	heat exchanger exit
9	exhaust exit

References

[1]   C. B. Meher-Homji, "The Development of the Whittle Turbojet," *J. Eng. Gas Turbines Power,* vol. 120, 1998.

[2]   C. B. Meher-Homji, "Pioneering Turbojet Developments of Dr. Hans Von Ohain—From the HeS 1 to the HeS 011," *J. Eng. Gas Turbines Power,* vol. 122, 2000.

[3]   J. A. a. A. Reed, A. A., "Intelligent Visualization and Control System for Multidisciplinary Numerical Propulsion System Simulation", paper 96-4034, presented at the 6th AIAA/USAF/NASA/ISSMO Multidisciplinary and Optimization Conference, Bellevue, WA, USA, 1996.

[4]   J. A. a. A. Reed, A.A., "Computational Simulation of Gas Turbines: Part I - Foundations of Component-based Models", ASME 99-GT-346, presented at the ASME IGTI Turbo Expo, 1999.

[5]   J. A. a. A. Reed, A.A., "Computational Simulation of Gas Turbines: Part II - Extensible Domain Frameworks", ASME 99-GT-347, presented at the ASME IGTI Turbo Expo, 1999.

[6]   Evans A.L. et al., "Intelligent Visualization and Control System for Multidisciplinary Numerical Propulsion System Simulation'", presented at the ASME Turbo Expo 1997, 1997.

[7]   P. Jeschke, Kurzke, J., Schaber, R. and Riegler,, "Preliminary Gas Turbine Design Using the Multidisciplinary Design System MOPEDS," *Journal of Engineering for Gas Turbine and Power,* vol. 126, pp. 258-264, 2004.

[8]   K. Lietzau and A. Kreiner, "Model Based Control Concepts for Jet Engines", 2001-GT-0016, presented at the ASME TURBO EXPO, 2001.

[9]   Several authors and contributors, "Performance Prediction and Simulation of Gas Turbine Engine Operation", NATO Research and Technology Organization RTO, 2003.

[10]   *Application lifecycle management* http://en.wikipedia.org/wiki/Application_lifecycle_management (10 March 2012)

[11]   J. Kurzke, "Advanced User-friendly Gas Turbine Performance Calculations on a Personal Computer", 95-GT-147, presented at the ASME IGTI Turbo Expo, 1995.

[12]   W. P. J. Visser and M. J. Broomhead, "GSP A generic object-oriented gas turbine simulation environment", ASME 2000-GT-0002, presented at the ASME TURBO EXPO, Munich, Germany, 2000.

[13]   Several authors and contributors, "Performance Prediction and Simulation of Vehicular Gas Turbines", NATO Research and Technology Organization RTO, 2007.

[14]   A. Bala, Sethi, V., Lo Gatto, E., Pachidis, V. and Pilidis, P., "PROOSIS – A Collaborative Venture for Gas Turbine Performance Simulation using an Object Oriented Programming Schema", ISABE 2007-1357, 2007.

References

[15]   Claus R.W. et al., "Multi disciplinary Propulsion Simulation Using NPSS", AIAA-92-4709-CP, 1992.

[16]   M. G. Turner, J. A. Reed, R. Ryder and J. P. Veres, "Multi-Fidelity Simulation of a Turbofan Engine With Results Zoomed Into Mini-Maps for a Zero-D Cycle Simulation", GT2004-53956, presented at the ASME IGTI Turbo Expo, Vienna, Austria, 2004.

[17]   T. Tinga, W. P. J. Visser, W. B. de Wolf and M. J. Broomhead, "Integrated Lifing Analysis Tool for Gas Turbine Components", ASME-2000-GT-0646, 2000.

[18]   *AspenONE* www.aspentech.com (2014)

[19]   *Cycle Tempo* www.asimptote.nl/software/cycle-tempo (2014)

[20]   J. J. Sellers and C. J. Daniele, "DYNGEN - A program for calculating steady-state and transient performance of turbojet and turbofan engines", NASA, 1975.

[21]   H. I. H. Saravanamuttoo, G. F. C. Rogers and H. Cohen, *Gas Turbine Theory*, 5th ed.: Pearson Education, 2001.

[22]   A. Whitfield and N. C. Baines, *Design of radial turbomachines*. New York: Longman Scientific & Technical, 1990.

[23]   J. Kurzke, "How to get Component Maps for Aircraft Gas Turbine Performance Calculations", ASME Paper 96-GT-164, 1996.

[24]   *Broyden's method* http://en.wikipedia.org/wiki/Broyden%27s_method (2014)

[25]   W. P. J. Visser, "Gas Turbine Simulation at NLR", MOD05, presented at the CEAS Symposium on Simulation Technology, Delft, 1997.

[26]   *Delphi* http://en.wikipedia.org/wiki/Delphi_(programming_language) (2014)

[27]   W. P. J. Visser, O. Kogenhop and M. Oostveen, "A Generic Approach for Gas Turbine Adaptive Modeling," *ASME Journal of Engineering for Gas Turbines and Power,* vol. 128 GTP-04-1039, 2004.

[28]   W. P. J. Visser and M. J. Broomhead, "GSP User Manual", National Aerospace Laboratory NLR, Amsterdam, the Netherlands, NLR TR-99410, 2000.

[29]   W. P. J. Visser, M. J. Broomhead, O. Kogenhop and E. R. Rademaker, "GSP Technical Manual", National Aerospace Laboratory NLR, Amsterdam, the Netherlands, NLR-TR-2010-343-Issue-2, 2014.

[30]   O. Kogenhop, M. J. D. Valens, W. P. J. Visser and M. J. Broomhead, "GSP Software Requirements Specification, version 2", National Aerospace Laboratory NLR, Amsterdam, the Netherlands, NLR-TR-2013-424, 2013.

[31]   M. J. D. Valens, W. P. J. Visser and M. J. Broomhead, "GSP Analysis and Design Document", National Aerospace Laboratory NLR, Amsterdam, the Netherlands, NLR-CR-2001-356, 2001.

[32]   G. Booch, *Object Oriented Design with Applications*: Benjamin/Cummings Publishing, 1991.

[33]   W. P. J. Visser and S. C. A. Kluiters, "Modeling the Effects of Operating Conditions and Alternative Fuels on Gas Turbine Performance and Emissions", RTO-MP-14, presented at the RTO-AVT symposium on "Gas Turbine Engine Combustion, Emissions and Alternative Fuels", Lisbon, Portugal, 1998.

[34]   J. Kurzke, "Advanced User-friendly Gas Turbine Performance Calculations on a Personal Computer", ASME Paper 95-GT-147, 1995.

[35]   U. Schumann, *Lecture Notes in Engineering. Air Traffic and the Environment-Background, Tendencies and Potential Global Atmospheric Effects*: Springer Verlag, Berlin, 1990.

[36]   H. W. Pohl, *Hydrogen and Other Alternative fuels for Air and Ground Transportation*. Chichester, UK: John Wiley & Sons Ltd., 1995.

[37]   H. W. Jentink and J. J. F. v. Veen, "In flight spectroscopic aircraft emission measurements" in proceedings of *RTO-AVT symposium on Gas Turbine Engine Combustion, Emissions and Alternative fuels*, Lisbon, Portugal, 1998.

[38]   D. Kretschmer and J. Odgers, "The characterization of combustion by fuel composition – measurements in a small conventional combustor" in proceedings of *AGARD-Conference Proceedings 422 on Combustion and Fuels in Gas Turbine Engines, paper 10*, 1988.

[39]   N. K. Rizk and H. C. Mongia, "Emissions Predictions of Different Gas Turbine Combustors", AIAA Paper 94-118, 1994.

[40]   S. Maidhof and J. Janicka, "Numerical modelling of turbine combustion chambers" in proceedings of *AGARD Conference on Fuels and Combustion Technology for Advanced Aircraft Engines - 536, paper 10*, 1993.

[41]   U. Schumann, "AERONOX, The impact of NOx Emissions from Aircraft Upon the Atmosphere at Flight Altitudes 8-15 km, Publication on research related to aeronautics and environment", DLR, Germany, 1995.

[42]   F. Bozza, R. Tuccillo and G. Fontana, "Performance and Emission Levels in Gas Turbine Plants," *ASME Journal of Engineering for Gas Turbines and Power,* vol. 116, pp. 53-62, 1994.

[43]   C. G. Rodriguez and W. F. O'Brien, "Unsteady, finite-rate model for application in the design of complete gas-turbine combustor configurations" in proceedings of *AGARD Conference on Design principles and methods for aircraft gas turbine engines*, RTO, Neuilly Sur Seine, 1998.

[44]   M. J. Botros and e. al, "One-dimensional predictive emission monitoring model for gas turbine combustors", ASME Paper 97-GT-414, presented at the ASME Turbo Expo, 1997.

[45]   K. K. Kuo, *Principles of Combustion*. New York: John Wiley & Sons, 1986.

[46]   I. Glassman, *Combustion*. Princeton NJ, USA: Academic Press., 1996.

[47]   S. Gordon and B. J. McBride, "Computer Program for Calculation of Complex Chemical Equilibrium Compositions and Applications. Part II Users Manual and Program Description", National Aeronautics and Space Administration, Lewis Research Center, NASA Reference Publication 1311, 1994-1996.

[48]   S. Gordon and B. J. McBride, "Computer Program for Calculation of Complex Chemical Equilibrium Compositions and Applications. Part I Analysis", National Aeronautics and Space Administration, Lewis Research Center, NASA Reference Publication 1311, 1994-1996.

[49]   G. J. Sturgess, R. McKinney and S. Morford, "Modification of Combustor Stoïchiometry Distribution for Reduced NOx Emission From Aircraft Engines", ASME Paper 92-GT-108, 1992.

References

[50]   A. W. Lefebvre, *Gas Turbine Combustion*: Hemisphere Publishing Corporation, Washington, 1983.

[51]   D. C. J. Hammond and A. M. Mellor, "Analytical Calculations for the Performance and Pollutant Emissions of Gas Turbine Combustors" in proceedings of *Combustion Science and Technology, vol.4, p.101-112*, 1971.

[52]   R. S. Fletcher and J. B. Heywood, "A model for nitric oxide emissions from aircraft gas turbine engines", AIAA Paper 71-123, 1971.

[53]   M. Barrère, "Modélisation des foyers de turboréacteur en vue de l'étude de la pollution" in proceedings of *AGARD Conference on Atmospheric Pollution by Aircraft Engines 125, paper 27*, 1973.

[54]   J. A. Miller and C. T. Bowman, "Mechanism and modelling of nitrogen chemistry in combustion," *Progress in Energy and Combustion Science, Oxford: Pergamon Press plc.,* vol. 15, pp. 287-338, 1989.

[55]   J. L. Toof, "A Model for the Prediction of Thermal, Prompt, and Fuel NOx Emissions From Combustion Turbines", ASME Paper 85-GT-29, 1985.

[56]   F. Bachmaier, K. H. Eberius and T. Just, "The formation of Nitric Oxide and the detection of HCN," *Combustion Science and Technology,* vol. 7, p.77., 1973.

[57]   C. P. Fenimore, "Formation of Nitric Oxide from Fuel Nitrogen in Ethylene Flames," *Combustion and Flame, American Elsevier Publishing Company Inc.,* vol. 19, pp. 289-297, 1972.

[58]   G. J. Kelsall, et al., "Combustion of LCV Coal Derived Fuel Gas for High Temperature, Low Emissions Gas Turbines in the British Coal Topping Cycle", ASME Paper 91-GT-384, 1991.

[59]   M. Sato, et al., "Coal Gaseous Fueled, Low Fuel-NOx Gas Turbine Combustor", ASME Paper 90-GT-381, 1990.

[60]   T. Nakata, et al., "Experimental Evaluation of a Low NOx LBG Combustor Using Bypass Air", ASME Paper 90-GT-380, 1990.

[61]   G. A. Lavoie, J. B. Heywood and J. C. Keck, "Experimental and Theoretical Study of Nitric Oxide formation in Internal Combustion Engines," *Combustion Science and Technology, Gordon and Breach Science Publishers Ltd.,* vol. 1, pp. 313-326, 1970.

[62]   A. A. Westenberg, "Kinetics of NO and CO in Lean, Premixed Hydrocarbon-Air Flames," *Combustion Science and Technology, Gordon and Breach Science Publishers Ltd.,* vol. 4, pp. 59-64, 1971.

[63]   F. L. Dryer and I. Glassman, "High-Temperature oxidation of CO and CH4" in proceedings of *Pollutant Formation and Destruction in flames, 14th Symposium (Int.) on Combustion*, 1973, pp. 987-1003.

[64]   P. V. Chleboun, K. P. Hubbert and C. G. W. Sheppard, "Modelling of CO Oxidation in Dilution Jet Flows" in proceedings of *Combustion and Fuels in Gas Turbine Engines, AGARD-Conference Proceedings-422, paper 38*, 1988.

[65]   D. T. Pratt, "Coalescence/Dispersion Modelling of Gas Turbine Combustors" in proceedings of *Combustor Modelling, AGARD-Conference Proceedings-275, paper 15*, 1980.

[66]   J. P. Appleton, "Soot oxidation kinetics at combustion temperatures',
        Atmospheric Pollution by Aircraft Engines" in proceedings of *AGARD
        Conference on Atmospheric Pollution by Aircraft Engines*, Neuilly Sur Seine,
        France, 1973.

[67]   J. Nagle and R. F. Strickland-Constable, "Oxidation of carbon between
        1000oC-2000oC" in proceedings of *Proceedings 5th Conference on Carbon,
        page 154, Pergamon*, 1961, p. 154.

[68]   *ICAO Engine Exhaust Emissions Data Bank,* issue 1, Appendix C, data for
        CF6-80C2B1F, pp. C-41, vol., 1993.

[69]   P. D. J. Hoppesteyn, J. Andries and K. R. G. Hein, "Biomass/coal derived gas
        utilization in a gas turbine combustor", ASME Paper 98-GT-160, 1998.

[70]   W. d. Jong, A. J. and K. R. G. Hein, "Coal-biomass gasification in a
        pressurized fluidized bed gasifier", ASME Paper 98-GT-159, 1998.

[71]   W. P. J. Visser and I. D. Dountchev, "Modeling Thermal Effects on
        Performance of small Gas Turbines", GT2015-42744, to be presented at the
        ASME IGTI Turbo Expo 2015, Montreal, Canada, 2015.

[72]   C. Rodgers, "Some Effects of Size on the Performances of Small Gas
        Turbines," *ASME Paper GT-2003-38027,* pp. 17-26, June 16–19 2003.

[73]   B. F. Kolanowski, *Guide to Microturbines*. Lilburn, USA: The Fairmont Press,
        2004.

[74]   J. H. LienHardt IV and J. H. LienHardt V, *A Heat Transfer Text Book*, 3rd ed.
        Cambridge (MA) USA: Phlogiston Press, 2008.

[75]   W. P. J. Visser, *WVCOMPS14 Delphi component library code* (2014)

[76]   W. P. J. Visser, *GSP11 code* (2014)

[77]   D. L. Doel, "Temper - a Gas Path Analysis tool for commercial jet engines",
        92-GT-315, presented at the ASME Turbo Expo, 1992.

[78]   P. Kamboukos and K. Mathioudakis, "Comparison of linear and non-linear gas
        turbine performance diagnostics", ASME GT-2003-38518, 2003.

[79]   L. A. Urban, "Gas Path analysis applied to turbine engine condition
        monitoring", AIAA 72-1082., presented at the AIAA, 1972.

[80]   B. Lambiris, K. Mathioudakis, A. Stamatis and K. Papailiou, "Adaptive
        modeling of jet engine performance with application of condition monitoring,"
        ASME Journal of propulsion and power, vol. 10, 1994.

[81]   A. Stamatis, K. Mathioudakis and K. Papailiou, "Adaptive simulation of gas
        turbine performance", 89-GT-205, 1989.

[82]   S. Bin, Z. Jin and Z. Shaoji, "An investigation of artificial neural networks
        (ANN) in quantitative fault diagnosis for turbofan engine", ASME 2000-GT-
        32, 2000.

[83]   M. J. Embrechts, A. L. Schweizerhof, M. Bushman and M. H. Sabatella,
        "Neural network modeling of turbofan parameters", ASME 2000-GT-0036,
        2000.

[84]   K. Kanelopoulos, A. Stamatis and K. Mathioudakis, "Incorporating neural
        networks into gas turbine performance diagnostics", ASME 97-GT-035, 1997.

[85]   P. J. Lu, M. C. Zhang, T. C. Hsu and J. Zhang, "An evaluation of engine faults
        diagnostics using artificial neural networks", ASME 2000-GT-0029, 2000.

[86]   C. Romessis and K. Mathioudakis, "Setting up of a probabilistic neural network for sensor fault detection including operation with component fault", ASME GT-2002-30030, 2002.

[87]   T. U. J. Grönstedt, "Identifiability in multi-point Gas Turbine Parameter estimation problems", ASME GT-2002-30020, 2002.

[88]   S. Sampath, A. Gulati and R. Singh, "Fault diagnostics using genetic algorithm for advanced cycle gas turbine", ASME GT-2002-30021, 2002.

[89]   S. Sampath, S. O. T. Ogaji, Y. G. Li and R. Singh, "Fault diagnosis of a two spool turbo-fan engine using transient data: a genetic algorithm approach ", ASME GT-2003-38300, 2003.

[90]   M. Zedda and R. Singh, "Gas turbine engine and sensor diagnostics", ISABE 99-7238, 1999.

[91]   P. Kamboukos, P. Oikonomou, A. Stamatis and K. Mathioudakis, "Optimizing diagnostic effectiveness of mixed turbofan by means of adaptive modelling and choice of appropriate monitoring parameters" in proceedings of *RTO symposium on aging mechanisms and control*, 2001.

[92]   K. Mathioudakis, A. Stamatis, A. Tsalavoutas and N. Aretakis, "Instructing the principles of gas turbine performance monitoring and diagnostics by means of interactive computer models", ASME 2000-GT-584, 2000.

[93]   *GSP web site*   www.gspteam.com

[94]   J. A. Moreno Barragán, "Engine Vibration monitoring and diagnosis based on On-Board captured data', " in proceedings of *NATO/RTA AVT symposium*, Manchester, 2001.

[95]   M. J. Roemer and G. J. Kacprzynski, "Advance diagnostics and prognostic technologies for gas turbine engine risk assessment", ASME 2000-GT-30, 2000.

[96]   A. Stamatis, K. Mathioudakis, J. Ruiz and B. Curnock, "Real time engine model implementation for adaptive control & performance monitoring of large civil turbofans", ASME 2001-GT-0362, 2001.

[97]   A. Tsalavoutas, N. Aretakis, K. Mathioudakis and A. Stamatis, "Combining advanced data analysis methods for the constitution of an integrated gas turbine condition monitoring and diagnostic system", ASME 2000-GT-0034, 2000.

[98]   T. Zoller, "Advanced engine monitoring and diagnosis systems: Actual system for the EJ200 engine of the Eurofighter 2000 aircraft and future trends", RTO-MP-079(I)-Pt-A-B, presented at the RTO AVT Symposium on "Ageing Mechanisms and Control: Part B – Monitoring and Management of Gas Turbine Fleets for Extended Life and Reduced Costs", Manchester UK, 2001.

[99]   L. Dambrosio, S. M. Camporeale and B. Fortunato, "Performance of gas turbine power plants controlled by one step ahead adaptive technique", ASME 2000-GT-0037, 2000.

[100]   D. L. Doel, "Interpretation of weighted-least-squares gas path analysis results", ASME GT-2002-30025, 2002.

[101] A. Stamatis, K. Mathioudakis, G. Berios and K. Papailiou, "Jet engine fault detection with discrete operating points gas path analysis", ISABE meeting paper 89-7133, 1989

[102] N. Aretakis, K. Mathioudakis and A. Stamatis, "Non-Linear engine component fault diagnosis from a limited number of measurements using a combinatorial approach", ASME GT-2002-30031, 2002.

[103] S. O. T. Ogaji and R. Singh, "Study of the optimization of measurement sets for gas path fault diagnosis in gas turbines", ASME GT-2002-30050, 2002.

[104] M. L. Verbist, W. P. J. Visser, R. Pecnik and J. P. van Buijtenen, "Experience with Gas Path Analysis for On-Wing Turbofan Condition Monitoring," *ASME Journal of Engineering for Gas Turbines and Power,* GTP-13-1212, 2014.

[105] M. L. Verbist, W. P. J. Visser, R. Pecnik and J. P. van Buijtenen, "Component Map Tuning Procedure using Adaptive Modeling", GT2012-68688, presented at the ASME TURBO EXPO, Copenhagen, Denmark, 2012.

[106] W. P. J. Visser, M. J. Broomhead and J. v. d. Vorst, "TERTS, A Generic Real-Time Gas Turbine Simulation Environment", 2001-GT-0446 presented at the ASME TURBO EXPO, New Orleans, Louisiana, USA, 2001.

[107] "Real-Time Modeling Methods for Gas Turbine Engine Performance".

[108] M. W. French, "Development of a Compact Real-Time Turbofan Engine Dynamic Simulation", SAE paper 821401, 1982.

[109] M. G. Ballin, "A High Fidelity Real-Time Simulation of a Small Turboshaft Engine" in *NASA TM-100991*, 1988.

[110] W. W. P. J. v. Oosterhout, "Development of the Generic Thermodynamic Turboshaft Engine Real-Time Simulation (TERTS) Model", Delft Technical University, Faculty of Aerospace, Delft, 1996,

[111] *RESPECT - Rotorcraft Efficient and Safe Procedures for Critical Trajectories* http://www.nlr.nl/public/hosted-sites/respect/index.html (2000)

[112] W. P. J. Visser, H. Pieters, M. Oostveen and E. v. Dorp, "Experience with GSP as a Gas Path Analysis Tool", ASME GT2006-90904, presented at the ASME TURBO EXPO 2006, Barcelona, Spain, 2006.

[113] J. Kurzke, "How to create a performance model of a gas turbine from a limited amount of information", ASME paper GT2005-68537, 2005.

[114] W. P. J. Visser, S. A. Shakariyants and M. Oostveen, "Development of a 3kw Micro Turbine for CHP Applications," *Journal of Engineering for Gas Turbines and Power,* vol. 116, 2011.

[115] W. P. J. Visser, S. A. Shakariyants, M. T. L. d. Later, A. Haj Ayed and K. Kusterer, "Performance Optimization of a 3kW Microturbine for CHP Applications", GT2012- 68686, presented at the ASME Turbo Expo 2012, Copenhagen, Denmark, 2012.

[116] A. J. Head and W. P. J. Visser, "Scaling 3-36kW Microturbines", ASME GT2012-68685, 2012.

[117] O. E. Balje, "Turbomachines: A Guide to Design, Selection and Theory", ed New York: J. Wiley & Sons, 1981, pp. 37, 49, 74.

References

[118]   T. Tetsui, M. Kyoya and Y. Miura, "Development of a TiAl Turbocharger for Passenger Vehicles" in *Mitsubishi Heavy Industries Technical Review* vol. 37, 2000.

[119]   K. Matsumoto, M. Tojo, Y. Jinnai, N. Hayashi and S. Ibaraki, "Development of Compact and High-Performance Turbocharger for 1,050C Exhaust Gas" in *Mitsubishi Heavy Industries Technical Review* vol. 45, 2008.

[120]   "Super MWE" in *Holset HTi Magazine*. www.holset.co.uk, 2009, pp. 7-8.

[121]   O. Ryder, "The Worldwide Efficiency Drive" in *Cummins/Holset HTi Magazine*. www.holset.co.uk, 2009, pp. 5–6.

[122]   A. T. Simpson, S. W. T. Spence and J. K. Watterson, "A Comparison of the Flow Structures and Losses Within Vaned and Vaneless Stators for Radial Turbines," *ASME Journal of Turbomachinery,* vol. 131, p. 031010, 2009.

[123]   S. W. T. Spence, R. S. E. Rosborough, D. Artt and G. McCullough, "A Direct Performance Comparison of Vaned and Vaneless Stators for Radial Turbines," *ASME Journal of Turbomachinery,* vol. 129, pp. 53–61, 2007.

[124]   Y. Kang and R. McKeirnan, "Annular Recuperator Development And Performance Test for 200 kW Microturbine", ASME Paper GT2003-38522, 2003.

[125]   C. F. McDonald, "Recuperator Considerations for Future Higher Efficiency Microturbines," *Appl. Therm. Eng.,* vol. 23, pp. 1463–1487, 2003.

[126]   W. J. Matthews, K. L. More and L. R. Walker, "Long-Term Microturbine Exposure of an Advanced Alloy for Microturbine Primary Surface Recuperators", ASME Paper GT2008-50037, 2008.

[127]   P. J. Maziasz, B. A. Pint, J. P. Shingledecker, N. D. Evans, Y. Yamamoto, K. L. More and E. Lara-Curzio, "Advanced Alloys for Compact, High-Efficiency, High-Temperature Heat-Exchangers," *Int. J. Hydrogen Energy,* vol. 32, pp. 3622–3630, 2007.

[128]   C. Rodgers, "Turbochargers to small gas turbines!", ASME 97-GT-200, presented at the ASME Paper 97-GT-200, 1997.

[129]   C. Rodgers and C. F. McDonald, "Small Recuperated Gas Turbine APU Concept To Abate Concern About Emissions, High Fuel Cost, And Noise", , presented at the ASME paper GT-27913 Montreal, Canada 2007.

[130]   F. L. Moody, T. Zowski, C. V. Davis and E. S. K., *Hydraulic Machinery: Handbook of Applied Hydraulics*: McGraw Hill, 1969.

[131]   H. Addison, *A treatise on Applied Hydraulics*. London: Aberdeen University Press, 1954.

[132]   B. S. Massey, *Mechanics of Fluids*. New York: Litton Educational Publishing 1979.

[133]   M. V. Casey, "The Effect of Reynolds Number on the Effecncy of Centrifugal Compressor Stages," *Engineering for Gas Turbines and Power,* vol. 107, pp. 541-549, 1985.

[134]   C. Rodgers, "A cycle analysis technique for small gas turbines," *Solar Division,* pp. 37-49, 1969.

[135]   T. C. Capstone, "Technical Reference: Capstone Model C30 Performance ", ChatsworthApril 2006.

[136]   C. Capstone, "Capstone Hybrid Vehicle Experience", Capstone Turbines, California, USA2009.

[137]   G. c. Congress. (2010, June 22). Capstone Launches CARB-Certified Microturbine Range Extender for Hybrid Electric Vehicles. *Green car Congress; Energy, technology, issues and policies for sustainable mobility*. Available: http://www.greencarcongress.com/2010/06/capstone-20100622.html#more

[138]   D. E. Holeski and S. M. Futral, "Experimental performance evaluation of a 6.02 inch radial inflow turbine over a range of Reynolds number", Lewis Research Center, Cleveland, Ohio1967.

[139]   W. J. Nusbaum and C. A. Wasserbauer, "Experimental performance evaluation of a 4.59inch radial inflow turbine over a range of Reynolds numbers", NASA, Washington, D. C., D-38351967.

[140]   A. J. Glassman, *Turbine Design and Application* Washington Lewis Research Center 1994.

[141]   E. J. Logan, *Handbook of Turbomachinery* New York Marcel Dekker, 2003.

[142]   M. Olivero, A. Javed, R. Pecnik, P. Colonna and J. P. van Buijtenen, "Study on the Tip Clearance Effects in the Centrifugal Compressor of a Micro Gas Turbine by means of Numerical Simulations", presented at the IGTC2011-0233, 2011.

[143]   C. Pfleiderer, *Die Kreisel Pumpen* vol. 5. Berlin Sringer Verlag, 1961.

[144]   T. C. Capstone. *Overview of Capstone* http://www.usea.org/Programs/APP/Kolkata_Workshop_4-08/Capstone_OverviewKolkataApr08.pdf (2009, 25-07-2011)

[145]   T. C. Capstone. *Capstone MicroTurbine: Model 330 HEV MicroTurbine Multi Fuels* http://www.metadope.com/Bus/Capstone/Capstone30hev.pdf (2010, 25-07-2011)

[146]   W. P. J. Visser, S. A. Shakariyants and M. Oostveen, "Development of a 3kw Micro Turbine for CHP Applications", presented at the ASME GT2010-22007, 2010.

[147]   T. C. Capstone, "Capstone Drive Solution Range Extender". Chatsworth 2010.

[148]   S. M. Y. A. Denis L. D. H., "Gas turbine plant acting as generator of gas under pressure," Patent nr. GB 818,063, 1959.

[149]   P. A. Jeschke P., "A Novel Gas Generator Concept for Jet Engines using a Rotating Combustion Chamber", GT2013-95574, presented at the ASME Turbo Expo 2013, San Antonio TX, USA, 2013.

[150]   S. Z. Boksteen, J. P. van Buijtenen, D. J. v. d. Vecht and R. Pecnik, "Performance Modeling of a Modern Gas Turbine for Dispatch Optimization", GT2012-68137, presented at the ASME Turbo Expo, Copenhagen, Denmark, 2012.

[151]   F. Yin, A. G. Rao and J. P. van Buijtenen, "Performance Cycle Analysis for a Multi-Fuel Hybrid Engine", GT2013-94601, presented at the ASME Turbo Expo, San Antonio TX, USA, 2013.

[152]   S. A. Shakariyants, "Generic Methods for Aero-Engine Exhaust Emission Prediction", Delft University of Technology, 2008, ISBN 978-90-9023346-8.

References

[153]   S. A. Shakariyants, W. P. J. Visser, A. Tarasov and J. P. van Buijtenen, "Generic Airplane and Aero-Engine Simulation Procedures for Exhaust Emission Studies", GT2007-27943, presented at the ASME TURBO EXPO 2007, Montreal, Canada, 2007.

[154]   I. Goulos, V. Pachidis, R. d'Ippolito, J. Stevens and C. Smith, "An Integrated Approach for the Multidisciplinary Design of Optimum Rotorcraft Operations", GT2012-69583, presented at the ASME TURBO EXPO, Copenhagen, Denmark, 2012.

[155]   U. E. L. Locadia, W. P. J. Visser and J. P. van Buijtenen, "Integral Performance Modelling Of Biomass Gasifiers And Gas Turbines", ASME/JPG paper JPGC2001/PWR-19006, presented at the International Joint Power Generation Conference, New Orleans, Louisiana, USA, 2001.

[156]   M. H. van Klooster, W. P. J. Visser and J. P. van Buijtenen, "Effects of mixed low calorific fuel on GE MS 9001FA gas turbine performance", Delft University of Technology, TUD-EV-2104, 2002.

[157]   J. P. van Buijtenen et al, "Co-combustion of syngas from biomass gasification in a gas turbine", SDE-KEMA, Projectnumber 50180312-KPS/TPE 02-1102, 2002.

Acknowledgements

The work described in this thesis has been performed over a period of at least 15 years. During this period, many people have been involved in the work in some way and without them this thesis could not have been written.

First, I like to thank my doctoral advisor Prof. Jos van Buijtenen for providing me with the opportunity to work on gas turbine simulation technology in an academic environment. For many years, our collaboration on gas turbine education combined with the application of GSP in many research projects has been an essential element.

Another essential element was my employment at the National Aerospace Laboratory NLR where I enjoyed many years of work on gas turbine performance and simulation, until I left in 2004. In the early years Jan Vleghert taught me many things about gas turbines. In the 1990s, NLR still made time available for younger engineers to develop knowledge and this led to the development of the object oriented version of GSP. I also wish to thank the other colleagues at NLR: Oscar Kogenhop, Michael Broomhead, Jan Derk Stegeman and Edward Rademaker who contributed to GSP. Oscar and Edward continue to develop GSP at NLR together with Delft University. They have also provided valuable comments during the writing of this thesis.

To Wim de Wolf of NLR I thank the involvement in the RTO (NATO Research and Technology Organisation) working groups on gas turbine simulation. This has helped me develop my current network in the international gas turbine community and ASME IGTI (International Gas Turbine Institute).

The work described in Chapter 12 was funded by the Netherlands Agency for Aerospace Programmes NIVR as a Basic Research Program (BRP) with project number 49212N. The author wishes to express his gratitude to KLM Royal Dutch Airlines CF6 engine maintenance facility Amsterdam, and in particular Rob Duivis, for their cooperation.

For more recent development I wish to thank my colleagues at MTT (Micro Turbine Technology b.v.) who have helped adding several capabilities to GSP that were required for micro turbine conceptual design and simulation. First of all Savad Shakariyants, the perfect sparring partner with whom working on several gas turbine cycle analysis and design problems was a lot of fun. Further thanks to Mark Oostveen, Ilian Dountchev and Viktor Kornilov. Thanks to MTT, I got the opportunity to apply GSP to all stages of gas turbine development.

At Delft University, I further owe gratitude to the past students Steven Kluiters for his contribution to the development of the chemical gas and emission formation model, Michel Verbist and Hanneke Pieters for their contributions to the adaptive modelling capability and Adam Head for his work on the scaling rules for efficiency, his reviewing and, as a native speaker of English, his invaluable help as a proof-reader.

Thanks go to Steven Kok for his comments, from today's information technology viewpoints, on the description of object orientation in Chapter 6. Paul Holden of Saturn Systems Engineering U.K., I wish to thank for his input in the configuration and case management functionality.

Finally, thanks go to my wife Anne-Marie and children Elise and Jules who have kindly allowed me to spend so much time to prepare this thesis in between the normal family businesses.

Wilfried Visser
Susteren, October 2014

About the author

Wilfried Visser was born on 18 October 1958 in Bovenkarspel, the Netherlands. He grew up in an agricultural environment. After completing secondary school he studied mechanical engineering at Delft University of Technology (TU Delft) where he earned his MSc degree in 1983 on performance simulation of large turbocharged diesel engines. From 1984 to 1986 he was drafted as a reserve officer in the Royal Dutch Army where he was occupied with endurance testing of military vehicles. From 1986 until 2004, he worked for National Aerospace Laboratory NLR in Amsterdam on aircraft propulsion performance and simulation. From 2004 to 2006 he was business development manager at Delta Consult b.v. (later SKF Asset Management Services, in Nieuwegein, the Netherlands), leading the development and marketing of industrial maintenance engineering tools and methods. Since 2006, Wilfried is working both as CTO for Micro Turbine Technology b.v. in Eindhoven and as lecturer at TU Delft.

The PhD research work described in this thesis has been carried out between 1996 and 2014, mainly at NLR and TU Delft. Wilfried is continuously involved in the development of GSP together with NLR and colleagues at TU Delft.

Wilfried is an active member in the organization of the ASME International Gas Turbine Institute (IGTI) Aircraft Engine Committee.

Outside his work, he is a certified and active Judo instructor, holding the 4th Dan.

Wilfried is married and has two children.

Selected Publications

- Visser, W.P.J. and Broomhead M.J., 2000, 'GSP, a generic object-oriented gas turbine simulation environment', ASME paper 2000-GT-2, presented at the ASME TURBO EXPO 2000, 8-11 May 2000, Munich, Germany,

- Visser W.P.J., Kogenhop O., Oostveen O., 'A Generic Approach for Gas Turbine Adaptive Modelling', ASME Journal of Engineering for Gas Turbines and Power, January 2006, Volume 128, GTP-04-1039

- Visser W.P.J., Shakariyants S.A. , Oostveen M. 'Development of A 3kW Micro Turbine For CHP Applications', ASME Journal of Engineering for Gas Turbines and Power, April 2011, Vol. 133 / 042301-1

- Verbist M.L., Visser W.P.J., Pecnik R., Buijtenen J.P. van, 'Experience with Gas Path Analysis for On-Wing Turbofan Condition Monitoring', ASME Journal of Engineering for Gas Turbines and Power, GTP-13-1212, 2014